NASA TN D-901

TECHNICAL NOTE

D-901

AERODYNAMIC CHARACTERISTICS OF A FOUR-PROPELLER TILT-WING VTOL MODEL WITH TWIN VERTICAL TAILS, INCLUDING EFFECTS OF GROUND PROXIMITY

By Kalman J. Grunwald

Langley Research Center
Langley Field, Va.

NATIONAL AERONAUTICS AND SPACE ADMINISTRATION
WASHINGTON June 1961

J

NATIONAL AERONAUTICS AND SPACE ADMINISTRATION

TECHNICAL NOTE D-901

AERODYNAMIC CHARACTERISTICS OF A FOUR-PROPELLER TILT-WING VTOL MODEL WITH TWIN VERTICAL TAILS, INCLUDING EFFECTS OF GROUND PROXIMITY

By Kalman J. Grunwald

SUMMARY

Results are presented of a wind-tunnel investigation of the aerodynamic stability, control, and performance characteristics of a model of a four-propeller tilt-wing VTOL airplane employing flaps and speed brakes through the transition speed range. The results indicate that the wing was stalled for steady level flight for all conditions of the investigation; however, the flapped configuration did produce a higher maximum lift. The effectiveness of the flap in delaying the stall in the present investigation was not as great as in some previous investigations because the flap used was smaller than that used previously. The wing stall resulted in an appreciable reduction of aileron effectiveness during the transition. Out of ground effect the low horizontal tail did not appear to be in an adverse flow field as had been expected and showed no erratic changes in effectiveness; however, in ground effect a large nose-down moment was experienced by the model. In general, the lateral aerodynamic data indicate that the configuration is directionally stable and possesses positive dihedral effect throughout the transition, and the data show no signs of erratic flow at the vertical tails.

INTRODUCTION

Previous investigations of tilt-wing configurations have indicated the importance of using an adequate ratio of wing chord to propeller diameter and the need for high-lift devices to minimize the wing stall problem during transition (ref. 1). Unfortunately, the wing size determined from these considerations is larger than would be desirable in cruise flight. While previous investigations have indicated the general considerations to be followed in avoiding stall in transition, they have not closely defined the sizes of flaps, slats, and so forth, needed.

The flapped tilt-wing configuration of reference 2 (referred to as "combination configuration" in ref. 2) appears to have an adequate stall margin but accomplishes this by the use of a large (40-percent chord) full-span Fowler flap.

One purpose of the present investigation was to determine the effectiveness of slats and a partial-span single-slotted flap (which, from weight and structural considerations, may be preferred to the 40-percent-chord Fowler flap of ref. 2) in controlling the stall on a model using a wing size which was chosen as a compromise between the cruise and transition conditions. Another purpose was to investigate the effectiveness of wing-mounted speed brakes in reducing the stall. It was reasoned that the increased thrust required to overcome the drag of the speed brakes would increase the slipstream velocity over the wing and thereby reduce the tendency to stall.

L 1 4 9 1

A third purpose of the investigation was to obtain additional lateral stability and control data on a tilt-wing configuration.

SYMBOLS

The force and moment coefficients presented in this report are based on the dynamic pressure in the slipstream. This system is used because when a wing is located in a propeller slipstream, large forces and moments can be produced even though the free-stream velocity decreases to zero, and in this condition coefficients based on the free-stream dynamic pressure approach infinity and therefore become meaningless. It appears appropriate, therefore, to base the coefficients on the dynamic pressure in the slipstream. The coefficients based on this dynamic pressure are indicated in the present paper by the use of the subscript s. The relations between the thrust and dynamic pressure in the slipstream have been derived in reference 3. The more familiar coefficient forms based on the free-stream dynamic pressure can be found by dividing by $(1 - C_{T,s})$; that is, $C_L = \frac{C_{L,s}}{1 - C_{T,s}}$.

All forces and moments are presented about the stability axis system. The positive sense of forces, moments, and angles is indicated in figure 1. The moments are presented with reference to the center-of-gravity locations, which varied with wing tilt angle as shown in figure 2. The coefficients for all configurations are based on the area of the short-span wing.

b	short wing span, 5.73 ft
c	wing reference chord, 1.055 ft

C_L lift coefficient based on free stream, $\frac{L}{\frac{\rho}{2}V^2S}$

$C_{L,s}$ lift coefficient based on slipstream, L/q_sS

$C_{l,s}$ rolling-moment coefficient based on slipstream, M_X/q_sSb

$C_{m,s}$ pitching-moment coefficient based on slipstream, M_Y/q_sSc

$C_{n,s}$ yawing-moment coefficient based on slipstream, M_Z/q_sSb

$C_{T,s}$ thrust coefficient, $\frac{T}{q_sN\frac{\pi}{4}d^2}$

$C_{X,s}$ longitudinal-force coefficient, F_X/q_sS

$C_{Y,s}$ side-force coefficient based on slipstream, F_Y/q_sS

d propeller diameter, 1.5 ft

F static resultant force, lb

F_X longitudinal force, lb

F_Y side force, lb

h height from wing-down ($i_w = 0^o$) moment reference point to ground, ft

h' height from trailing edge of wing root chord to ground, ft

i_t tail incidence, deg

i_w wing tilt angle, deg

L lift, lb

M moment, ft-lb

M_X rolling moment, ft-lb

M_Y	pitching moment, ft-lb
M_Z	yawing moment, ft-lb
N	number of propellers, 4
P	power, hp
q_s	dynamic pressure of slipstream, $\frac{\rho V^2}{2} + \frac{T}{N\frac{\pi}{4}d^2}$, lb/sq ft
S	area of short-span wing, 6.14 sq ft
T	total thrust, lb
T_t	thrust of tail fan, lb
V	free-stream velocity, ft/sec
α	angle of attack, deg
β	angle of sideslip, deg
$\beta_{.75}$	blade angle, measured at the 75-percent-radius location, deg
δ_a	aileron deflection, deg
δ_f	flap deflection, deg
δ_r	rudder deflection, deg
δ_{SB}	upper and lower speed-brake deflection, 60° from wing surface, except when noted
δ_e	elevator deflection, deg
ρ	mass density of air, slugs/cu ft
θ	slipstream turning angle, deg

Subscript:

o	power off

MODEL

Drawings of the model with pertinent dimensions are presented in figure 3, and photographs of the model mounted for testing are presented in figure 4. Figure 3(b) shows sketches of the flaps, speed brakes, and slats. The wing had an NACA 2415 airfoil section and pivoted about the 60-percent-chord line. For a few tests, the model was fitted with an electrically driven tail fan (figs. 3 and 4) in order to investigate the influence of the induced flow from the tail fan on the model stability characteristics.

The model consisted of a steel and aluminum frame to carry the loads and a wooden covering to give the desired contours. The three-blade propellers were made of bonded glass fiber and were driven by four variable-frequency electric motors. Most of the tests were run at a model propeller blade angle of approximately 6° and a rotational speed of 8,400 rpm. The direction of rotation of the propellers for most of the tests is shown in figure 3.

The forces and moments of the model were measured with an internally mounted strain-gage balance. The wing and tail incidence were changed by means of remotely controlled electric motors. The ailerons, elevator, and rudder were manually changed and locked in place with set screws. Each motor was mounted on ball bushing supports and restrained by strain-gage beams so that the thrust of each propeller could be measured.

TESTS AND CORRECTIONS

The investigation was made in the 17-foot test section of the Langley 300-MPH 7- by 10-foot tunnel, which is described in the appendix to reference 2.

A free-stream dynamic pressure of approximately 10 pounds per square foot was used for the propeller-off tests. The slipstream dynamic pressures for the power-on tests varied from about 7 to 14 pounds per square foot. The Reynolds number of the flow in the slipstream based on the wing reference chord of 1.055 feet varied from approximately 5×10^5 to 7×10^5.

The test procedure consisted of setting the propeller rotational speed with the model fuselage at zero angle of attack and then increasing the tunnel speed until zero longitudinal force was reached. The tunnel speed then corresponded to the condition for steady level flight at zero angle of attack (when the lift is made equal to the weight) and was held constant as the data were taken through the angle-of-attack range.

Usually subsequent tests were also made at tunnel dynamic pressures below and above the tunnel speed for steady level flight at zero angle of attack, in order to provide data on the variation of the characteristics under accelerating (or climb) and decelerating (or descending) conditions.

Corrections to the free-stream velocity to account for blockage and slipstream contraction were estimated and considered negligible. The jet-boundary corrections applied to the angle of attack and longitudinal force were estimated for a square test section by a method similar to that of reference 4. Inasmuch as these corrections depend on the circulation about the wing, it was necessary to subtract the direct thrust contribution to lift before applying them. The following relations were used:

$$\alpha = \alpha_{measured} + 0.2223C_{L,1}$$

$$C_{X,s} = \left(C_{X,s}\right)_{measured} - 0.0038\left(C_{L,1}\right)^2\left(1 - C_{T,s}\right)$$

where $C_{L,1}$ is the increment of lift coefficient that is approximately proportional to circulation and is obtained by subtracting the direct thrust contribution as follows:

$$C_{L,1} = \frac{C_{L,s} - C_{T,s}\dfrac{N\frac{\pi}{4}d^2}{S}\dfrac{F}{T}\sin\left(\vartheta + \alpha + i_w\right)}{1 - C_{T,s}}$$

where ϑ and F/T are the turning angle and thrust recovery factor determined from static tests.

A more rigorous correction procedure is now available in reference 5; however, this work became available after the present investigation was completed. Application of the corrections of reference 5 would change the absolute value of the coefficients slightly but would not significantly alter the general character of the curves or change any of the conclusions to be drawn from data.

PRESENTATION OF RESULTS

For most of the investigation three primary configurations were tested. These configurations are identified and defined in the following table:

Configuration	δ_f, deg	δ_a, deg	Wing extension	Slat position
Basic	0	0	Off	Retracted
Flapped	50	30	On	Low
Speed brake	0	0	Off	Low

The results of the investigation are presented in the following order (extraneous symbols on the data plots at the zero axes are reference points printed by the machine used for plotting the data):

The basic data obtained from the investigation are presented in figures 5 to 41. It should be remembered that the coefficients are based on the area of the short-span wing (tip extension off), except in figure 7(c). Figure 7(c) is a comparison of the lift-curve slopes and maximum lift coefficients of the basic configuration without wing extension (based on a wing area of 6.14 feet) and the basic configuration with wing extension (based on a wing area of 7.15 feet).

Complete analysis of the data has not been attempted; however, a few of the more significant results are analyzed on the basis of the performance and the stability and control characteristics that can be expected for an assumed airplane as determined from the tunnel data. The results of this analysis are presented in figures 42 to 50. A gross weight of 15,000 pounds and a model scale of 1/7.33 were assumed for the purpose of this analysis. The thrust required was computed from the experimental data and the power was calculated by using the characteristics of propeller 1 of reference 6.

DISCUSSION

Longitudinal Aerodynamic Characteristics

Transition performance.- Examination of the power-off data of figure 7 indicates that the lift-curve slope is somewhat lower than would be expected for a wing of this planform. About half of the discrepancy may be due to the relatively low Reynolds number of the tests.

The data for the basic configuration in the transition speed range investigated (i_w = 75° to 30°) are presented in figure 10. It can be

seen that at zero angle of attack and at a longitudinal force coefficient of zero (which corresponds to the steady-level-flight condition) the wing is stalled throughout most of the transition. This causes the thrust and power required in a steady-level-flight transition to remain relatively high, as shown in figures 42 and 43.

Somewhat higher lifts are obtained with the flapped configuration ($\delta_f = 50^o$, $\delta_a = 30^o$, slats in low position and wing extension on), as shown in figure 11, which results in a reduction in thrust and power required in steady level flight (figs. 42 and 43). However, the data of figure 11 indicates that the wing is still partially stalled, particularly in the descent condition (negative values of $C_{X,s}$), and the thrust and power required (figs. 42 and 43) are therefore higher than they might be if the wing were unstalled throughout the level flight and 10^o descent condition.

L
1
4
9
1

The wing center section, which was not in the propeller slipstream, was stalled throughout the transition, as would be expected. Tuft studies of the wing showed that the wing extensions (outboard panel) stalled at relatively low angles because the direction of rotation of the propellers was such as to increase the angle of attack over the outboard panel. Also, the aileron portion of the wing stalled before the flap section because the aileron was not a slotted configuration. The relatively small chord of the wing behind the outboard propeller is also believed to have contributed to the stall.

On the basis of past experience it is expected that appreciably better results would have been obtained if a larger tip chord and a full-span extendible slotted flap had been used. This effect is illustrated in figure 44, where the lift—longitudinal-force polars for the present configuration (at constant thrust coefficient) are compared with those of reference 2. The better aerodynamic characteristics obtained in reference 2 are due in part to the greater ratio of wing chord (with the flap extended) to propeller diameter for the configuration of reference 2. Also, the angle through which the slipstream is turned by the present configuration (fig. 5) is appreciably less than that for the wing of reference 2; thus the effective angle of attack required for a given condition is greater for the present configuration and stall occurs sooner. These points are discussed more fully in reference 1.

It should be observed that the stall would not prevent completion of transition from a performance standpoint if the power available exceeded that required in hovering. However, stall would greatly reduce the STOL performance, and experience has shown that the handling qualities in the transition speed range are adversely affected by the stall.

The basic data for configurations with speed brakes extended are presented in figure 12. Comparison of these data with data for the basic configuration (fig. 10) shows that, in general, speed brakes shifted the lift—longitudinal-force polars in the drag direction as intended. However, the thrust coefficient for a given condition was increased and there was little or no change in lift. As a result, the thrust and power required for level flight and 10° descent transitions were greatly increased, as shown in figures 42 and 43.

A limited investigation of the effects of the individual components added to the basic configuration to make up the flapped configuration was made. The effects of the wing extension are shown in figure 22, the effects of the slats are shown in figure 23, and the effects of the flaps are shown in figure 24.

Stability in transition.- In general, the data for all configurations (figs. 9 and 13 to 15) indicate longitudinal stability through most of the steady-level-flight ($C_{X,s} = 0$) transition except for some neutral stability or slight instability at the lowest speeds (highest thrust coefficients and wing incidence angles). In general, there is also a decrease in stability at the higher angles of attack. This is probably due primarily to the fact that the wing is stalled and the dynamic pressure in the wake from the wing decreases with increasing angle of attack as shown in reference 2. The erratic pitching-moment variations that it was feared would occur with a low tail, where there was the possibility of the tail moving into or out of the propeller slipstream, were not experienced.

The effect of the wake from the wing is believed to be the primary cause of the decrease in tail effectiveness $\partial M_Y/\partial i_t$ for the power-on conditions as compared with what would be expected from the power-off tail effectiveness as shown in figure 45. The fact that in the level flight conditions the power-on tail effectiveness for the basic configuration is fairly close to the power-off estimate indicates that there is only a small decrease in dynamic pressure at the tail. At lower speeds and in the descent condition (higher angles of attack) the greater difference indicates a further decrease in dynamic pressure at the tail. The wake from the speed brakes also causes a decrease in tail effectiveness for the steady-level-flight conditions.

The effects of the ground are shown in figures 16 to 18. In ground effect the slipstream impinges upon the ground and flows parallel to it, causing a change in the flow field at the tail. This change in the flow field causes an increase in stability at high angles of attack in ground effect due to the decrease in downwash and increase in dynamic pressure at the tail.

Trim in transition.- The variation of pitching moment in the transition speed range for the assumed airplane is presented in figures 46 to 48. The large nose-up moment in hovering is present because the configuration was designed with the concept that the tail fan would be lifting at the same disk loading as the main propellers in hovering.

The increase in nose-up moment for the basic configuration at low speeds (fig. 46) is due to the expected nose-up moments on the propellers (ref. 3). The decrease in moment at the higher speeds is due largely to the decrease in thrust and angle of attack required at these speeds (fig. 42) which reduces the direct contribution of the propellers. The forward shift of the center of gravity as the wing tilt angle is reduced also contributes to the reduction in nose-up moment.

As would be expected, the deflection of the flaps caused a decrease in nose-up moment (fig. 47) because of the direct contribution of the flap and because the angle of attack and thrust are further reduced (fig. 42) which further reduced the direct contribution of the propellers. The increase in nose-up moment due to the speed brakes (fig. 47) is due partly to the increase in thrust required (fig. 42) and partly to the reduction in tail effectiveness due to the wake from the speed brakes (fig. 45).

The presence of the ground causes a nose-down moment (fig. 48) due to the change in flow field at the tail. The change in moment due to entering ground effect does not appear to be serious at speeds above about 40 knots but would be serious at lower speeds in the descent conditions with high tail-incidence settings.

Tail-fan effectiveness.- For the most part, the tail fan did not change the overall stability (fig. 20). In figure 21(b), the increment of pitching moment calculated from the tail-fan thrust is compared with the increment obtained from the basic data of figure 20.

At the lower wing-incidence settings the horizontal tail was at moderate incidence settings and the tail fan and horizontal tail were in nearly the same plane. In this condition the flow through the tail fan induced a load on the horizontal tail that resulted in an appreciably larger contribution to the total model pitching moment than would be calculated from the direct tail-fan thrust. This induced load would also be expected to change the elevator hinge moment (which was not measured) and this would be a problem unless an irreversible power-boost control system were used.

With the tail at high incidence settings the tail was an appreciable distance from the fan and a load was not induced on the tail surface.

Lateral Aerodynamic Characteristics

The lateral aerodynamic characteristics are presented in figures 26 to 41. For the most part the basic data indicate directional stability and positive dihedral effect throughout the transition and show no obvious erratic flow characteristics at the vertical tail, both in and out of ground effect. With the tail off and with power off the configuration is directionally unstable, as would be expected. However, with power on and the tail off the configuration is directionally stable. The reason for this unexpected result is not known, but the fact that the tail-off directional stability increases with increasing thrust coefficient and wing-tilt angle indicates that it must be arising from the wing-propeller combination. The presence of the vertical hump (horizontal-tail mounting surface), which was left on in the tail-off tests, may also be a contributing factor. A similar tendency toward tail-off directional stability was also noted in the deflected-slipstream configuration of reference 7. (See fig. 12(c) of ref. 7.)

L 1 4 9 1

The aileron effectiveness is presented in figures 36 to 39 and summarized in figure 49. Accurate procedures for analytical predictions of the aileron effectiveness in the transition speed range are not available. However, two approximations have been made and are shown in figure 49. The first approximation is based on the use of the rolling-moment effectiveness $\frac{\partial C_{l,s}}{\partial \delta_a}$ at zero angle of attack as obtained from the power-off data of figure 36. It is assumed that the moment about a longitudinal axis lying in the plane of the wing at any tilt angle is proportional to the slipstream dynamic pressure $\left(\frac{\partial M}{\partial \delta_a} = \frac{\partial C_{l,s}}{\partial \delta_a} q_s Sb\right)$, and then this moment is resolved into rolling- and yawing-moment components. The second estimate is based on the power-on effectiveness in hovering taken from the yawing-moment data of figure 6. It is again assumed that the moment about a longitudinal axis in the plane of the wing is proportional to the slipstream dynamic pressure $\left(\frac{\partial M}{\partial \delta_a} = \frac{\partial M_Z/Tb}{\partial \delta_a} \frac{q_s}{q_{s_{hovering}}} Tb\right)$, and then this moment is resolved into rolling- and yawing-moment components. A more rigorous estimate would lie somewhere between these two estimates. It can be seen in figure 49 that both the stall procedures overestimate the aileron effectiveness; apparently the stall appreciably reduces the power-on aileron effectiveness in the transition speed range for all configurations.

Normally it is assumed that the thrust of the outboard propellers would be varied to provide roll control in hovering. In order to obtain

some information on the effects of a change in propeller thrust on the rolling and yawing moments in transition, a single condition of 2° reduction in blade angle on the left outboard propeller was investigated. The data are presented in figure 40. The propeller used was not a scale version of the propeller that would probably be used on a full-scale airplane of this type, and therefore only the ratio of the change in yawing moment to the change in rolling moment as presented in figure 50 can be used.

CONCLUSIONS

The results of an investigation to determine the aerodynamic characteristics of a four-propeller tilt-wing VTOL model with twin vertical tails, including effects of ground proximity, indicate the following conclusions:

1. The basic wing was stalled through most of the transition speed range of the investigation (wing tilt angles from 90° to 30°). The effectiveness of the flap in delaying the stall in the present investigation was not as great as in some previous investigations, primarily because the flap used was smaller than that used previously.

2. The speed-brake configuration required more thrust and power in the transition than the basic or flapped configurations.

3. Because of the wing stall experienced in transition with all configurations, the aileron effectiveness was appreciably lower than would be expected for an unstalled wing.

4. The present model did not encounter the nonlinearities in the pitching-moment characteristics that had been expected for a low-tail configuration. In ground effect, however, a nose-down pitching-moment was experienced at high wing incidence and low speed.

5. In general, the data for all configurations indicate longitudinal stability through most of the steady-level-flight transition except for some neutral stability or slight instability at lower speeds.

6. The tail fan did not change the overall stability of the configuration.

7. In general, the data indicate that the configuration is directionally stable and possesses positive dihedral effect through the transition. No signs of erratic flow were indicated at the tail.

Langley Research Center,
National Aeronautics and Space Administration,
Langley Field, Va., April 6, 1961.

REFERENCES

1. Kirby, Robert H.: Aerodynamic Characteristics of Propeller-Driven VTOL Aircraft. NASA TN D-730, 1961.

2. Kuhn, Richard E., and Hayes, William C., Jr.: Wind-Tunnel Investigation of Longitudinal Aerodynamic Characteristics of Three Propeller-Driven VTOL Configurations in the Transition Speed Range, Including Effects of Ground Proximity. NASA TN D-55, 1960.

3. Kuhn, Richard E., and Draper, John W.: Investigation of the Aerodynamic Characteristics of a Model Wing-Propeller Combination and of the Wing and Propeller Separately at Angles of Attack up to 90°. NACA Rep. 1263, 1956. (Supersedes NACA TN 3304 by Draper and Kuhn.)

4. Gillis, Clarence L., Polhamus, Edward C., and Gray, Joseph L., Jr.: Charts for Determining Jet-Boundary Corrections for Complete Models in 7- by 10-Foot Closed Rectangular Wind Tunnels. NACA WR L-123, 1945. (Formerly NACA ARR L5G31.)

5. Heyson, Harry H.: Wind-Tunnel Wall Interference and Ground Effect for VTOL-STOL Aircraft. Jour. Am. Helicopter Soc., vol. 6, no. 1, Jan. 1961, pp. 1-9.

6. Yaggy, Paul F., and Rogallo, Vernon L.: A Wind-Tunnel Investigation of Three Propellers Through an Angle-of-Attack Range From 0° to 85°. NASA TN D-318, 1960.

7. Kuhn, Richard E., and Grunwald, Kalman J.: Lateral Stability and Control Characteristics of a Four-Propeller Deflected-Slipstream VTOL Model Including the Effects of Ground Proximity. NASA TN D-444, 1961.

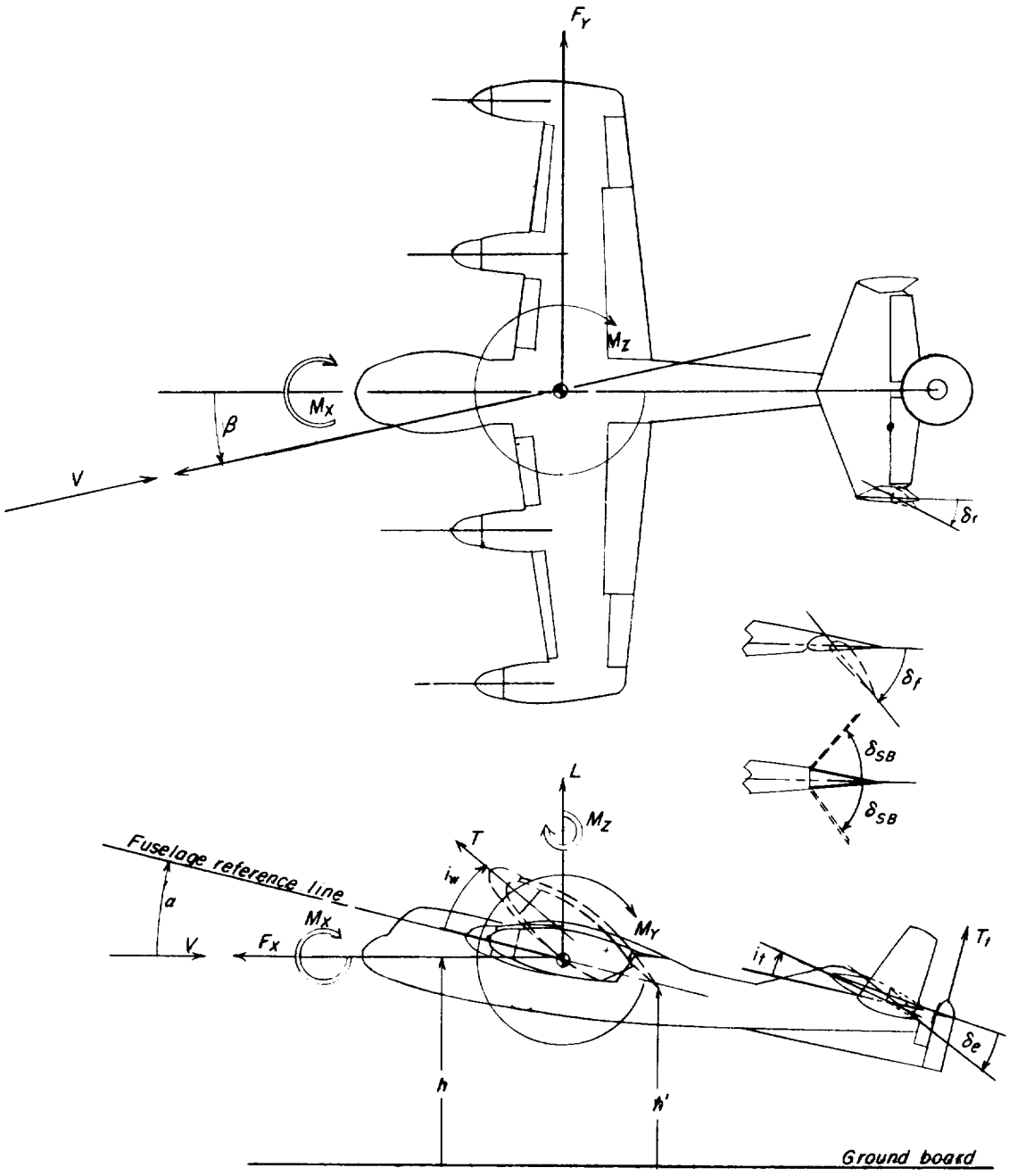

Figure 1.- Systems of axes used, showing positive sense of forces, moments, angles, and velocity.

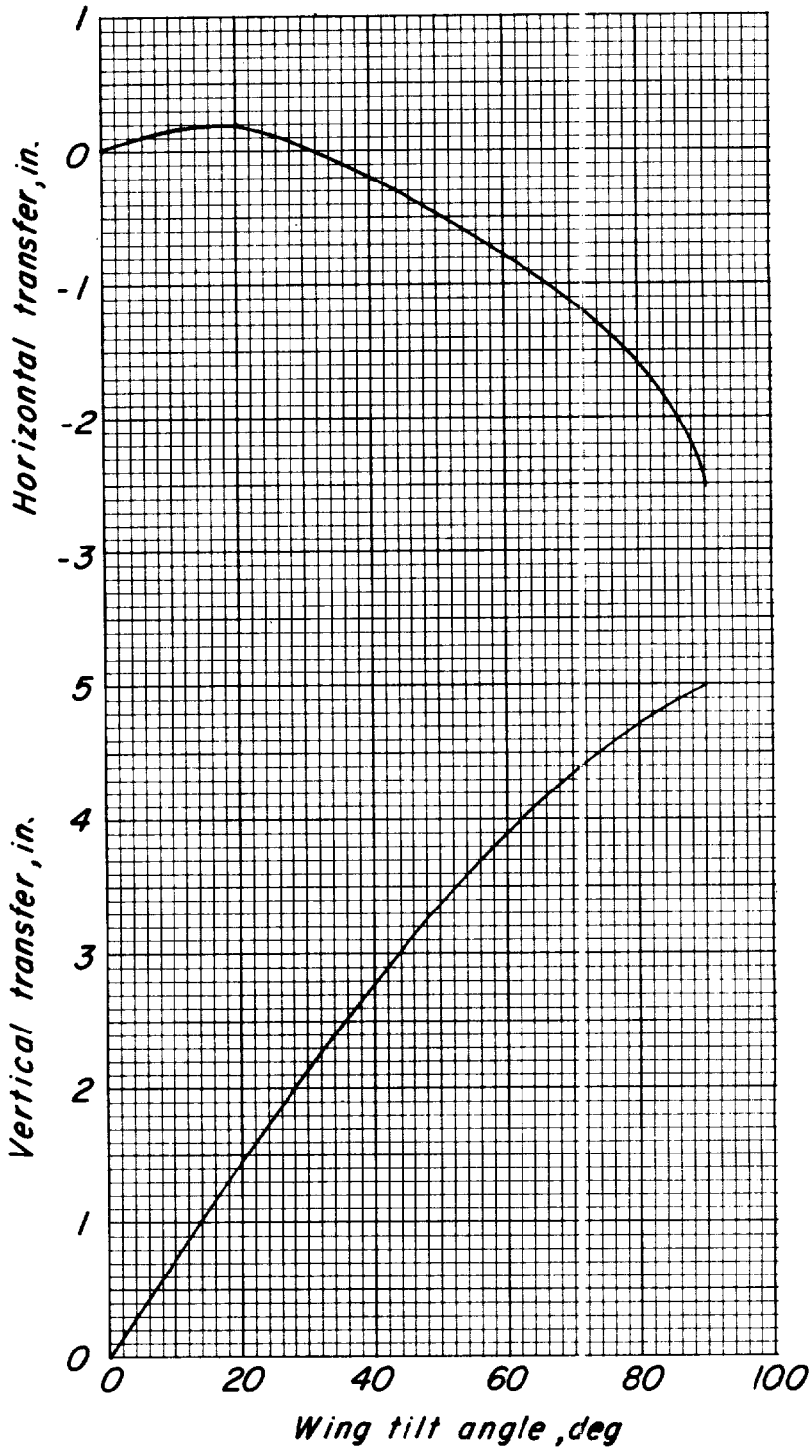

L-1491

Figure 2.- Variation of moment reference point with wing tilt angle.

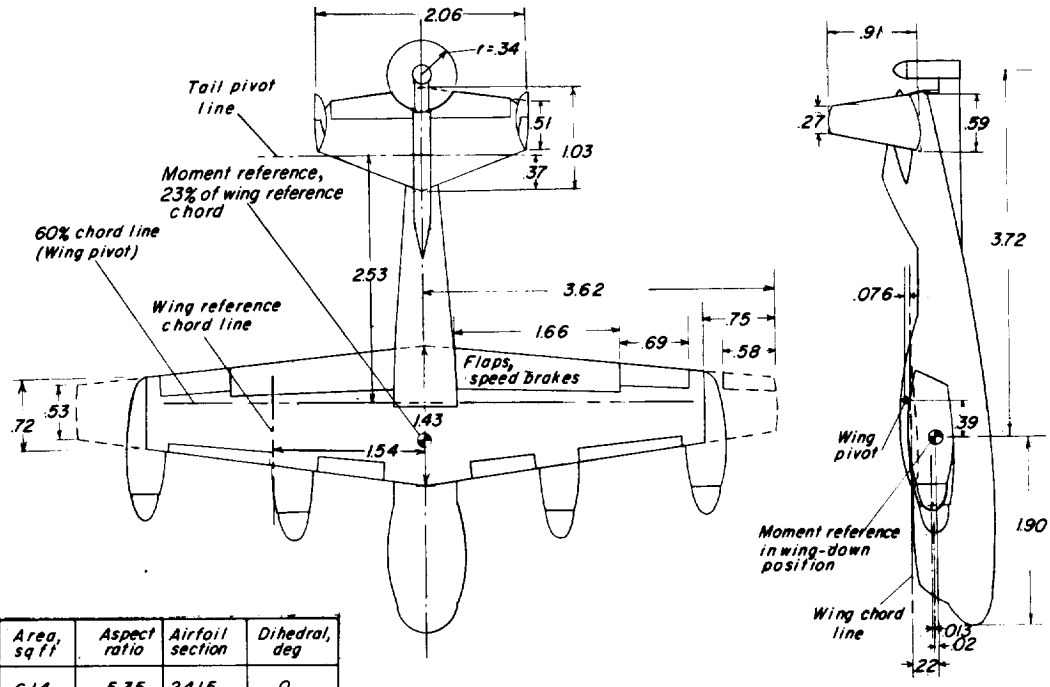

	Area, sq ft	Aspect ratio	Airfoil section	Dihedral, deg
Wing	6.14	5.35	2415	0
Wing and extension	7.15	7.95	2415	0
Horizontal tail	1.49	2.65	0012	6.5
Vertical tail	.80	2.06	0012	0

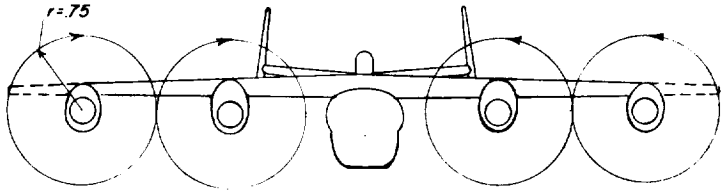

(a) Three-view drawing.

Figure 3.- Details of model. Dimensions are in feet.

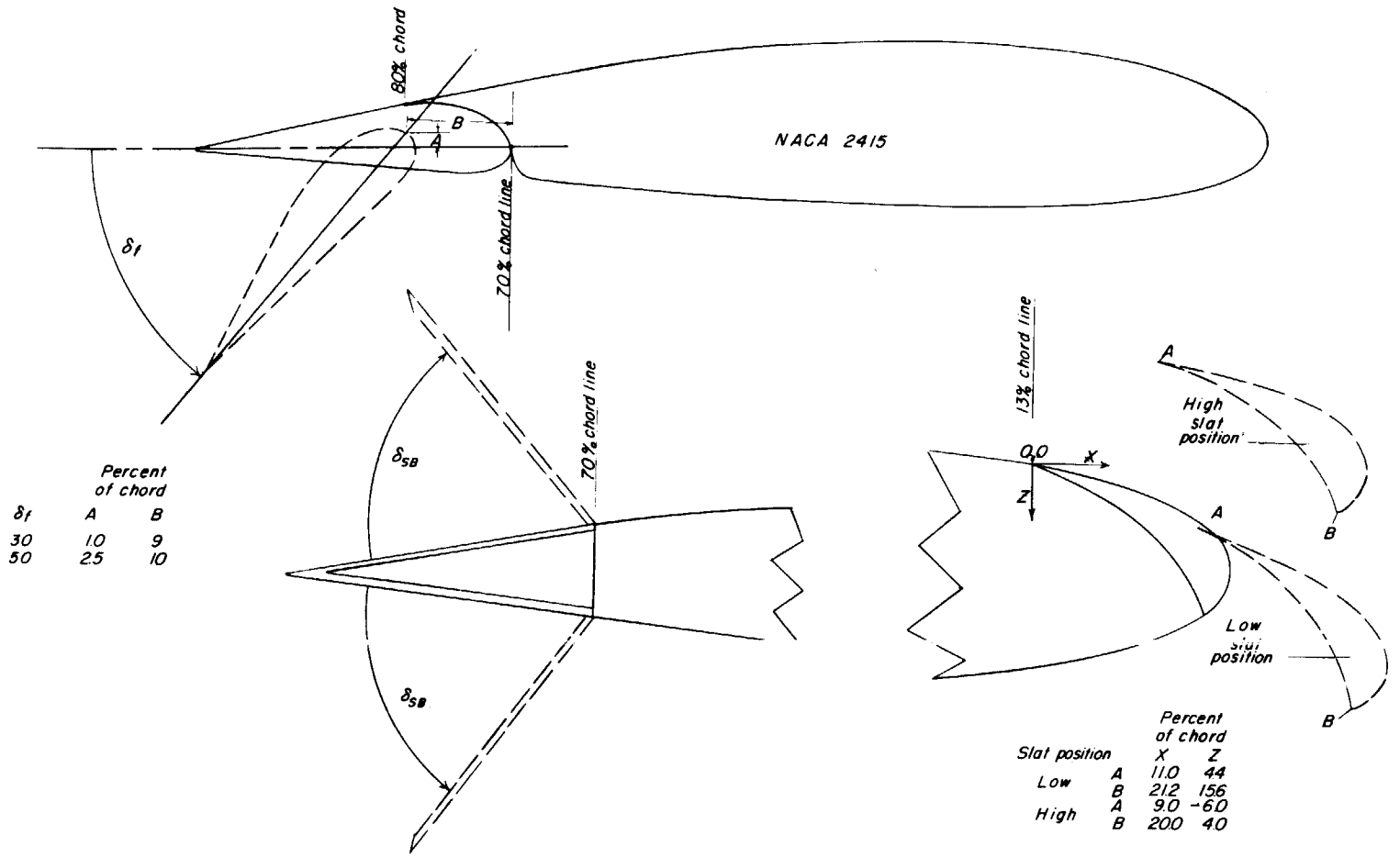

(b) Location of slat, speed brake, and flap.

Figure 3.- Concluded.

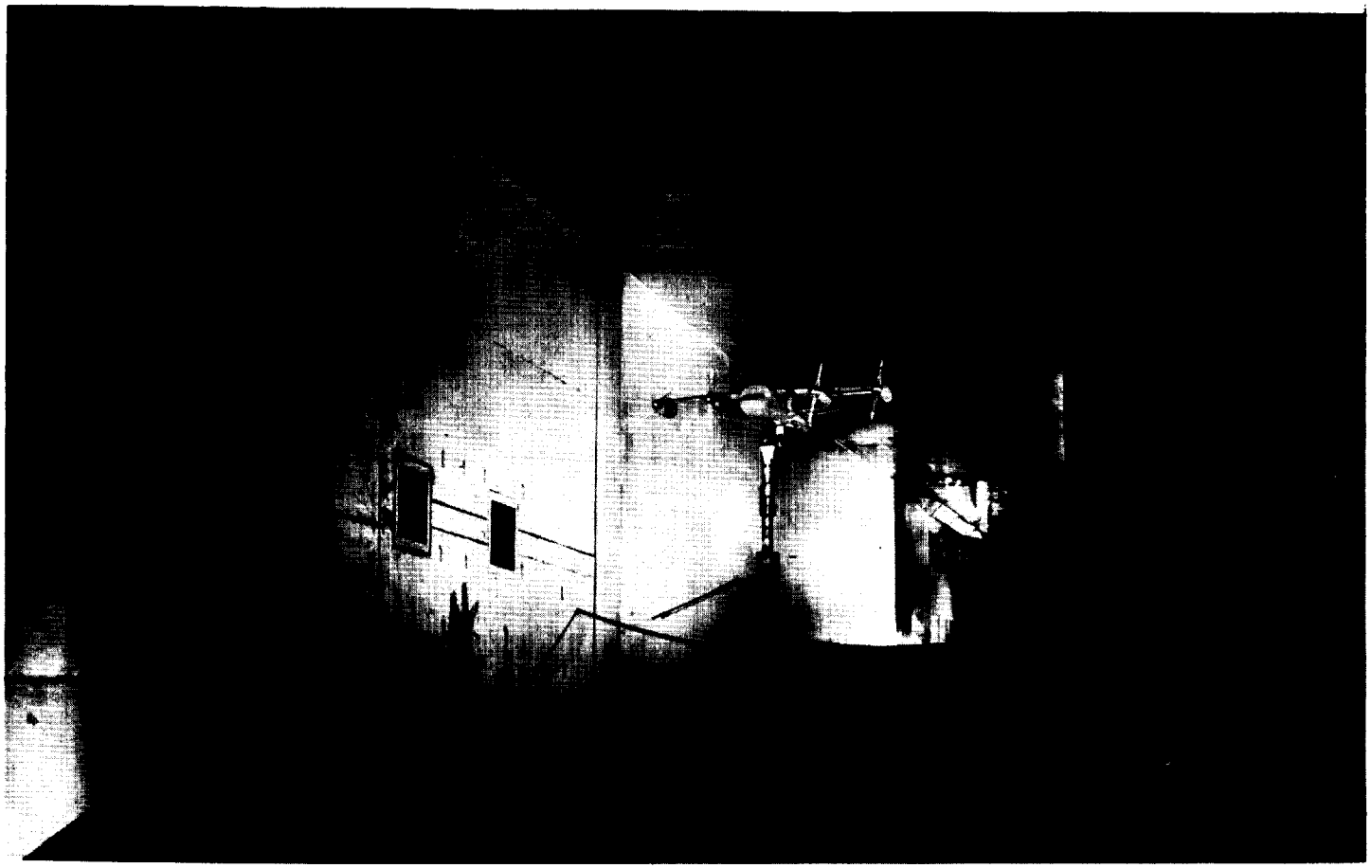

L-59-7553

(a) Model mounted in 17-foot test section of Langley 300-MPH 7- by 10-foot tunnel.

Figure 4.- Photographs of model.

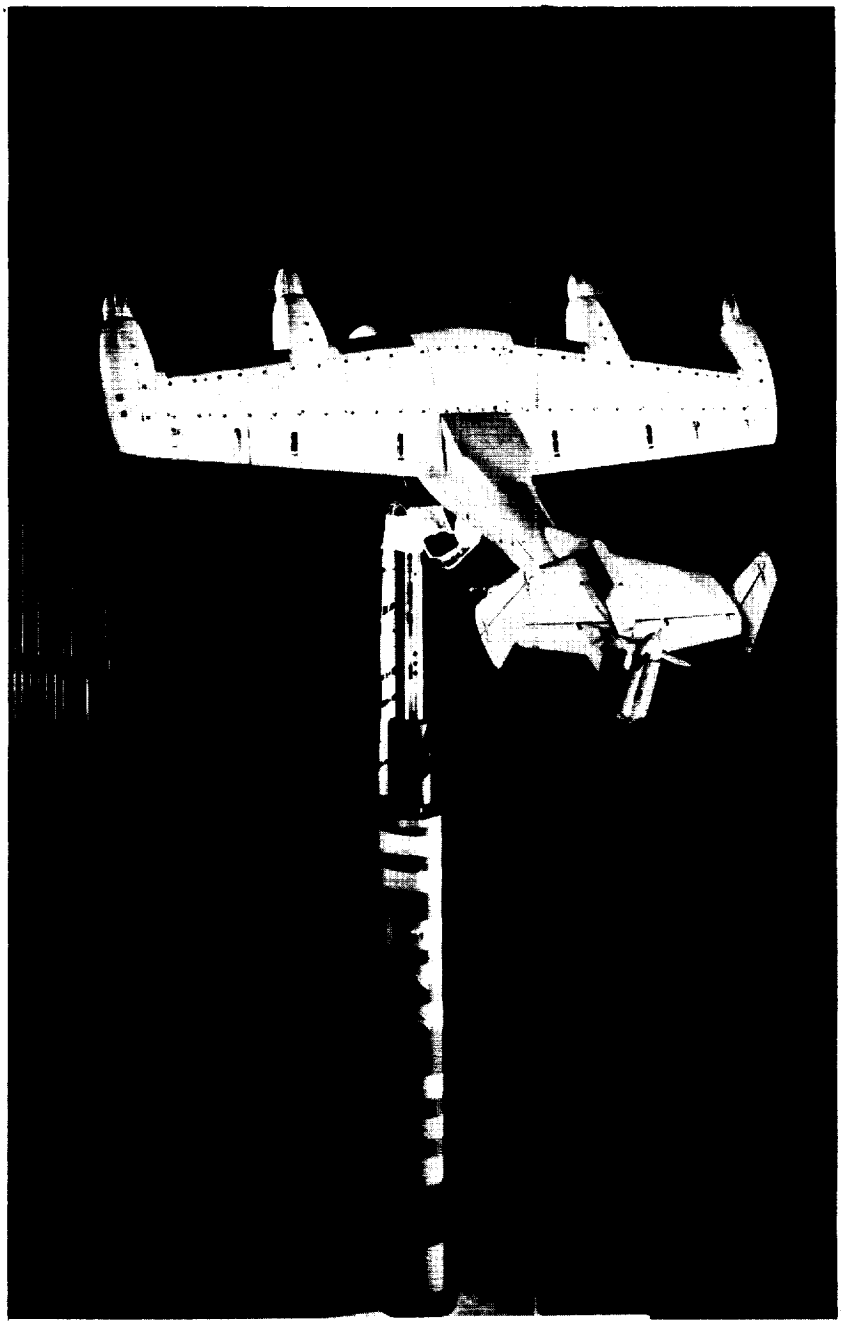

L-59-7556

(b) Model at positive angle of attack and positive wing tilt angle.

Figure 4.- Concluded.

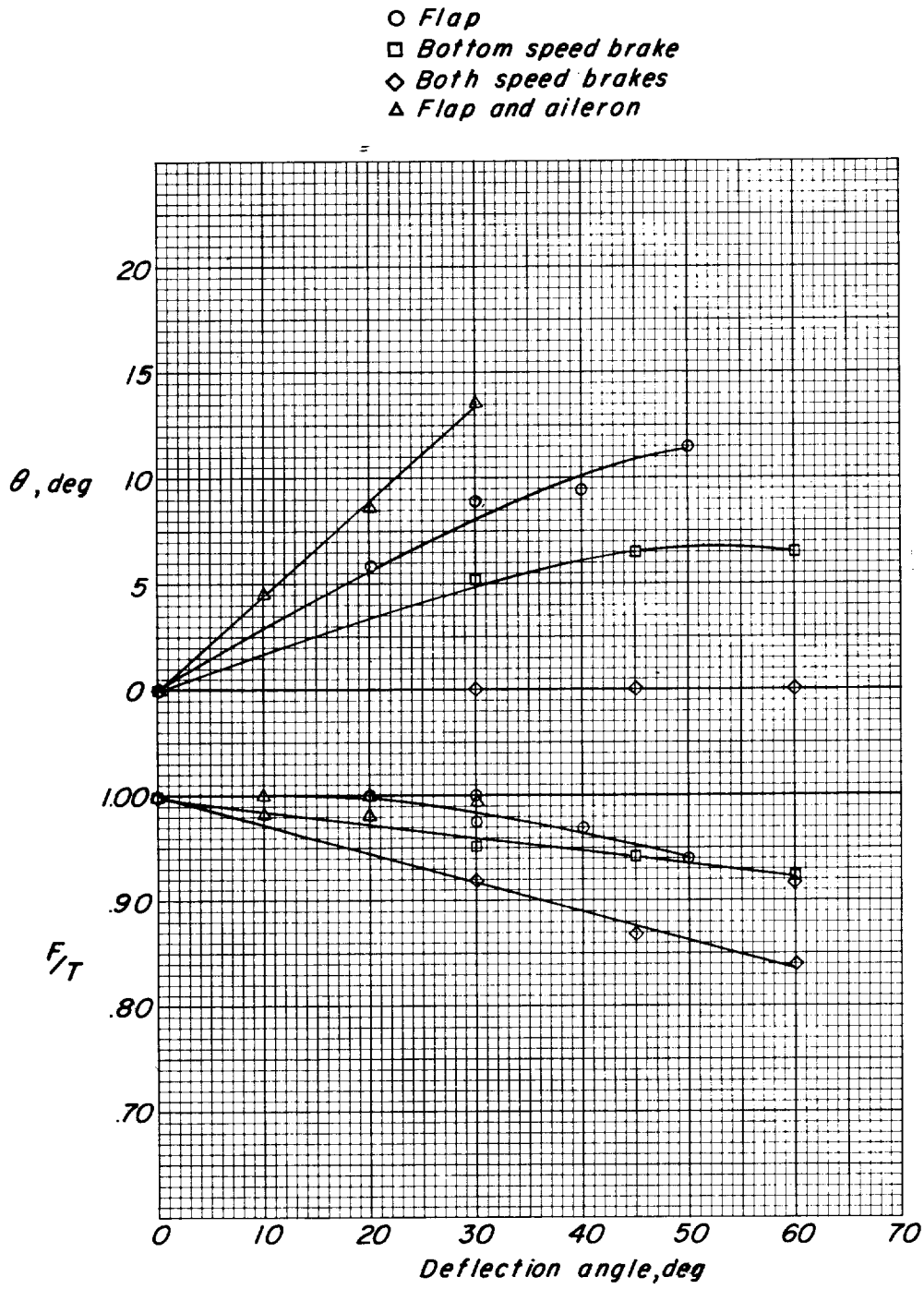

(a) Turning angle and thrust recovery factor.

Figure 5.- Static slipstream deflection characteristics.

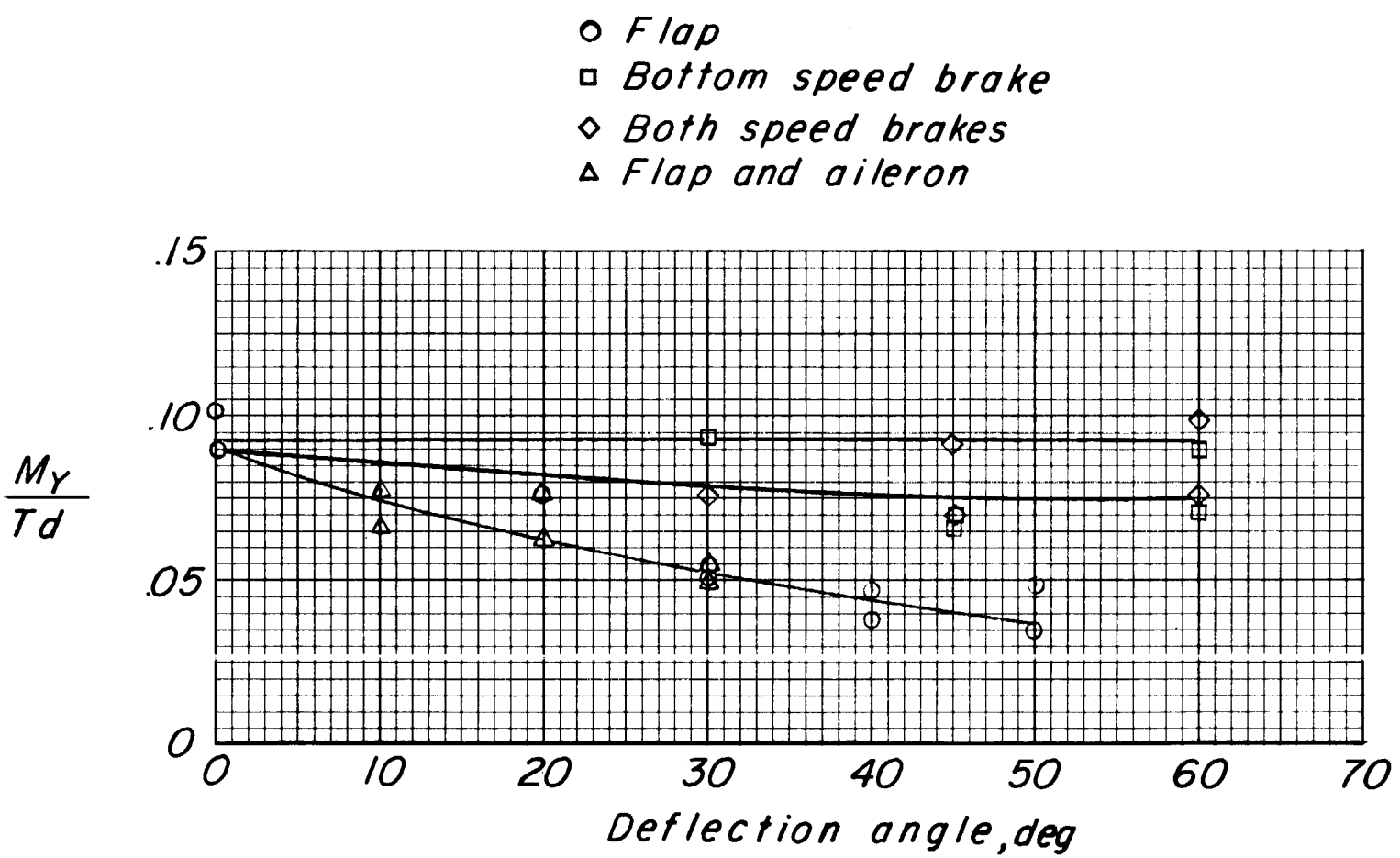

(b) Static pitching-moment characteristics.

Figure 5.- Concluded.

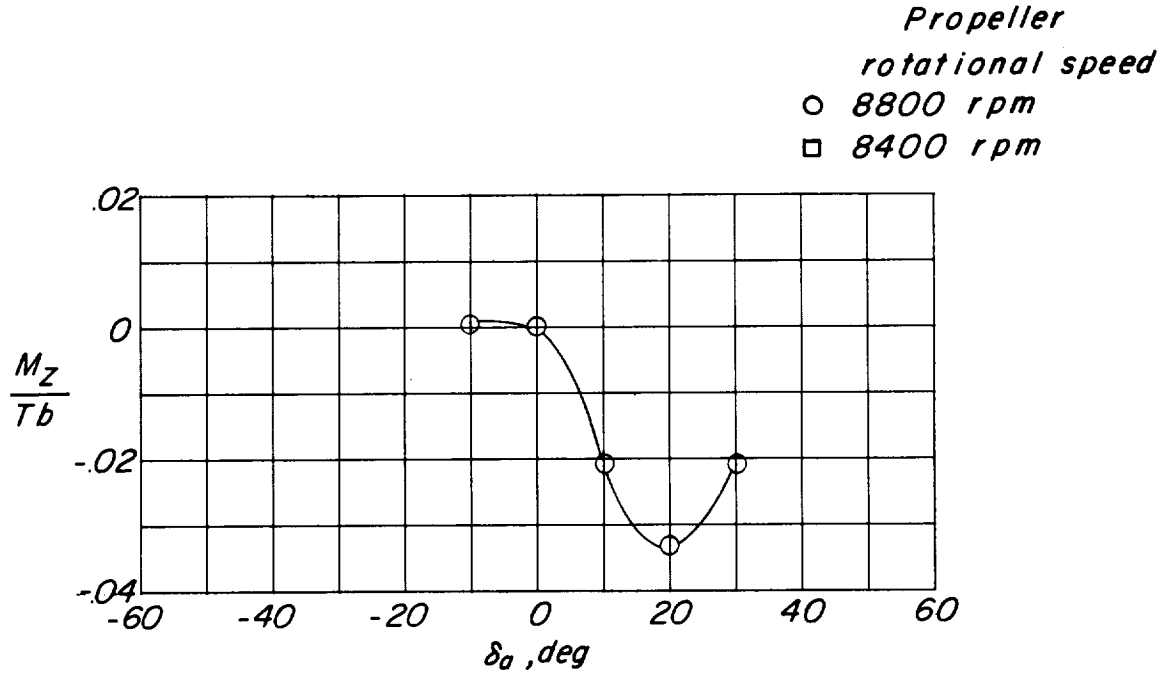

(a) Left inboard and outboard ailerons deflected (right aileron neutral); wing extensions on.

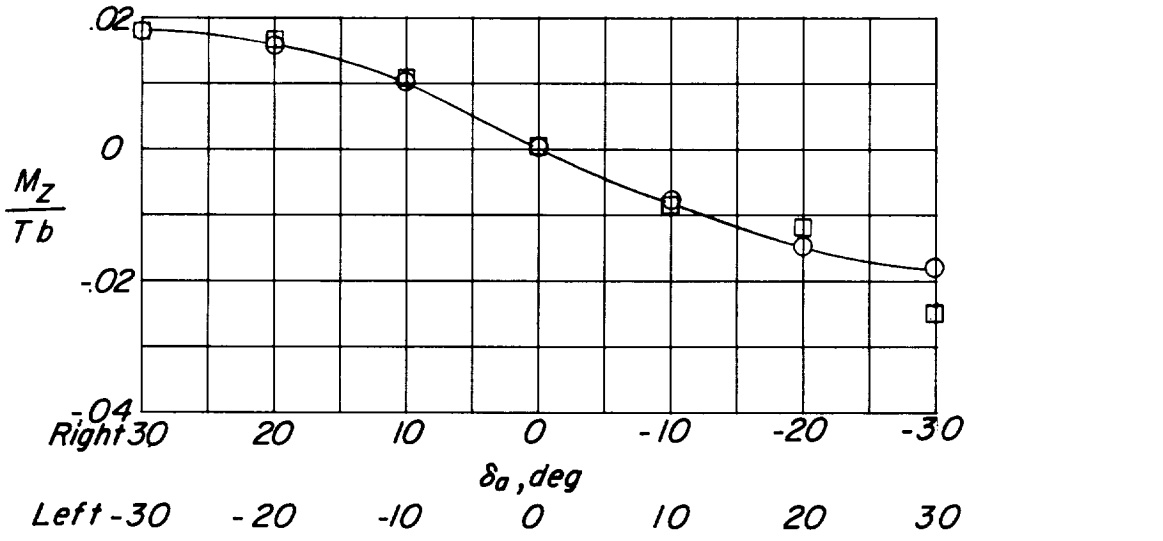

(b) Left and right inboard ailerons deflected; wing extension off.

Figure 6.- Static aileron effectiveness. $i_w = 90^\circ$.

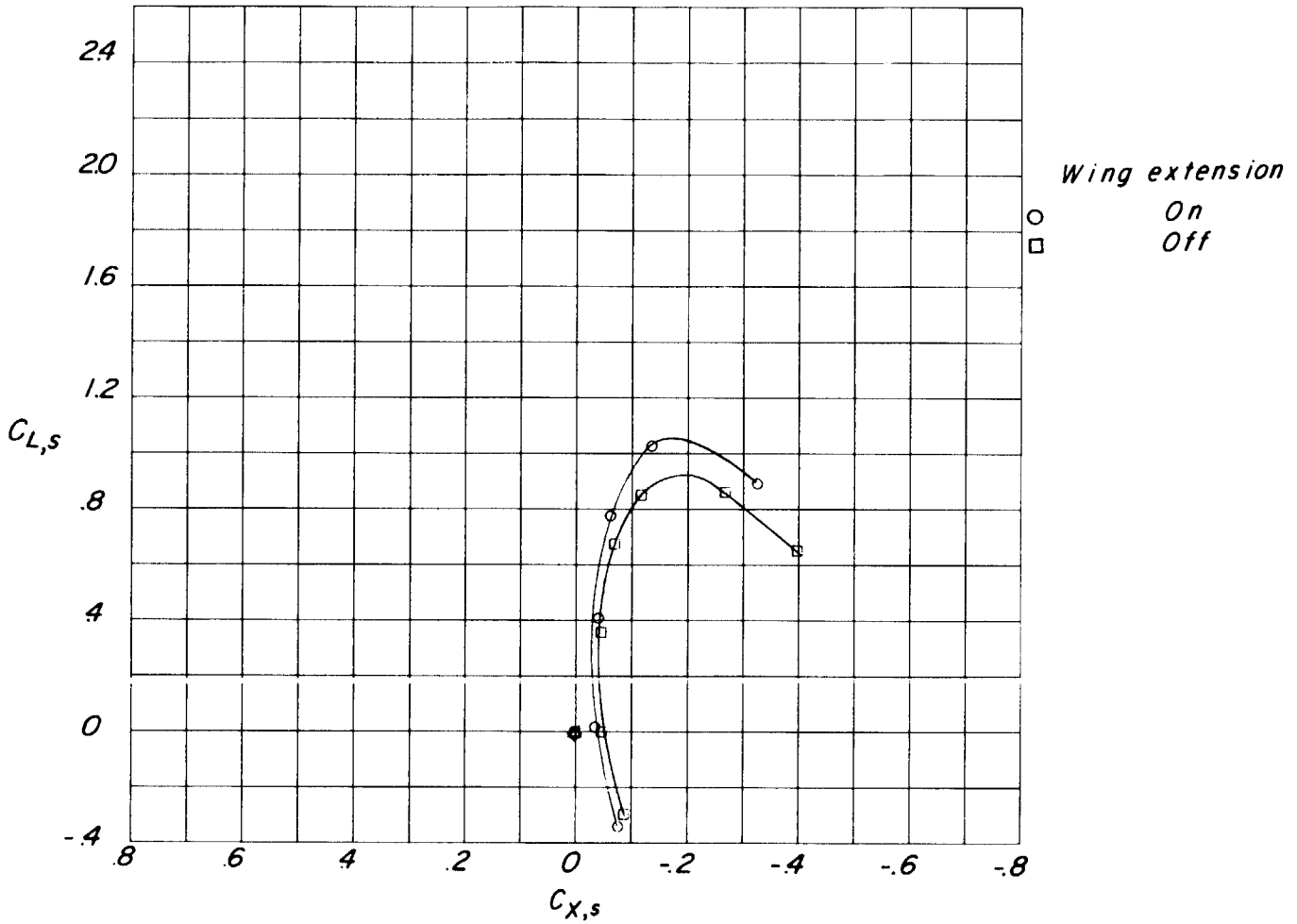

(a) Lift—longitudinal-force polars (coefficients based on area of short-span wing).

Figure 7.- Effect of wing extensions on power-off aerodynamic characteristics of basic configuration. Tail off; $i_w = 0^\circ$; slat retracted.

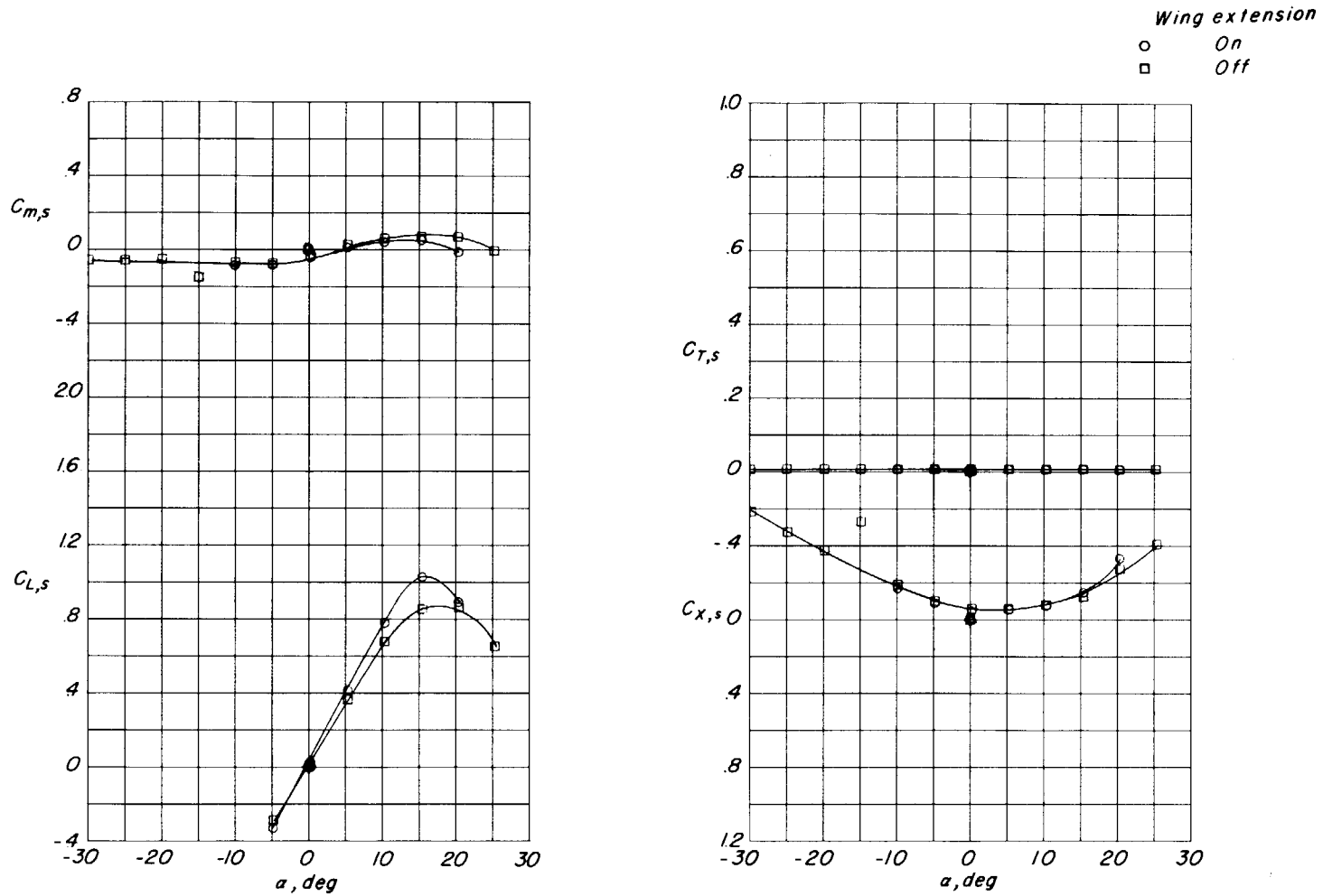

(b) Longitudinal aerodynamic characteristics through an angle-of-attack range (coefficients based on area of short-span wing).

Figure 7.- Continued.

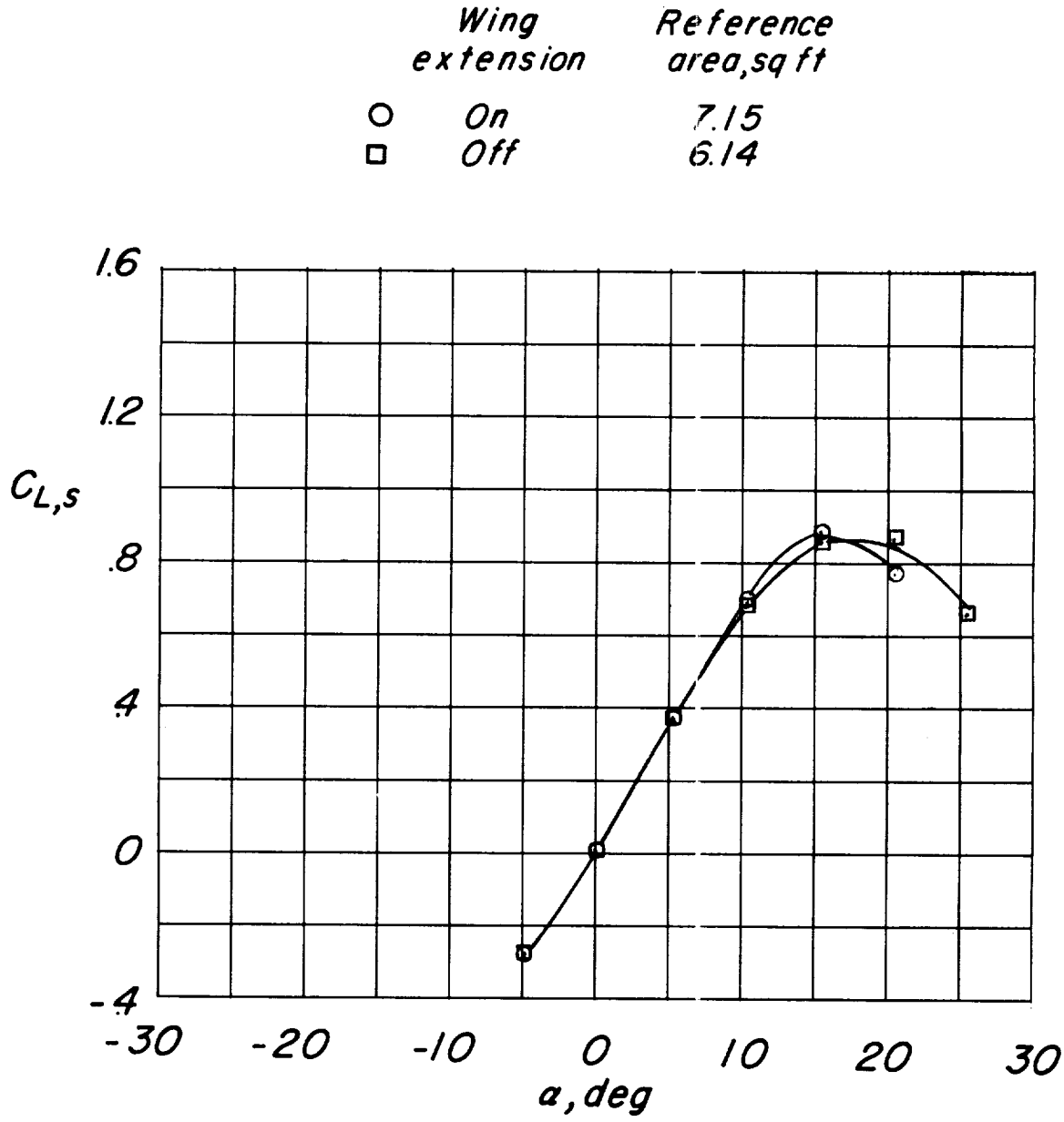

(c) Comparisons of lift curves for basic configuration with wing extension on and off (coefficients based on appropriate wing area).

Figure 7.- Concluded.

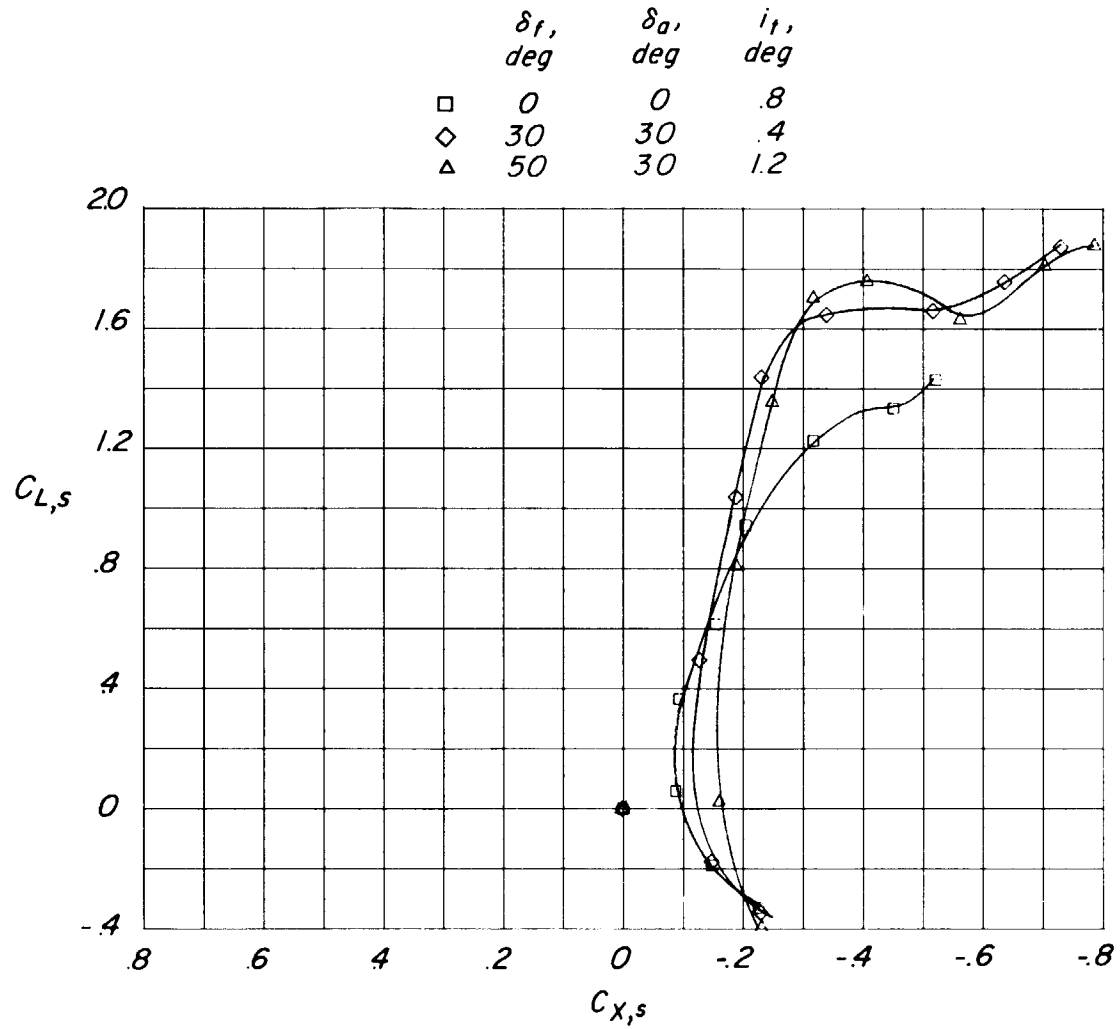

Figure 8.- Effect of flap deflection on power-off characteristics of flapped configuration. Tail incidence as required for trim; $i_w = 0^\circ$.

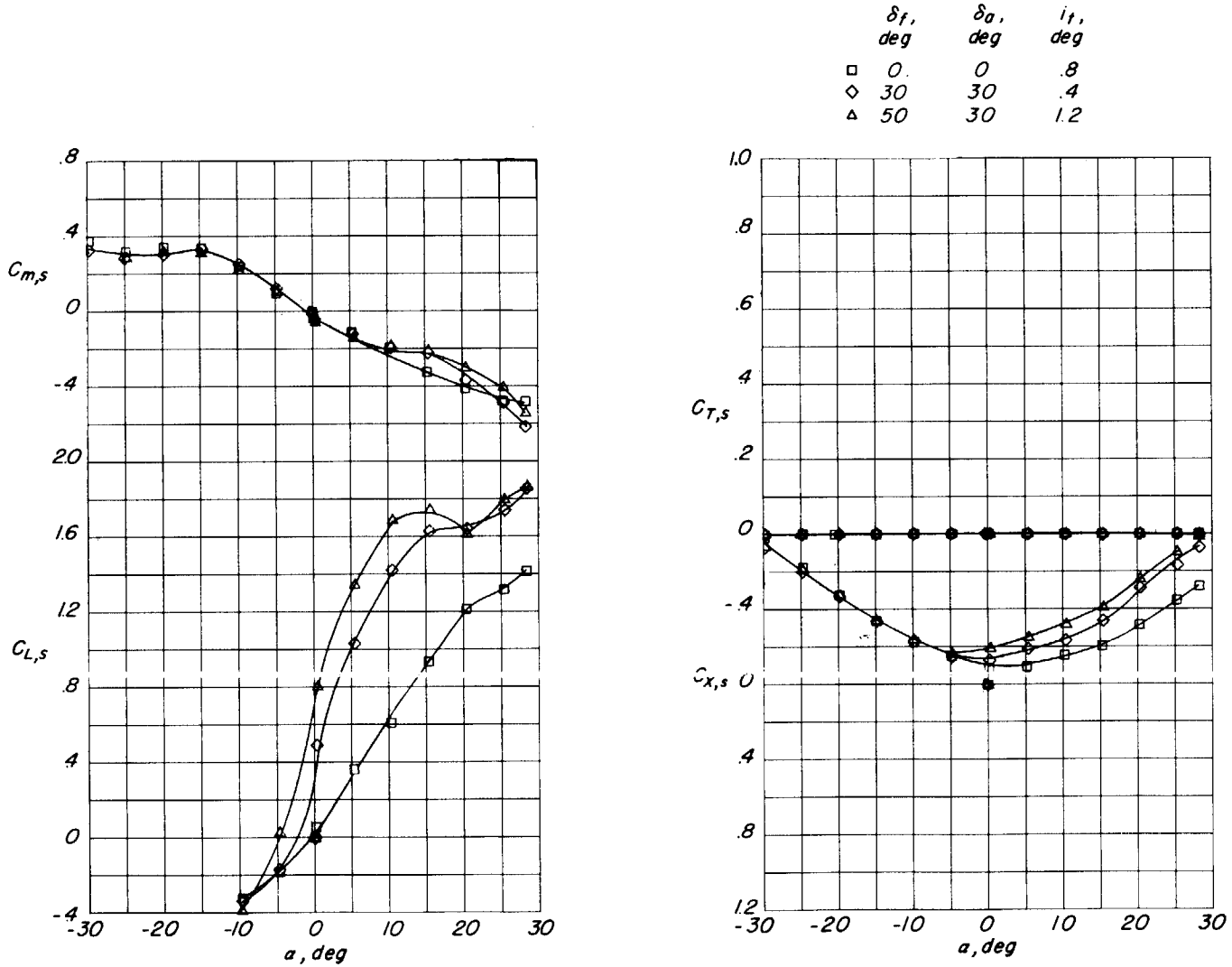

Figure 8.- Concluded.

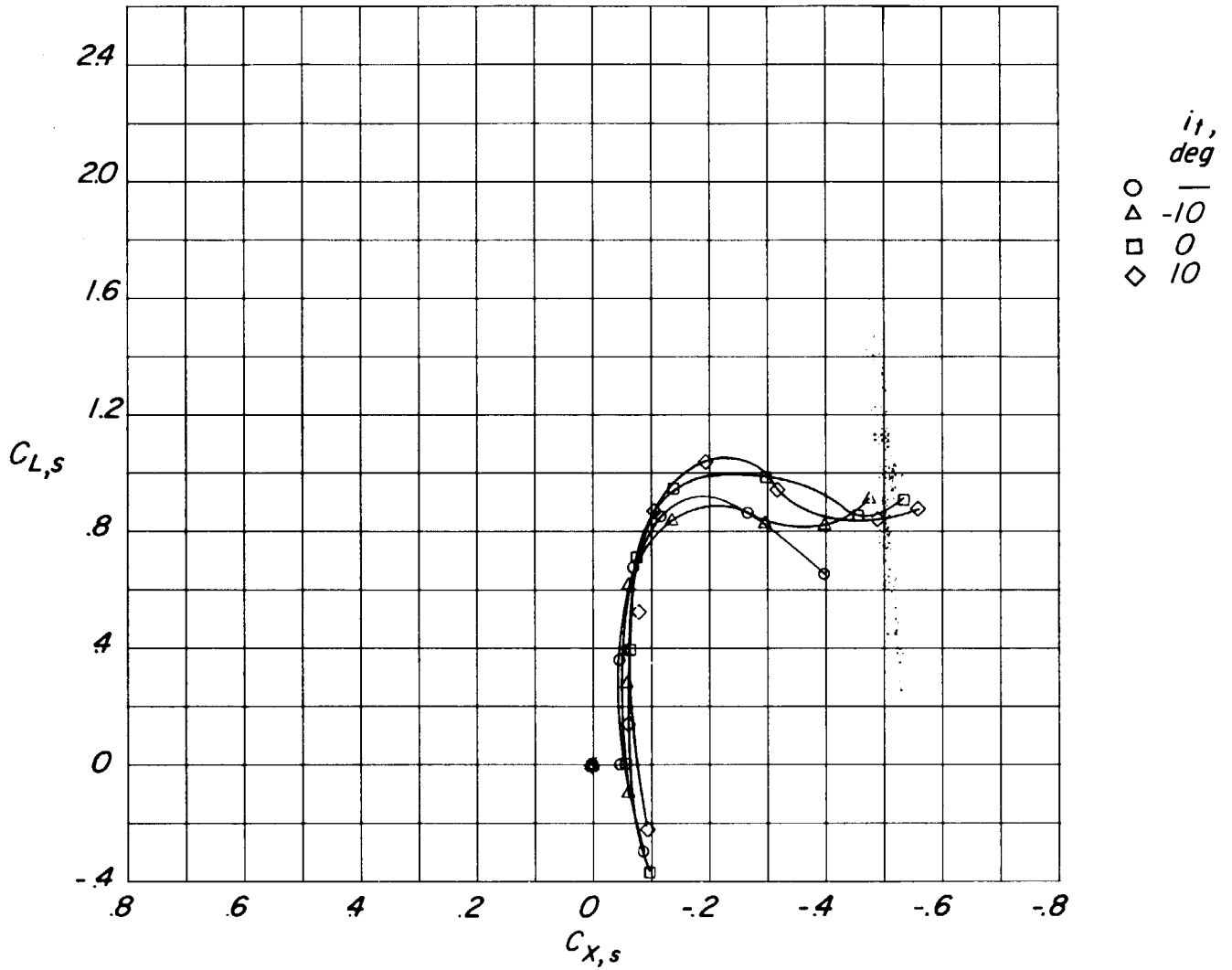

Figure 9.- Stabilizer effectiveness of basic configuration with power off. $i_w = 0^\circ$.

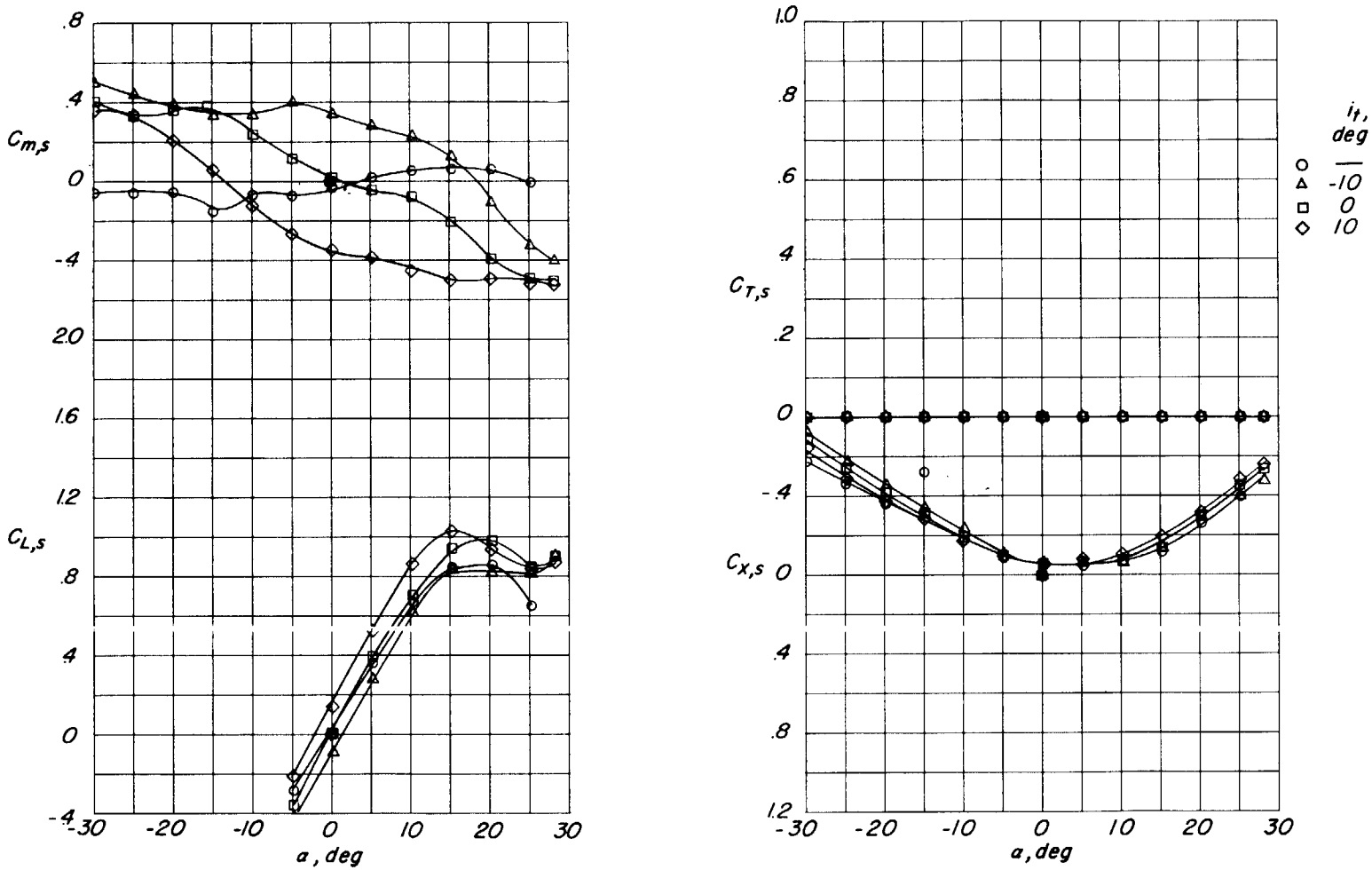

Figure 9.- Concluded.

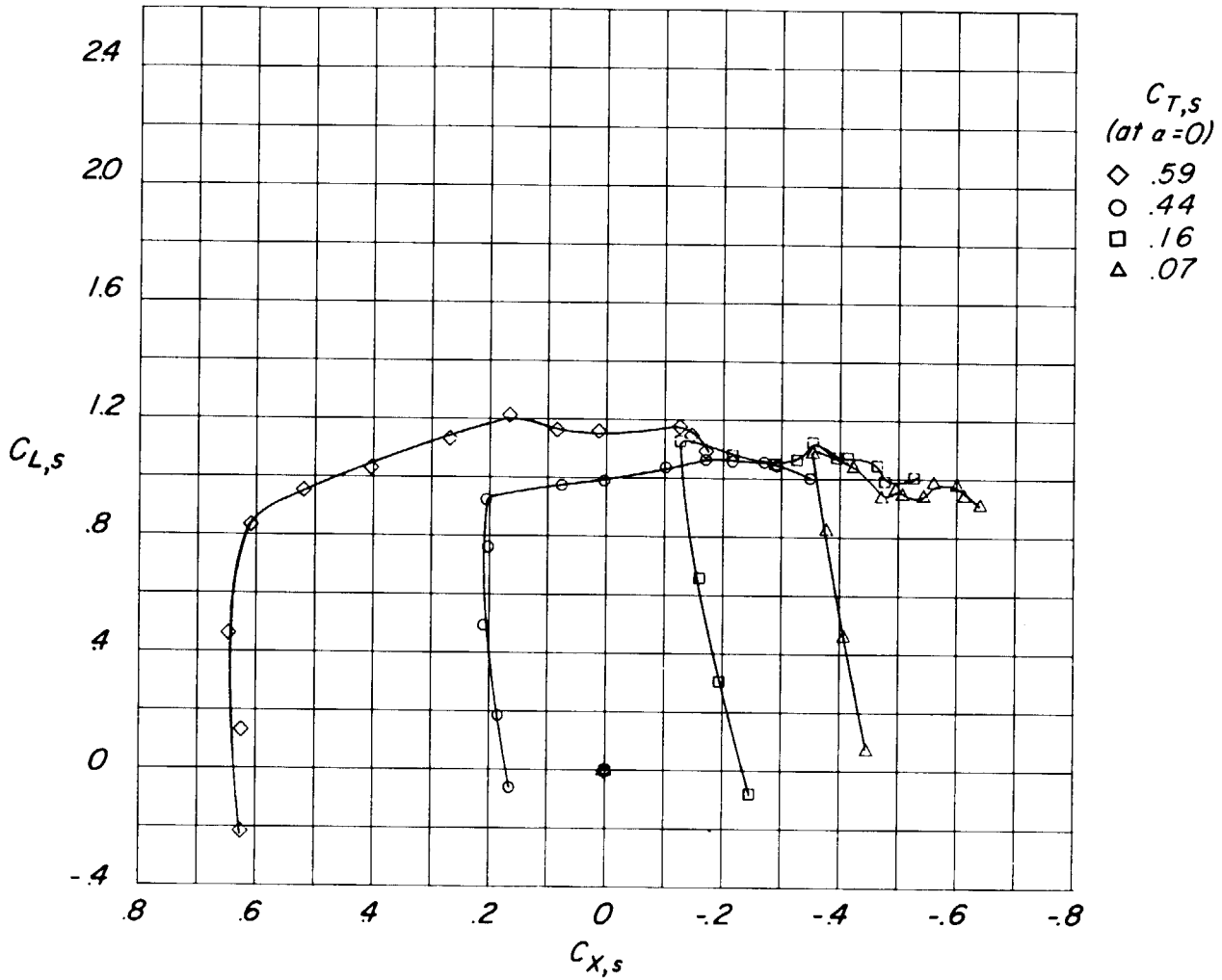

(a) Basic configuration; $i_w = 30^\circ$; $i_t = 9.2^\circ$.

Figure 10.- Effect of thrust coefficient and wing tilt angle for basic configuration.

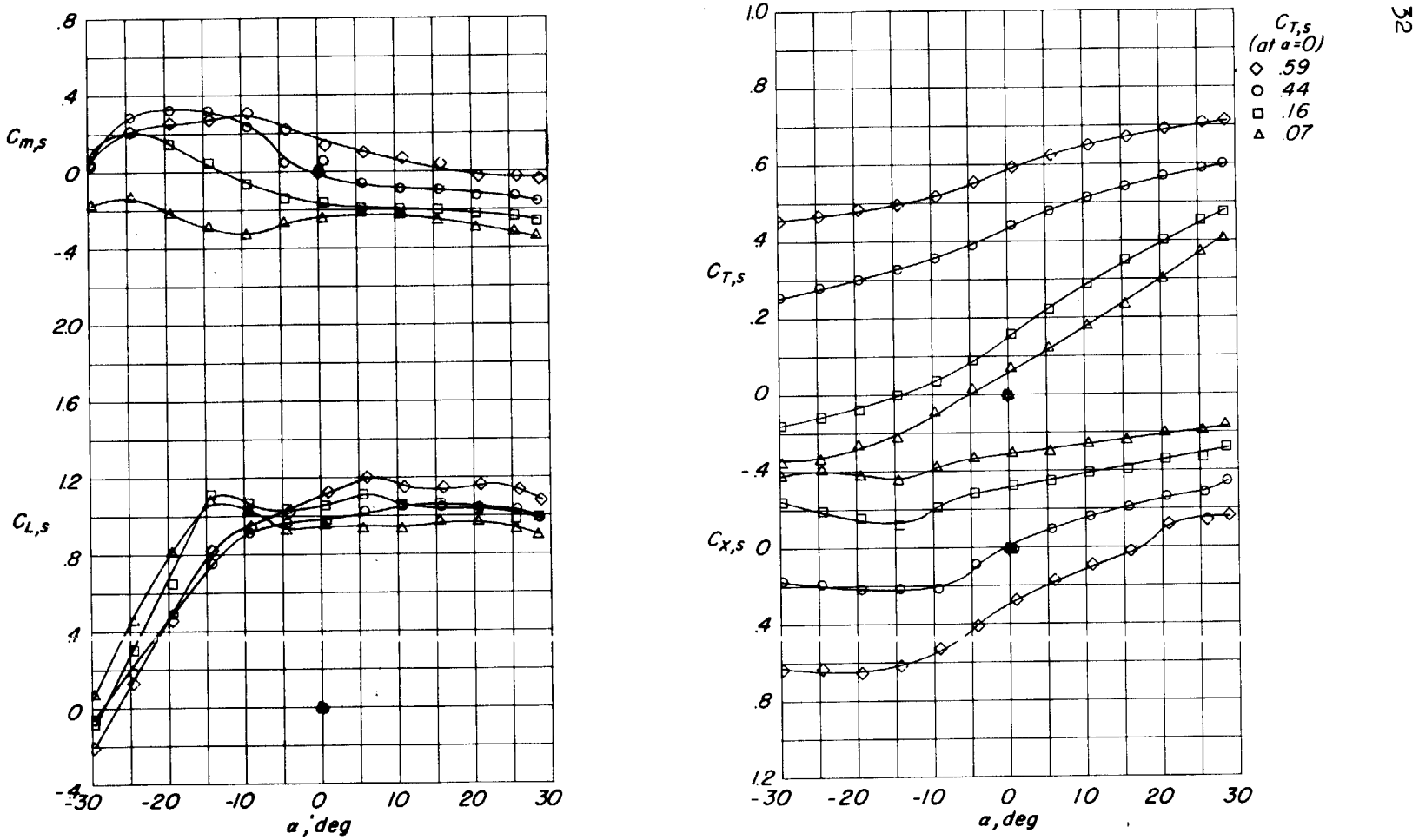

(a) Concluded.

Figure 10.- Continued.

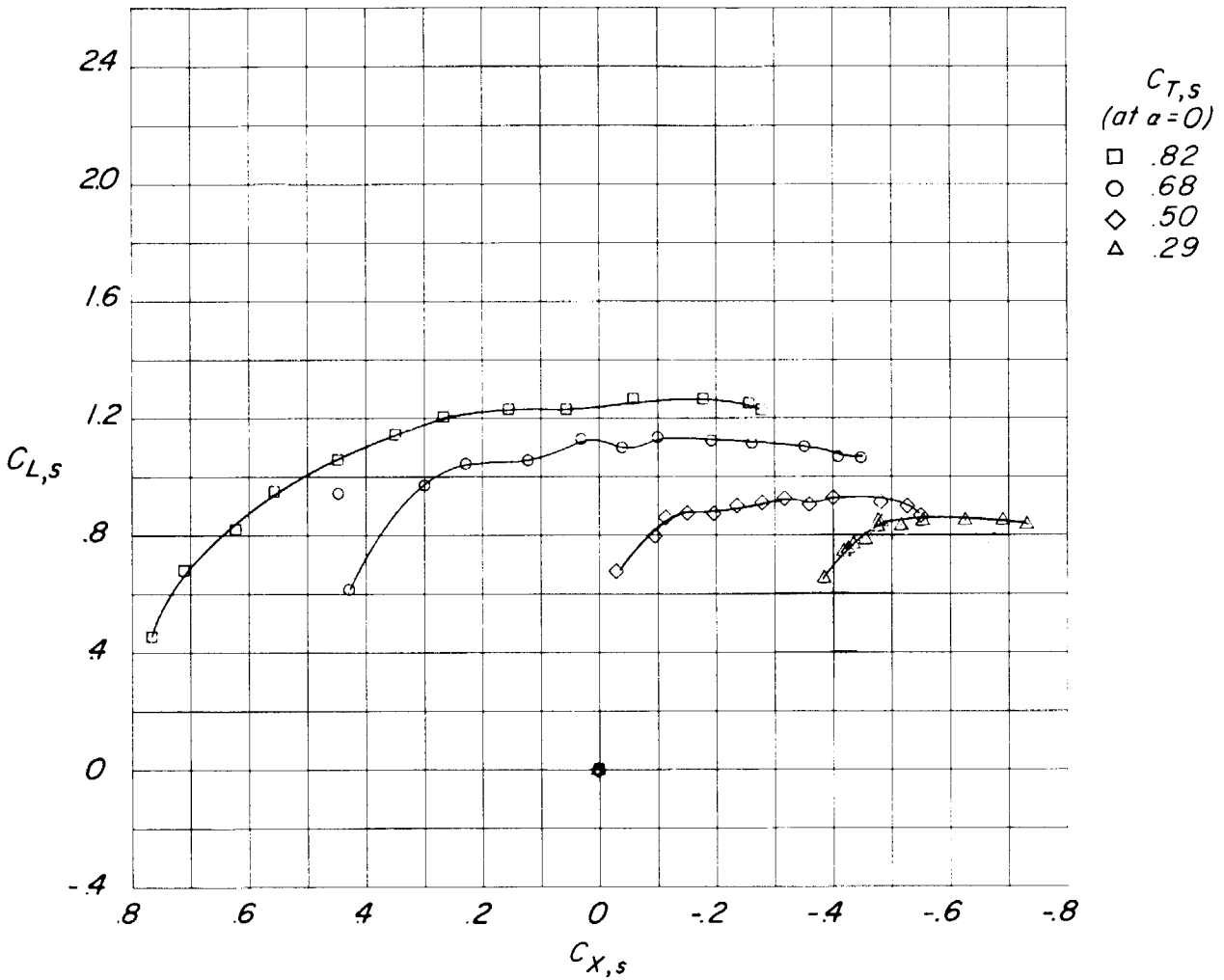

(b) Basic configuration; $i_w = 45^\circ$; $i_t = 19.2^\circ$.

Figure 10.- Continued.

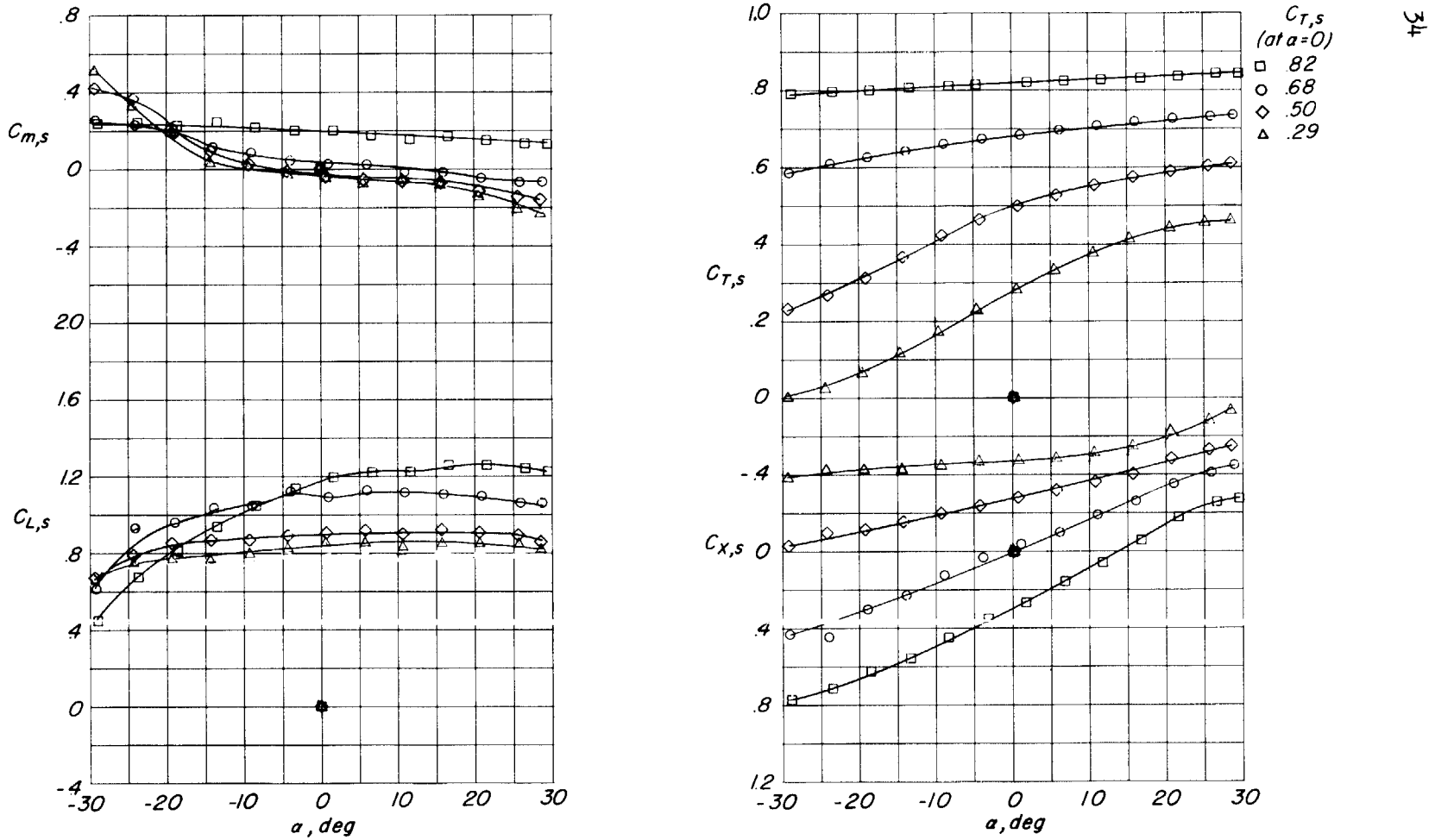

(b) Concluded.

Figure 10.- Continued.

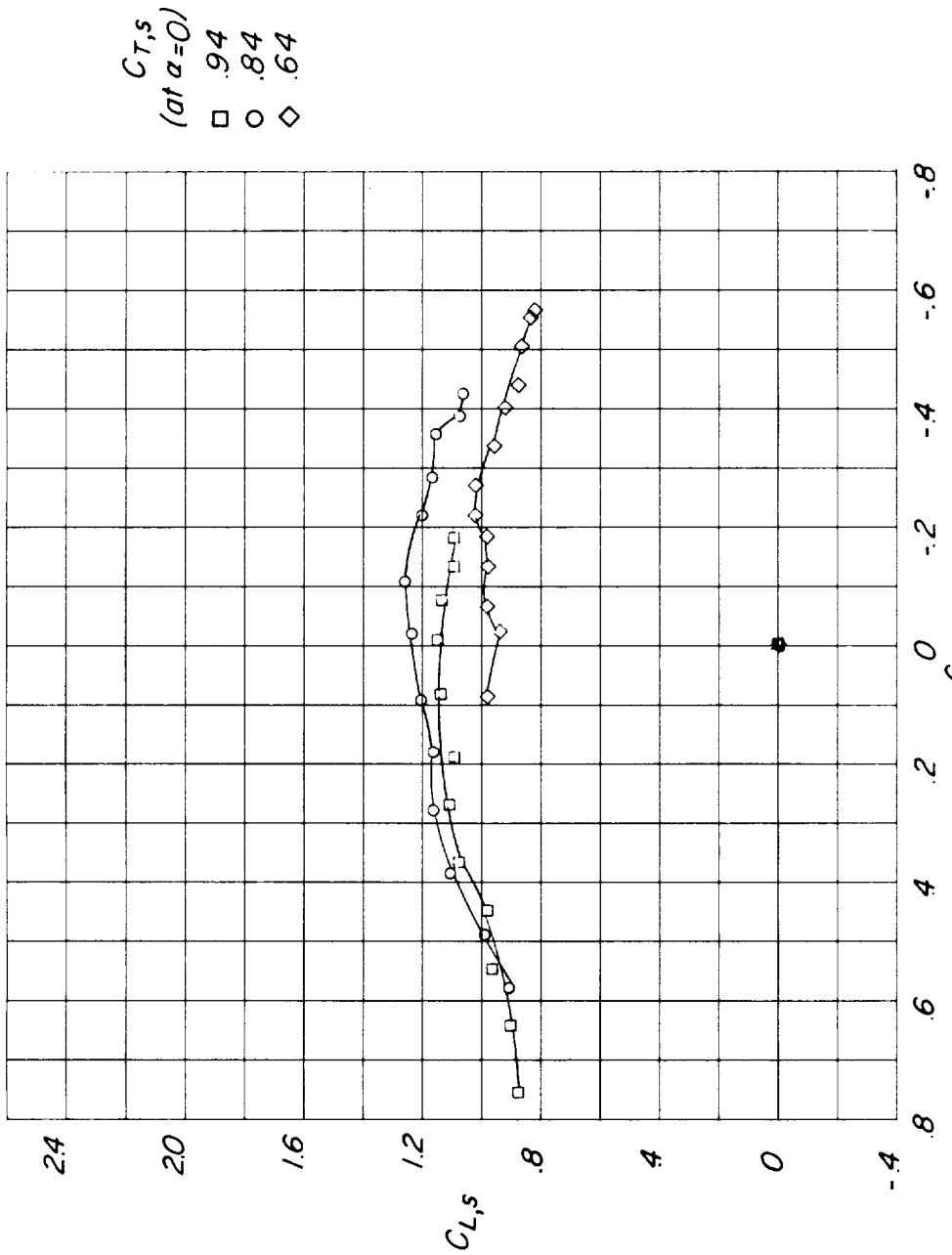

(c) Basic configuration; $i_w = 60^\circ$; $i_t = 30^\circ$.

Figure 10.- Continued.

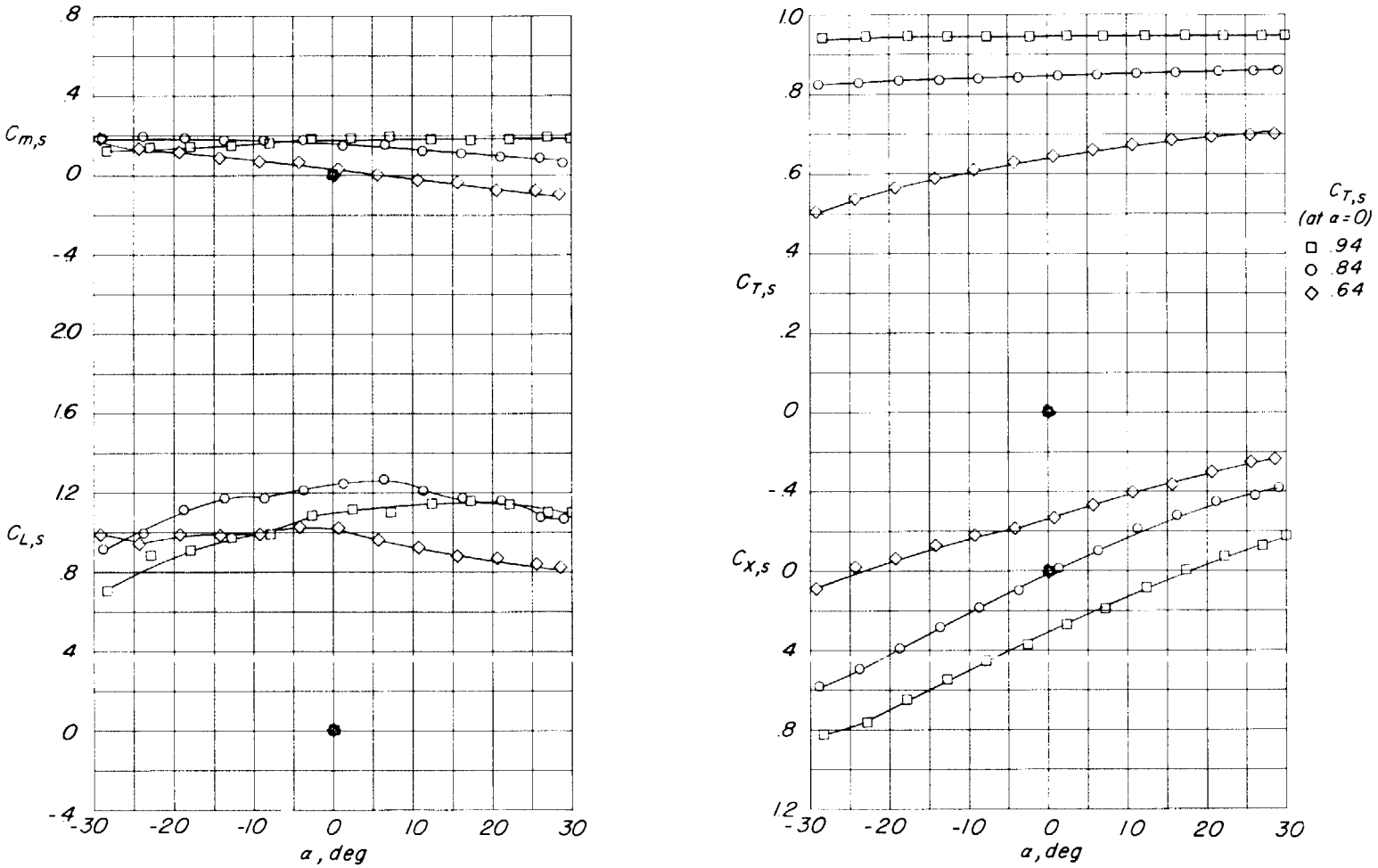

(c) Concluded.

Figure 10.- Continued.

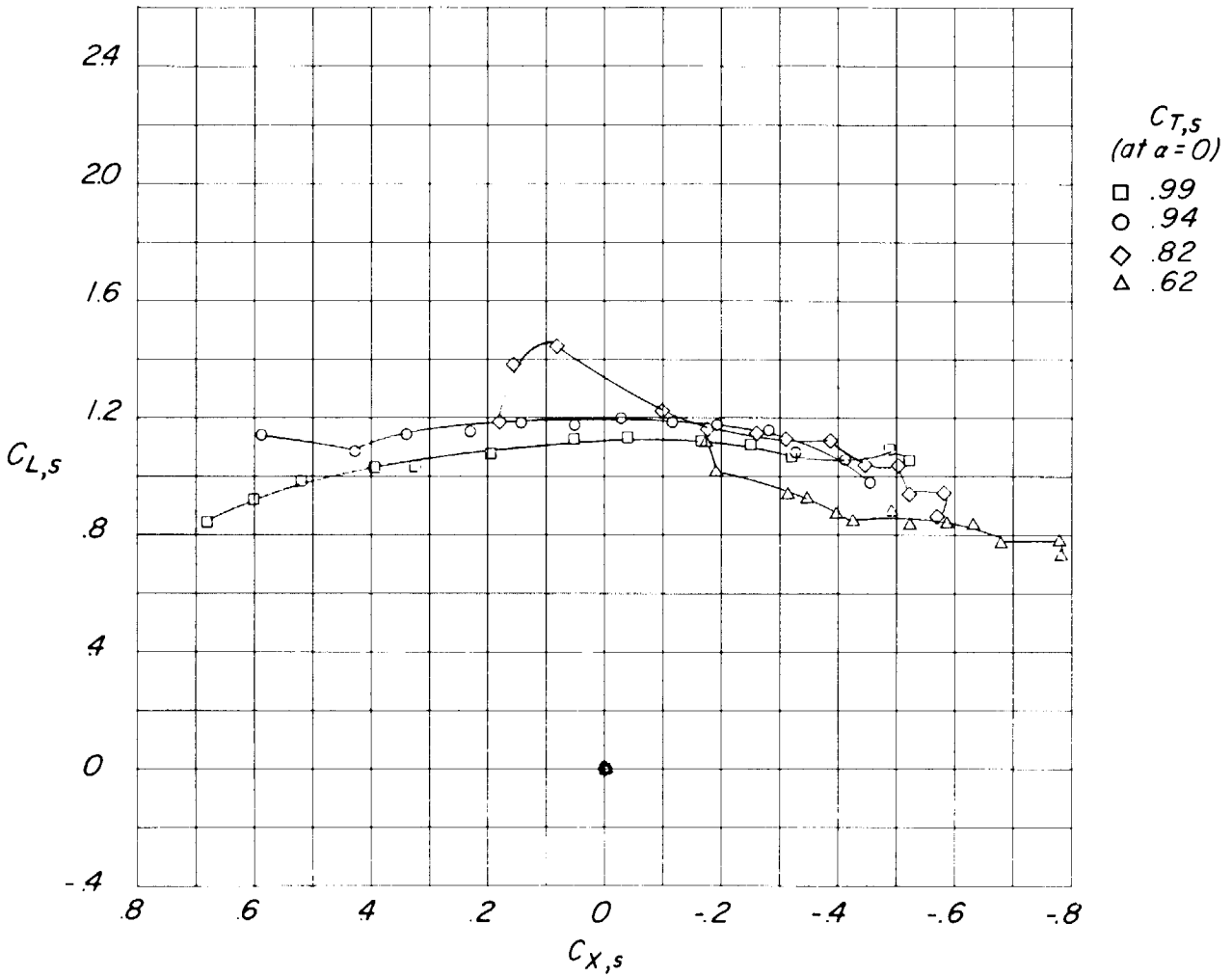

(d) Basic configuration; $i_w = 75^\circ$; $i_t = 30^\circ$.

Figure 10.- Continued.

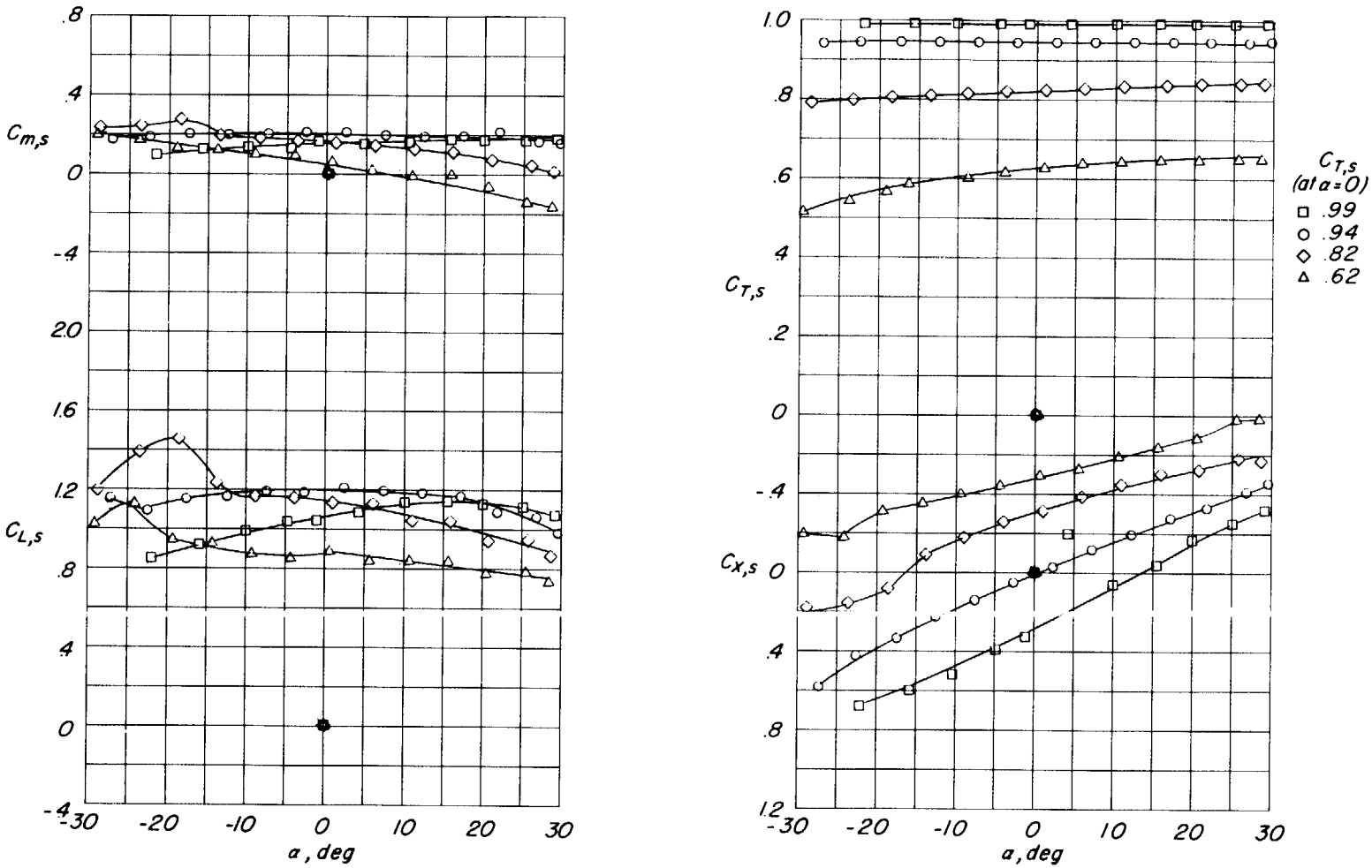

(d) Concluded.

Figure 10.- Concluded.

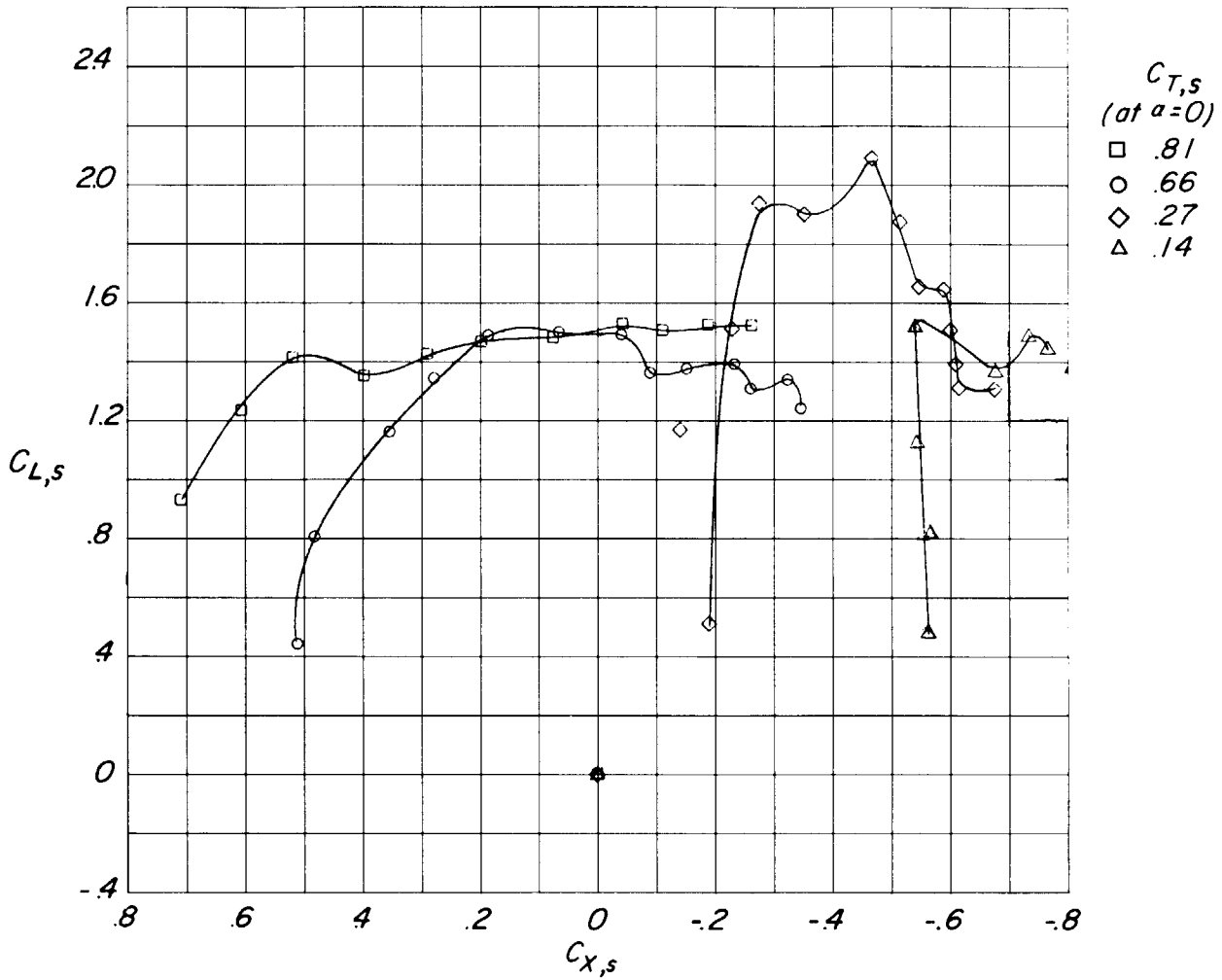

(a) Flapped configuration; $i_w = 30^\circ$; $i_t = 9.2^\circ$.

Figure 11.- Effect of thrust coefficient and wing tilt angle for flapped configuration.

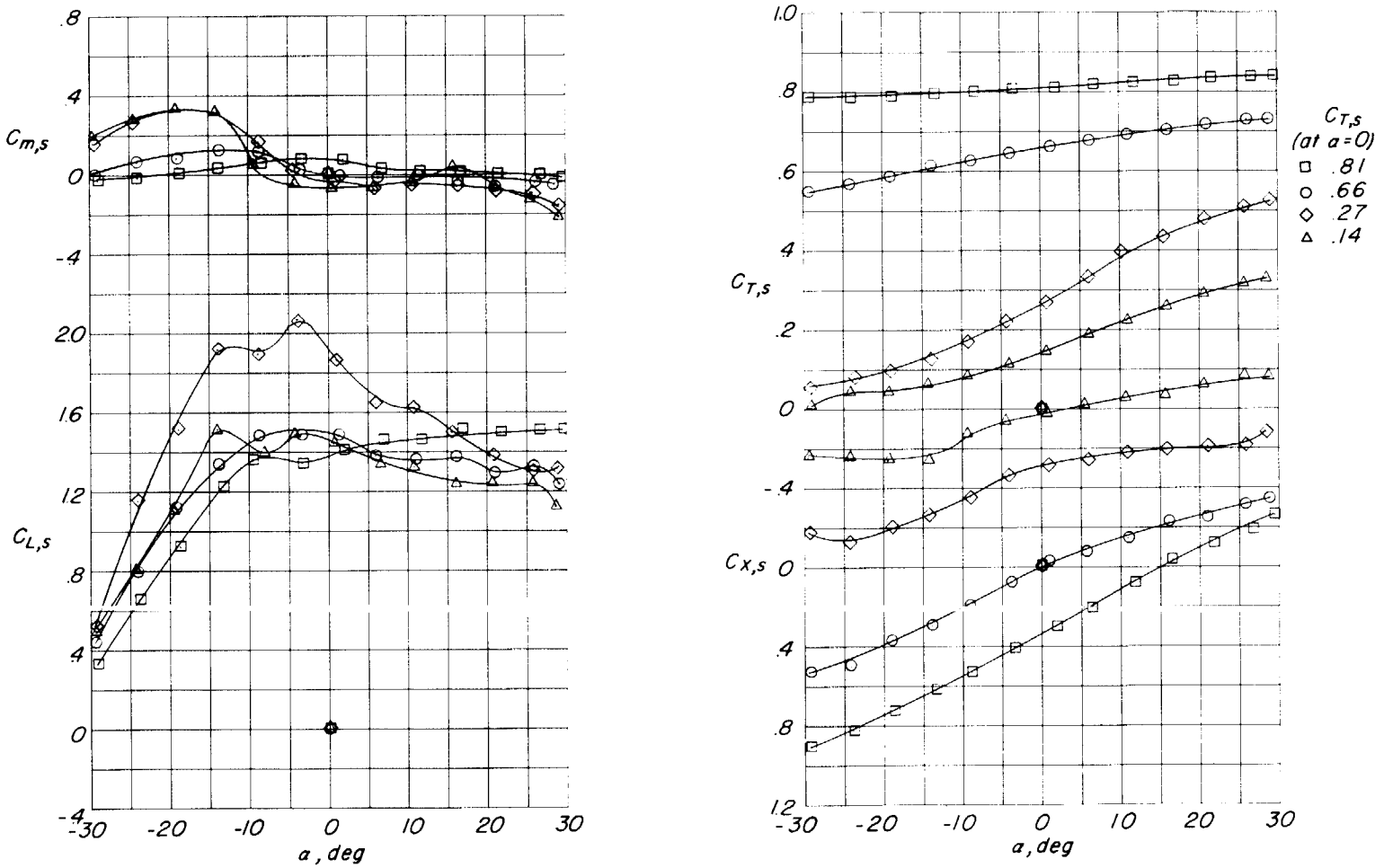

(a) Concluded.

Figure 11.- Continued.

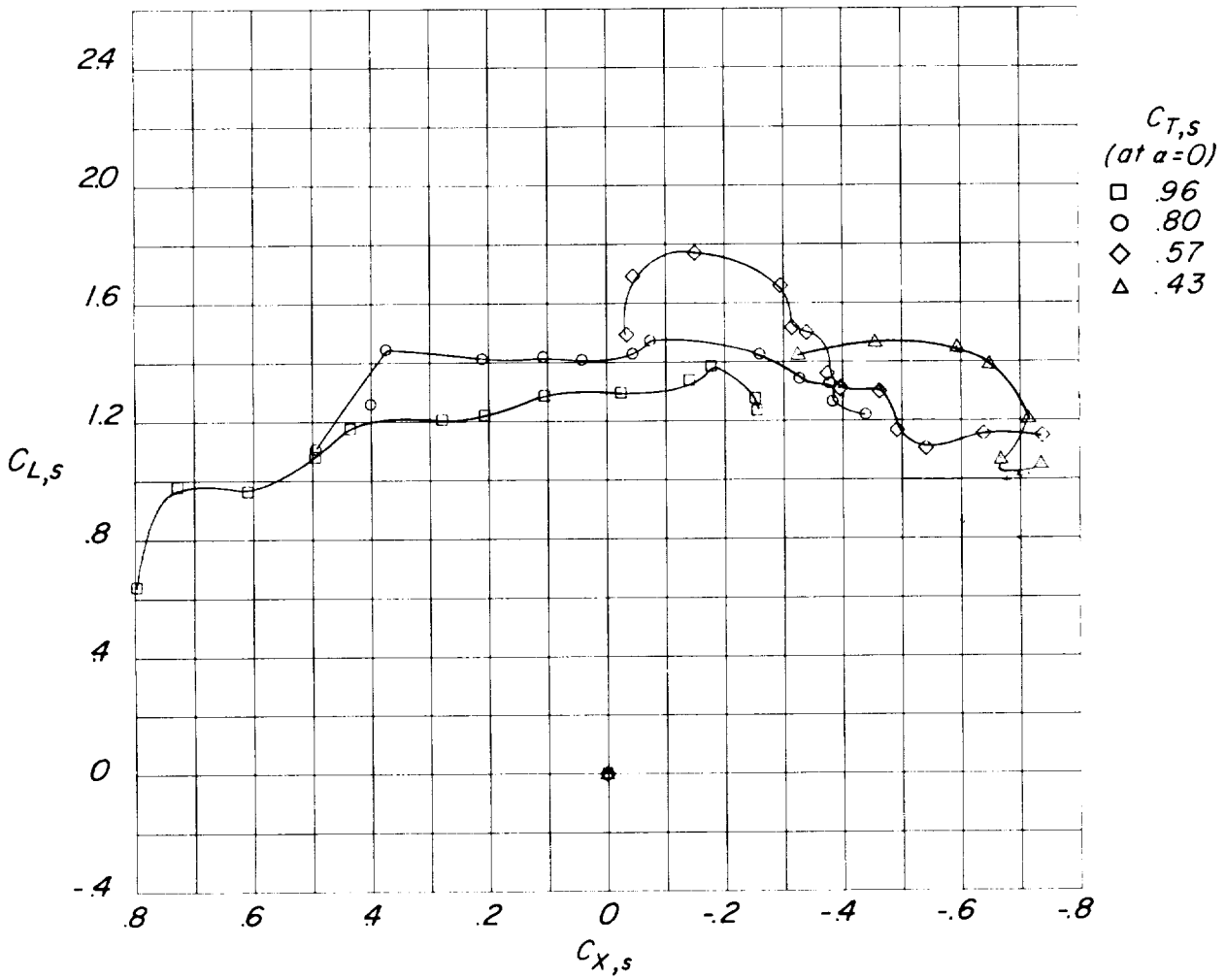

(b) Flapped configuration; $i_w = 45^\circ$; $i_t = 30^\circ$.

Figure 11.- Continued.

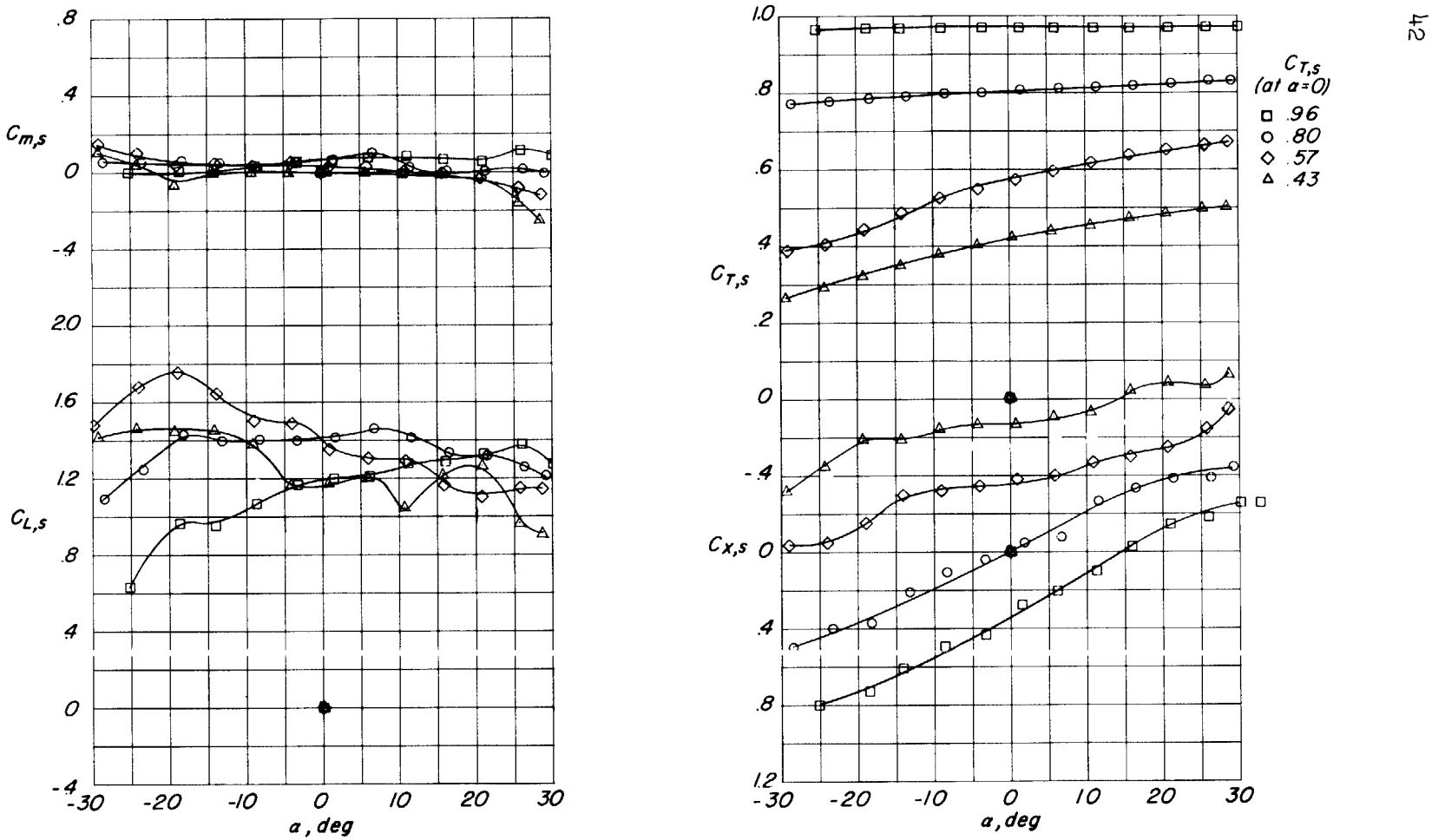

(b) Concluded.

Figure 11.- Concluded.

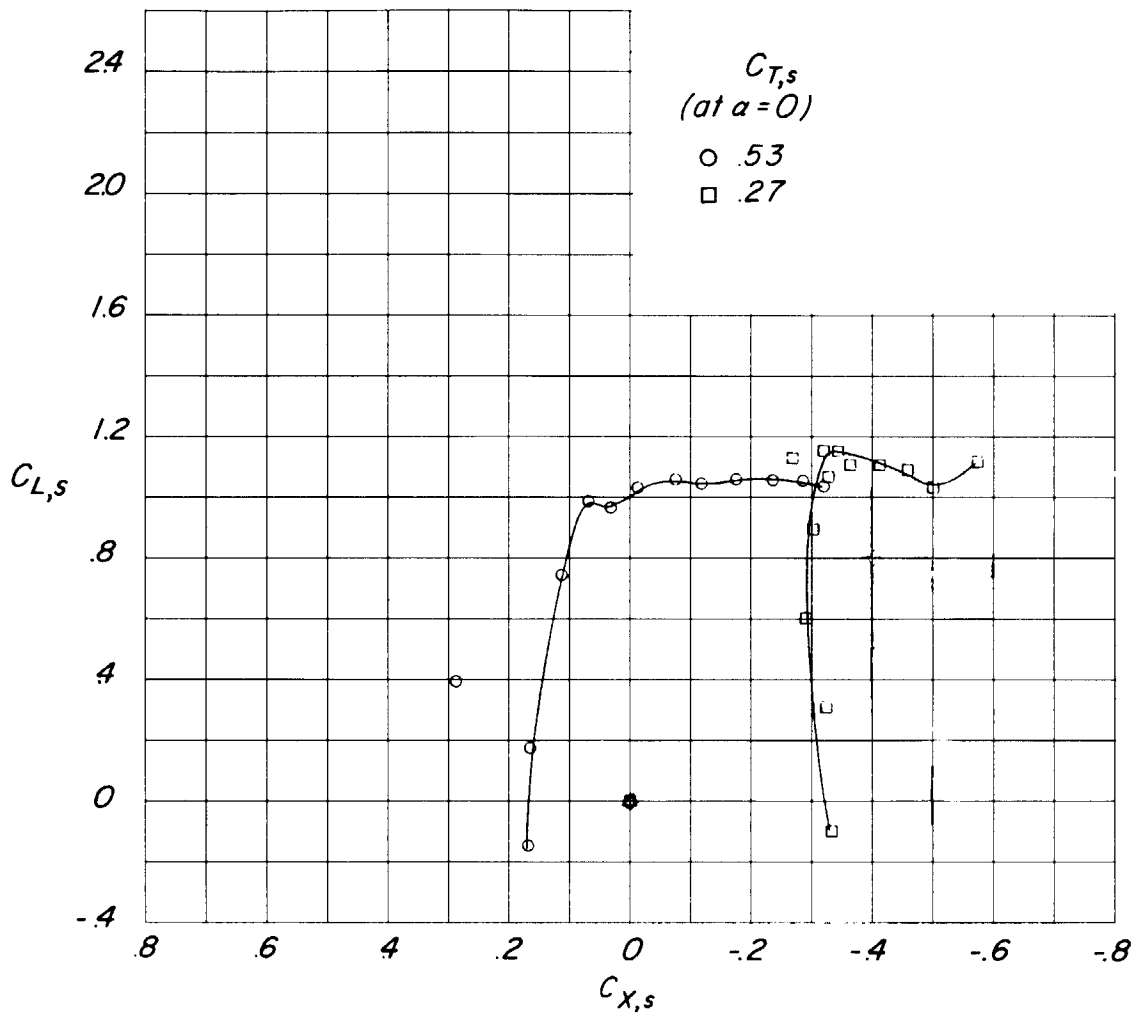

(a) Speed-brake configuration; $i_w = 30^\circ$; $i_t = 39.2^\circ$.

Figure 12.- Effect of thrust coefficient and wing tilt angle for speed-brake configuration.

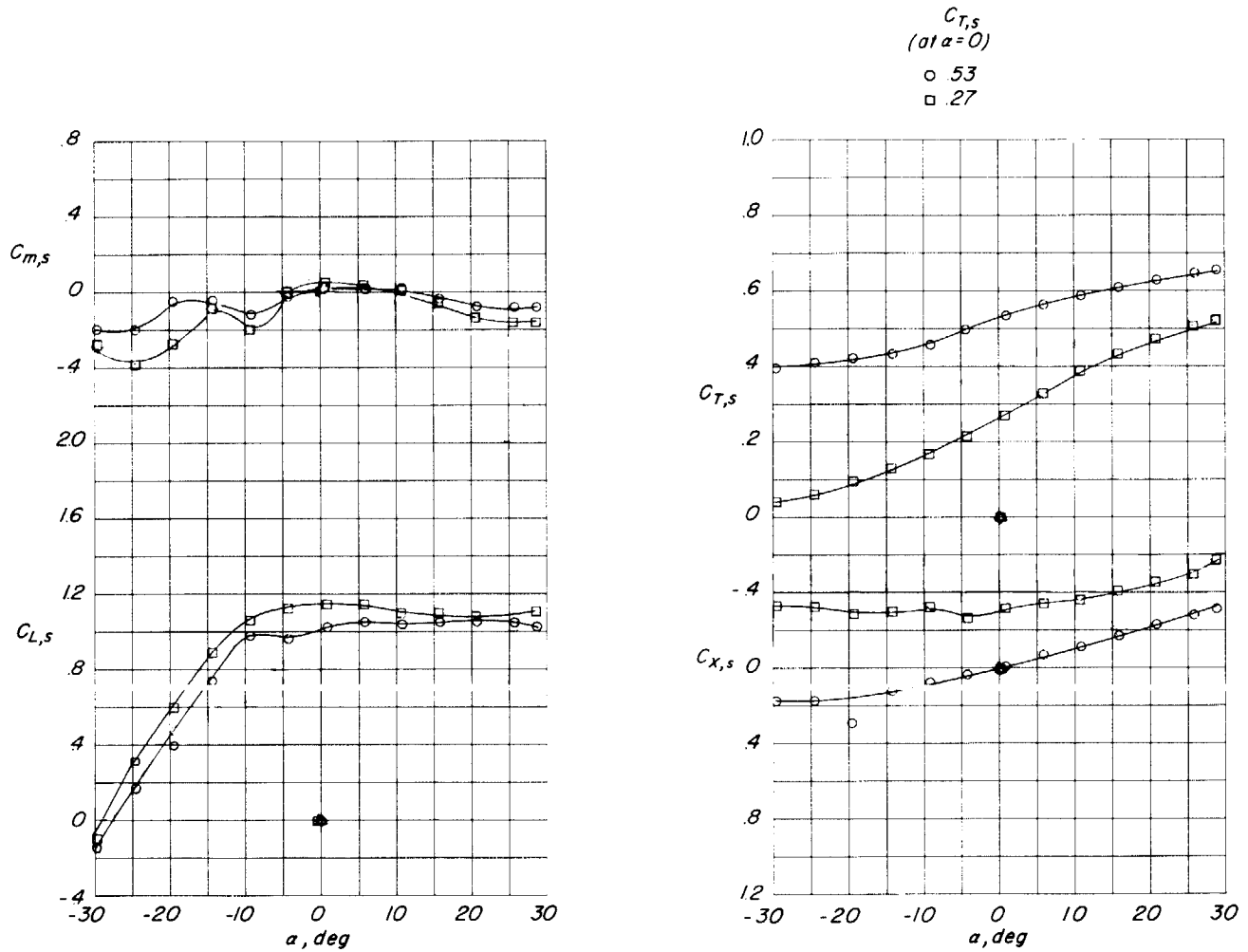

(a) Concluded.

Figure 12.- Continued.

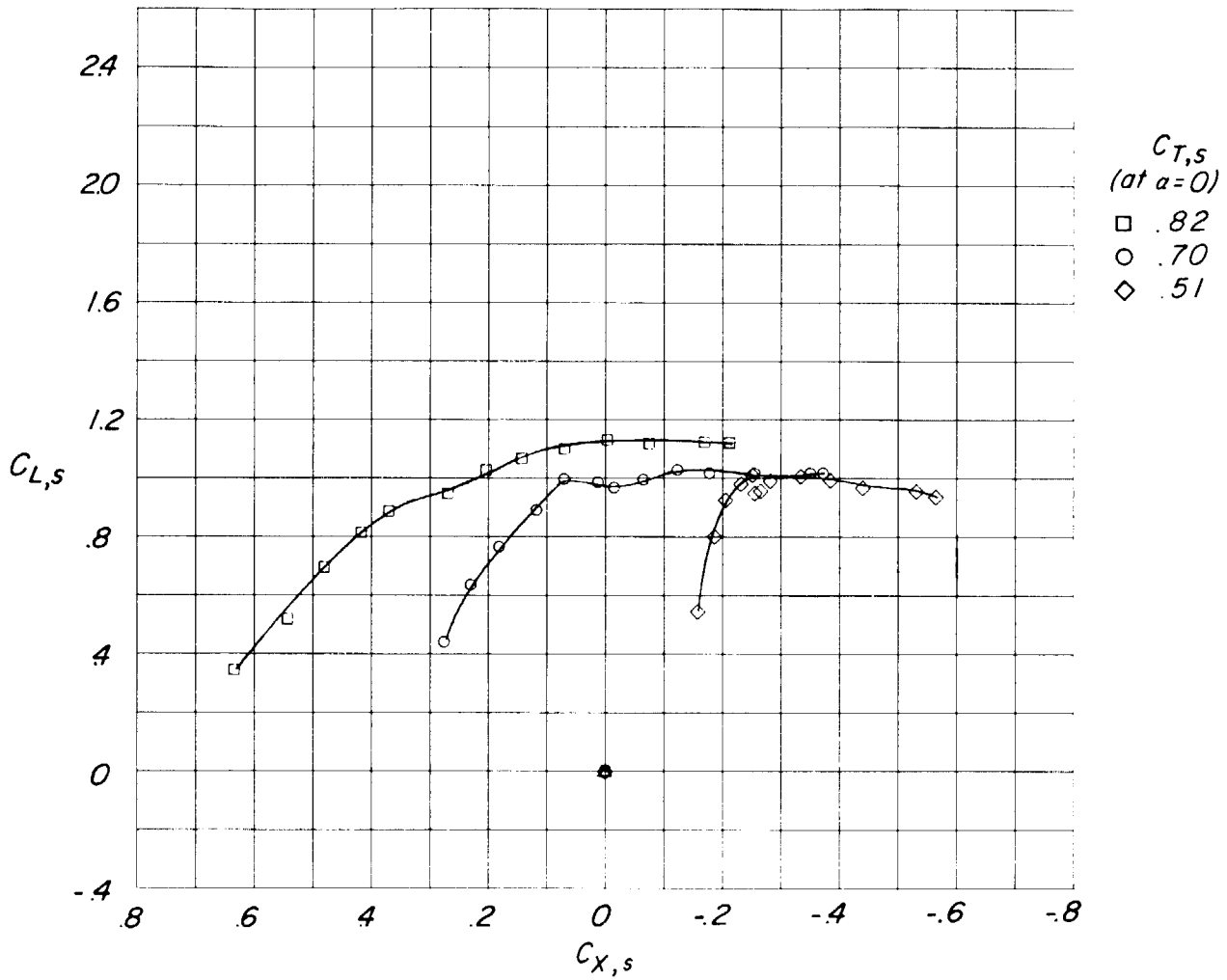

(b) Speed-brake configuration; $i_w = 45^\circ$; $i_t = 19.2^\circ$.

Figure 12.- Continued.

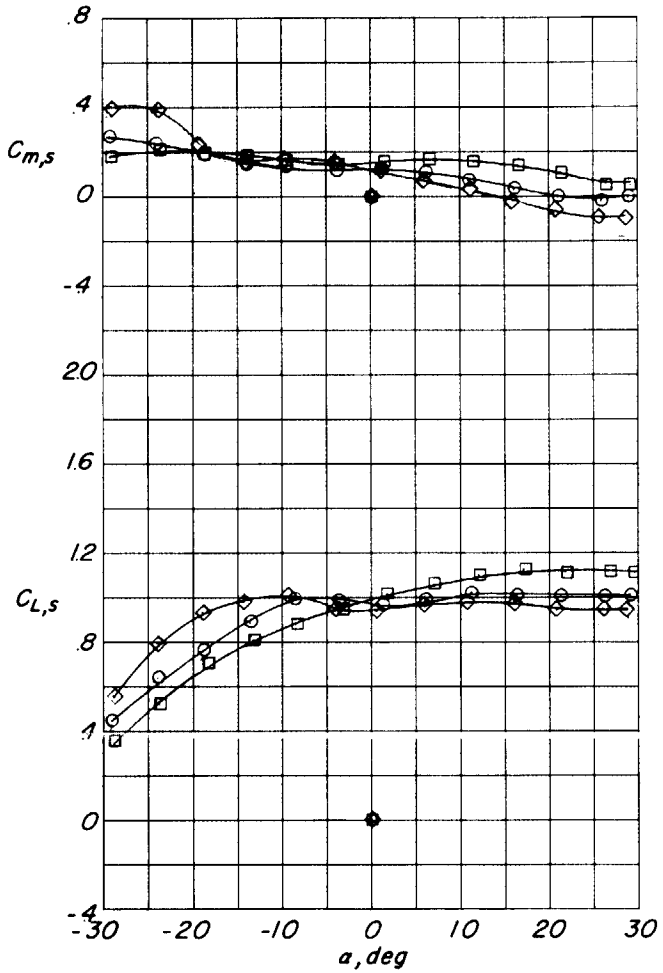

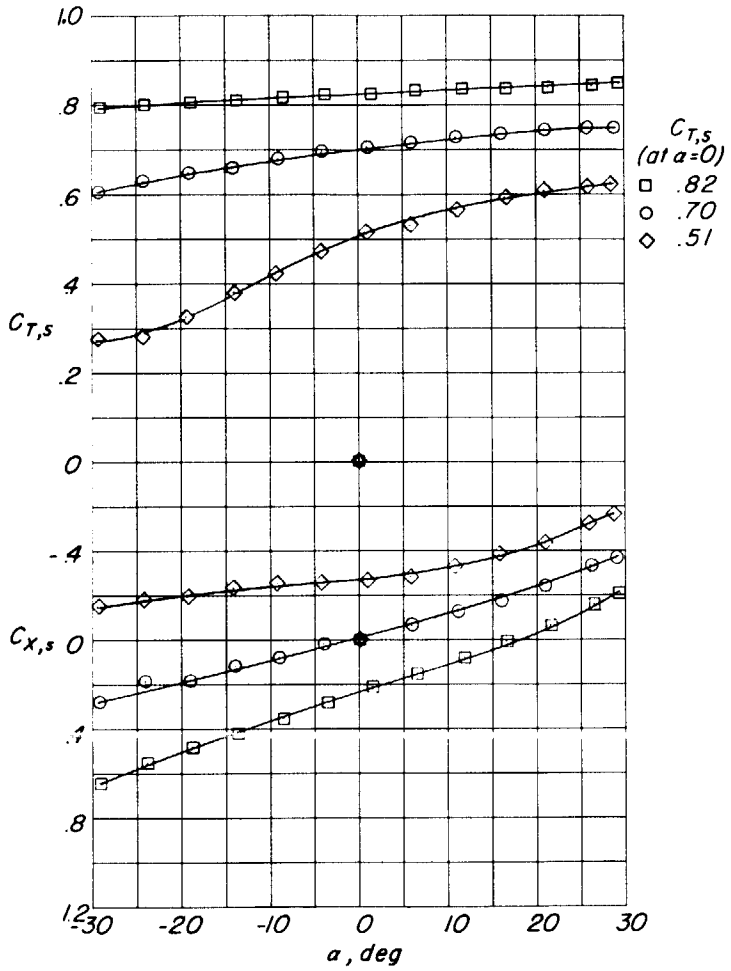

(b) Concluded.

Figure 12.- Concluded.

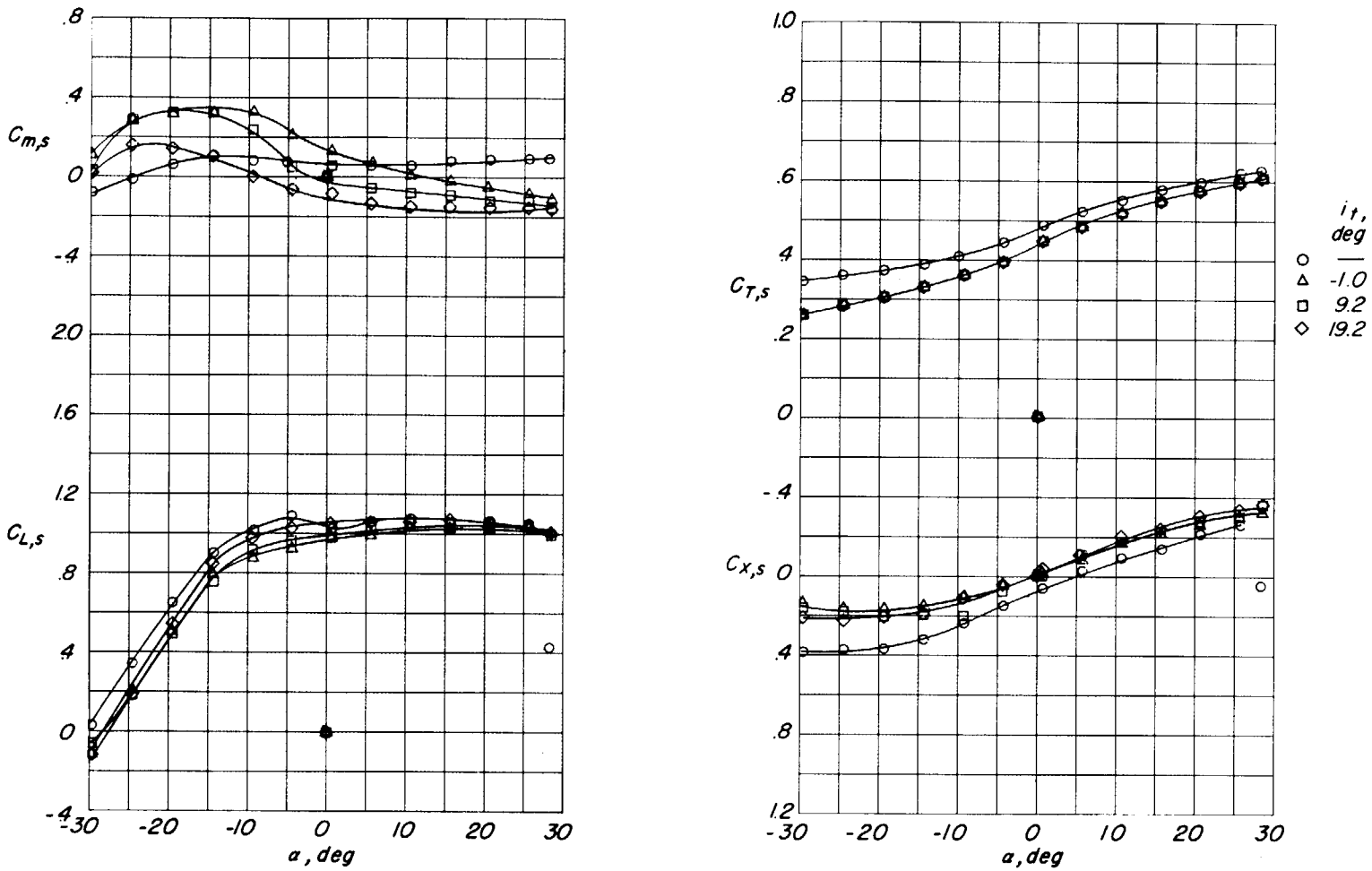

(a) Basic configuration; $i_w = 30^\circ$.

Figure 13.- Stabilizer effectiveness for the basic configuration.

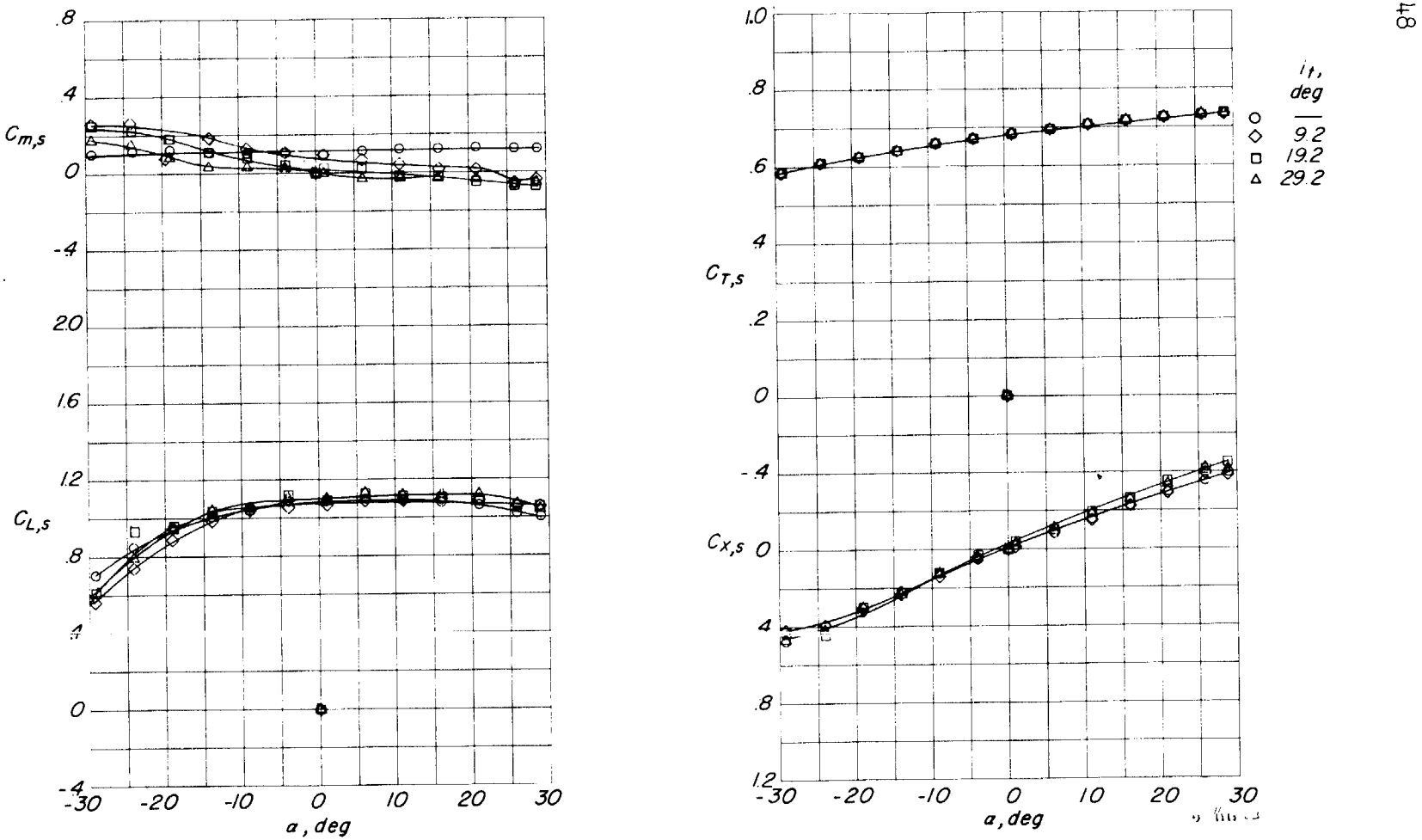

(b) Basic configuration; $i_w = 45°$.

Figure 13.- Continued.

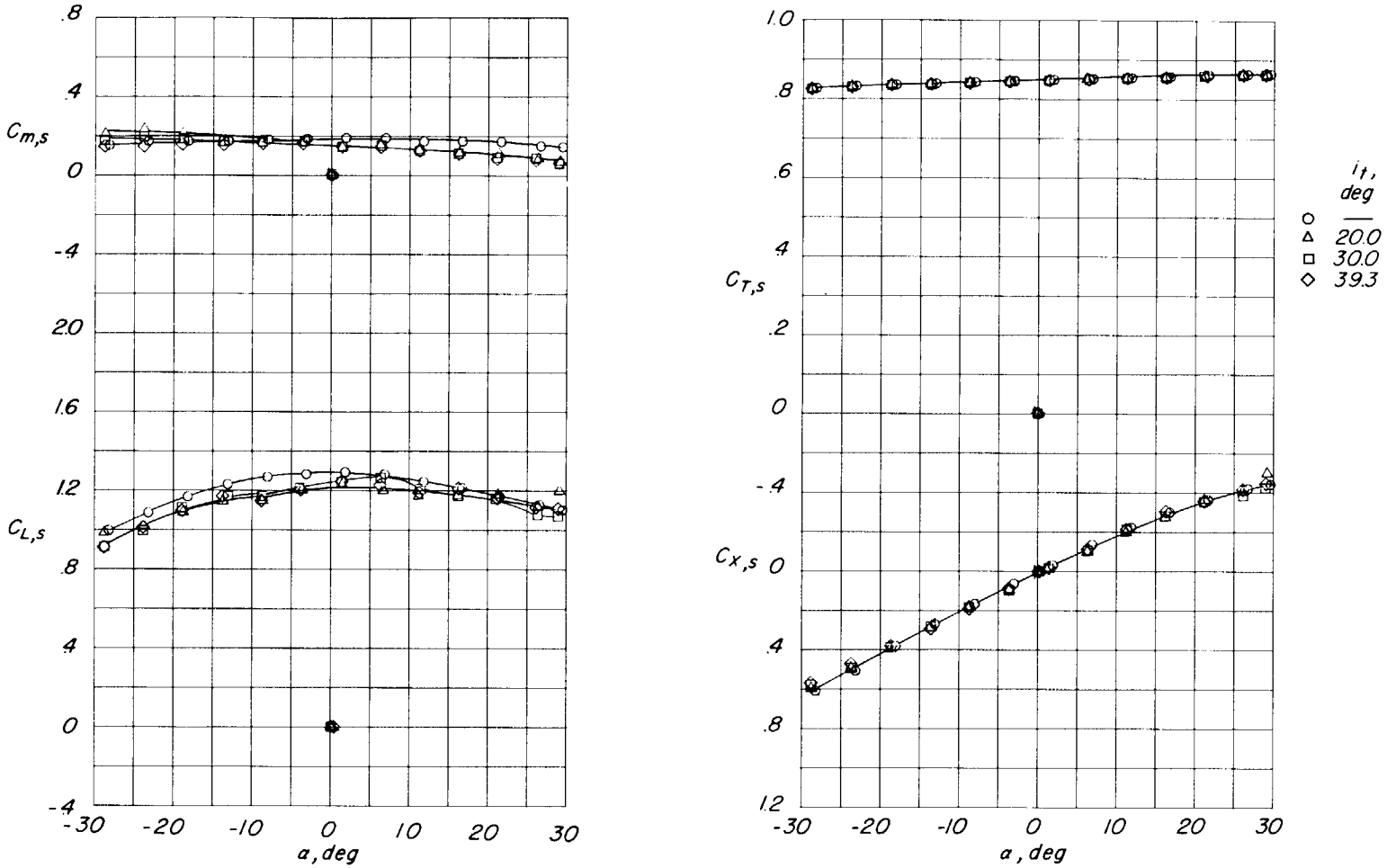

(c) Basic configuration; $i_w = 60^\circ$.

Figure 13.- Continued.

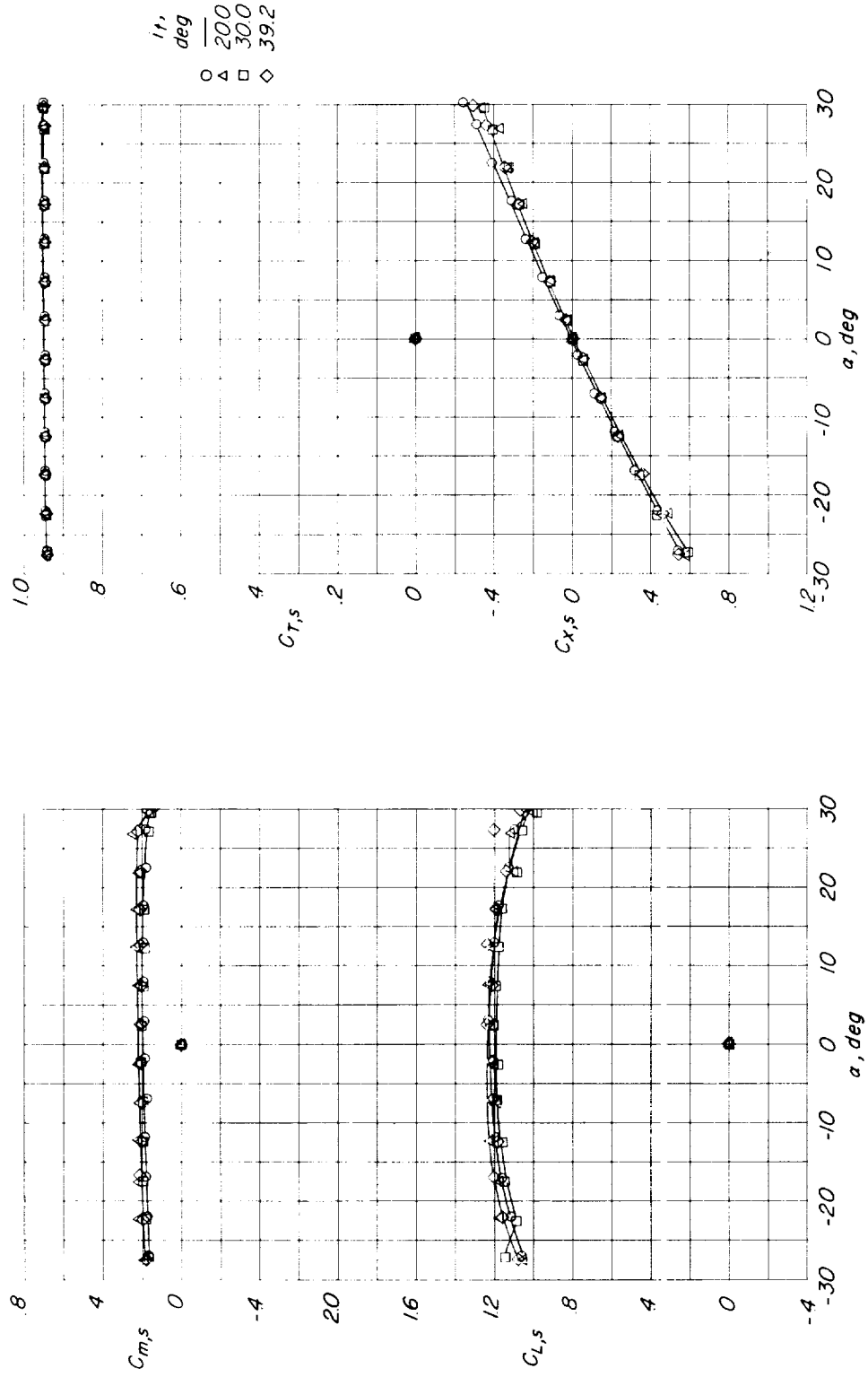

(d) Basic configuration; $i_w = 75°$.

Figure 13.- Concluded.

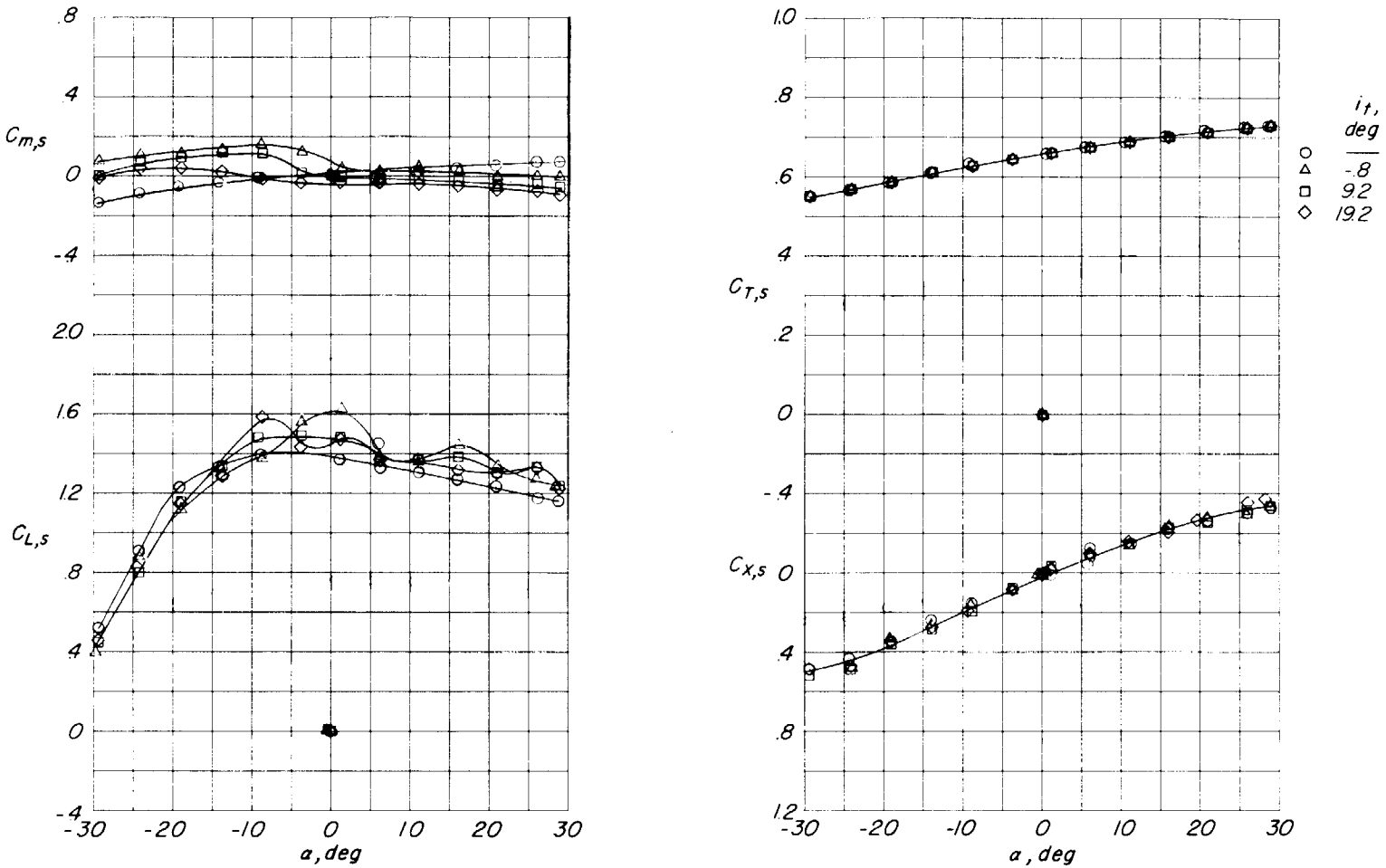

(a) Flapped configuration; $i_w = 30^\circ$.

Figure 14.- Stabilizer effectiveness for flapped configuration.

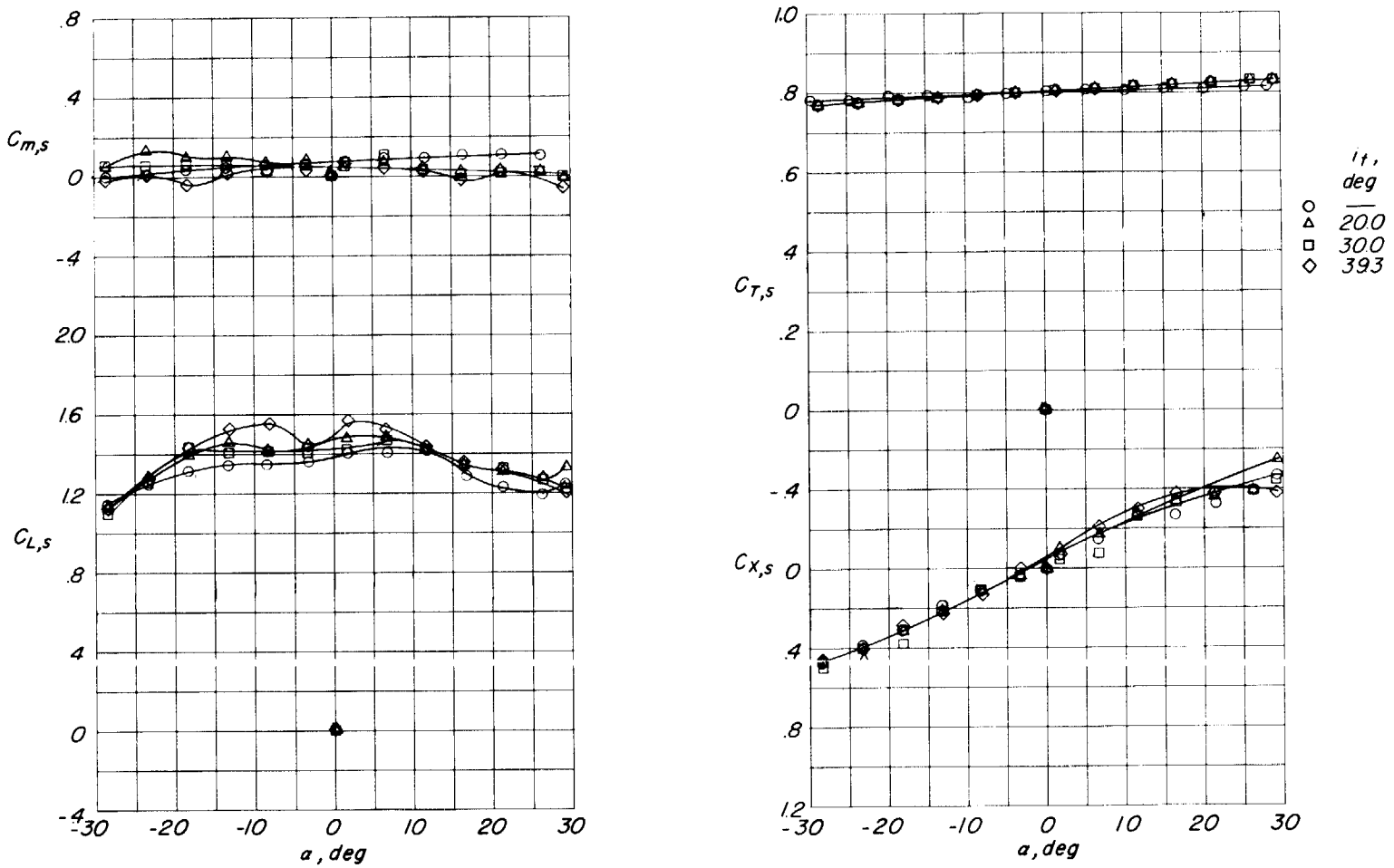

(b) Flapped configuration; $i_w = 45^\circ$.

Figure 14.- Concluded.

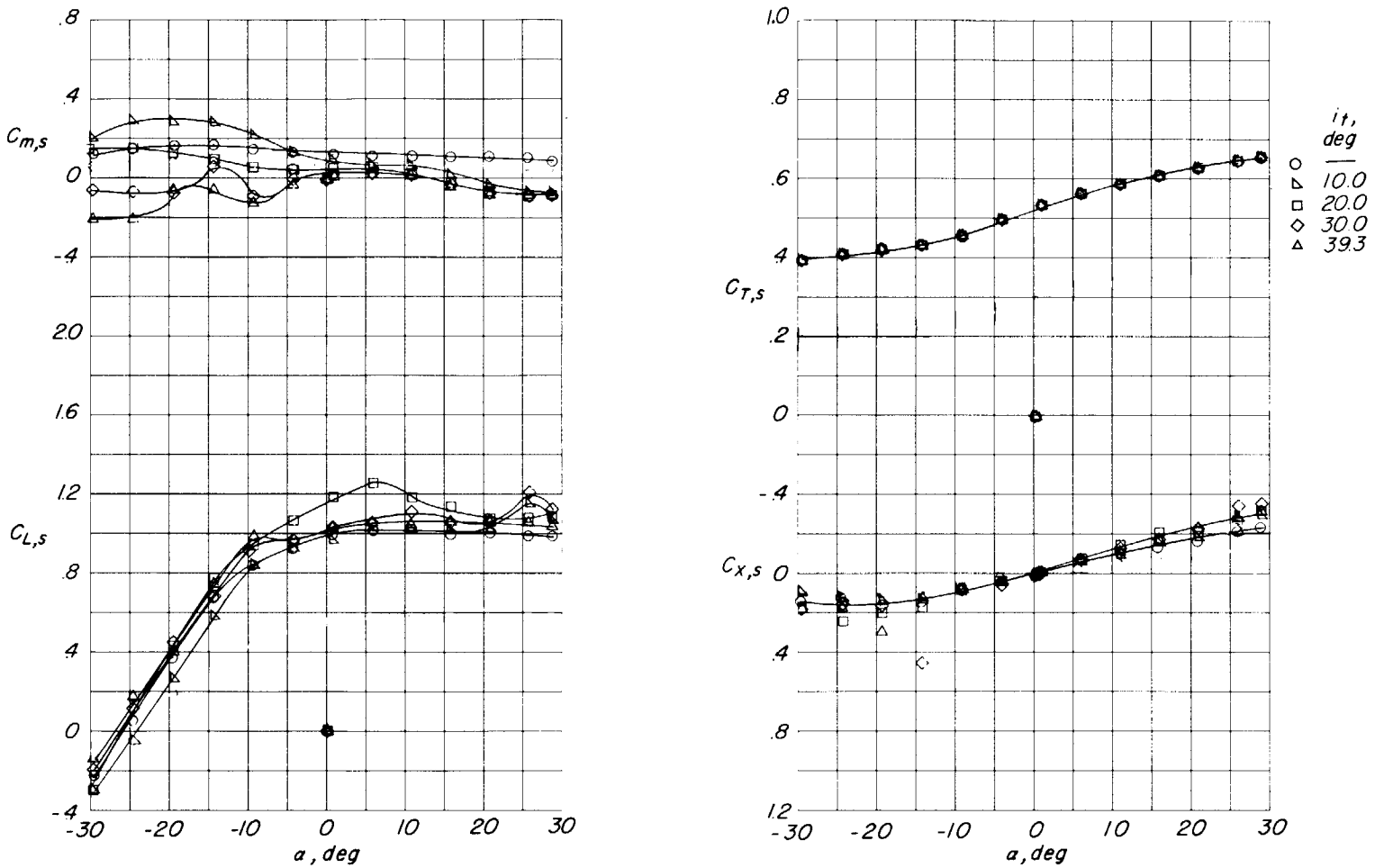

(a) Speed-brake configuration; $i_w = 30^\circ$.

Figure 15.- Stabilizer effectiveness for speed-brake configuration.

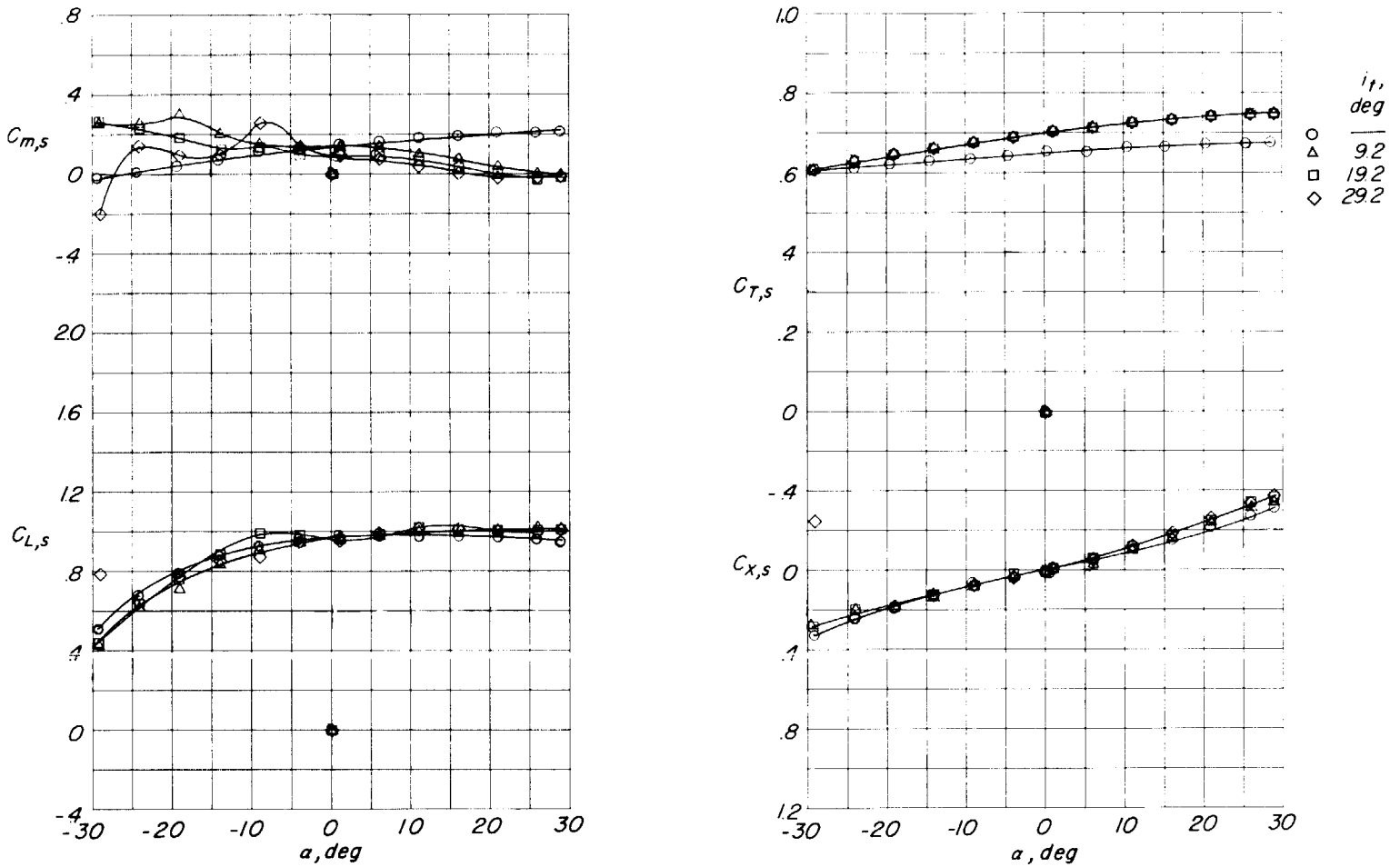

(b) Speed-brake configuration; $i_w = 45°$.

Figure 15.- Concluded.

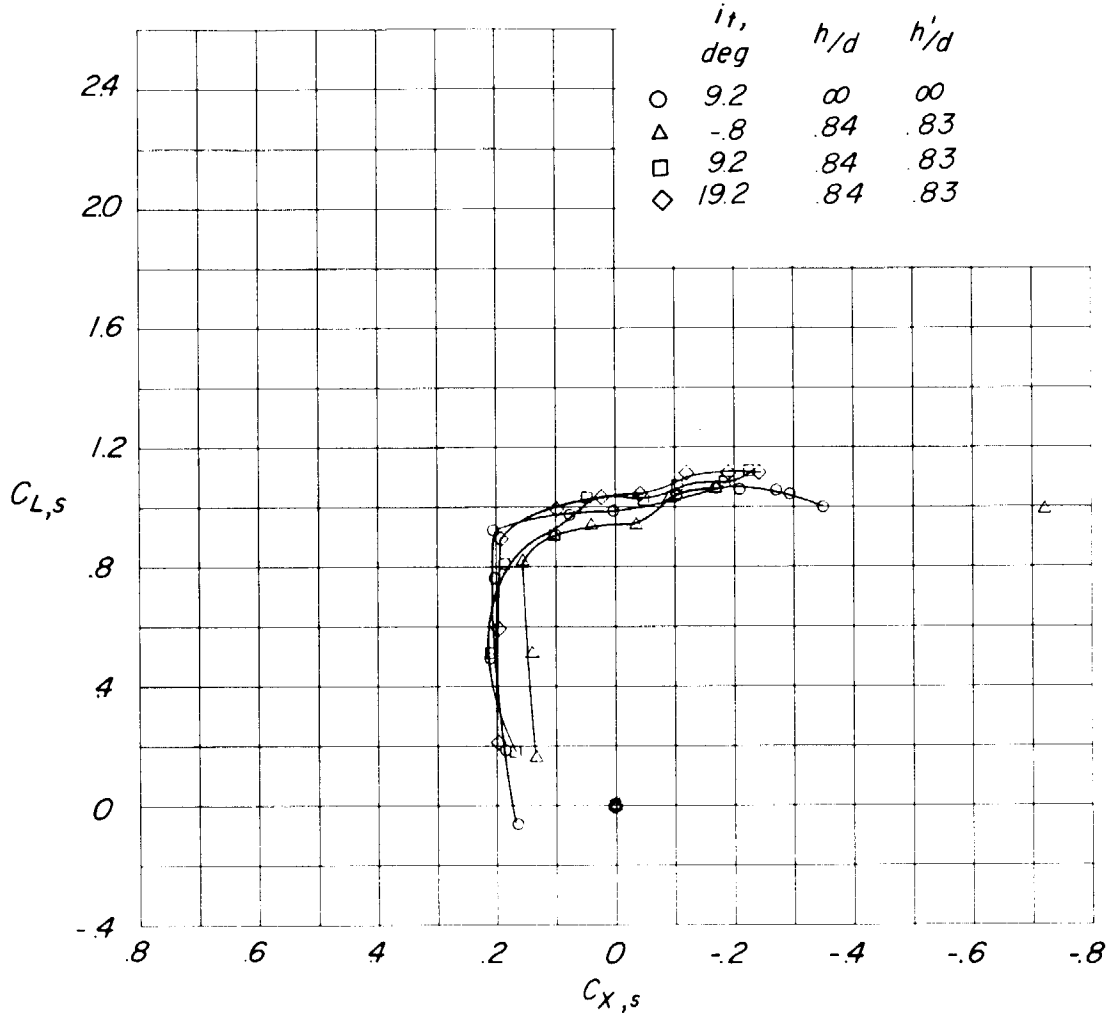

(a) Basic configuration; $i_w = 30^\circ$.

Figure 16.- Stabilizer effectiveness for the basic configuration in region of ground effect.

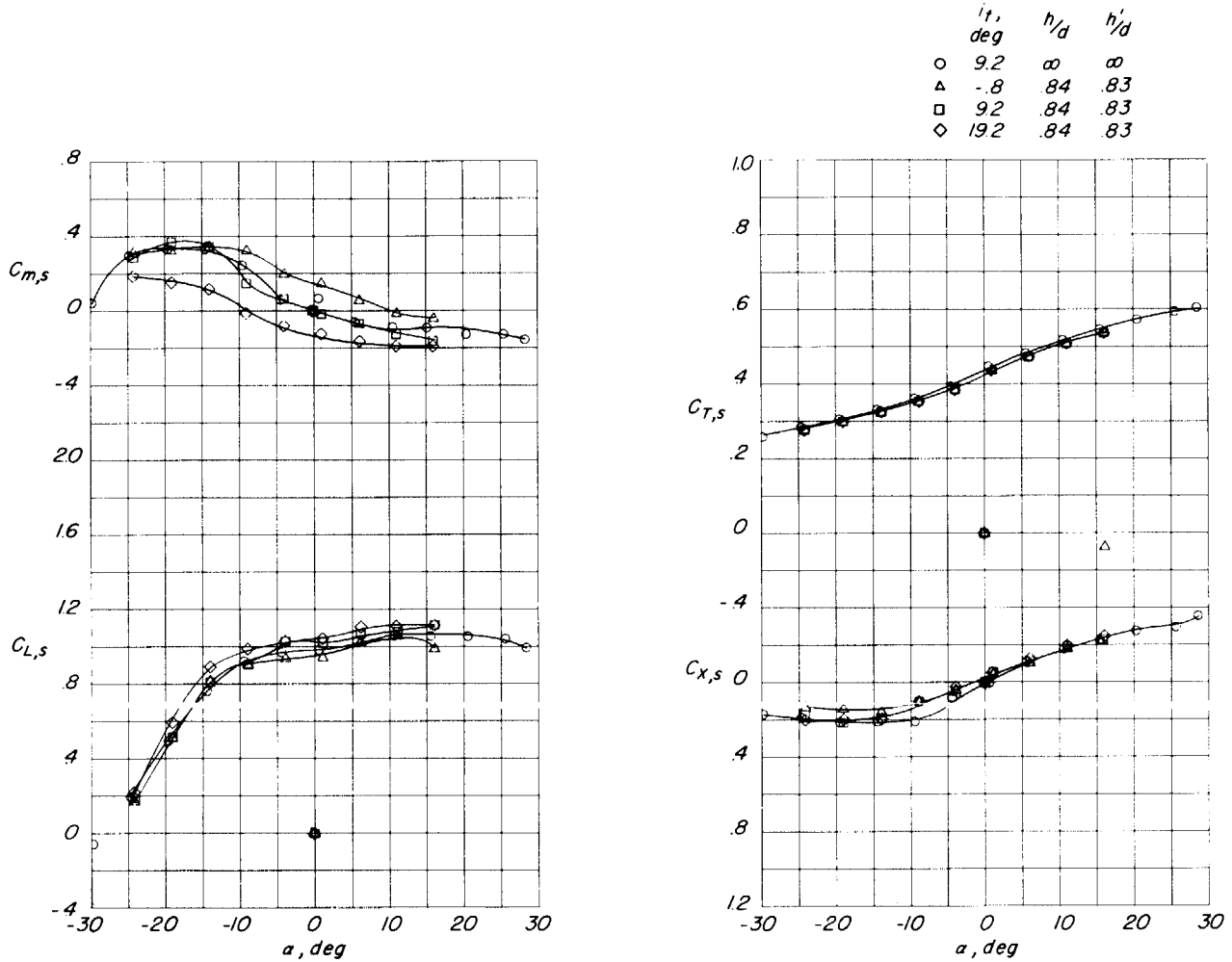

(a) Concluded.

Figure 16.- Continued.

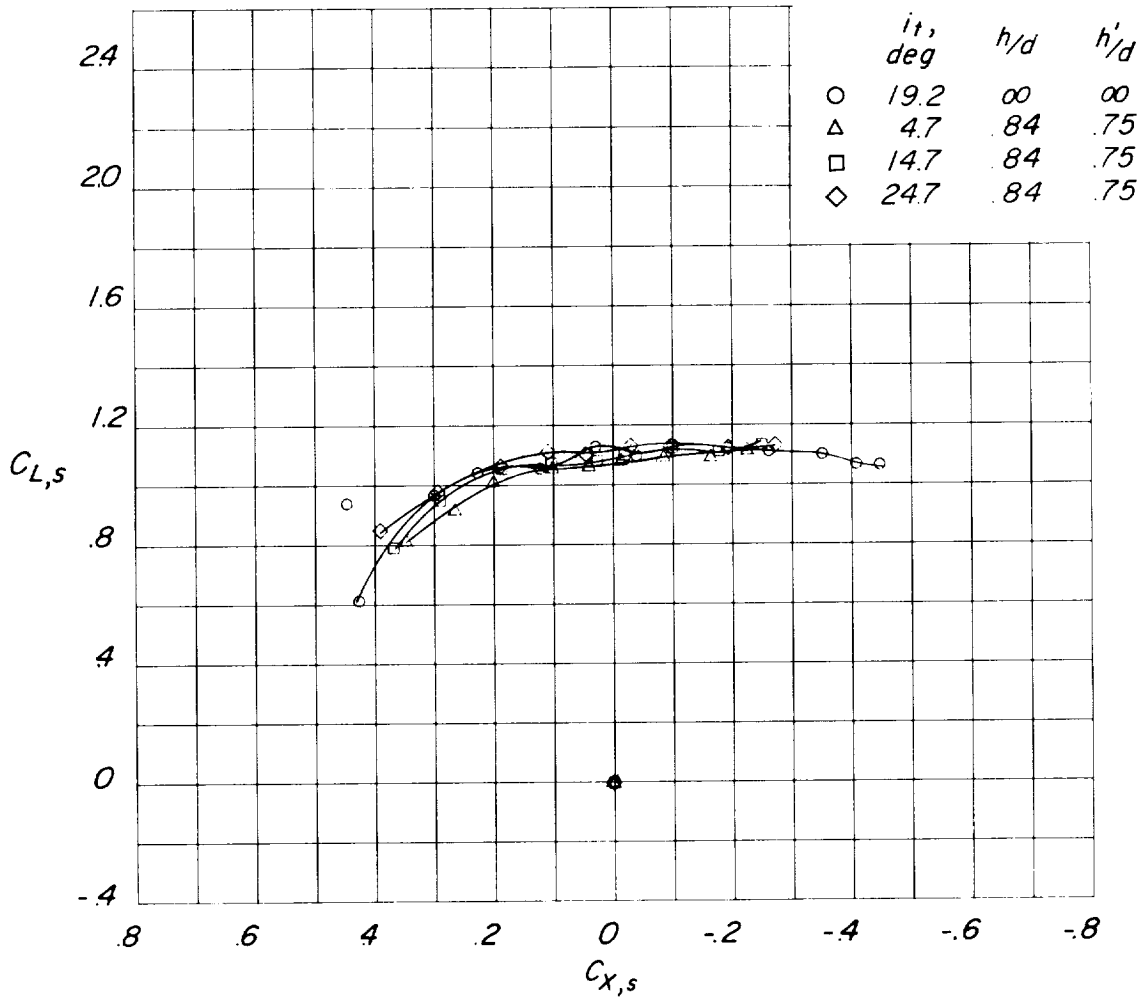

(b) Basic configuration; $i_w = 45°$.

Figure 16.- Continued.

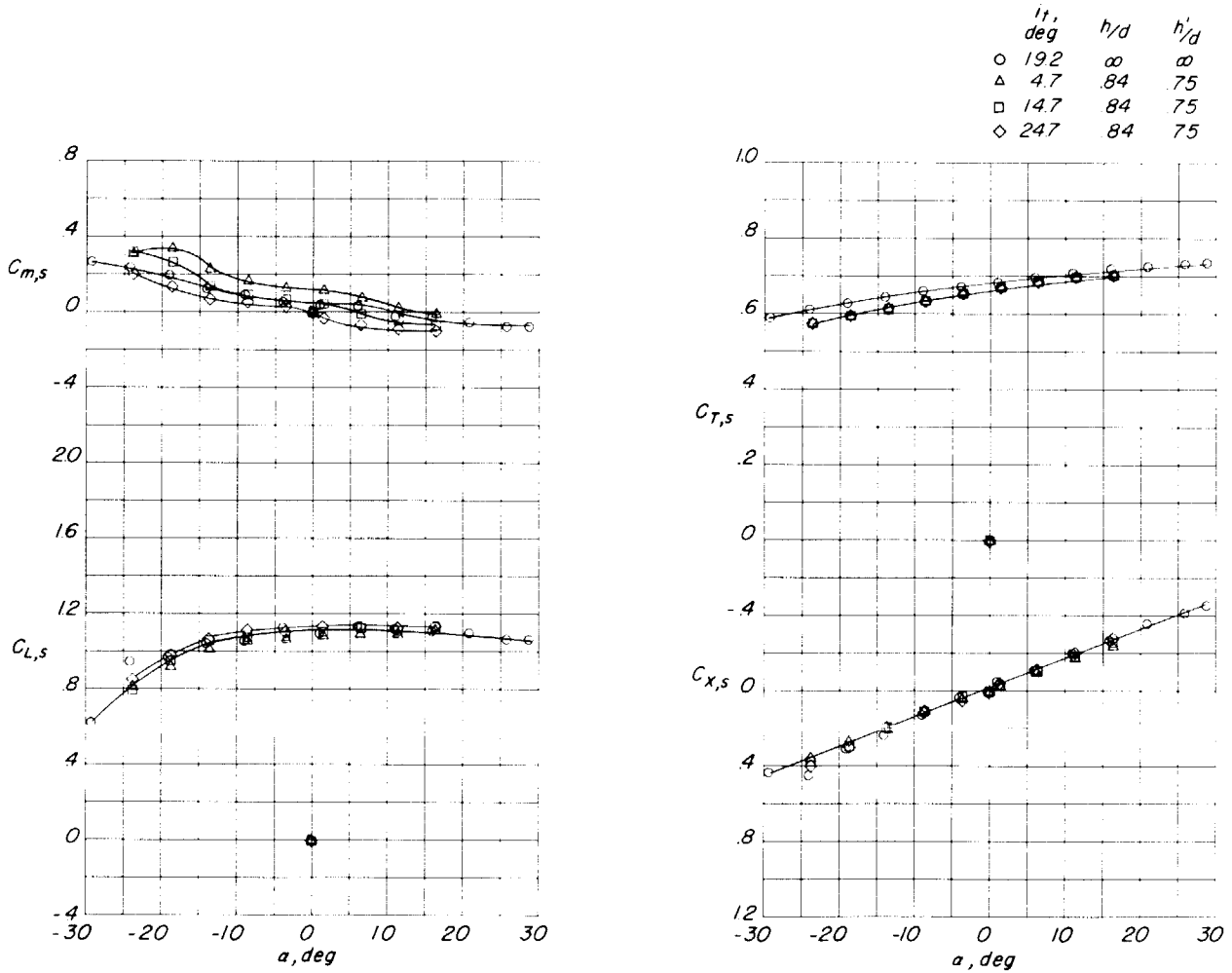

(b) Concluded.

Figure 16.- Continued.

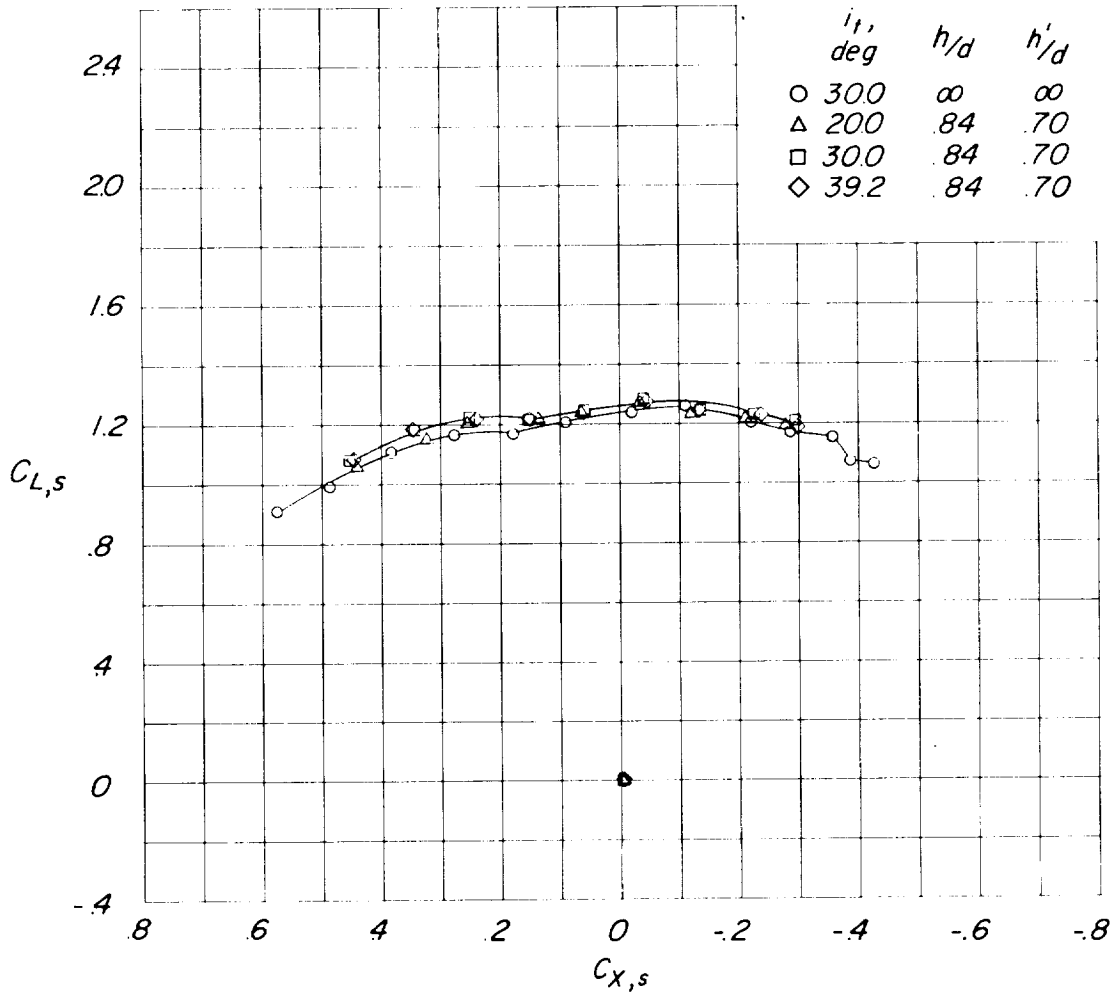

(c) Basic configuration; $i_w = 60^\circ$.

Figure 16.- Continued.

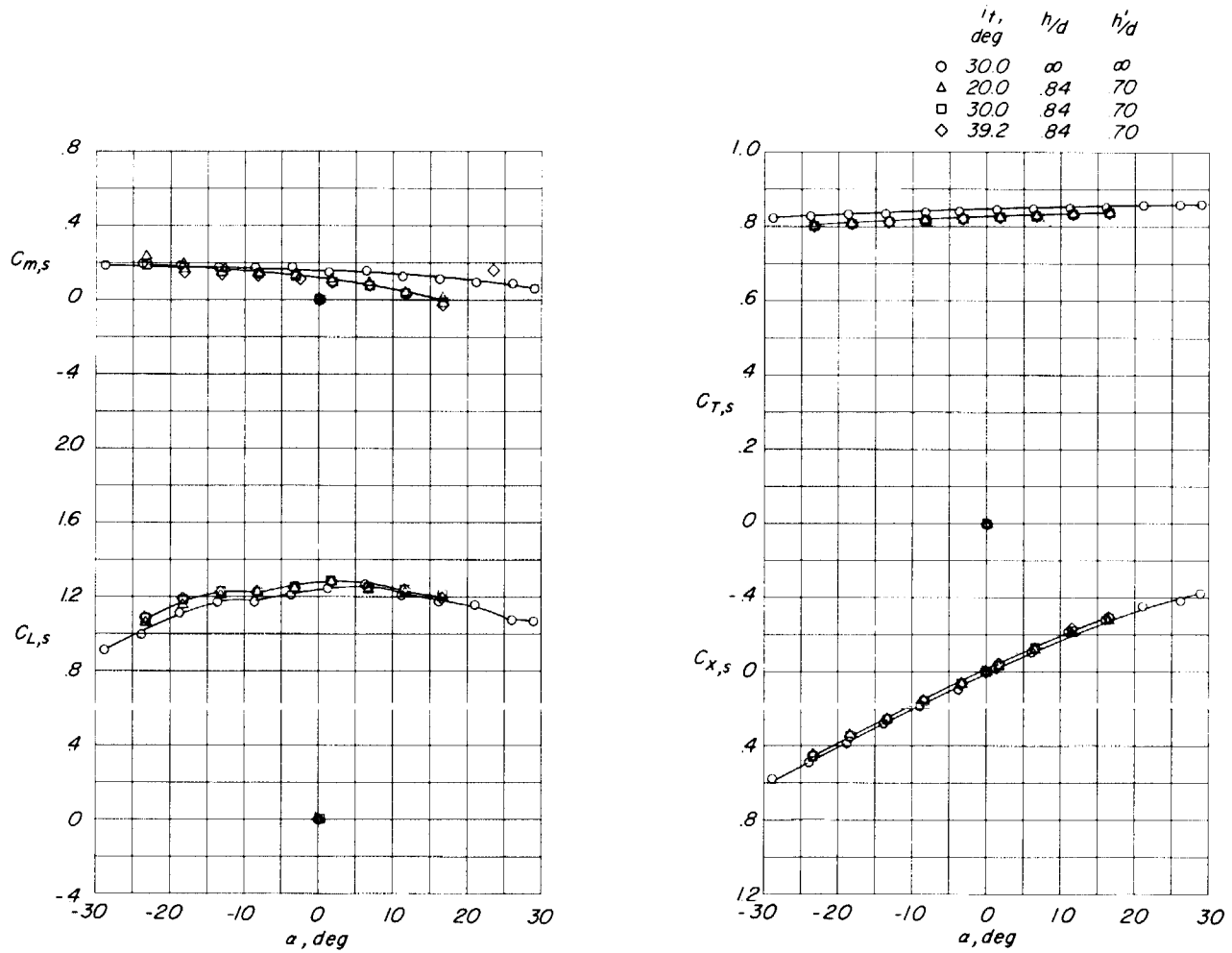

(c) Concluded.

Figure 16.- Continued.

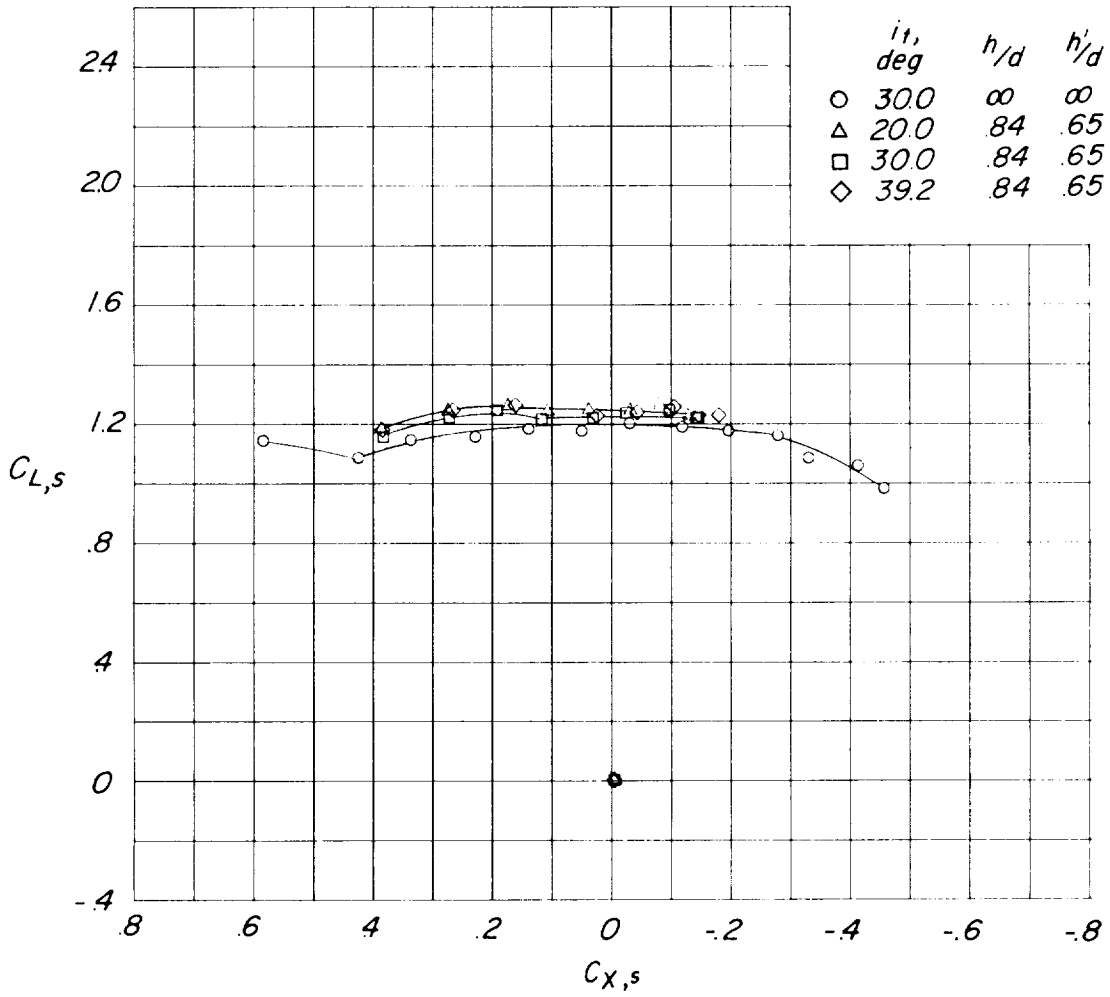

(d) Basic configuration; $i_w = 75^\circ$.

Figure 16.- Continued.

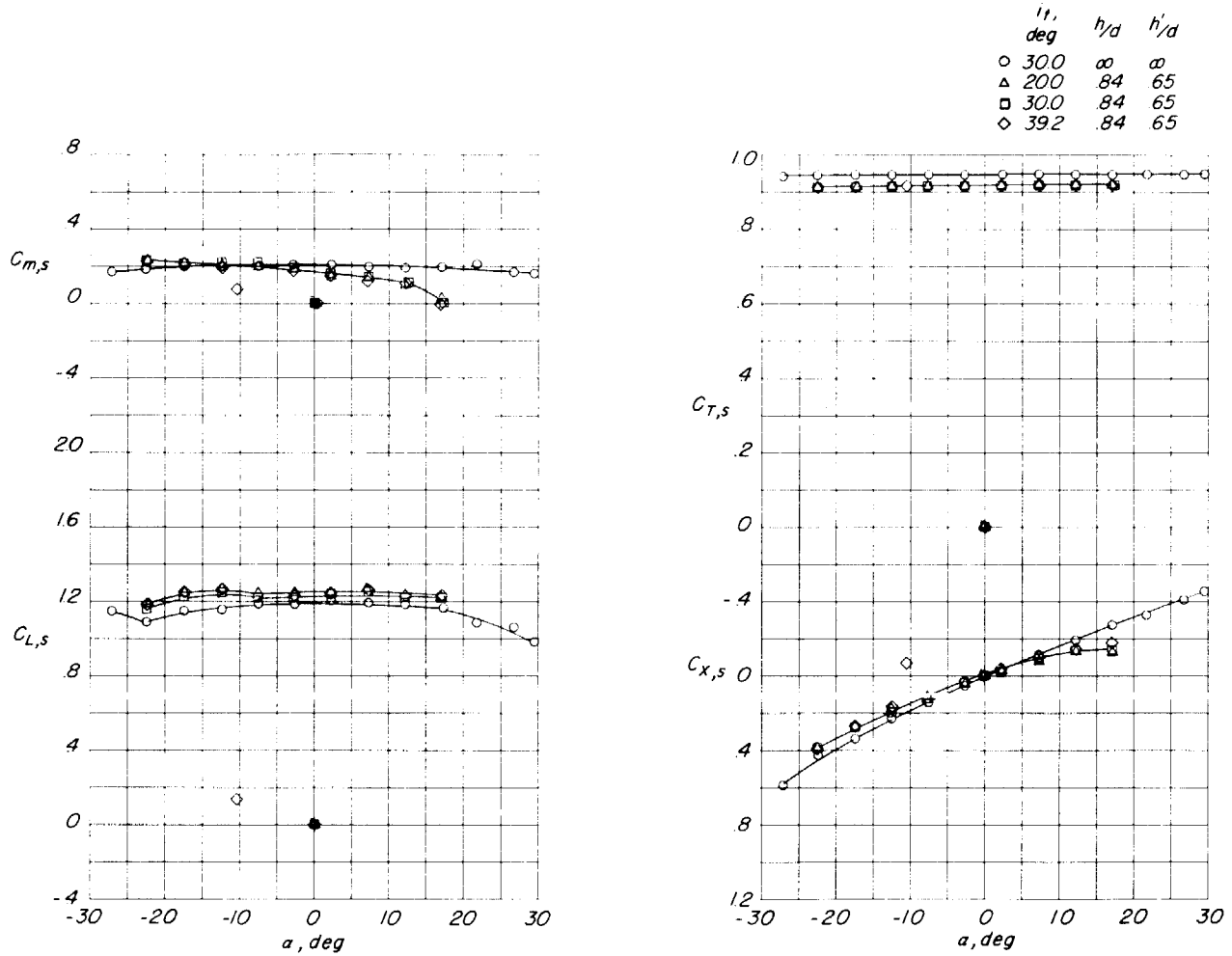

(d) Concluded.

Figure 16.- Concluded.

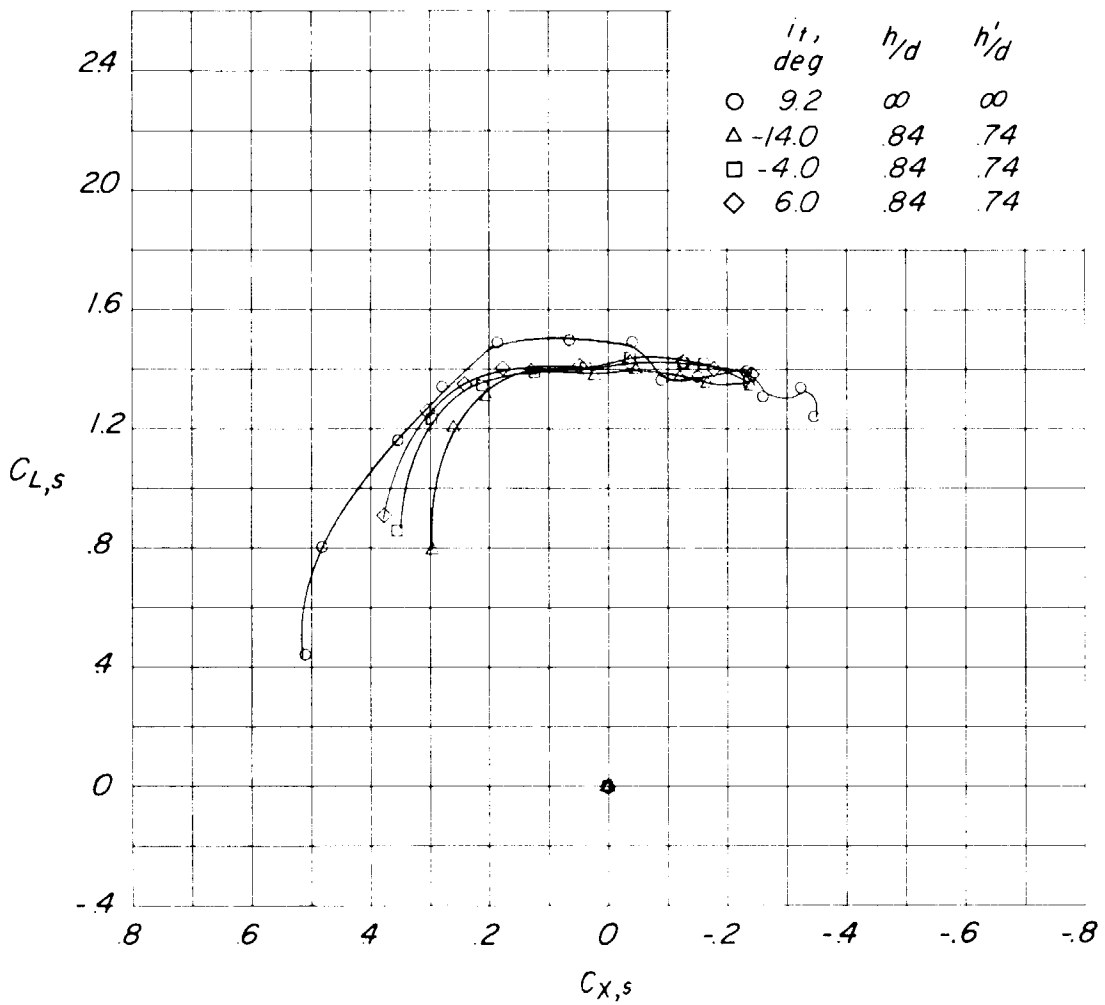

(a) Flapped configuration; $i_w = 30^\circ$.

Figure 17.- Stabilizer effectiveness for flapped configuration in region of ground effect.

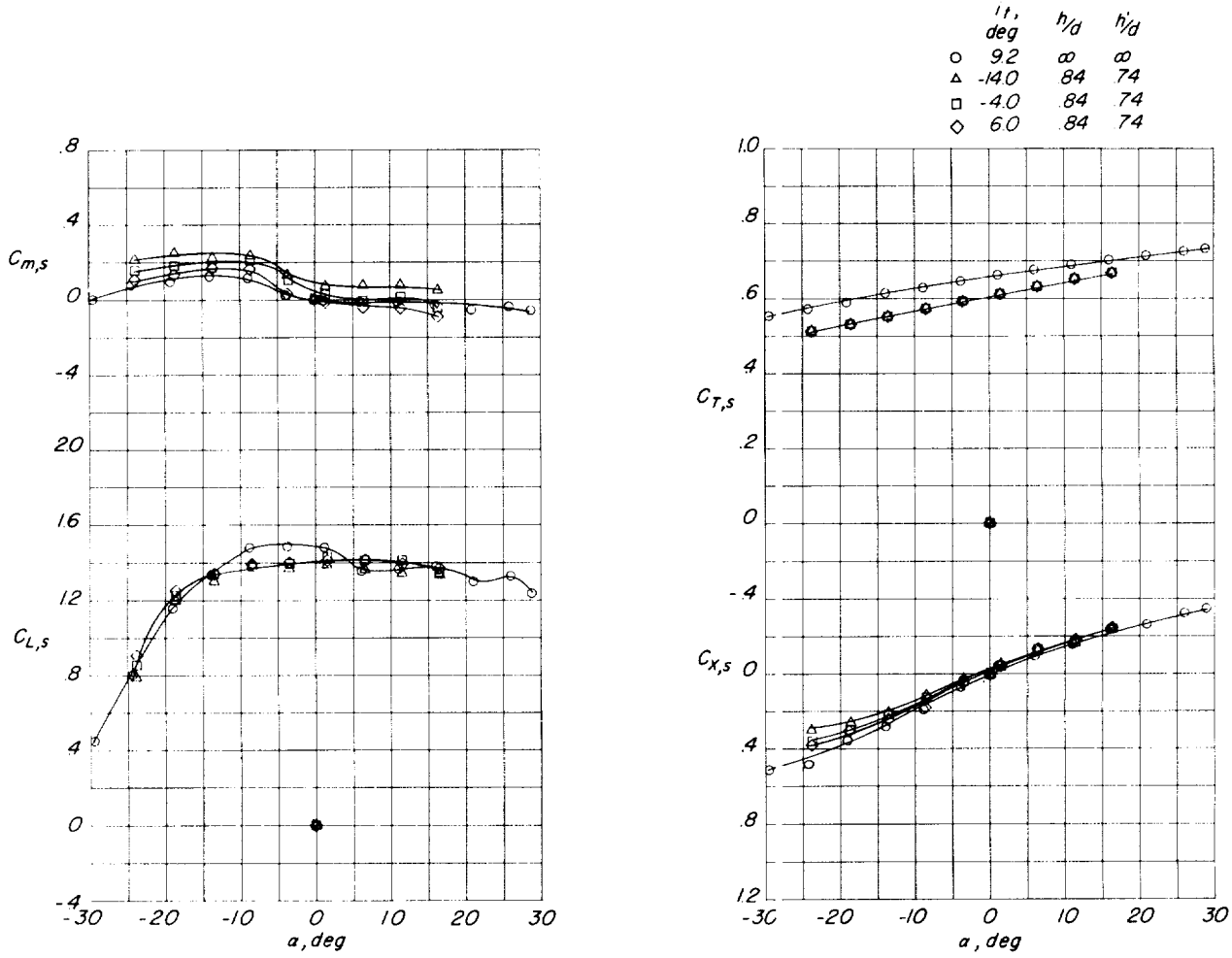

(a) Concluded.

Figure 17.- Continued.

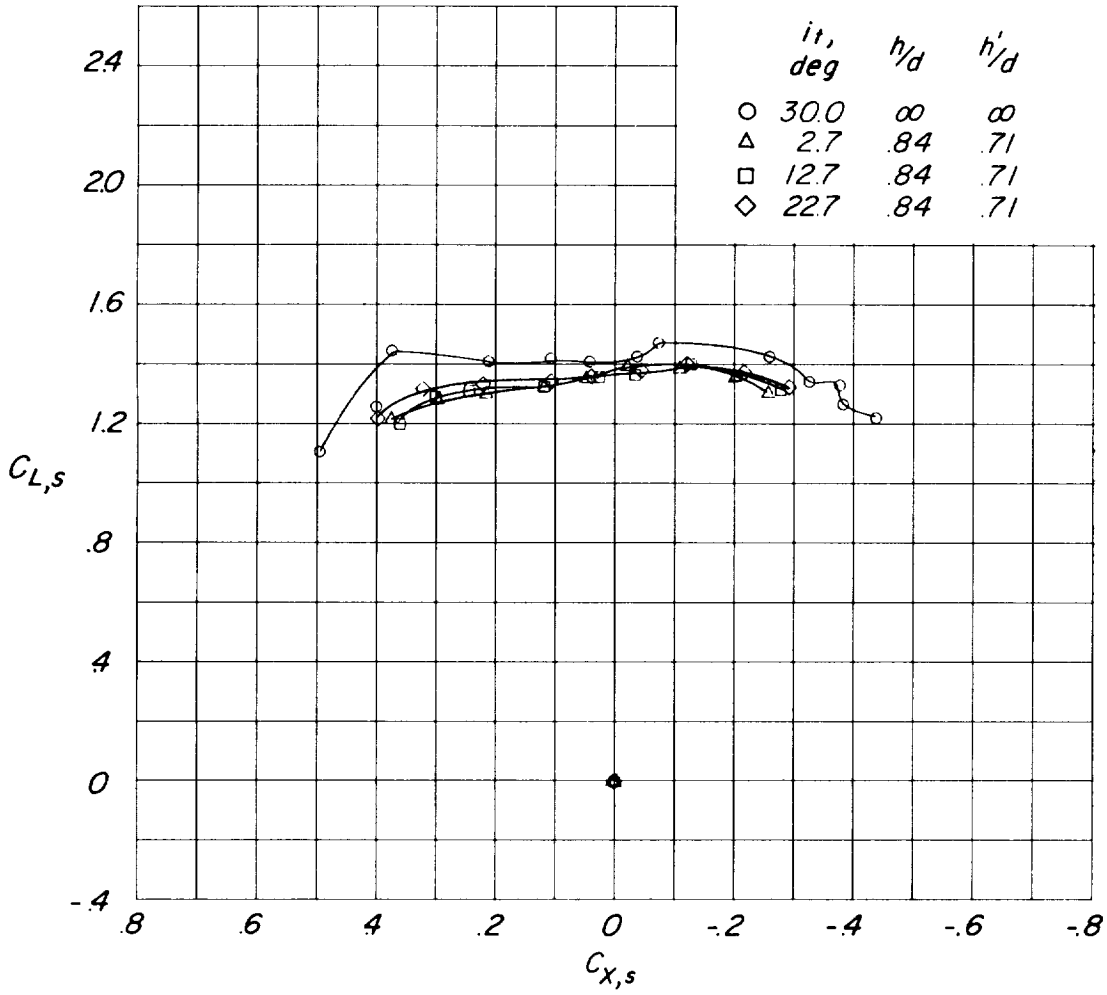

(b) Flapped configuration; $i_w = 45^\circ$.

Figure 17.- Continued.

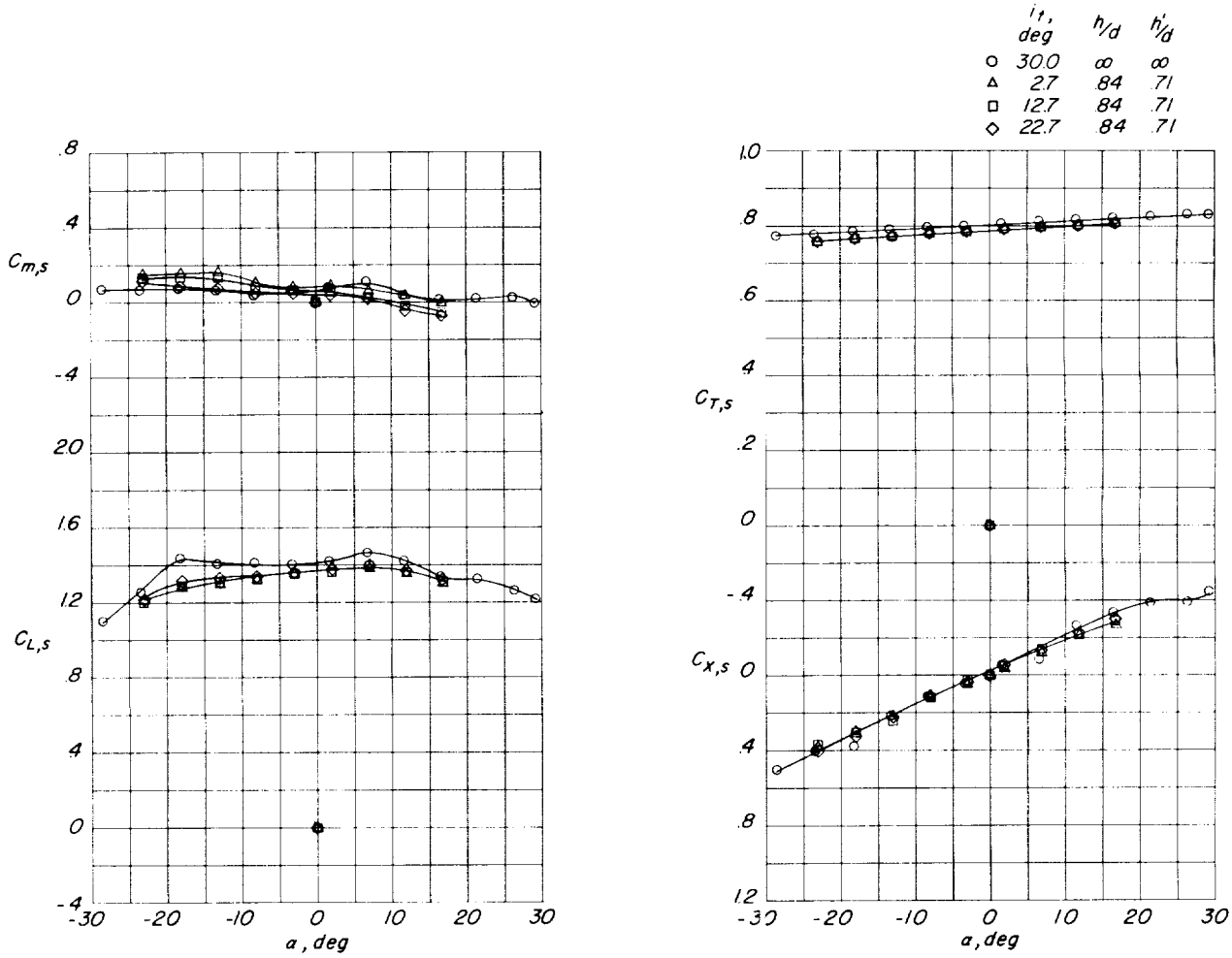

(b) Concluded.

Figure 17.- Concluded.

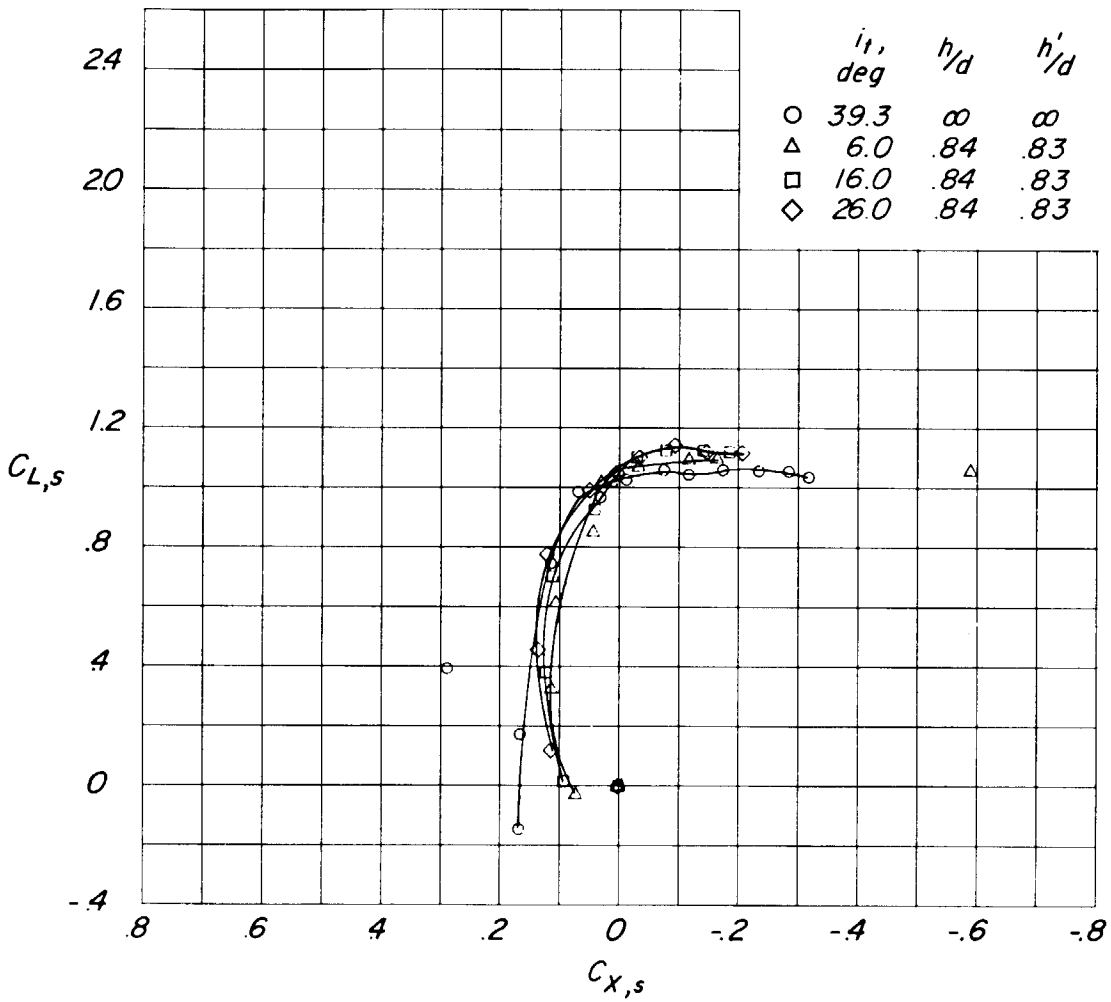

(a) Speed-brake configuration; $i_w = 30^\circ$.

Figure 18.- Stabilizer effectiveness for speed-brake configuration in region of ground effect.

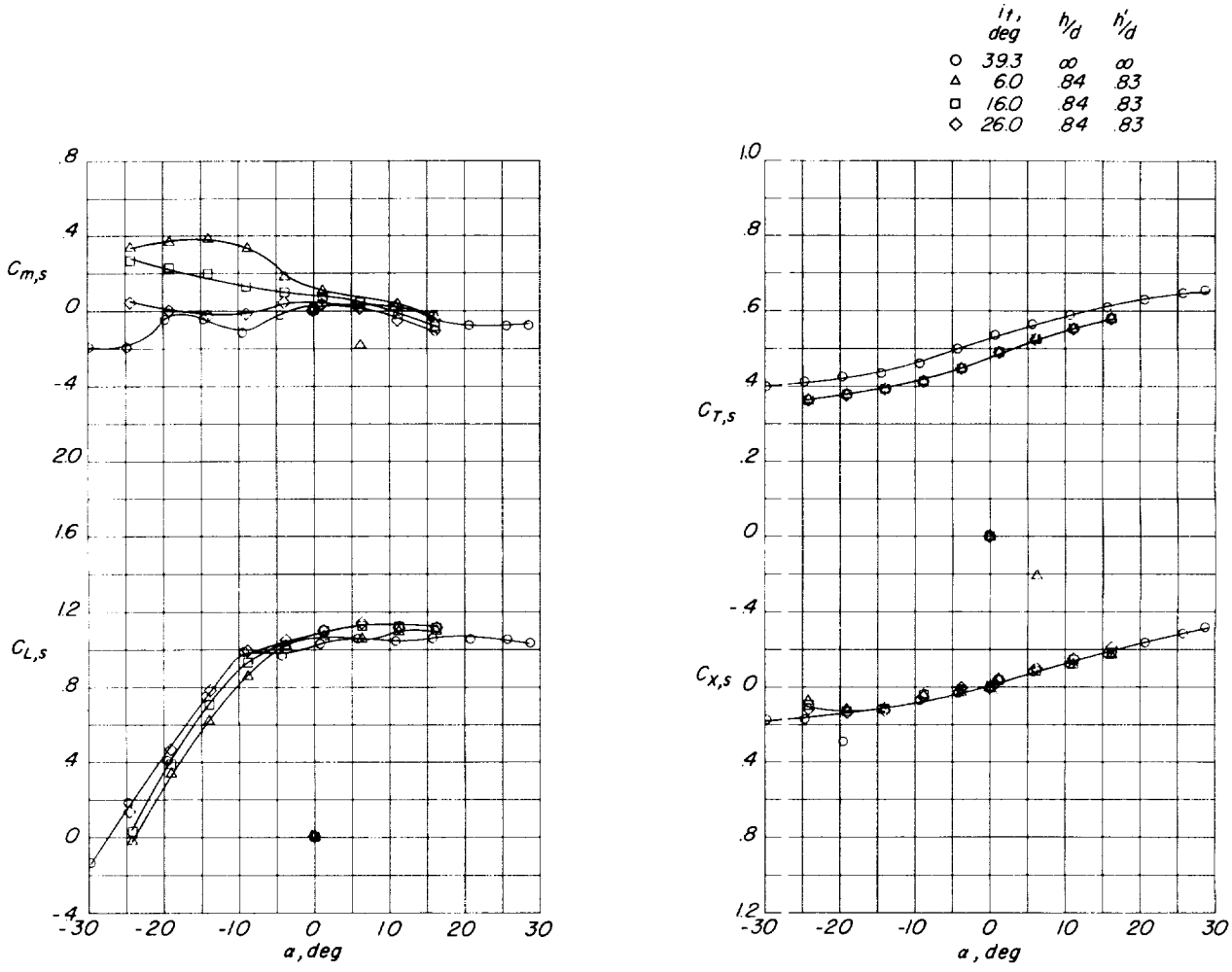

(a) Concluded.

Figure 18.- Continued.

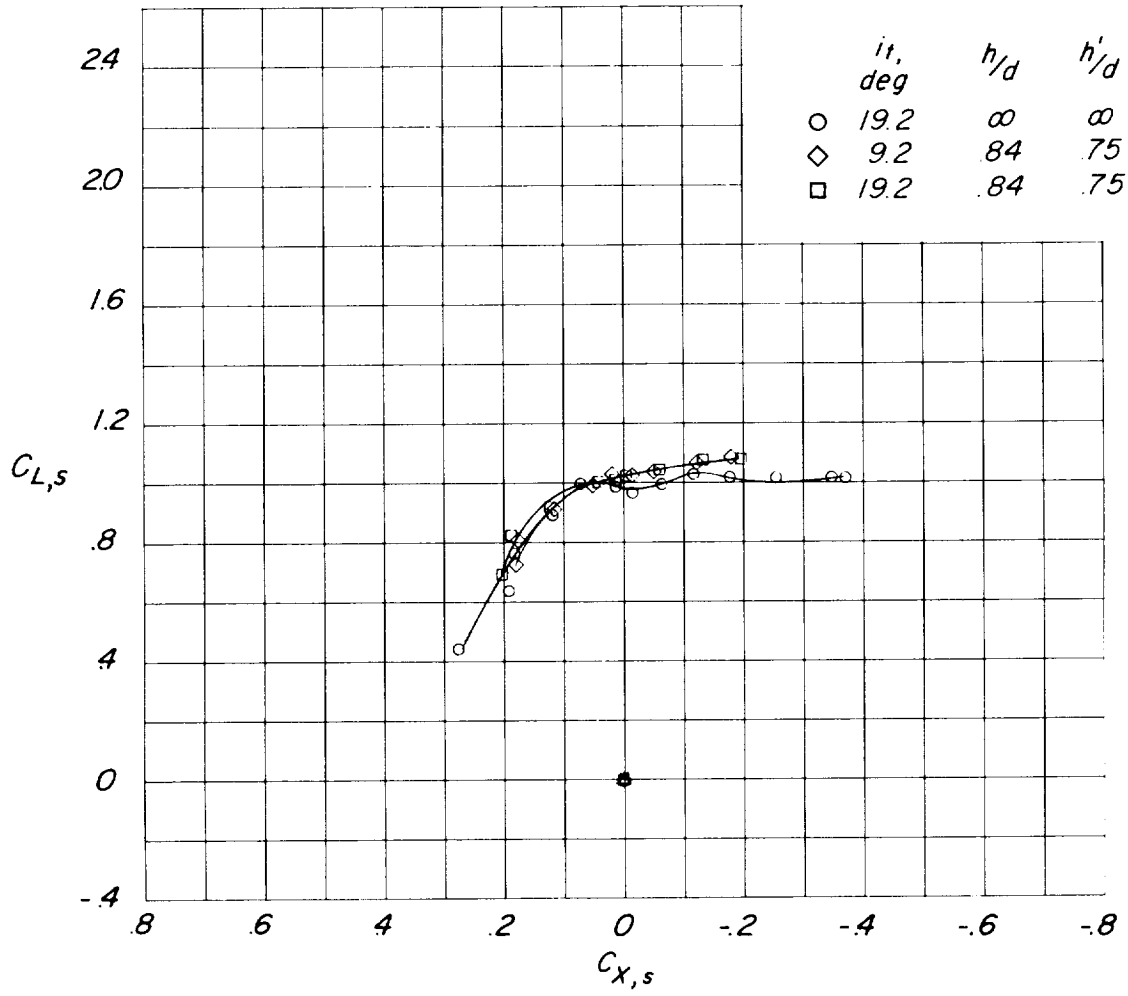

(b) Speed-brake configuration; $i_w = 45°$.

Figure 18.- Continued.

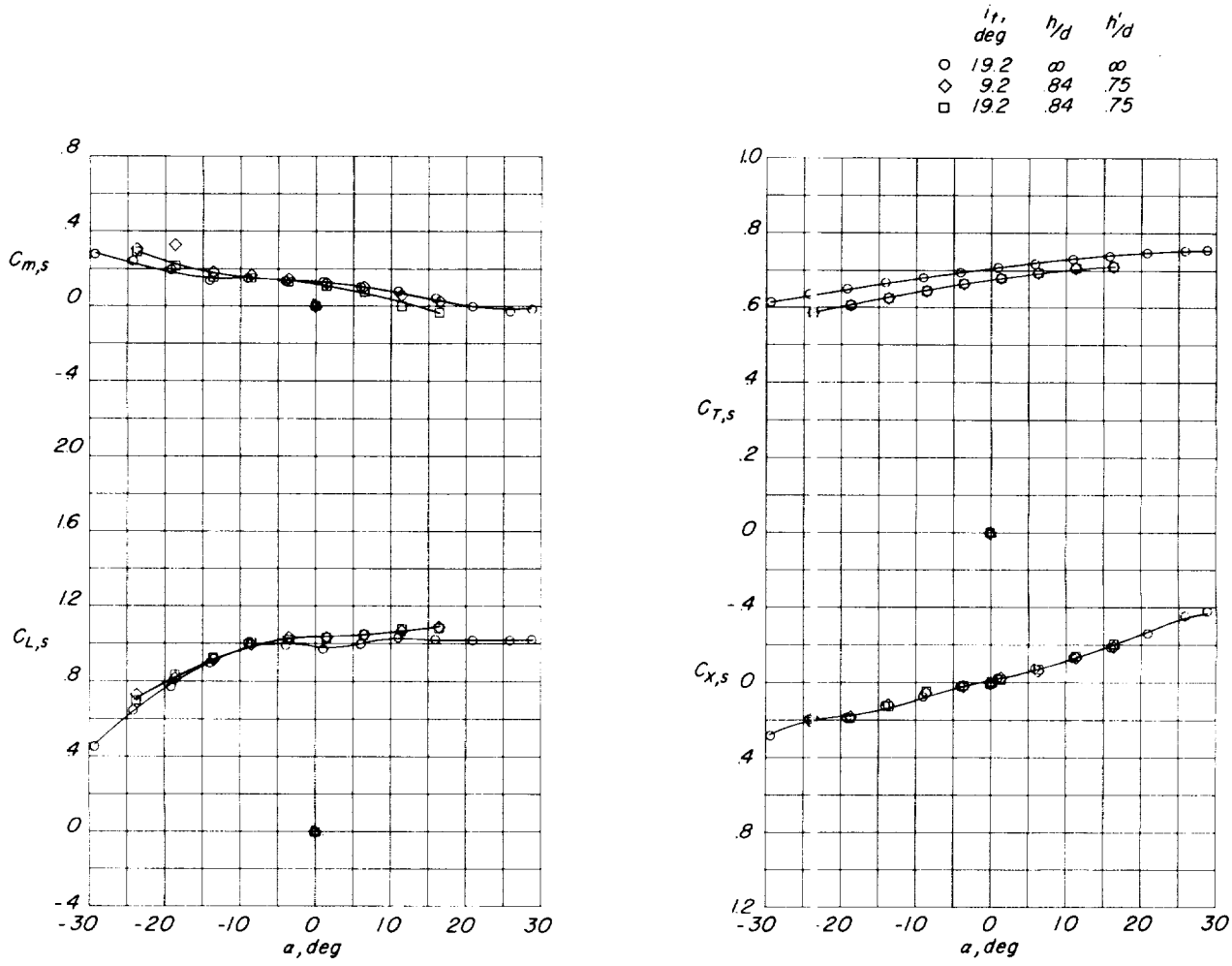

(b) Concluded.

Figure 18.- Concluded.

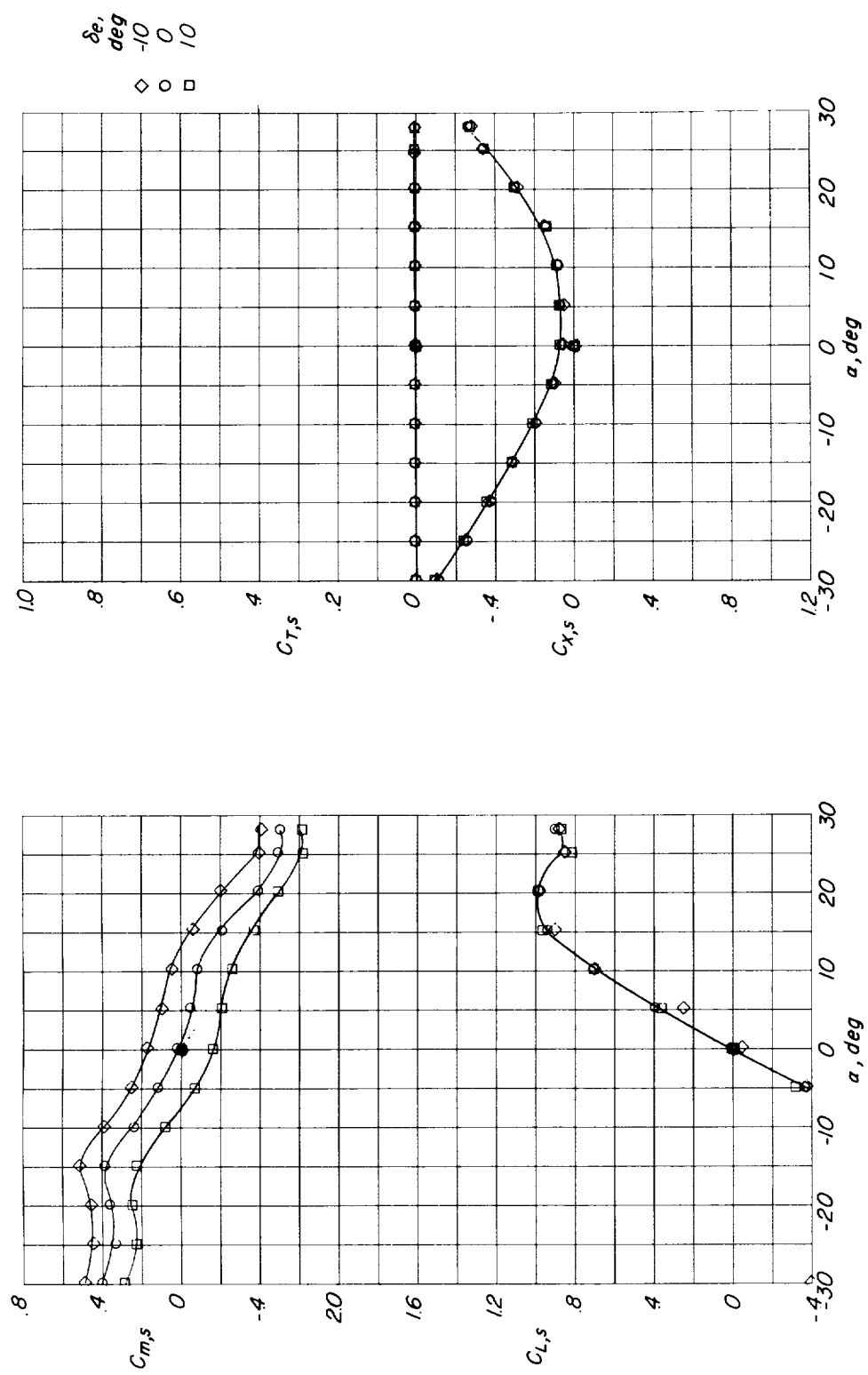

Figure 19.- Elevator effectiveness for basic configuration with power off. $i_w = 0^\circ$; $i_t = 0^\circ$.

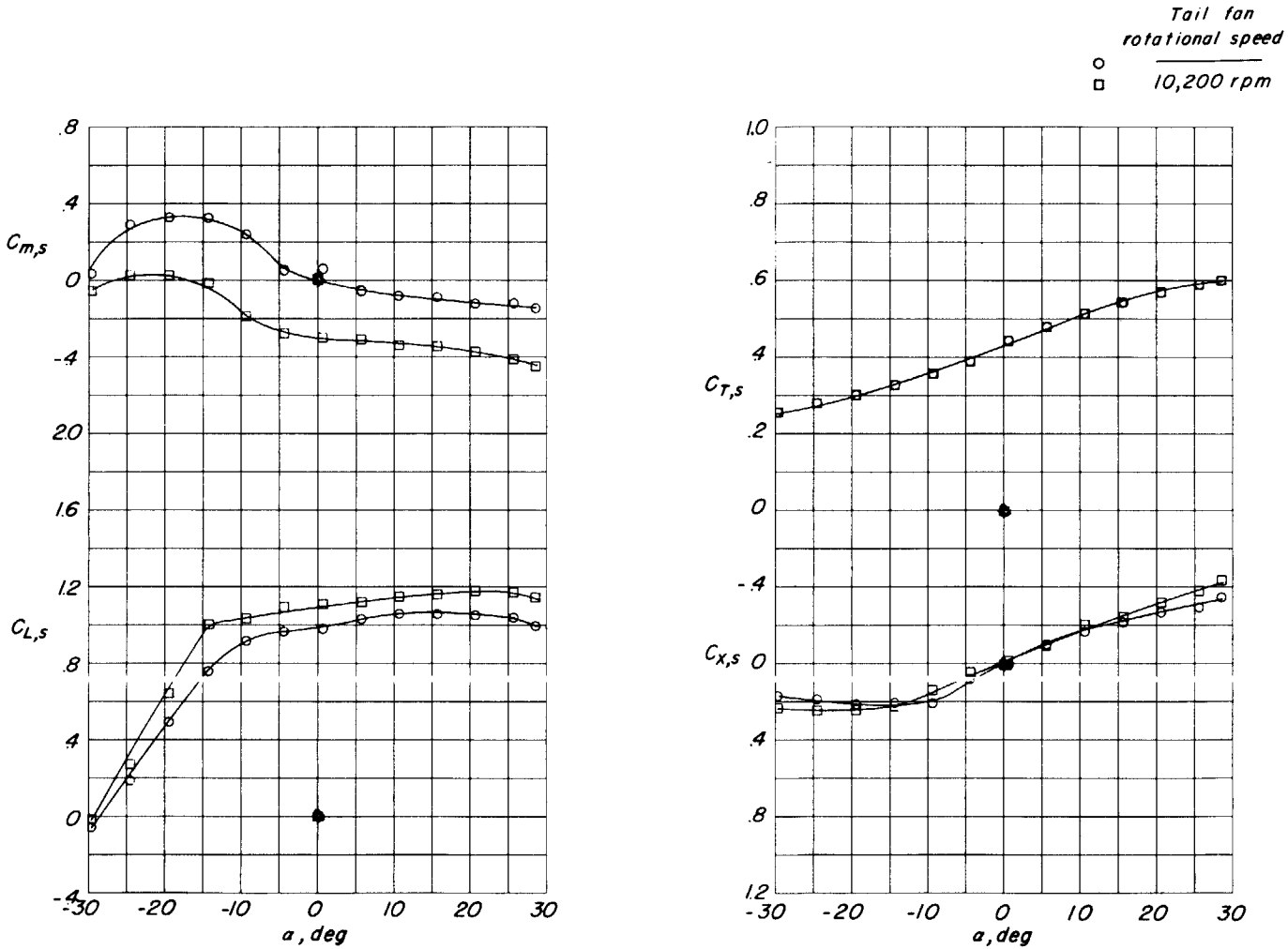

(a) Basic configuration; $i_w = 30^\circ$; $i_t = 9.2^\circ$.

Figure 20.- Tail-fan effectiveness for basic configuration.

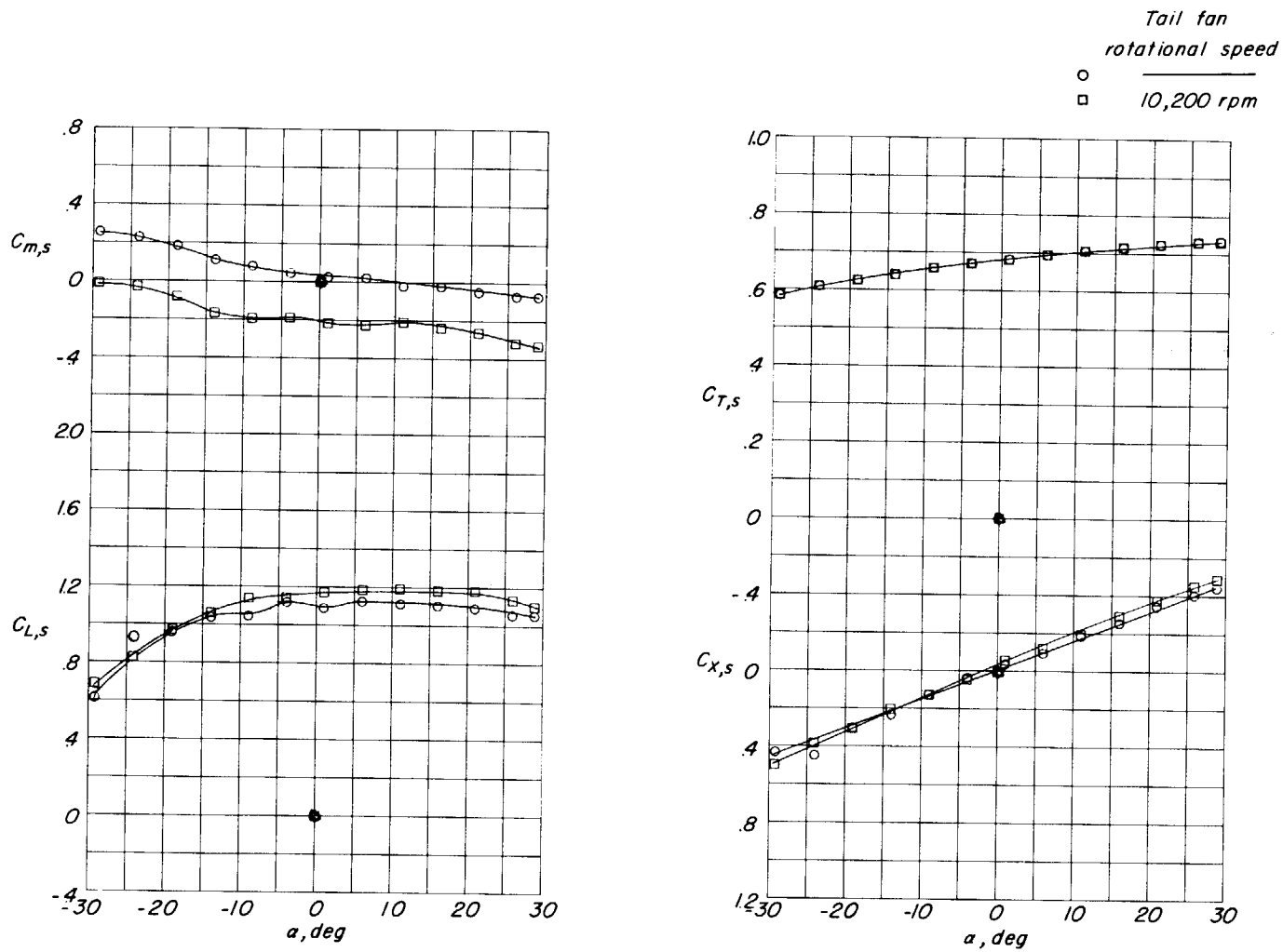

(b) Basic configuration; $i_w = 45^\circ$; $i_t = 19.2^\circ$.

Figure 20.- Continued.

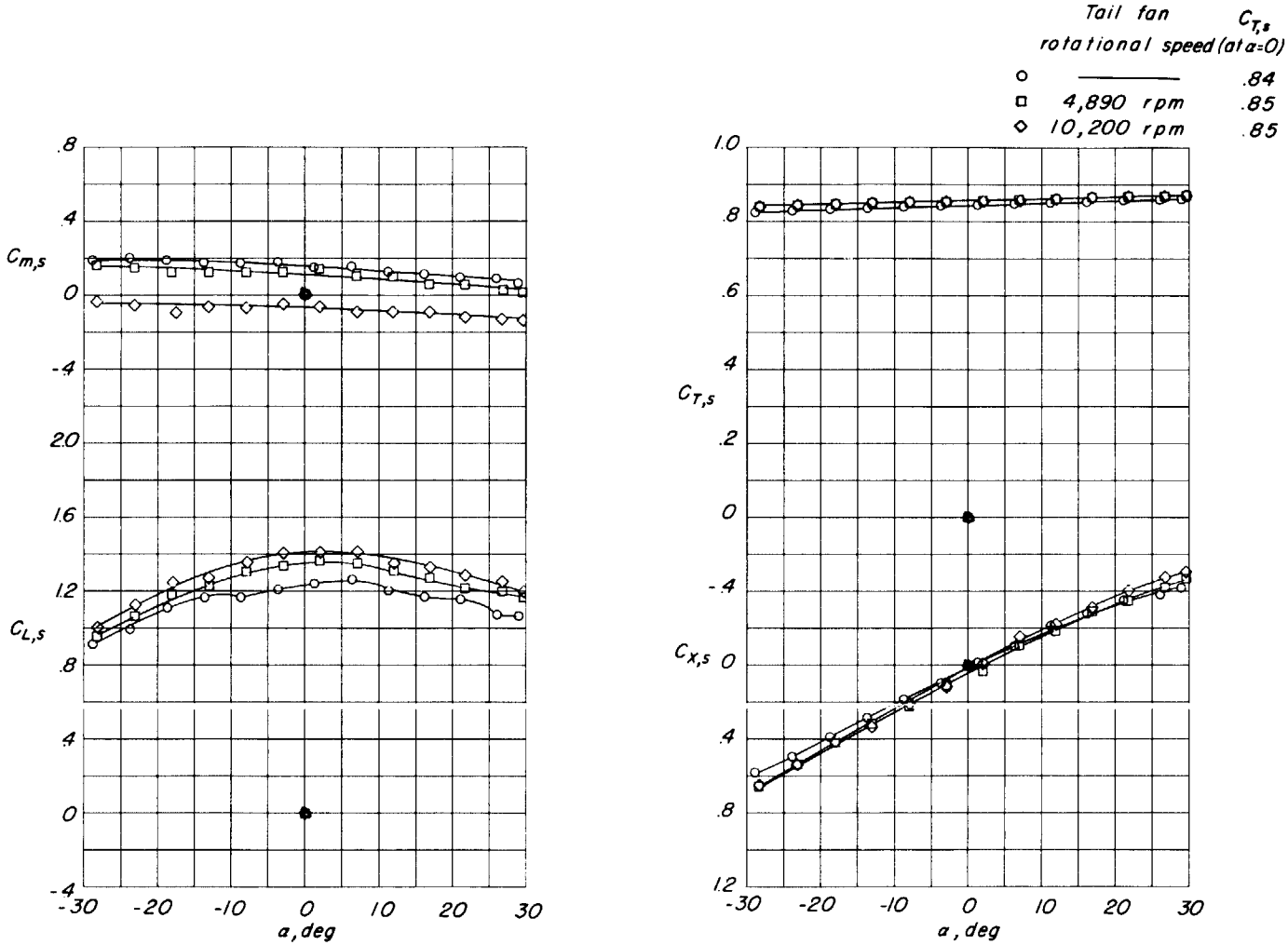

(c) Basic configuration; $i_w = 60^\circ$; $i_t = 30^\circ$.

Figure 20.- Continued.

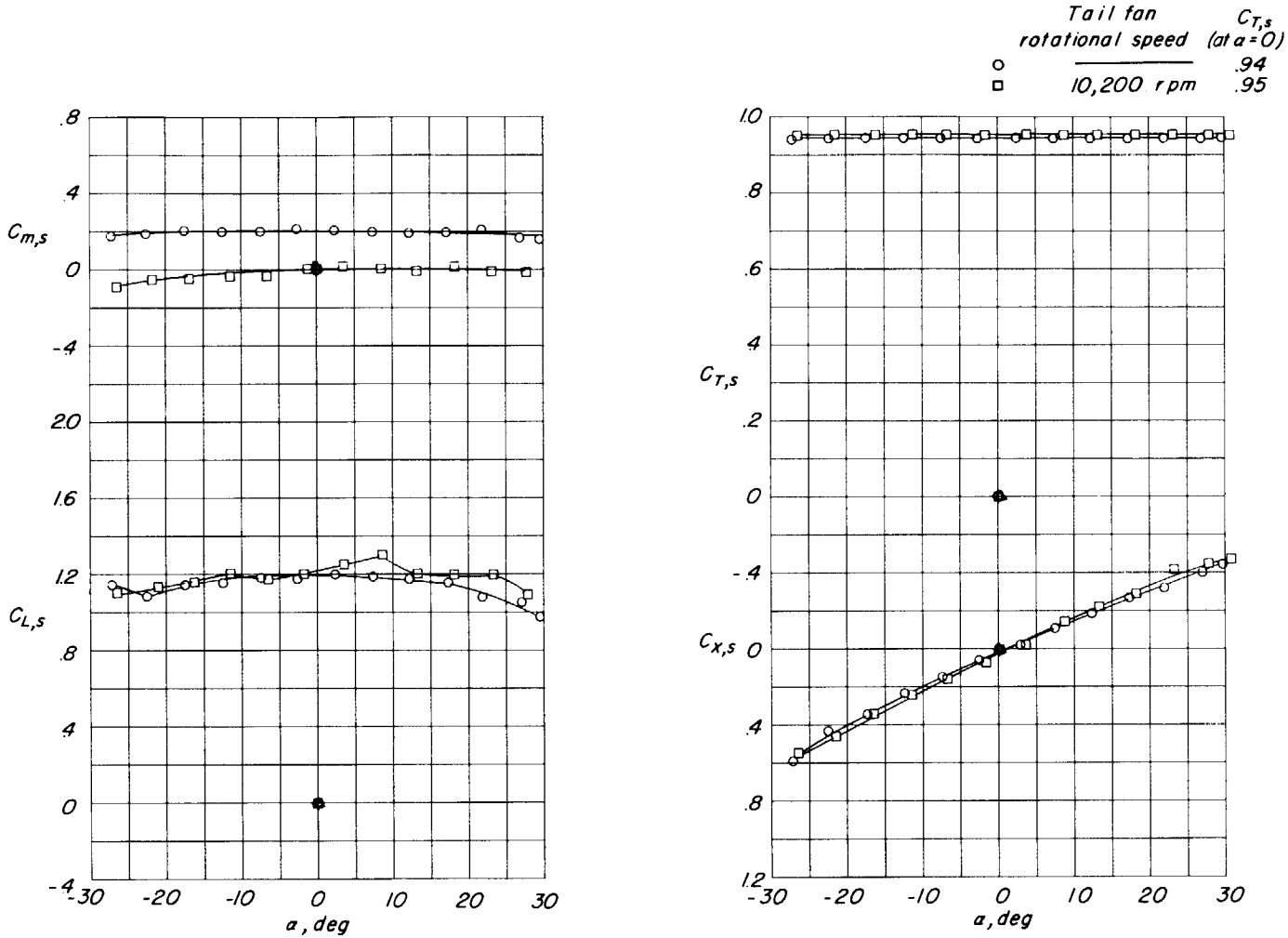

(d) Basic configuration; $i_w = 75^\circ$; $i_t = 30^\circ$.

Figure 20.- Concluded.

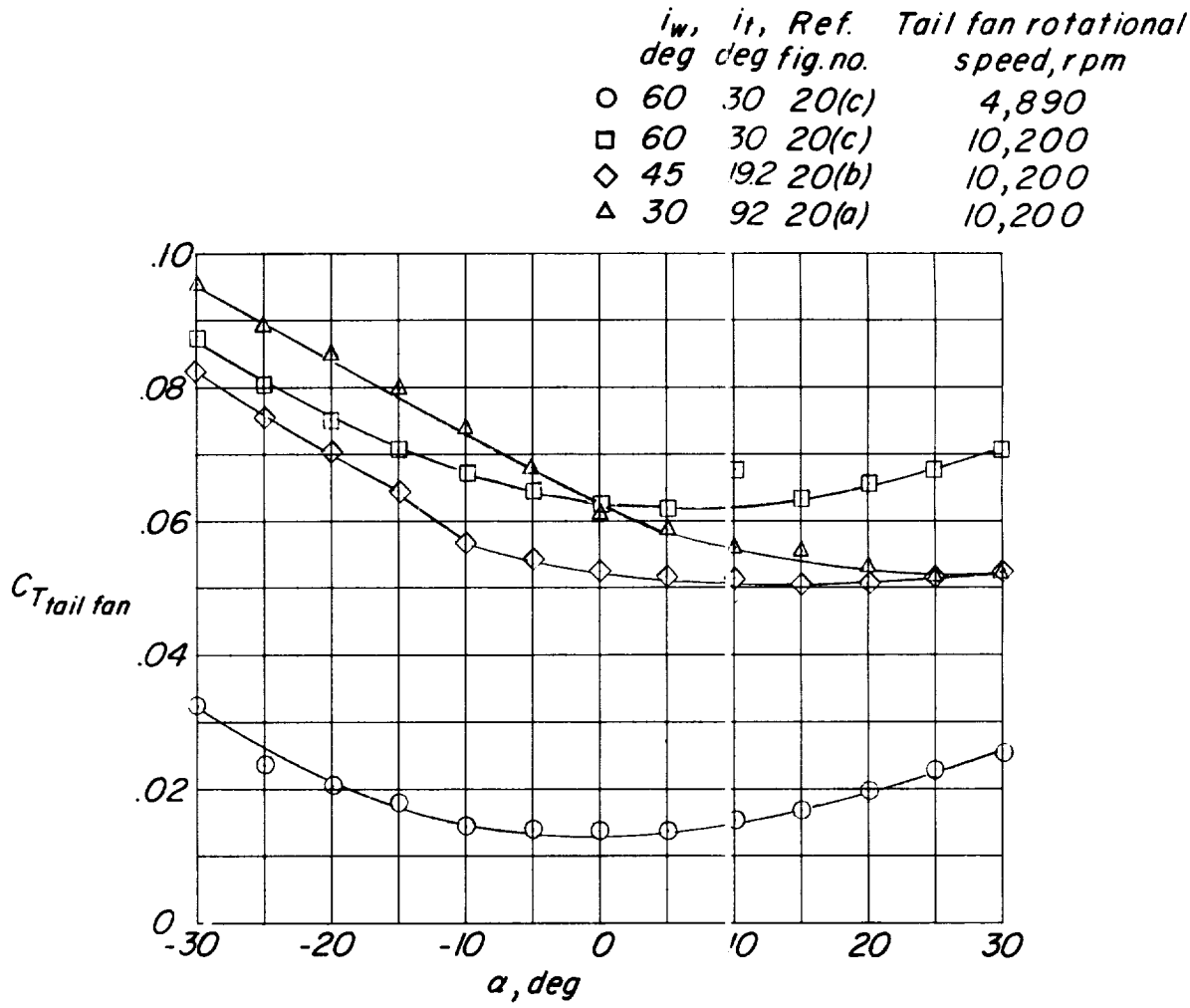

(a) Tail-fan thrust coefficients.

Figure 21.- Summary tail-fan effectiveness for basic configuration.

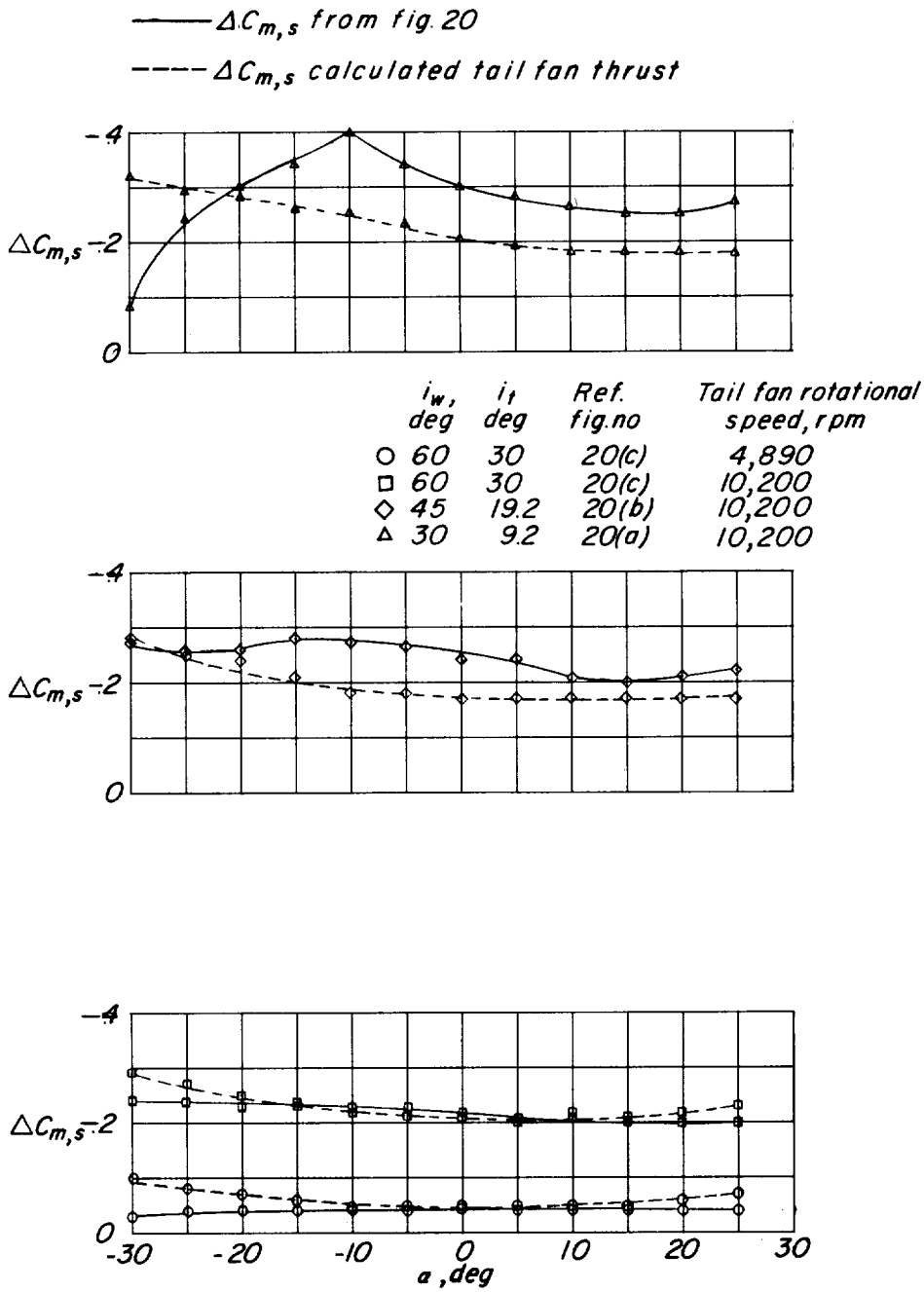

(b) Comparison of pitching-moment increments calculated from measured tail-fan thrust with measured increments in total model pitching moments from figure 20.

Figure 21.- Concluded.

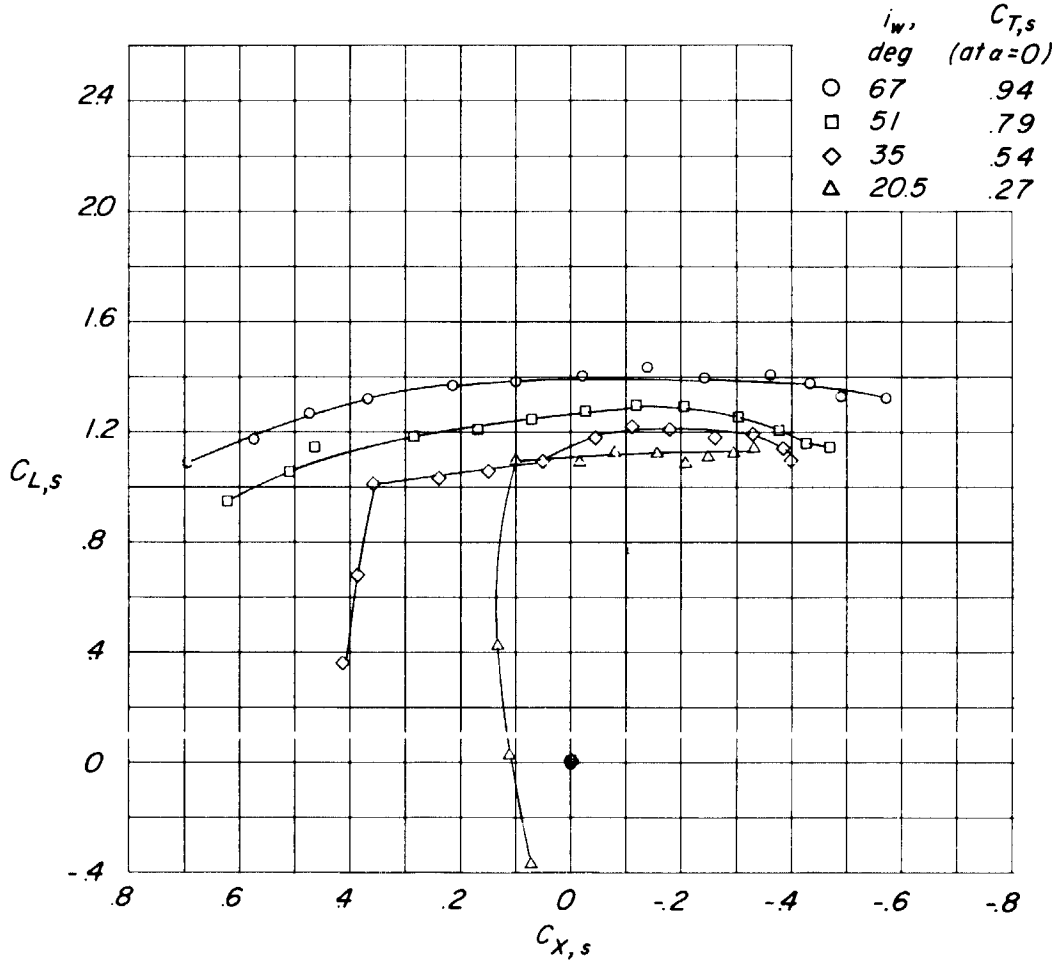

(a) Wing extensions on (coefficients based on area of short-span wing).

Figure 22.- Effect of wing extension for basic configuration for several thrust coefficients and wing tilt angles.

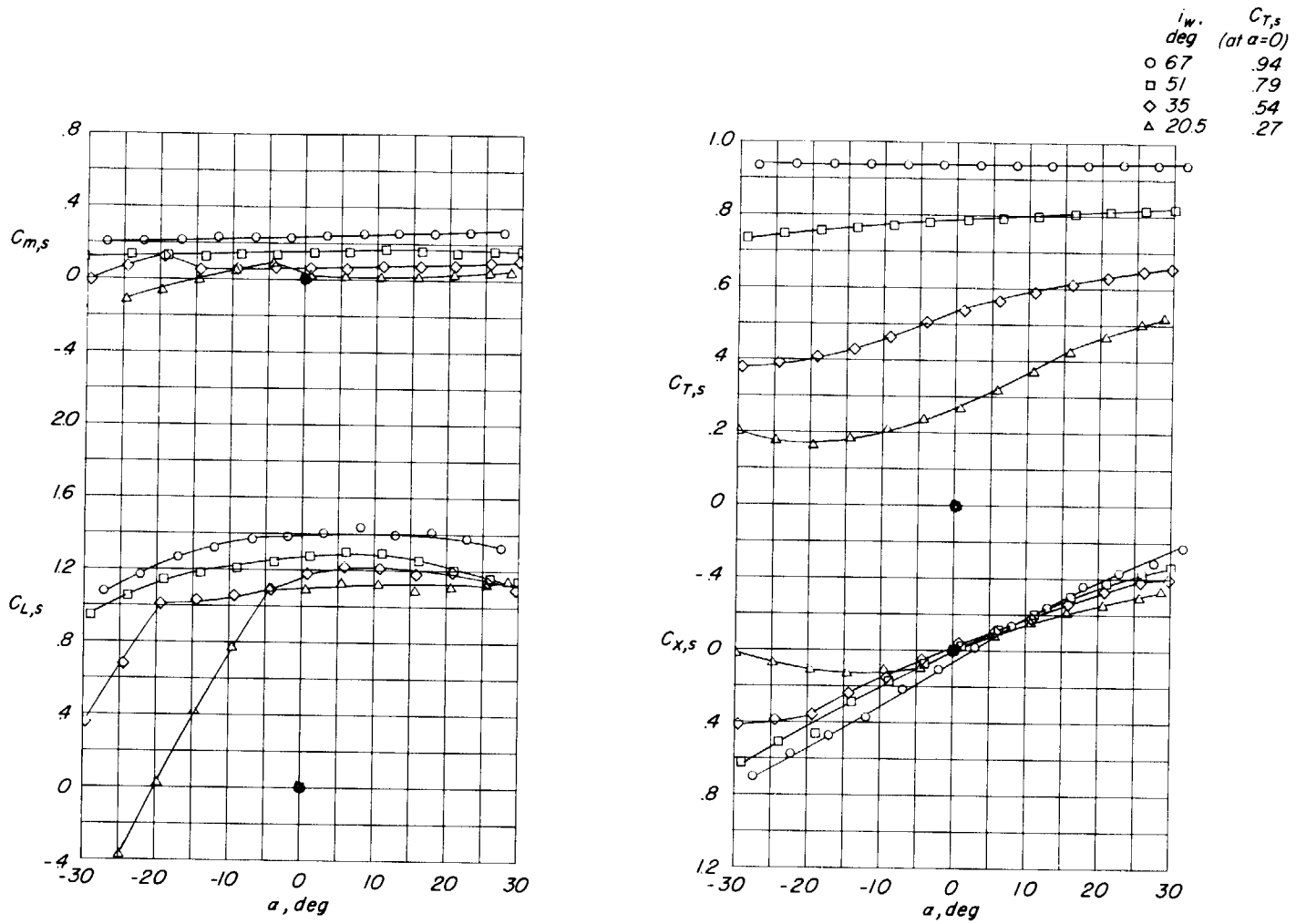

(a) Concluded. (Coefficients based on area of short-span wing.)

Figure 22.- Continued.

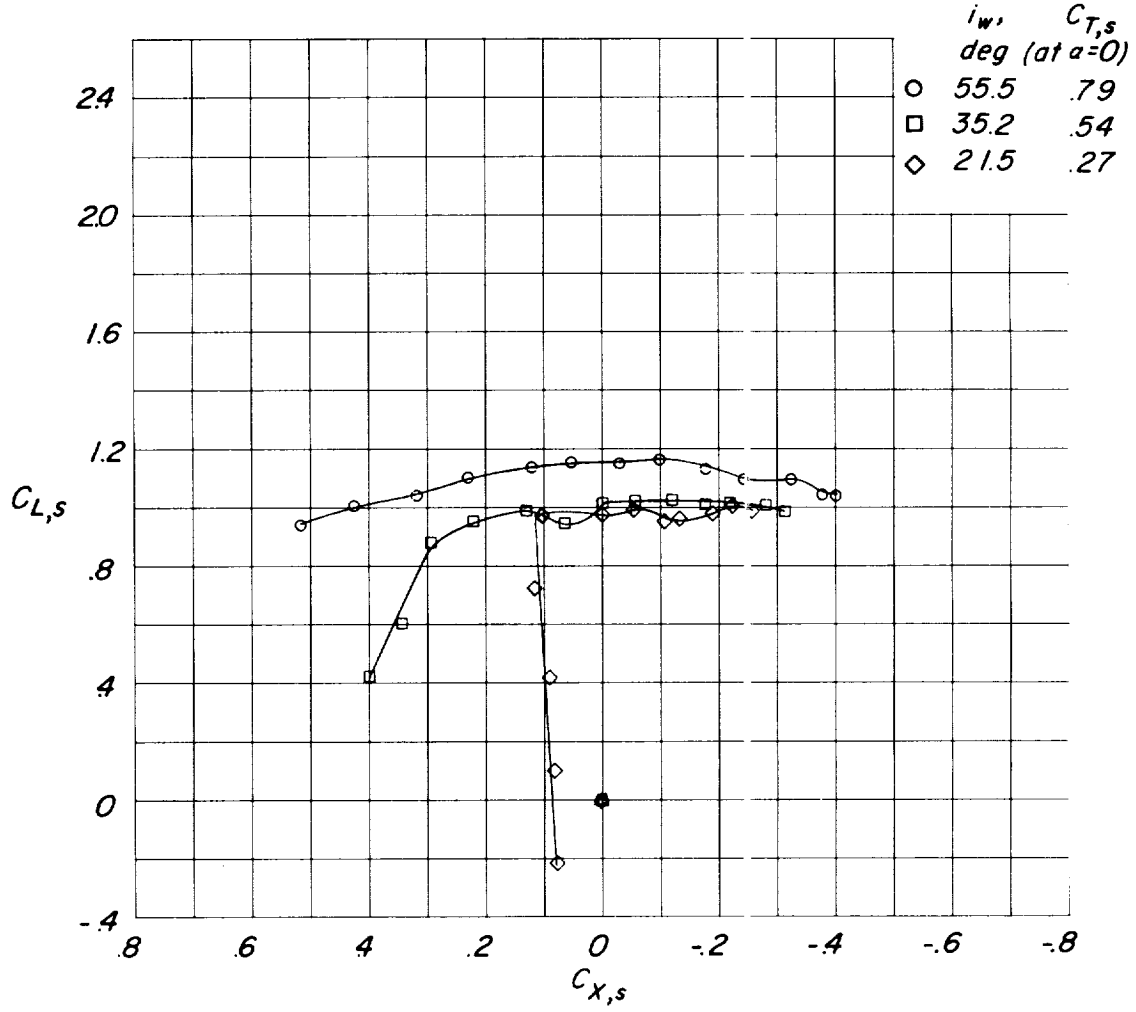

(b) Wing extension off (coefficients based on area of short-span wing).

Figure 22.- Continued.

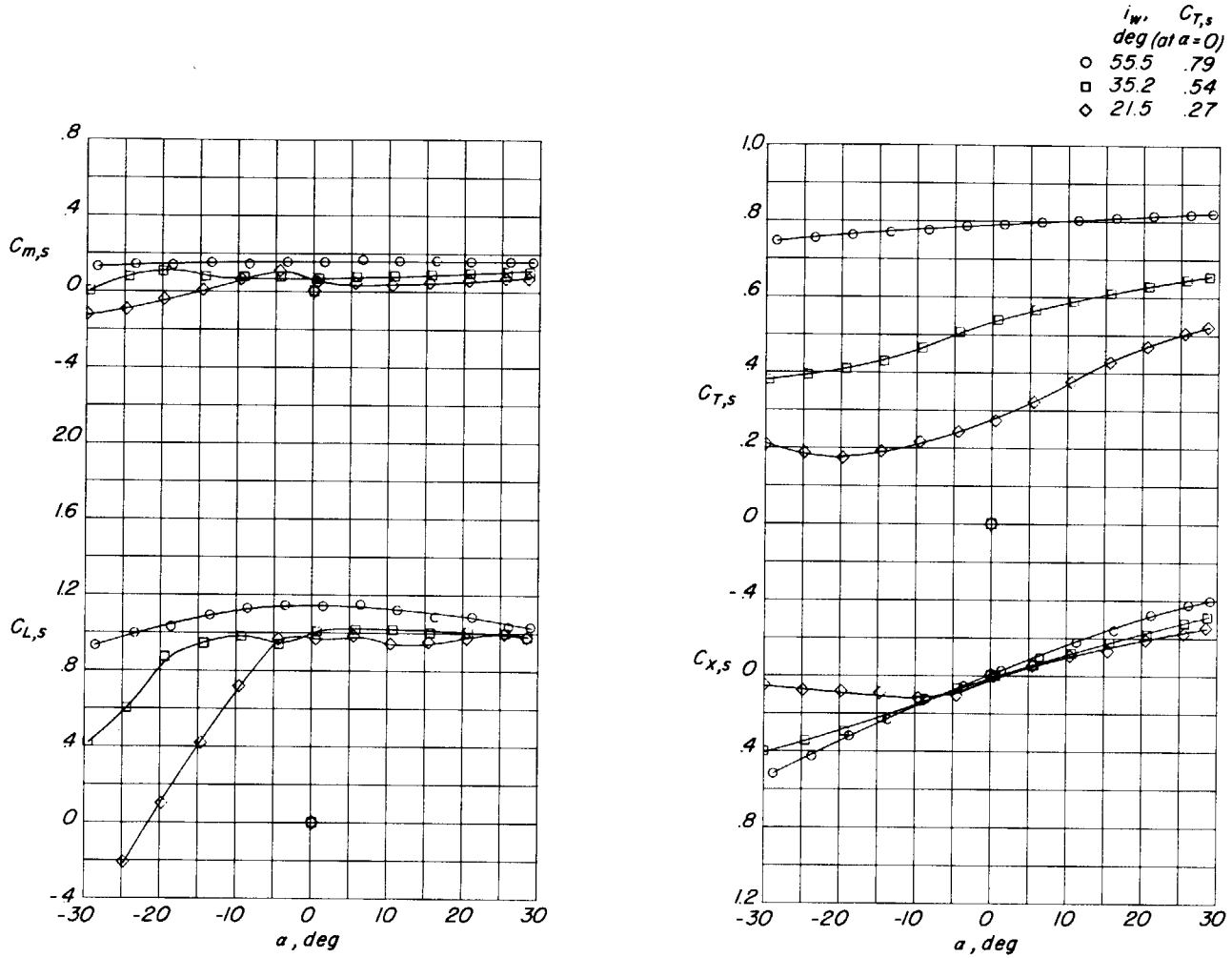

(b) Concluded. (Coefficients based on area of short-span wing.)

Figure 22.- Concluded.

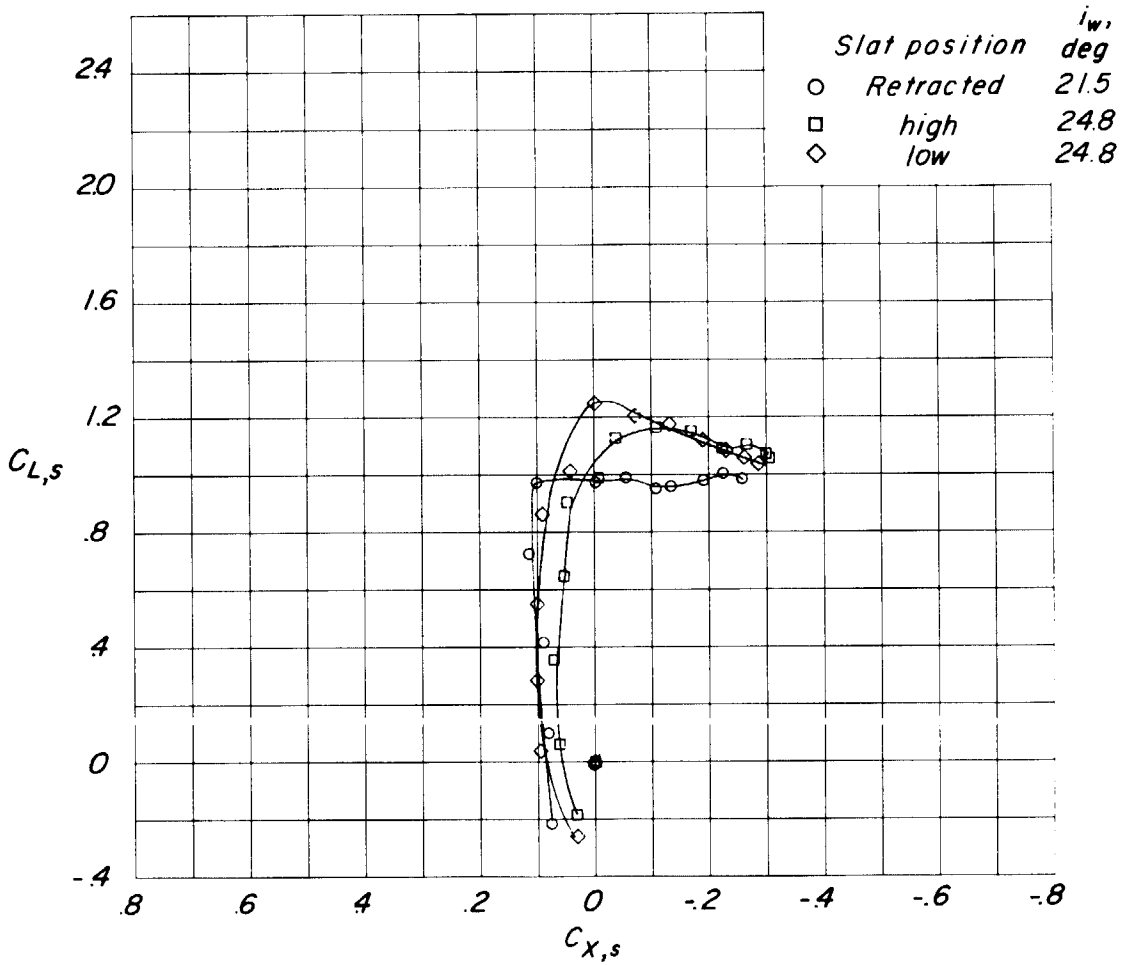

(a) Basic configuration; $i_w \approx 24^o$.

Figure 23.- Slat effectiveness for basic configuration for several thrust coefficients and wing tilt angles.

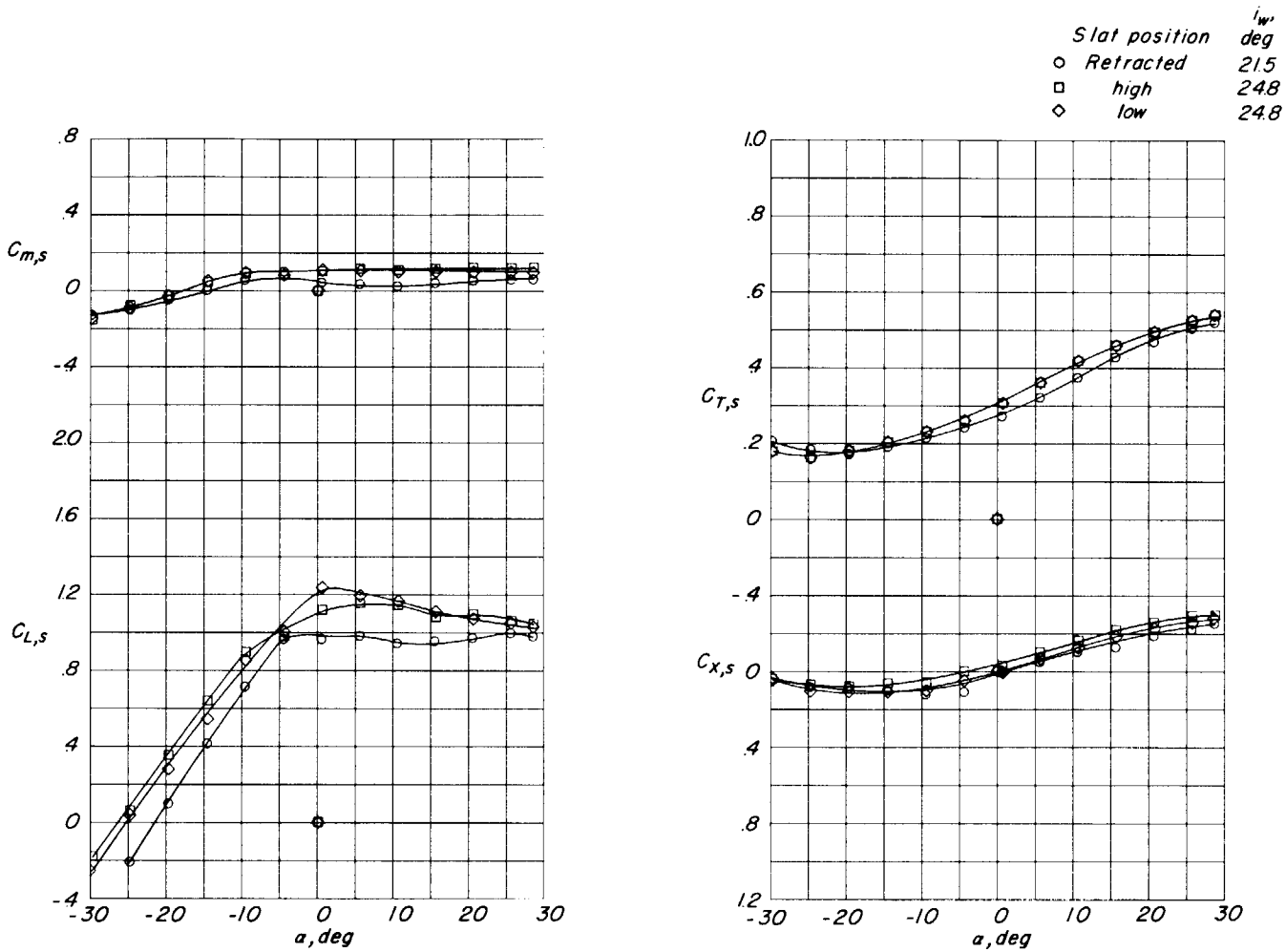

(a) Concluded.

Figure 23.- Continued.

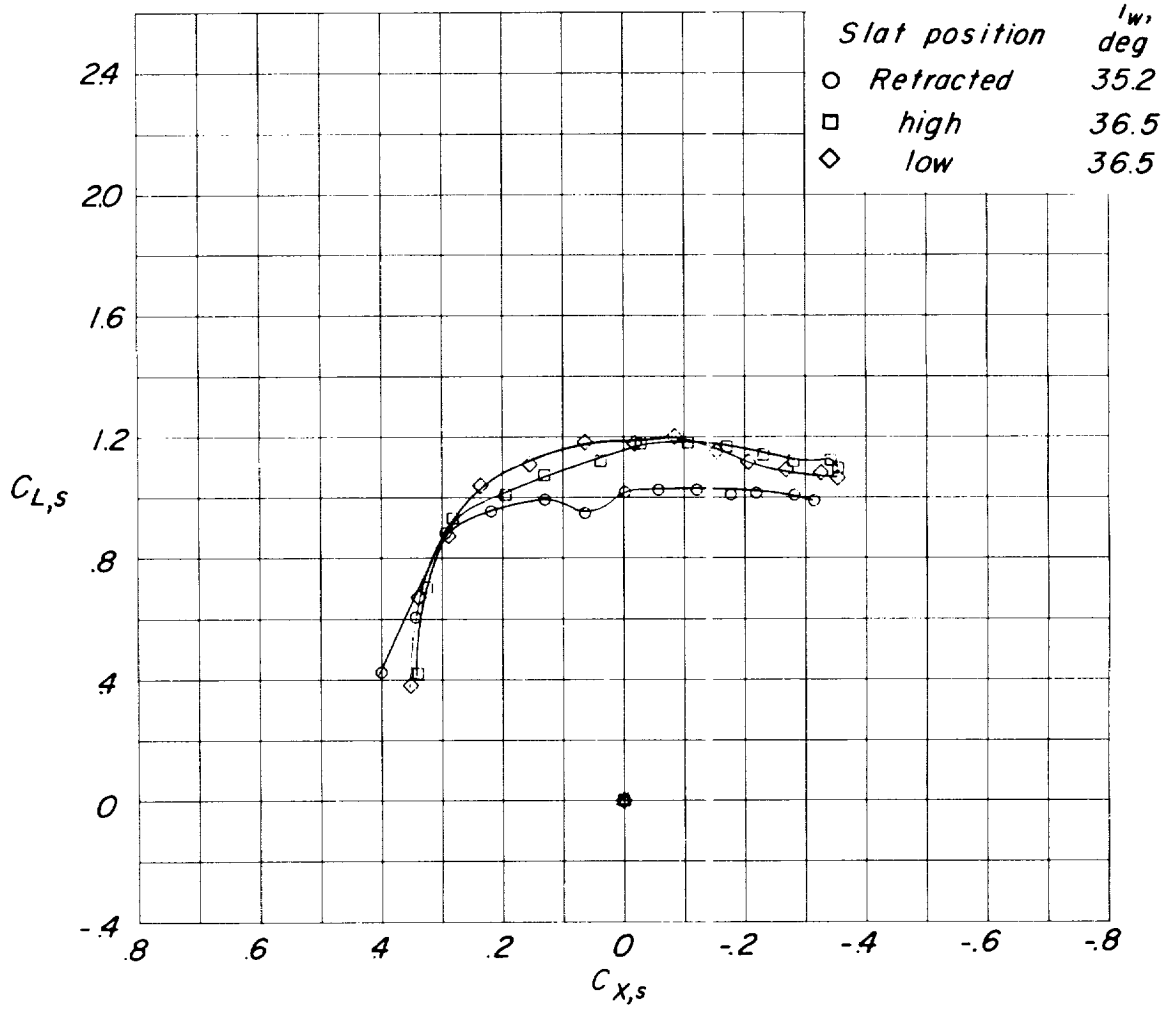

(b) Basic configuration; $i_w \approx 36°$.

Figure 23.- Continued.

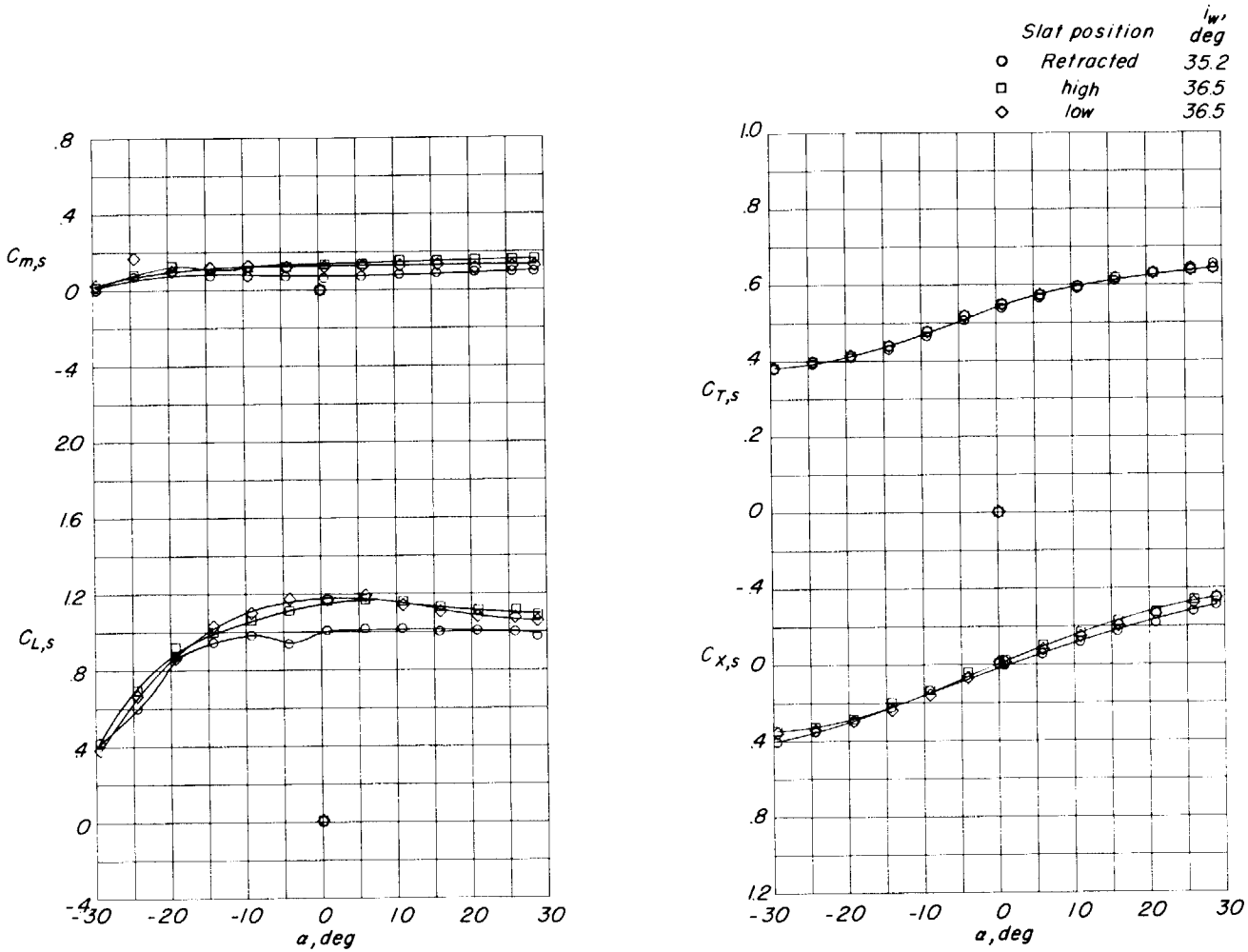

(b) Concluded.

Figure 23.- Continued.

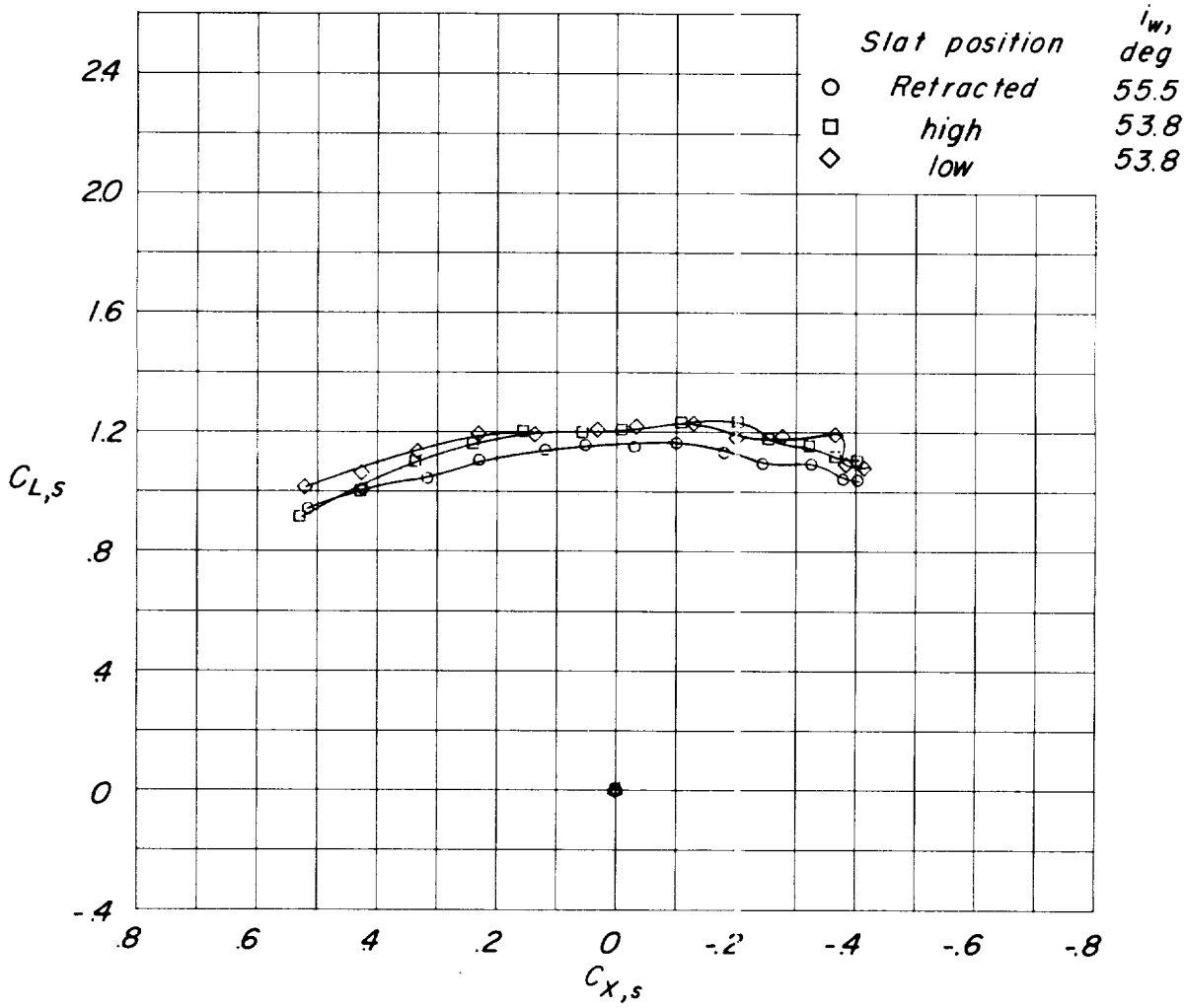

(c) Basic configuration $i_w \approx 55°$.

Figure 23.- Continued.

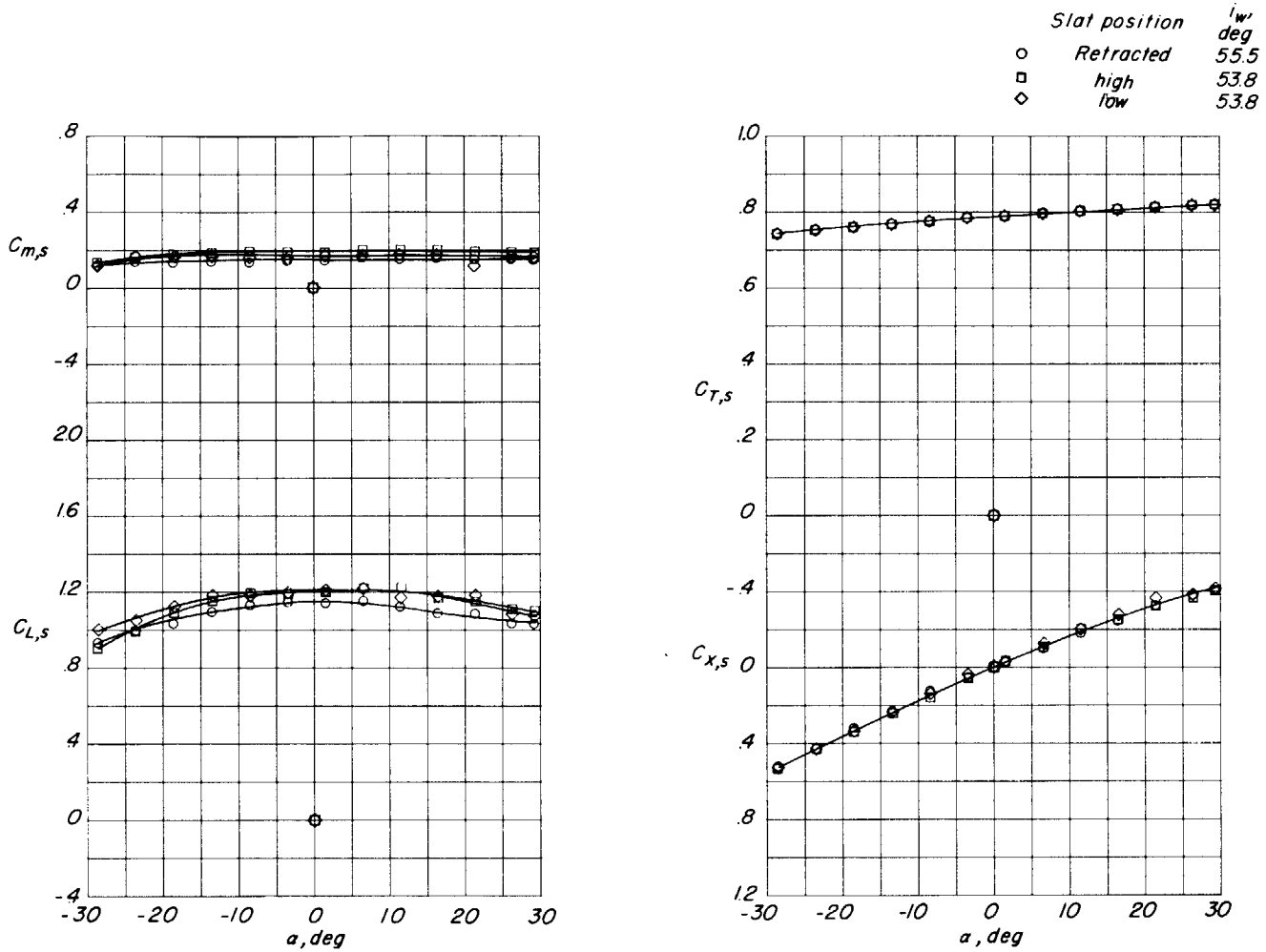

(c) Concluded.

Figure 23.- Concluded.

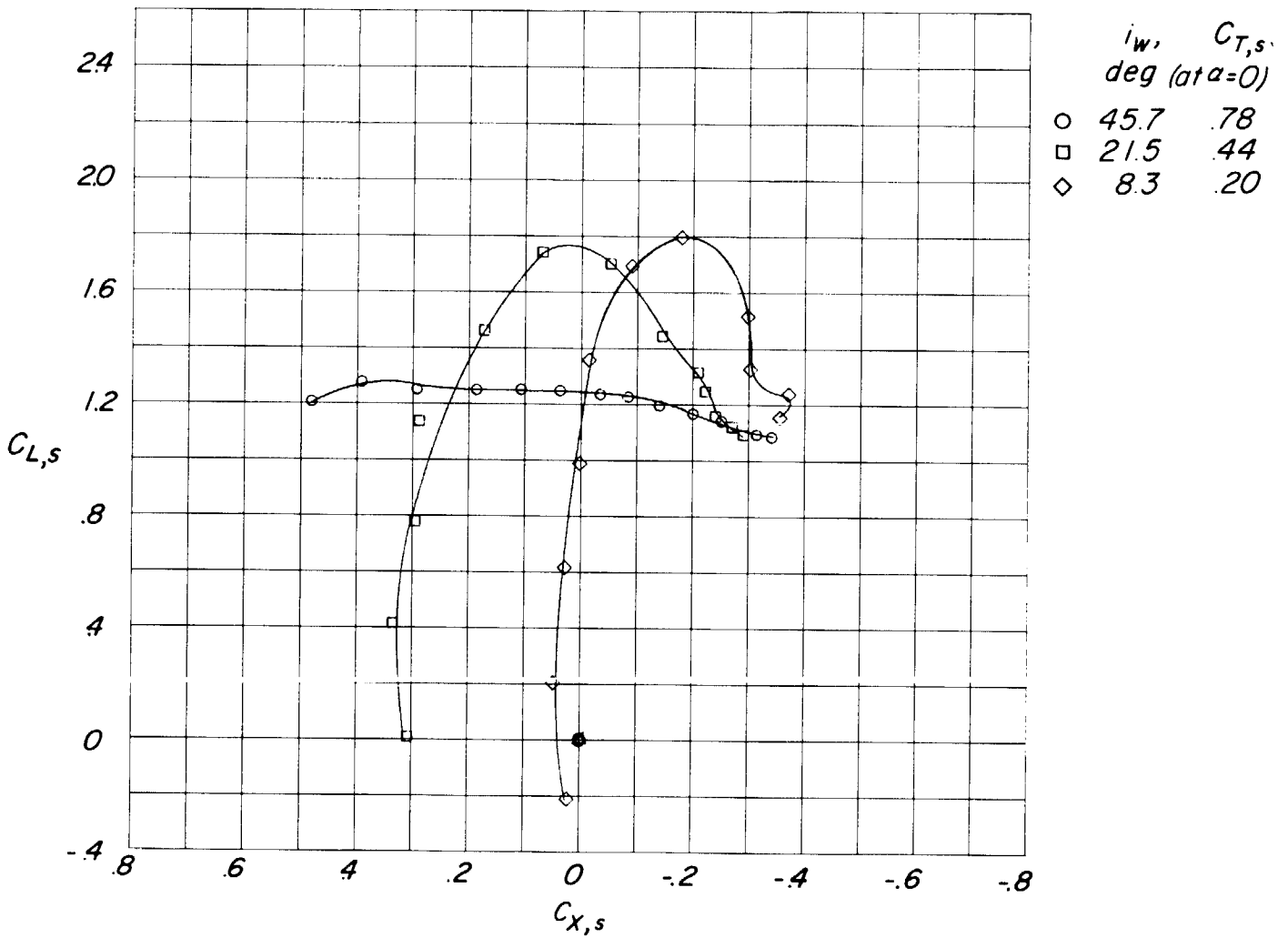

Figure 24.- Effect of thrust coefficient and wing tilt angle for basic configuration with flaps deflected 50°.

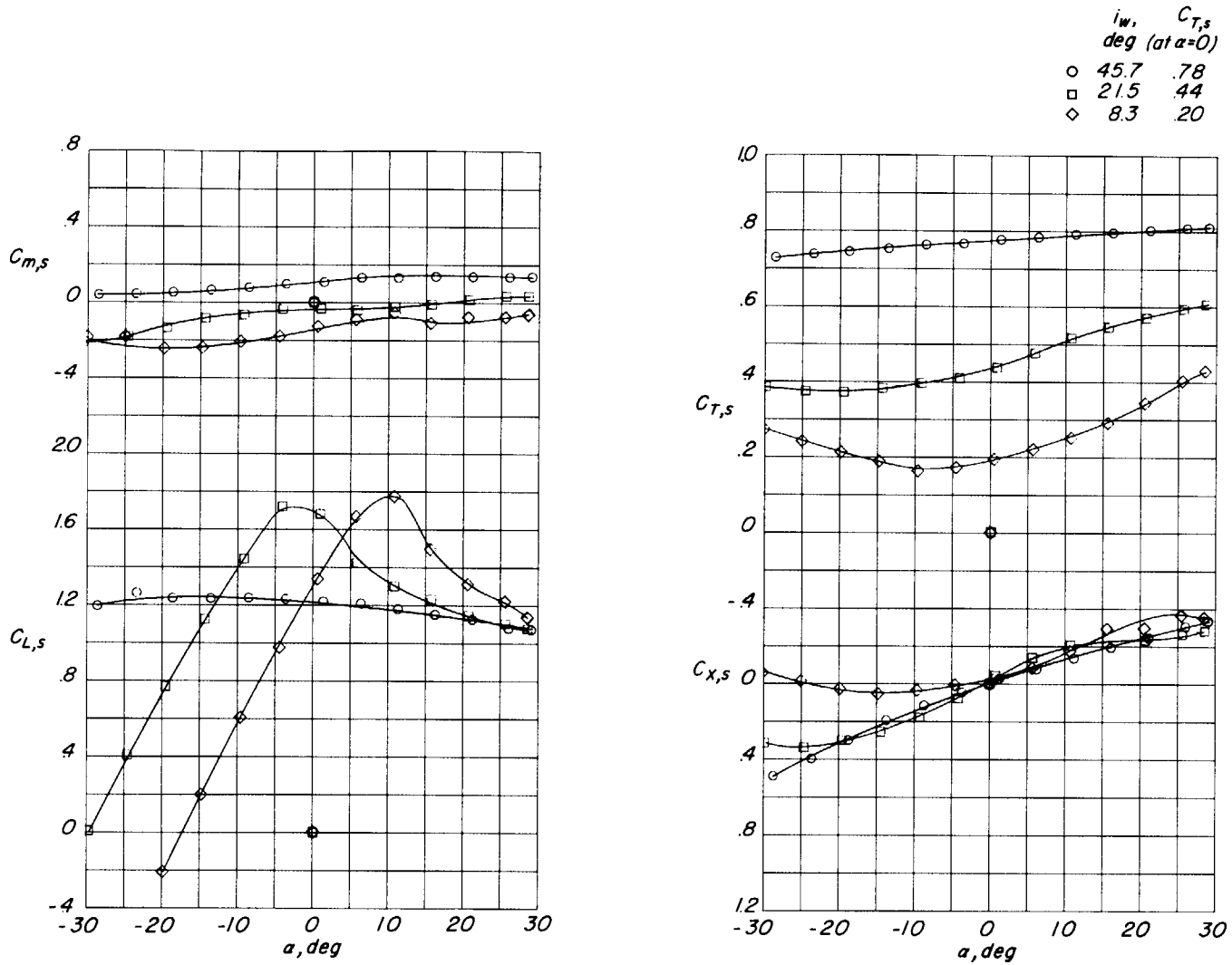

Figure 24.- Concluded.

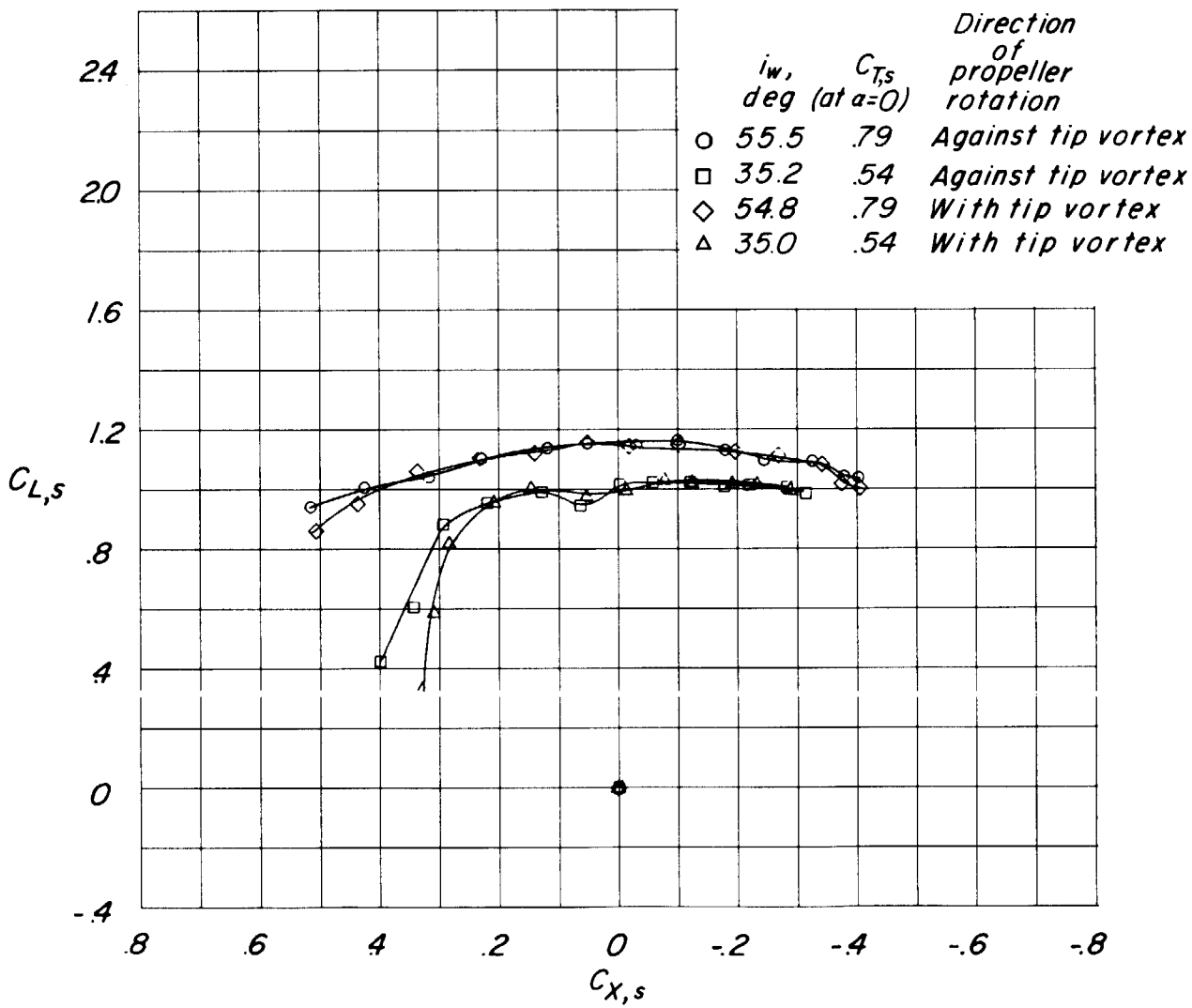

Figure 25.- Effect of direction of propeller rotation for basic configuration with tail off.

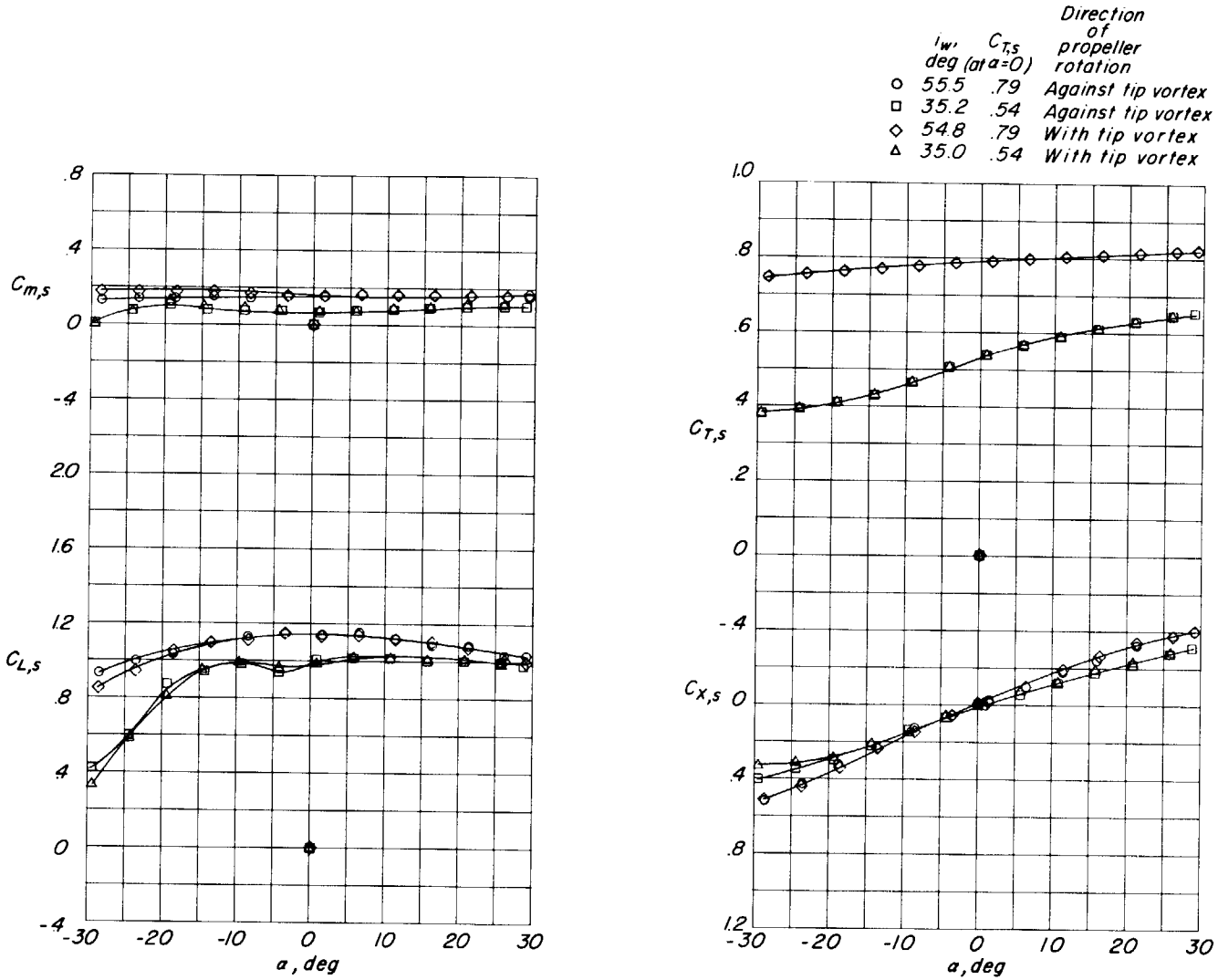

Figure 25.- Concluded.

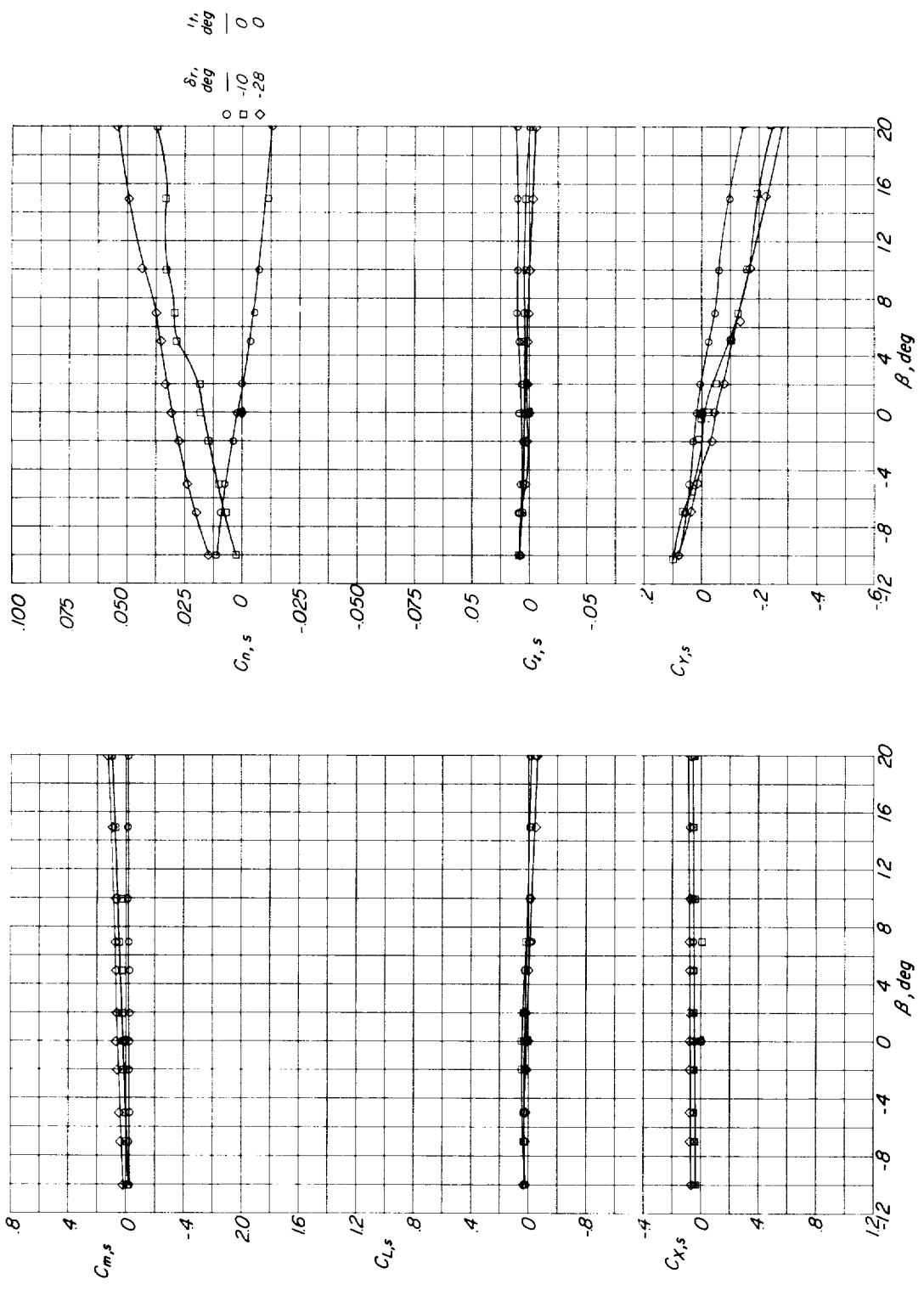

Figure 26.- Effect of rudder deflection for basic configuration with power off. $i_w = 0^\circ$; $\alpha = 0^\circ$.

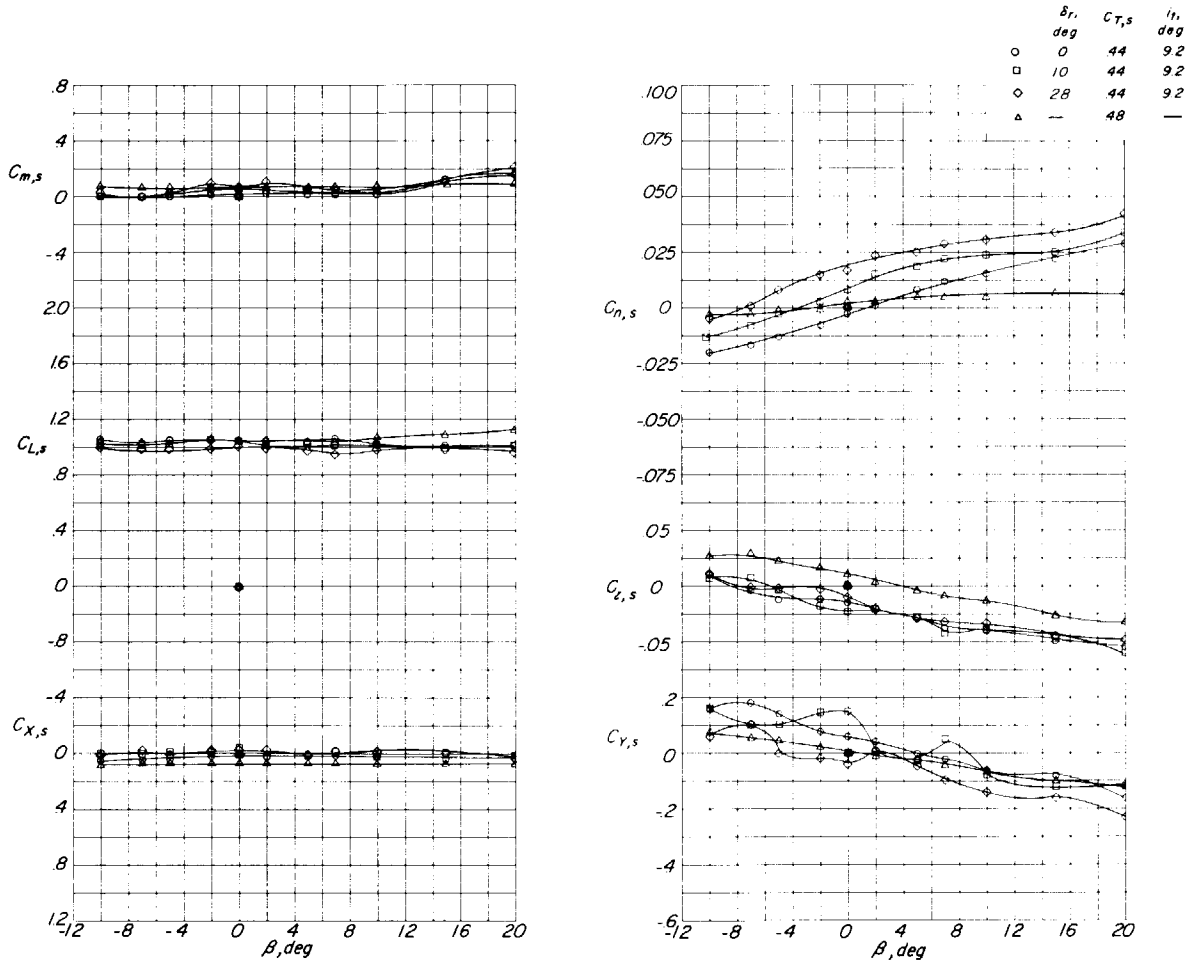

(a) Basic configuration; $i_w = 30^\circ$.

Figure 27.- Effect of rudder deflection for basic configuration for several thrust coefficients and wing tilt angles. $\alpha = 0^\circ$.

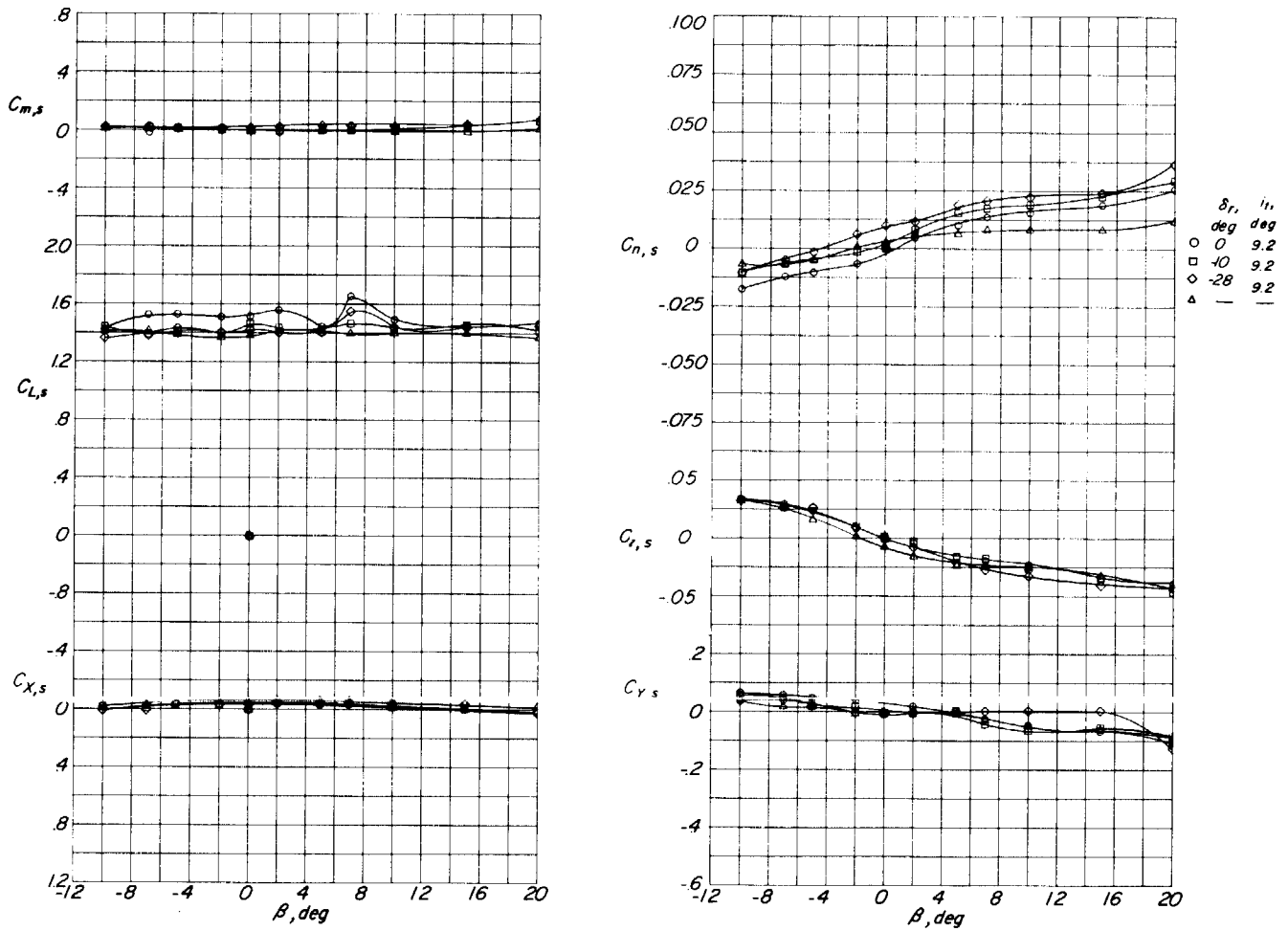

(a) Flapped configuration; $i_w = 30^\circ$; $C_{T,s} = 0.66$.

Figure 28.- Effect of rudder deflection for flapped configuration for several thrust coefficients and wing tilt angles. $\alpha = 0^\circ$.

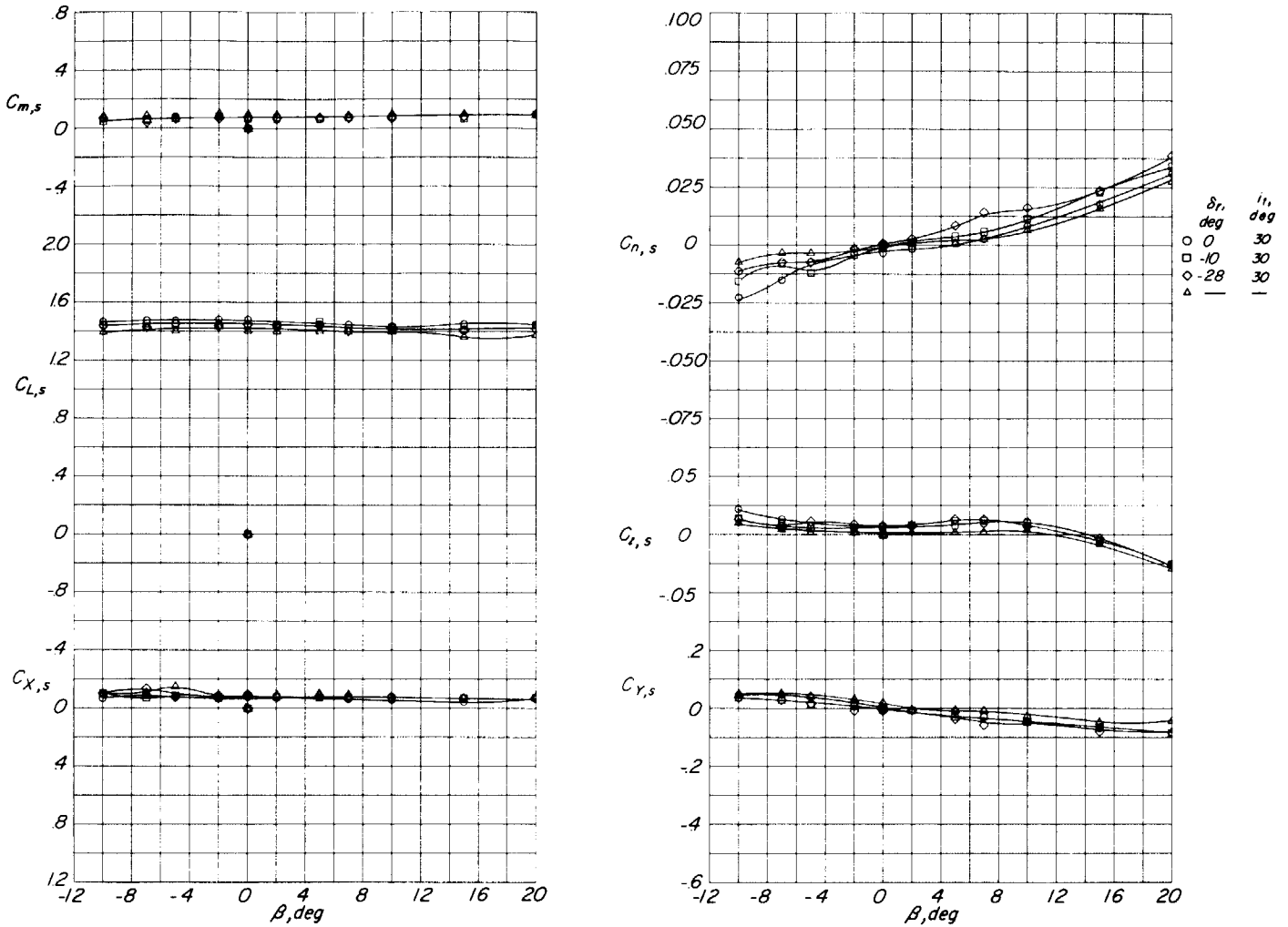

(b) Flapped configuration; $i_w = 45^\circ$; $C_{T,s} = 0.80$.

Figure 28.- Concluded.

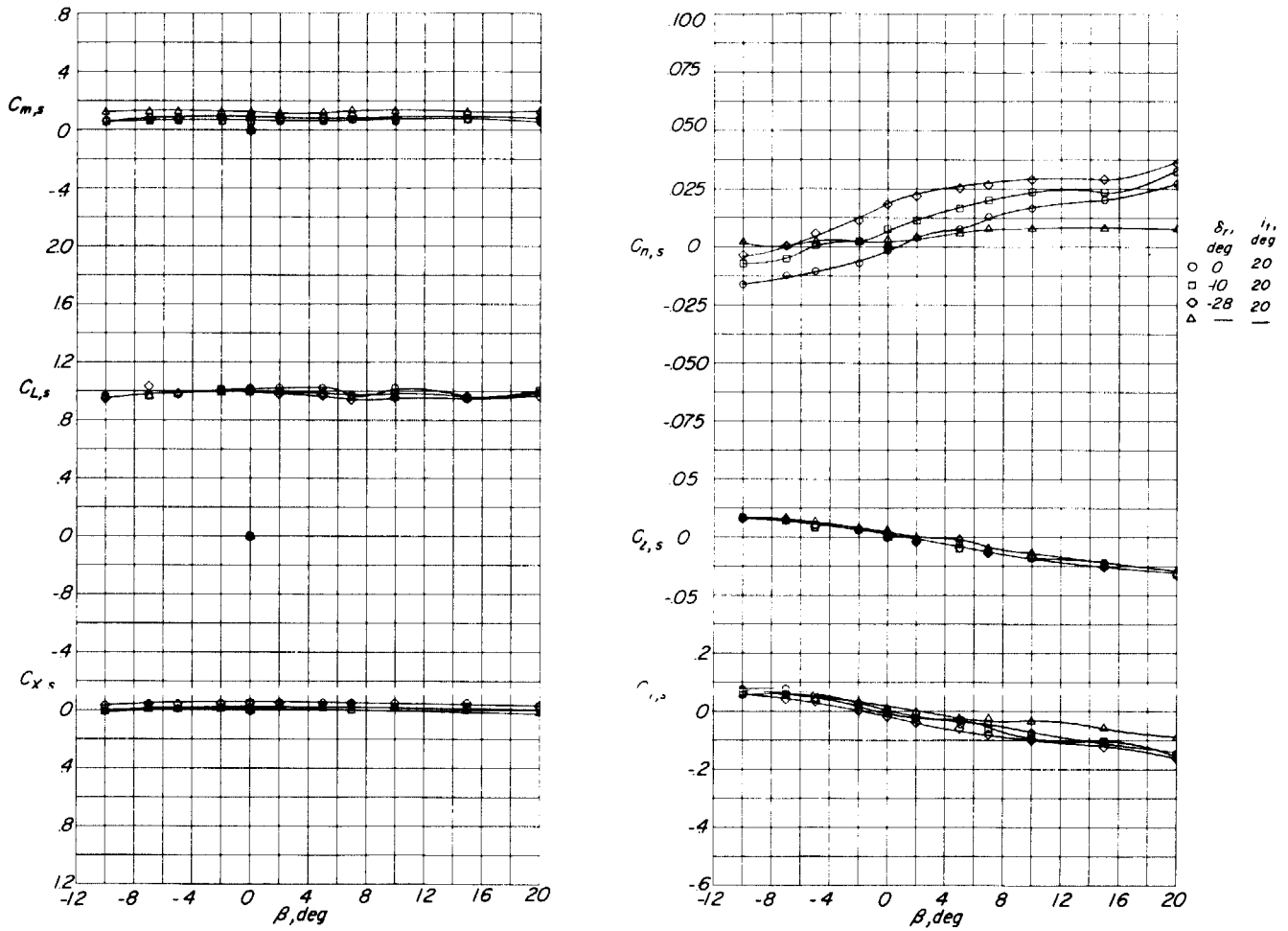

(a) Speed-brake configuration; $i_w = 30^\circ$; $C_{T,s} = 0.53$.

Figure 29.- Effect of rudder deflection for speed-brake configuration for several thrust coefficients and wing tilt angles. $\alpha = 0^\circ$.

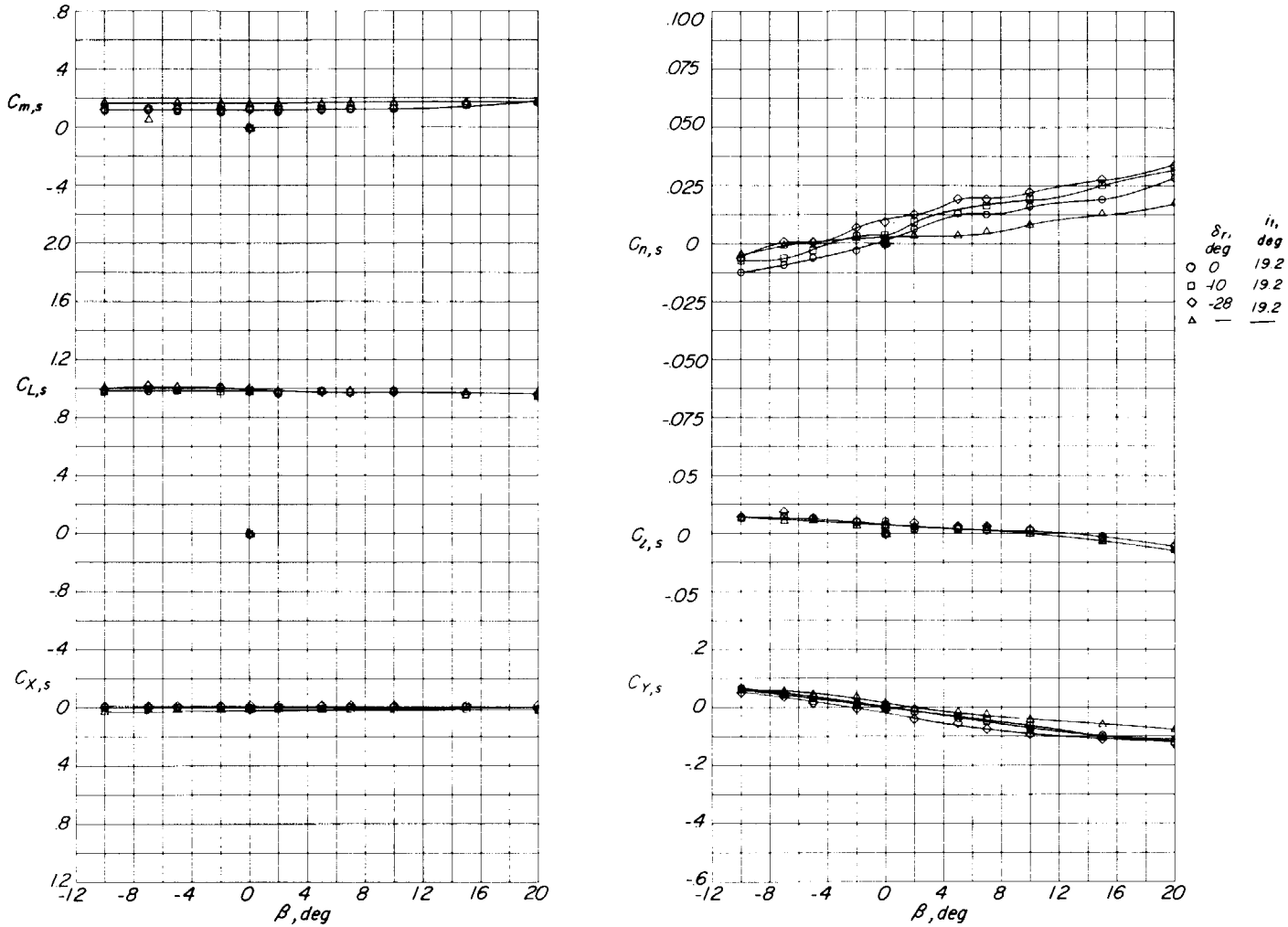

(b) Speed-brake configuration; $i_w = 45^\circ$; $C_{T,s} = 0.71$.

Figure 29.- Concluded.

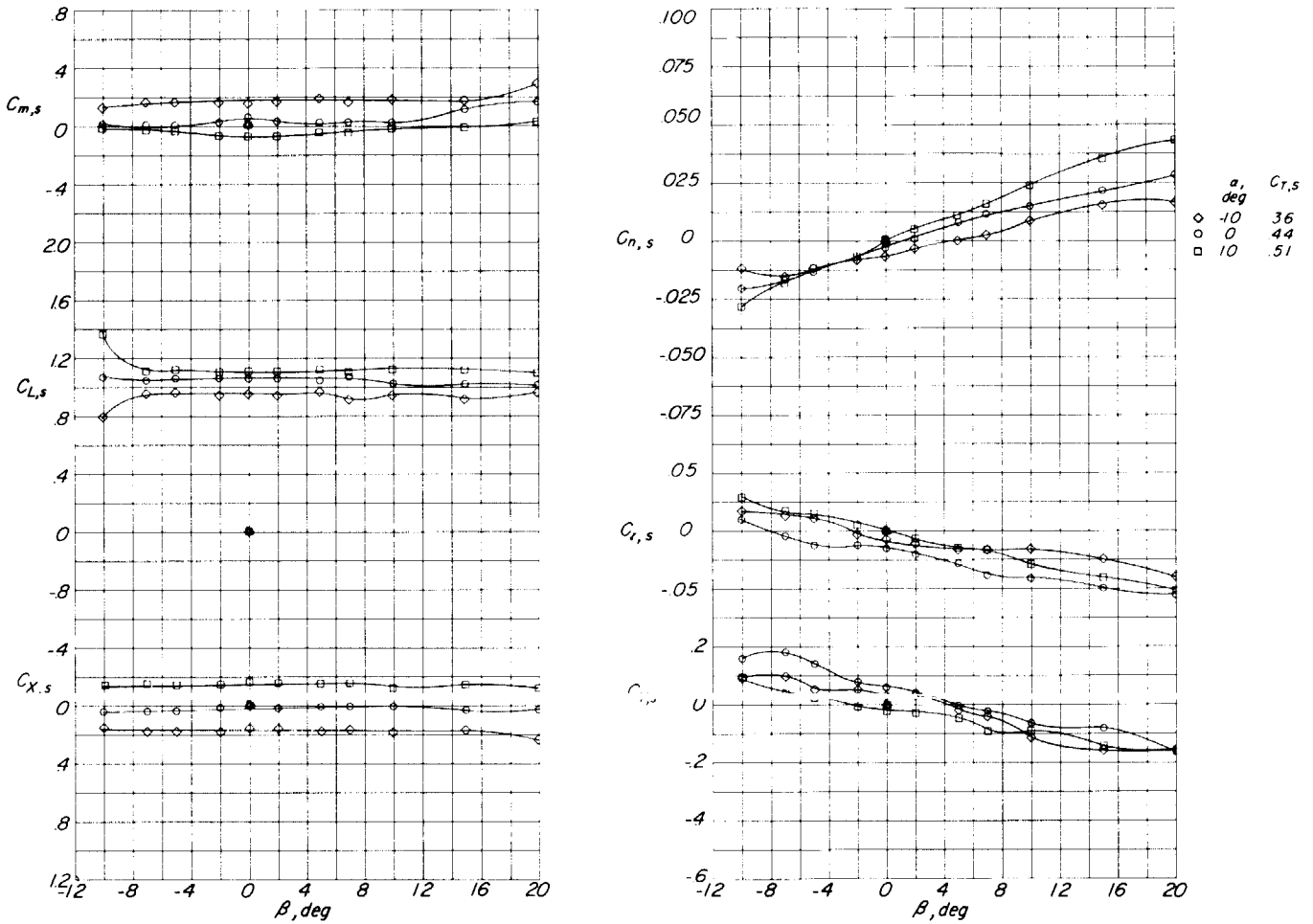

(a) Basic configuration; $i_w = 30^\circ$; $i_t = 9.2^\circ$.

Figure 30.- Effect of angle of attack and thrust coefficient on lateral stability characteristics of basic configuration.

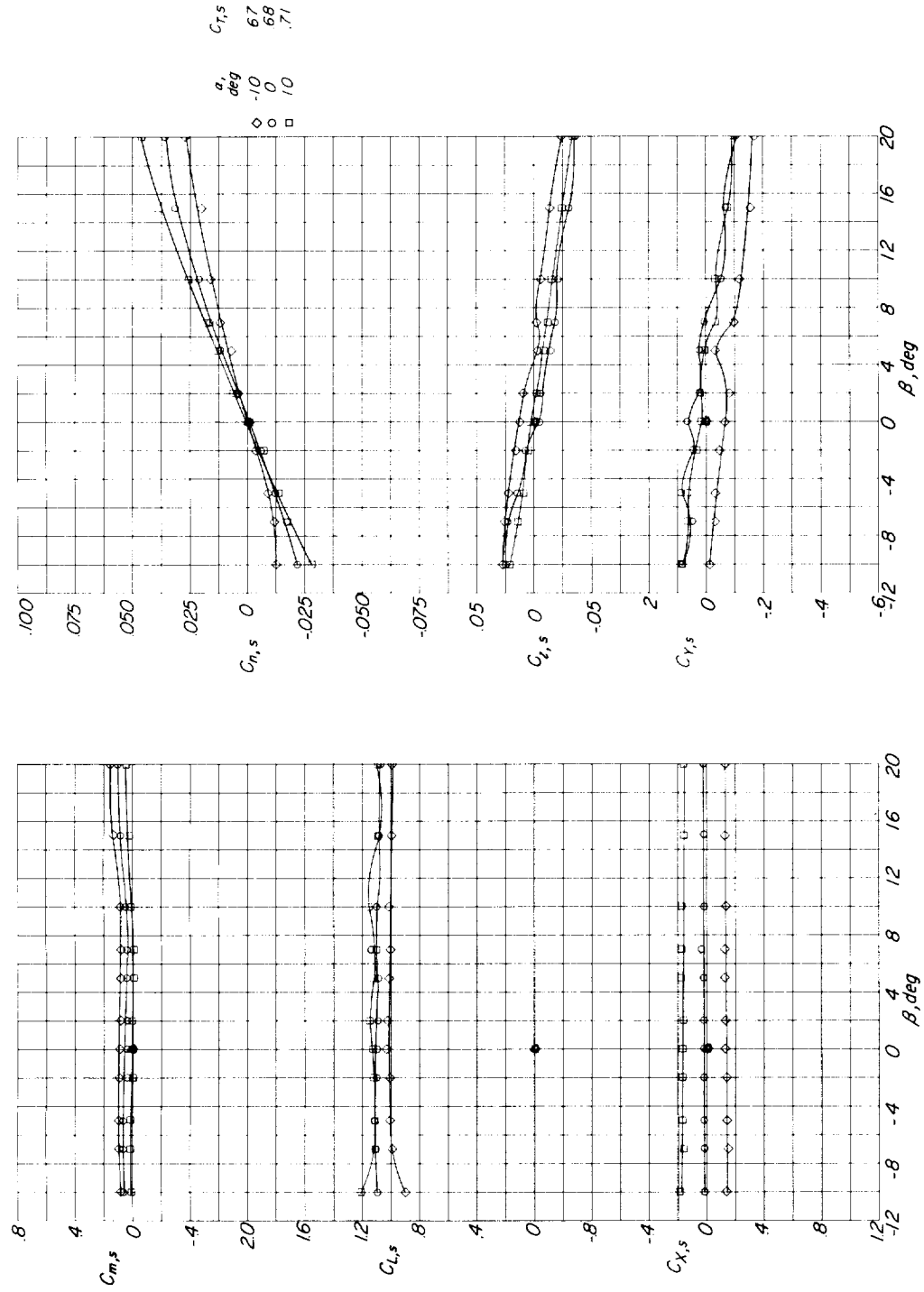

(b) Basic configuration; $i_w = 45^\circ$; $i_t = 19.2^\circ$.

Figure 30.- Continued.

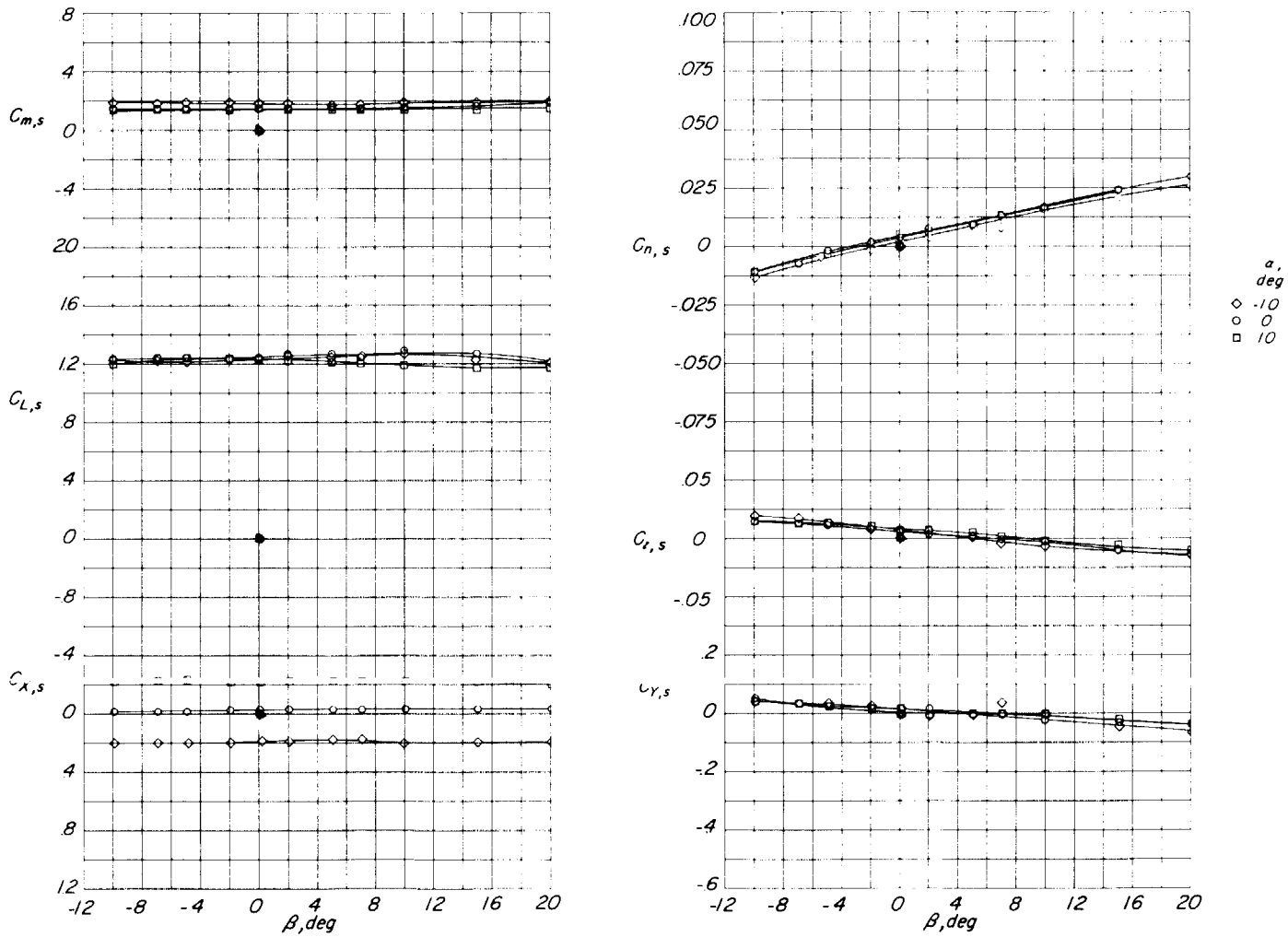

(c) Basic configuration; $i_w = 60^\circ$; $C_{T,s} = 0.84$; $i_t = 30^\circ$.

Figure 30.- Continued.

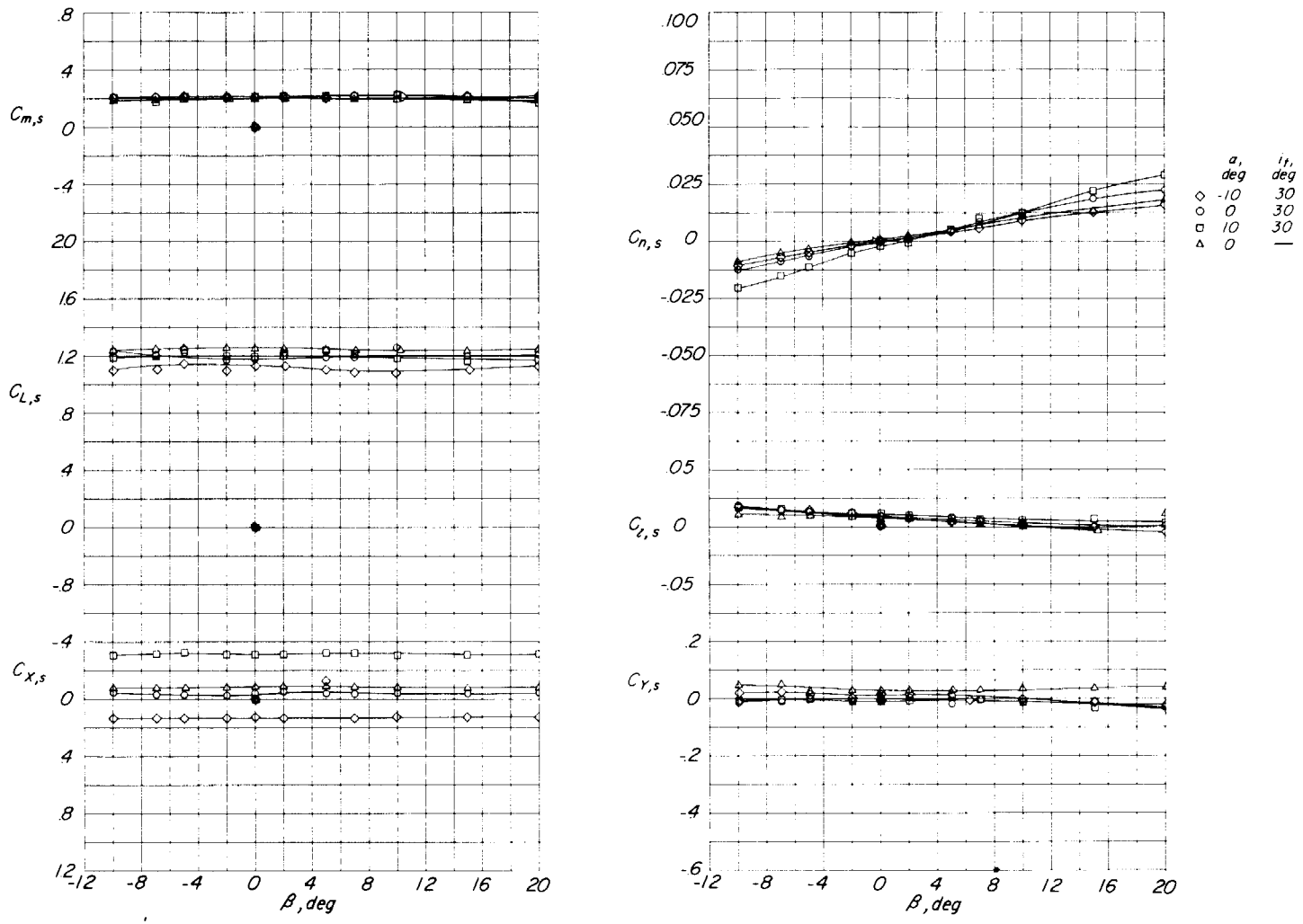

(d) Basic configuration; $i_W = 75^\circ$; $C_{T,s} = 0.94$.

Figure 30.- Concluded.

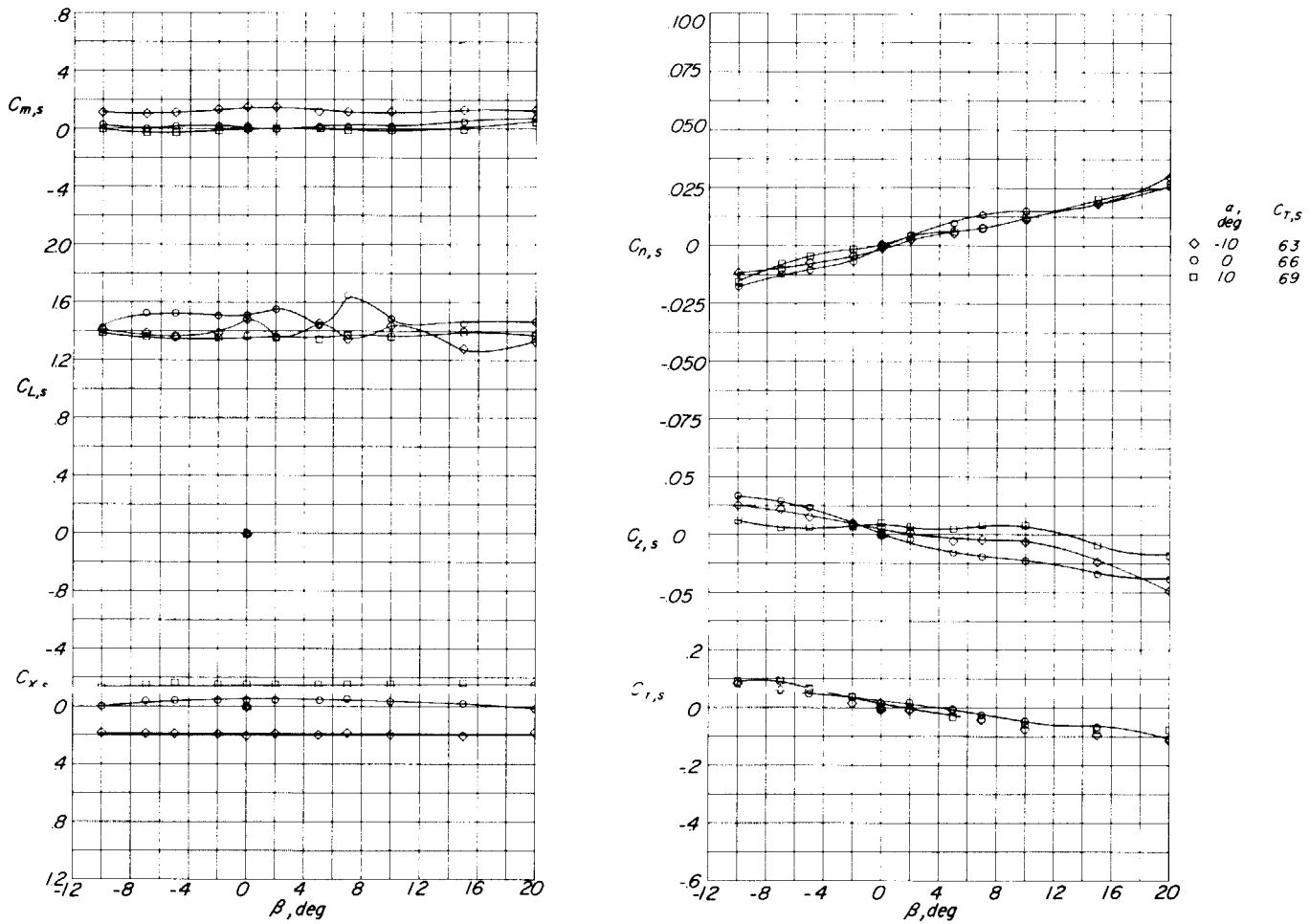

(a) Flapped configuration; $i_w = 30^\circ$; $i_t = 9.2^\circ$.

Figure 31.- Effect of angle of attack and thrust coefficient on lateral stability characteristics of flapped configuration.

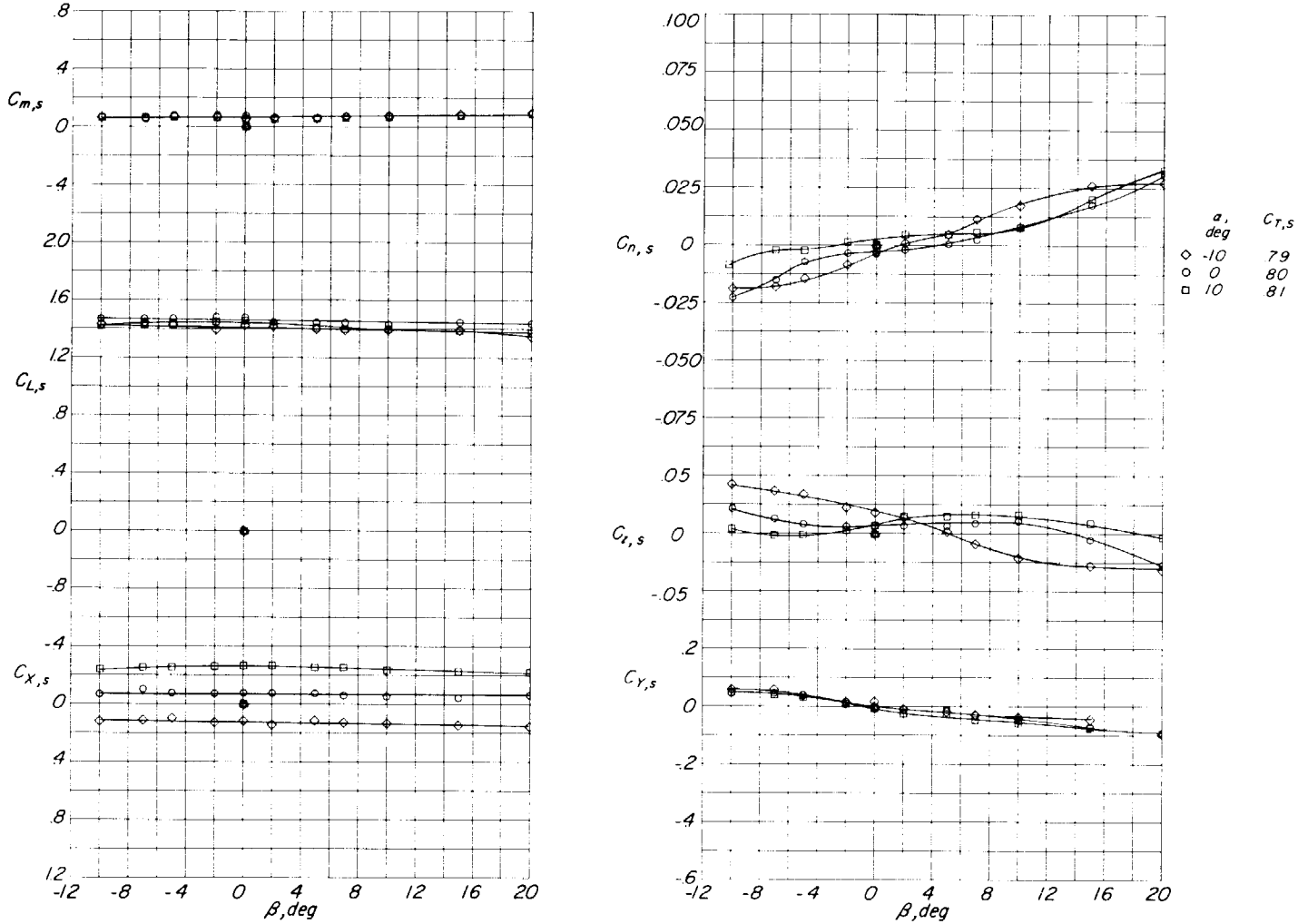

(b) Flapped configuration; $i_w = 45^\circ$; $i_t = 30^\circ$.

Figure 31.- Concluded.

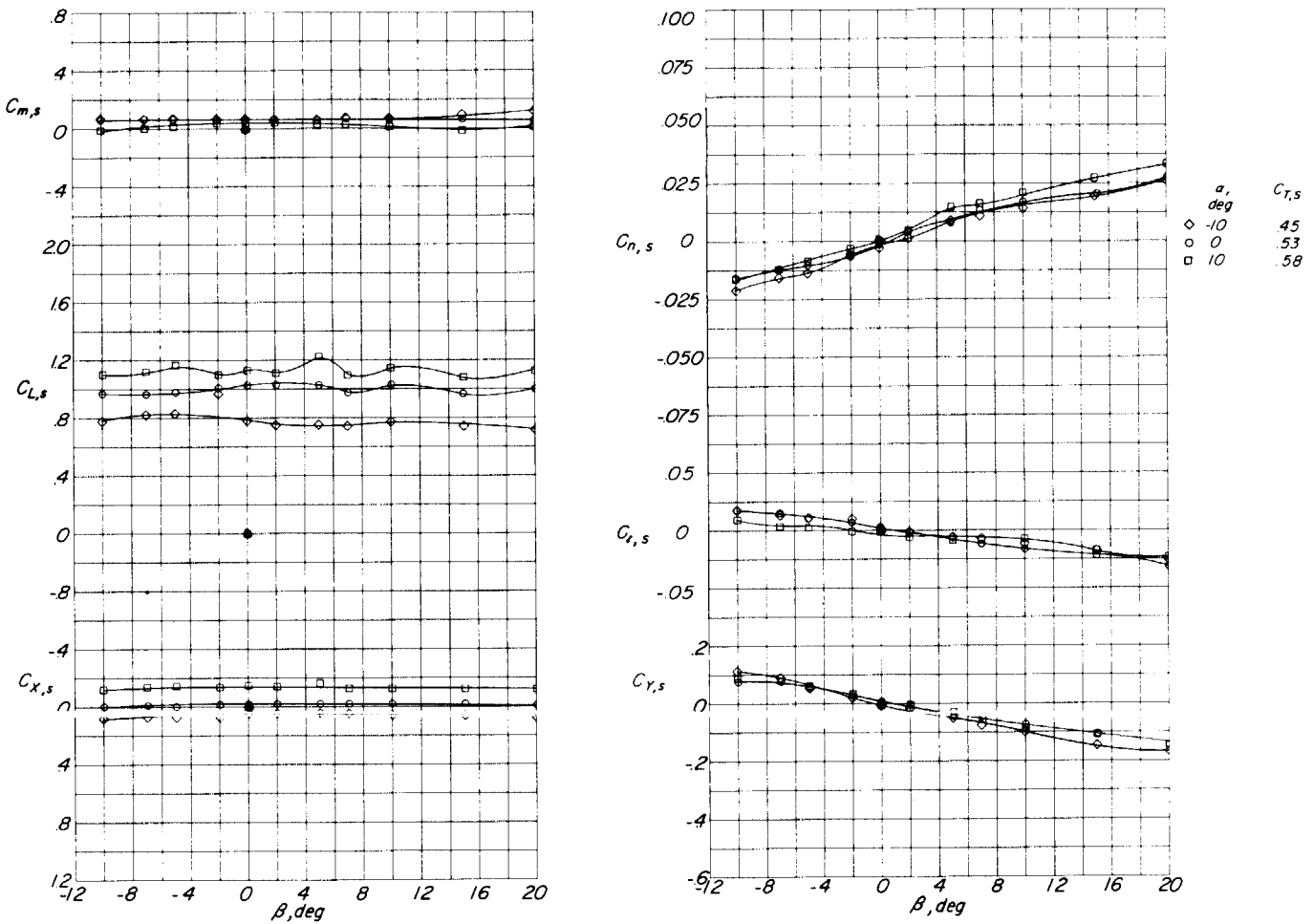

(a) Speed-brake configuration; $i_w = 30^o$; $i_t = 20^o$.

Figure 32.- Effect of angle of attack and thrust coefficient on lateral stability characteristics of speed-brake configuration.

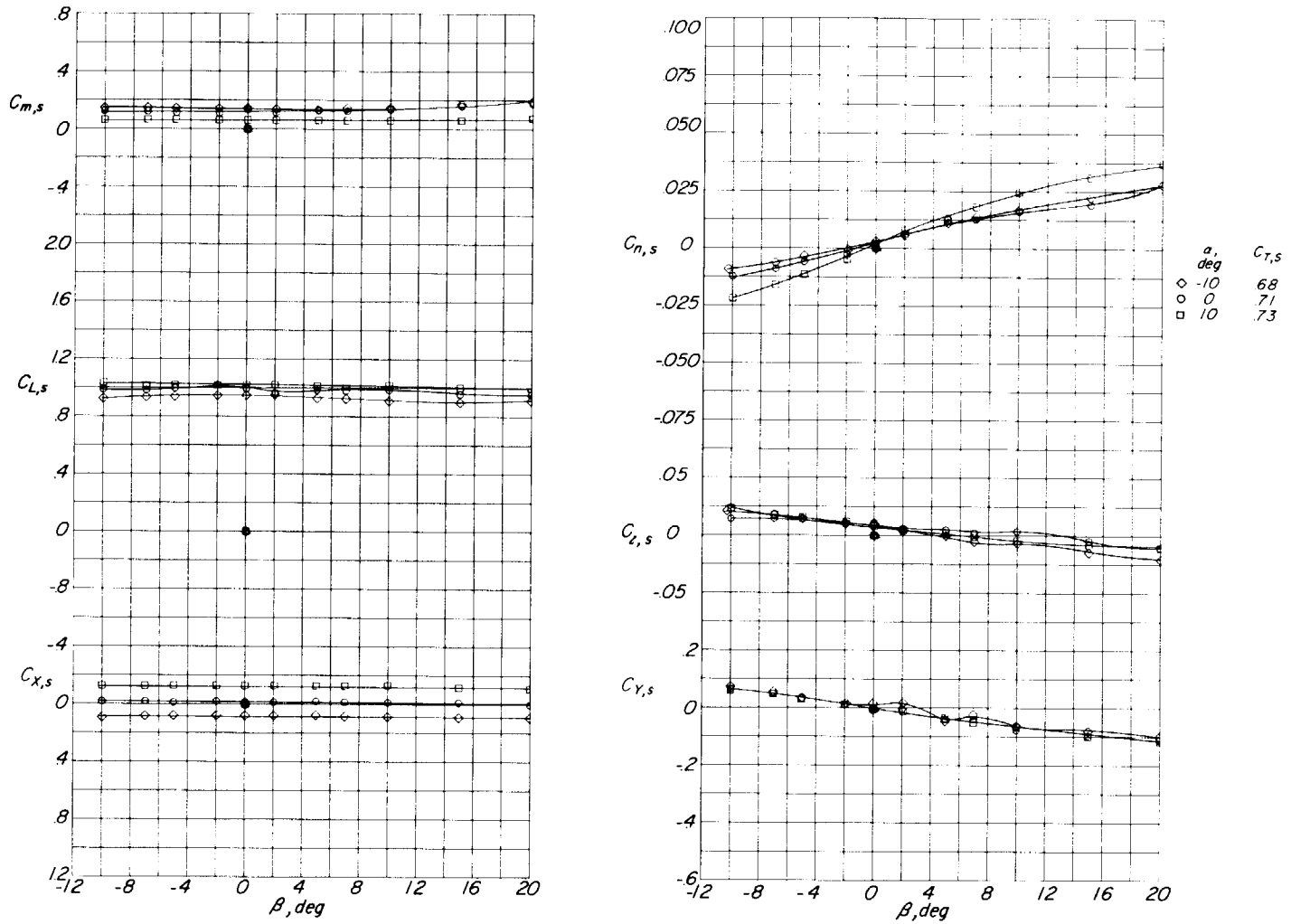

(b) Speed-brake configuration; $i_w = 45^\circ$; $i_t = 19.2^\circ$.

Figure 32.- Concluded.

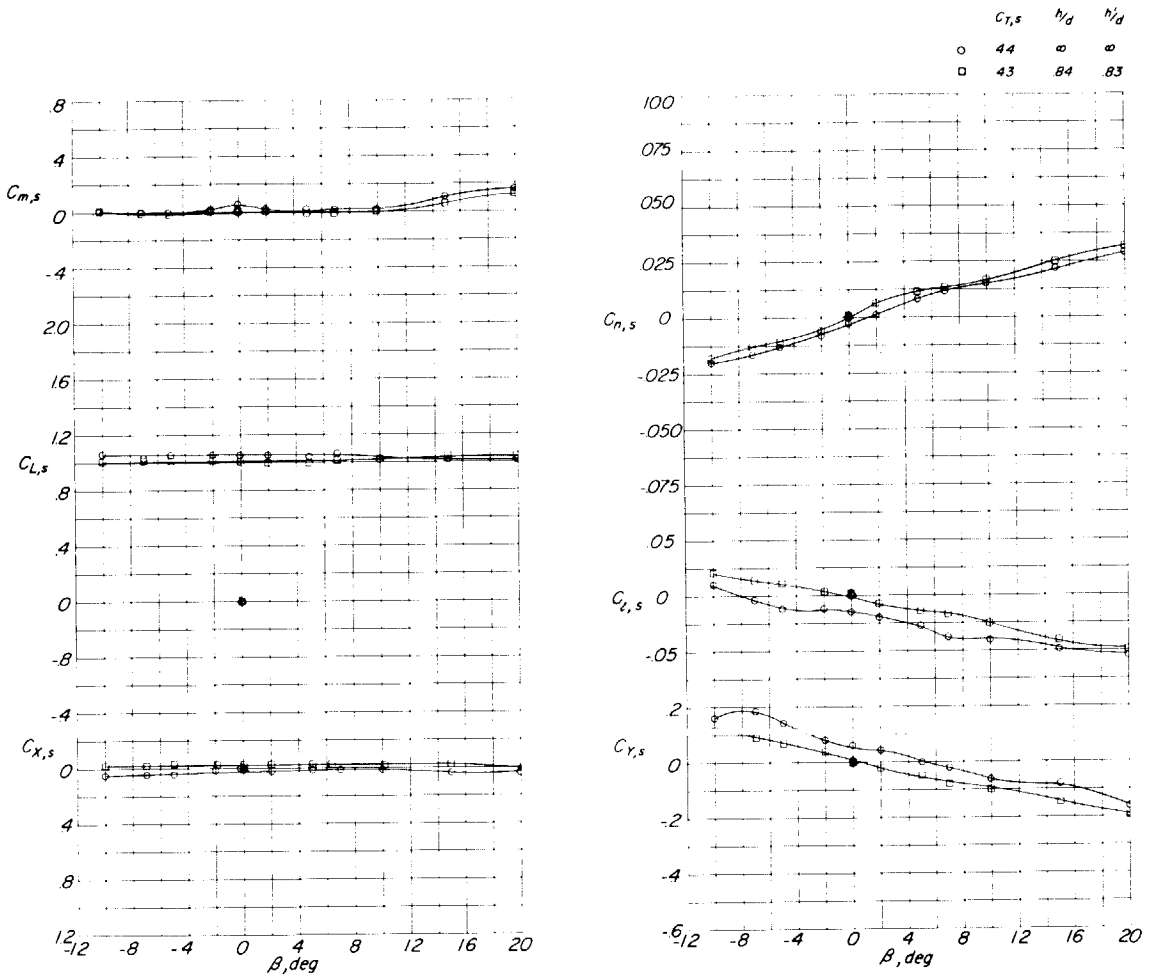

(a) Basic configuration; $i_w = 30^\circ$; $i_t = 9.2^\circ$.

Figure 33.- Effect of ground on lateral stability characteristics of basic configuration for several thrust coefficients and wing tilt angles. $\alpha = 0^\circ$.

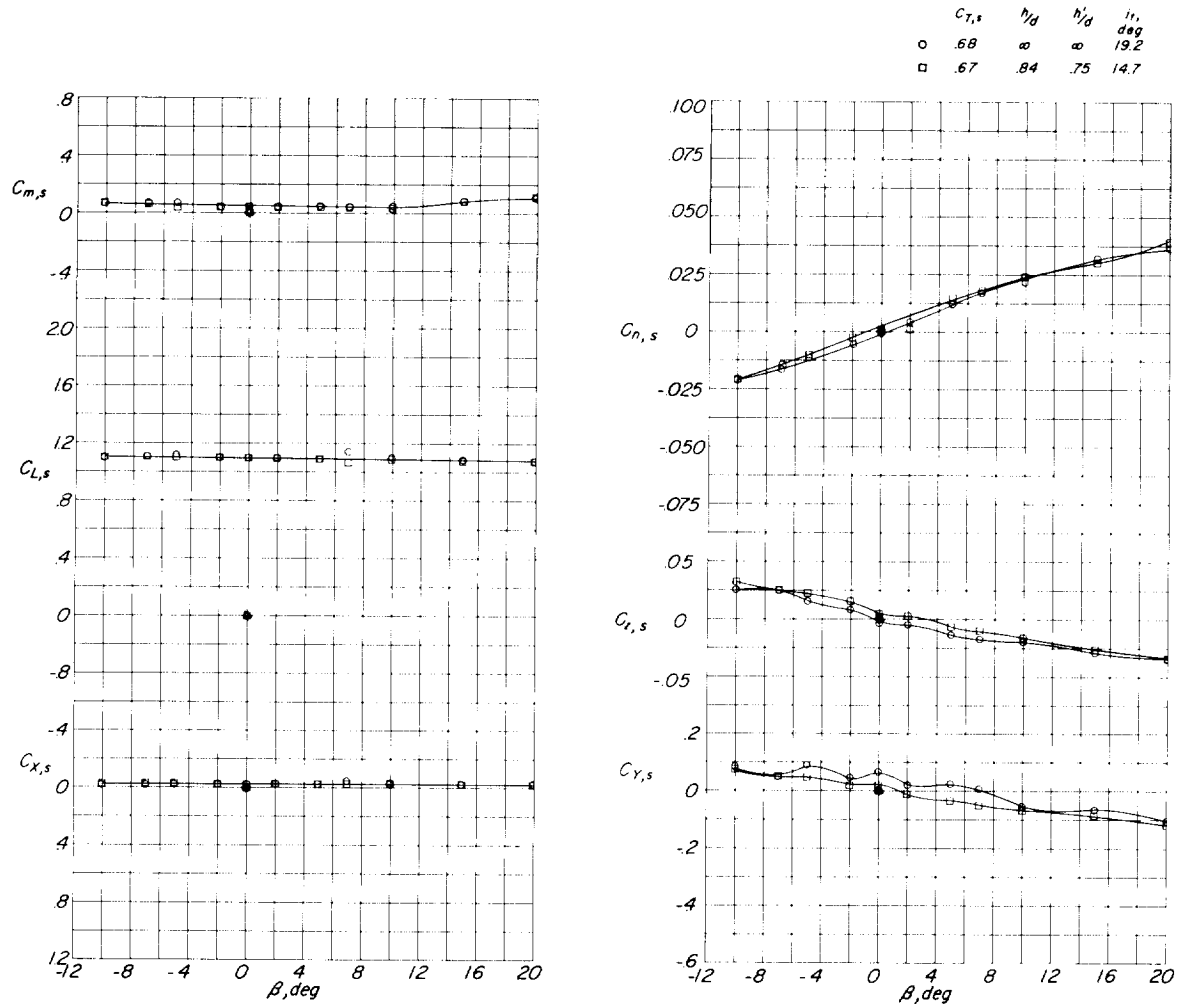

(b) Basic configuration; $i_w = 45^o$.

Figure 33.- Continued.

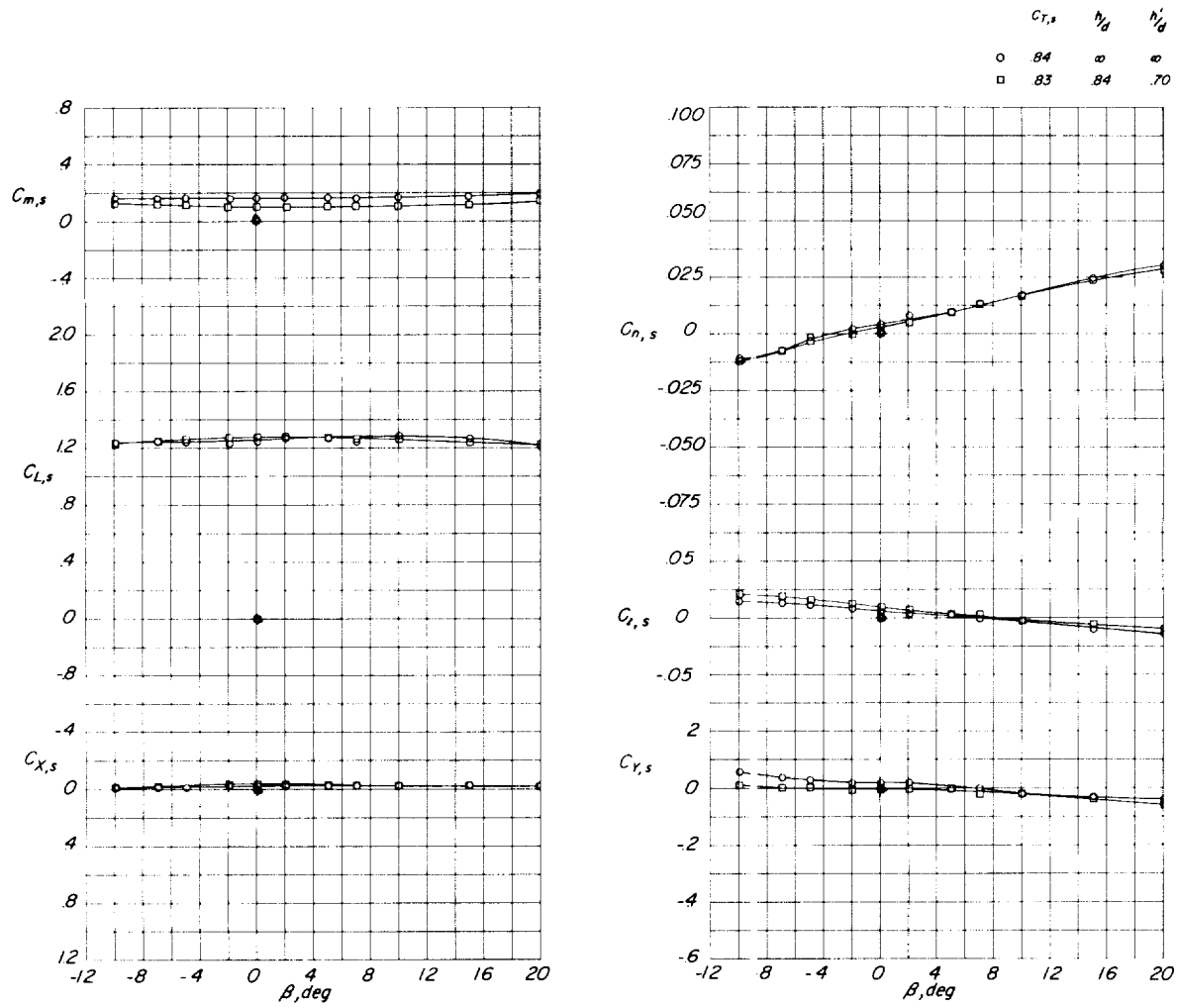

(c) Basic configuration; $i_w = 50^\circ$; $i_t = 30^\circ$.

Figure 33.- Continued.

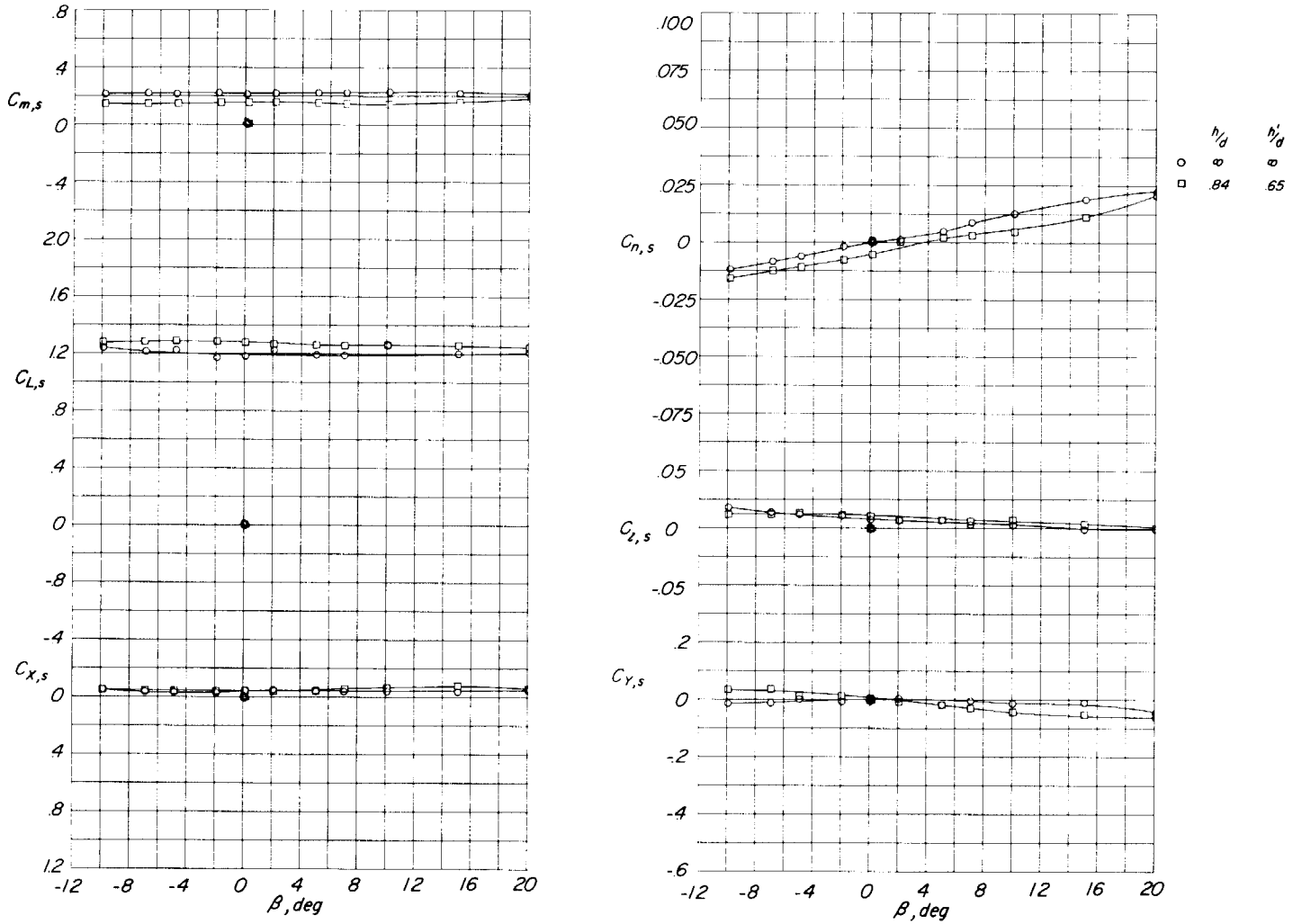

(d) Basic configuration; $i_w = 75^\circ$; $i_t = 30^\circ$; $C_{T,s} = 0.94$.

Figure 33.- Concluded.

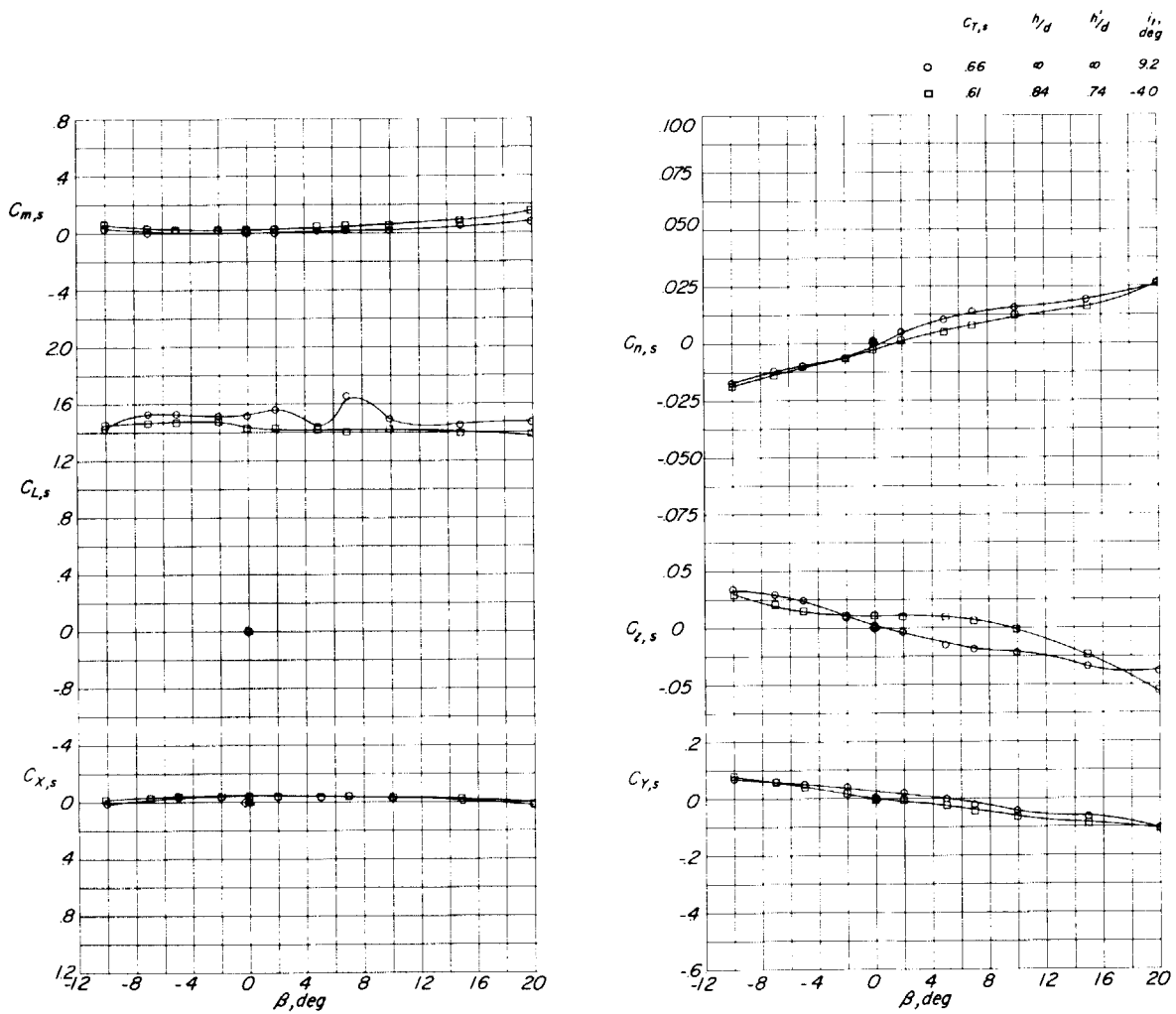

Figure 34.- Effect of ground on lateral stability characteristics of flapped configuration. $i_w = 30^o$; $\alpha = 0^o$.

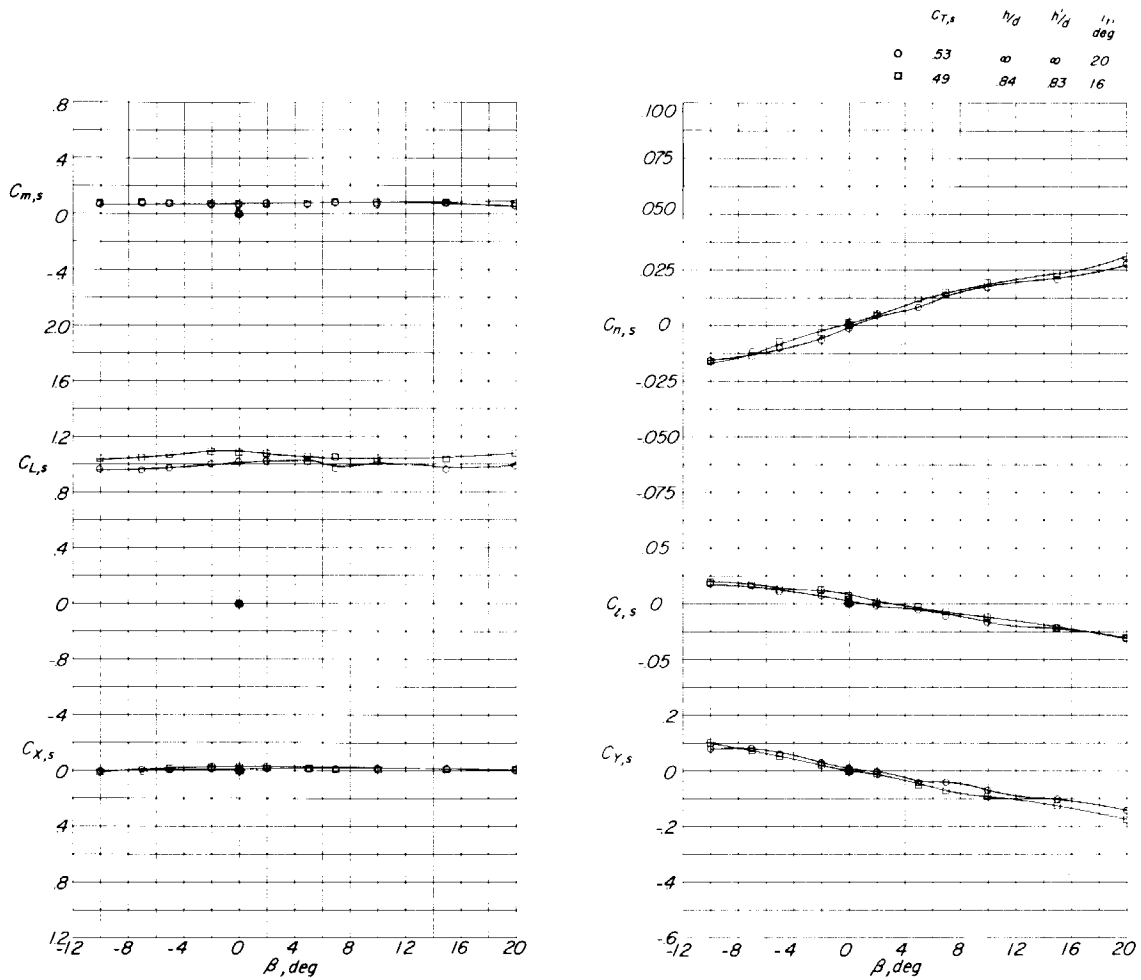

(a) Speed-brake configuration; $i_w = 30^\circ$.

Figure 35.- Effect of ground on lateral stability characteristics of speed-brake configuration for several thrust coefficients and wing tilt angles. $\alpha = 0^\circ$.

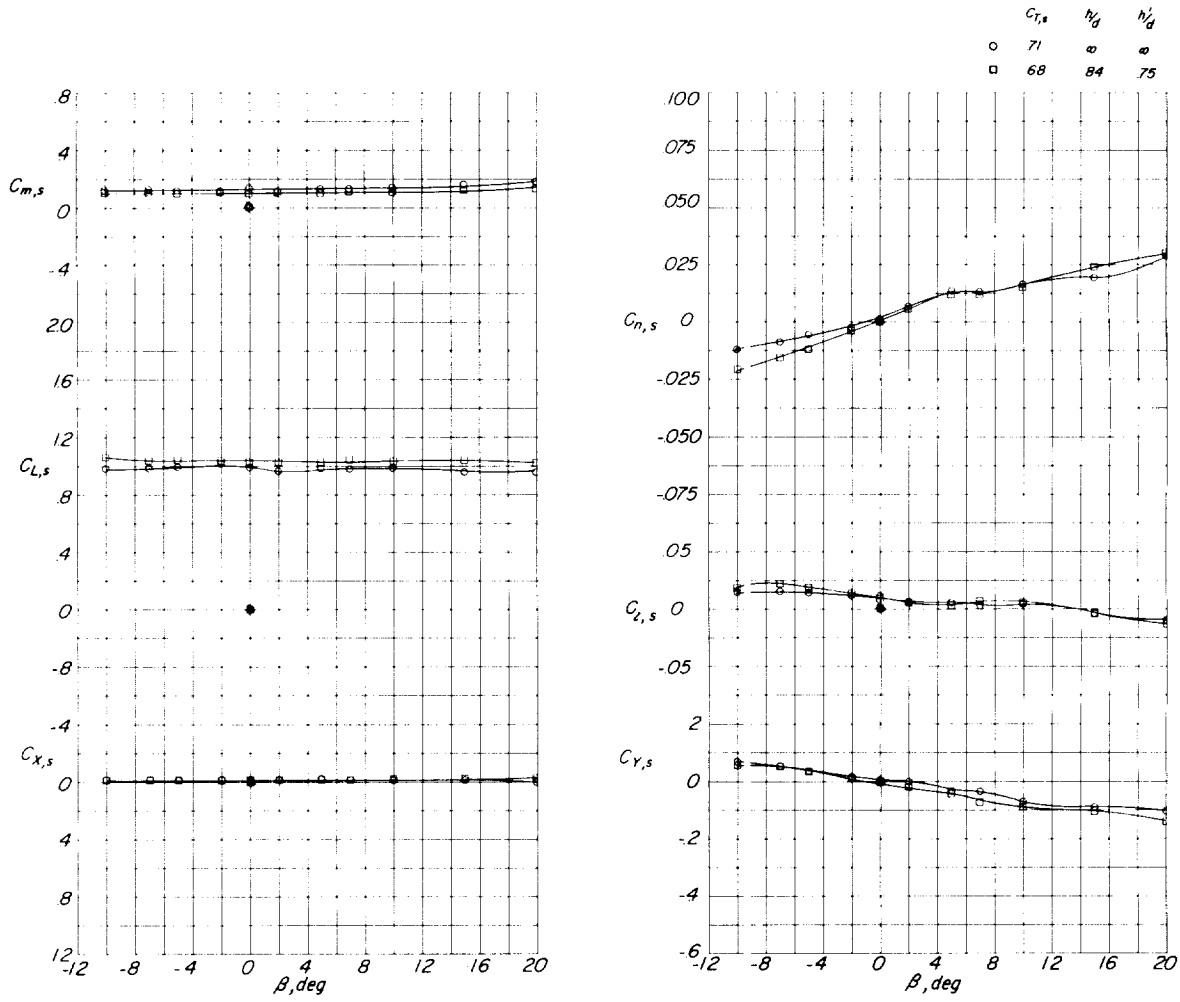

(b) Speed-brake configuration; $i_w = 45^\circ$; $i_t = 19.2^\circ$.

Figure 35.- Concluded.

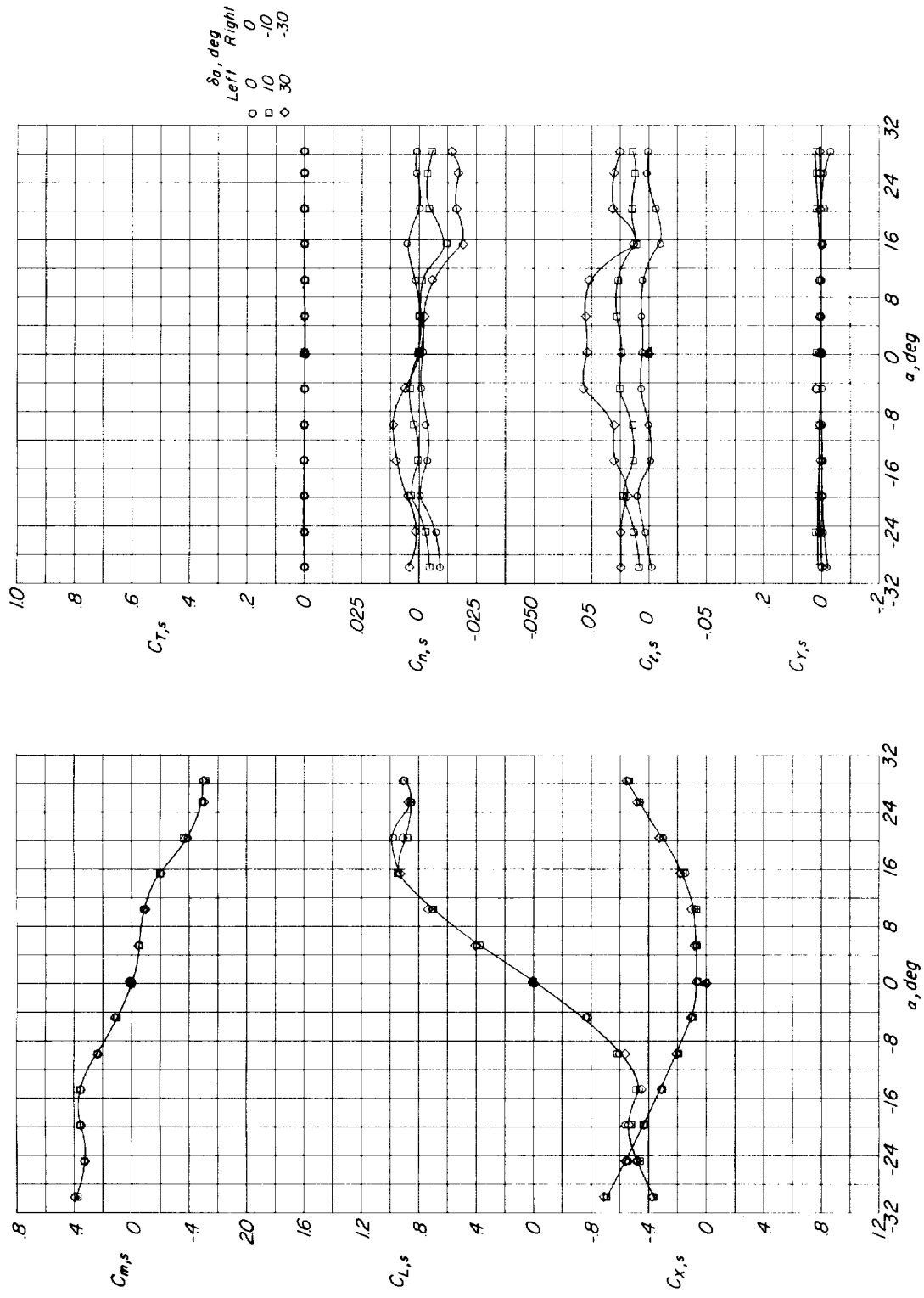

Figure 36.- Aileron effectiveness for basic configuration with power off. $i_w = 0^\circ$; $i_t = 0^\circ$.

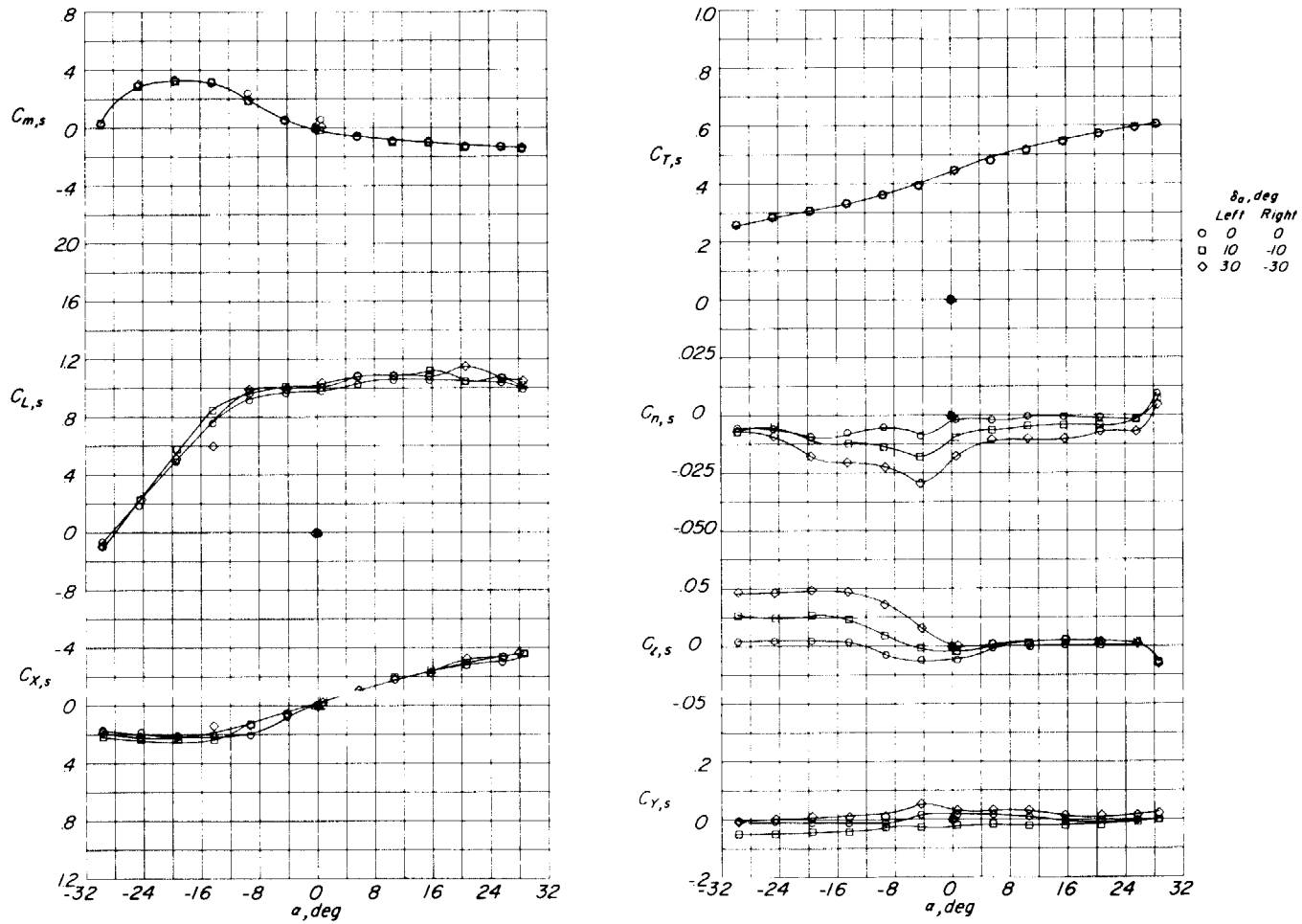

(a) Basic configuration; $i_w = 30^\circ$; $i_t = 9.2^\circ$.

Figure 37.- Aileron effectiveness for basic configuration for several thrust coefficients and wing tilt angles.

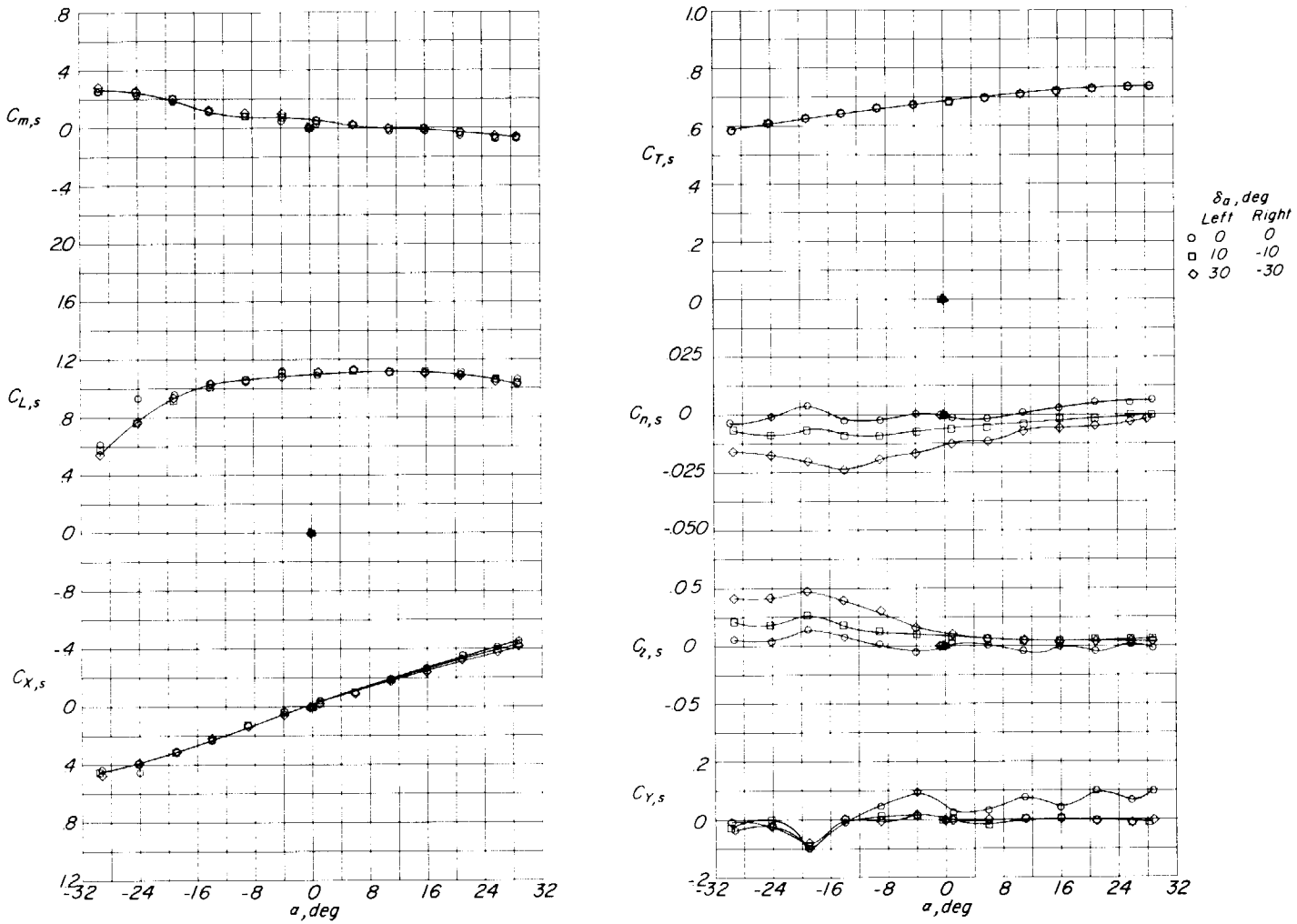

(b) Basic configuration; $i_w = 45^\circ$; $i_t = 19.2^\circ$.

Figure 37.- Continued.

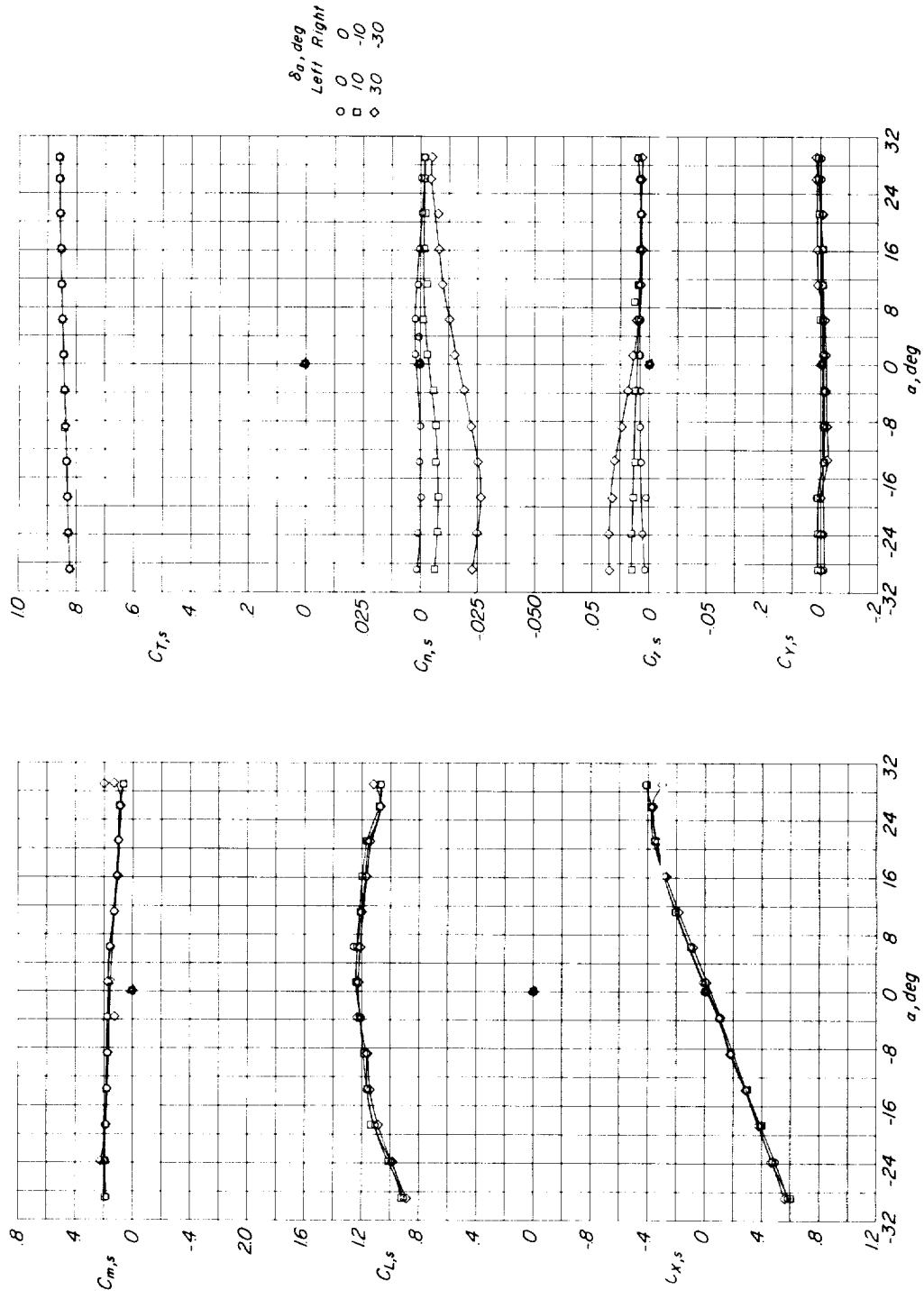

(c) Basic configuration; $i_w = 60^\circ$; $i_t = 30^\circ$.

Figure 37.- Continued.

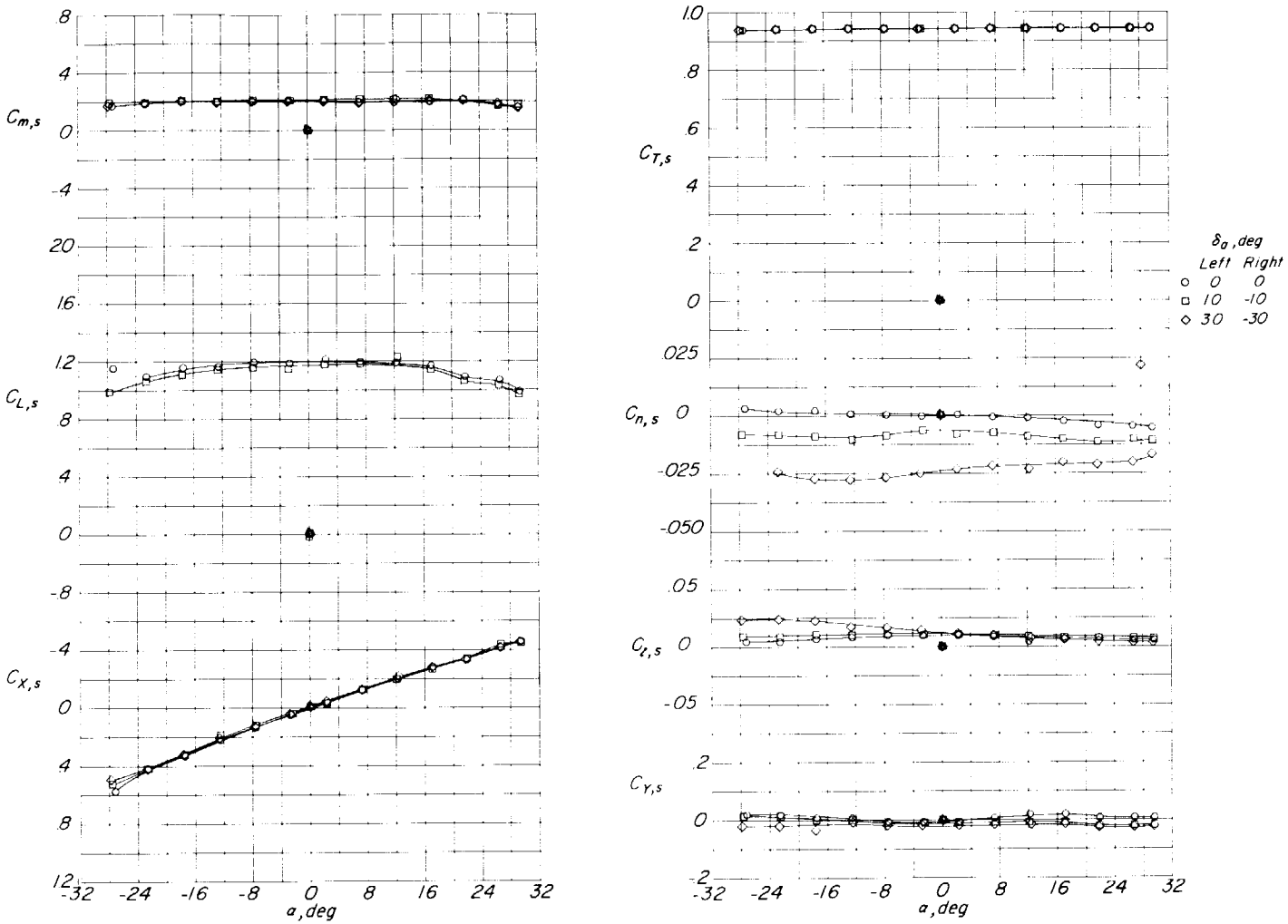

(d) Basic configuration; $i_w = 75^\circ$; $i_t = 30^\circ$.

Figure 37.- Concluded.

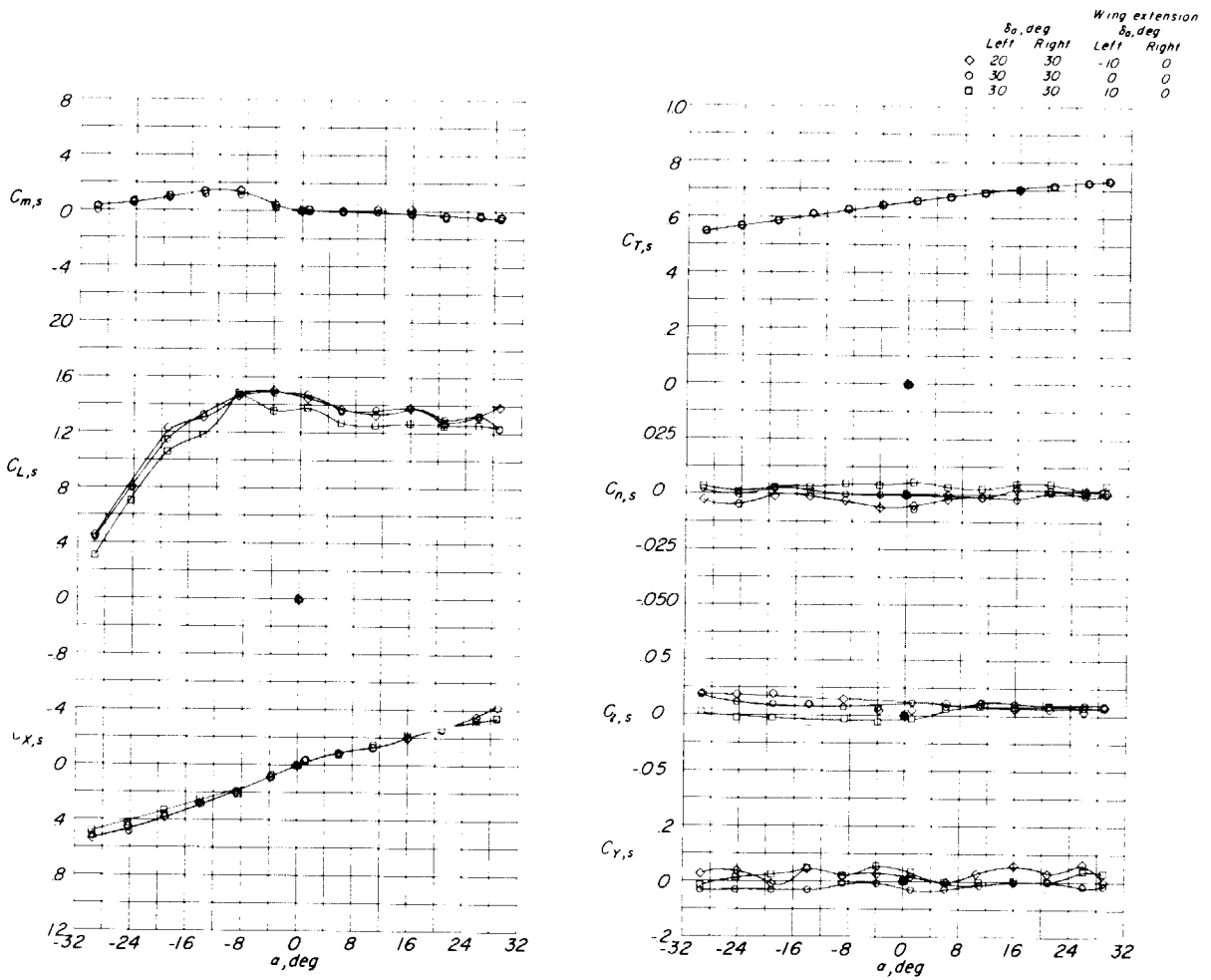

(a) Flapped configuration; $i_w = 30^\circ$; $i_t = 9.2^\circ$.

Figure 38.- Aileron effectiveness for flapped configuration for several thrust coefficients and wing tilt angles.

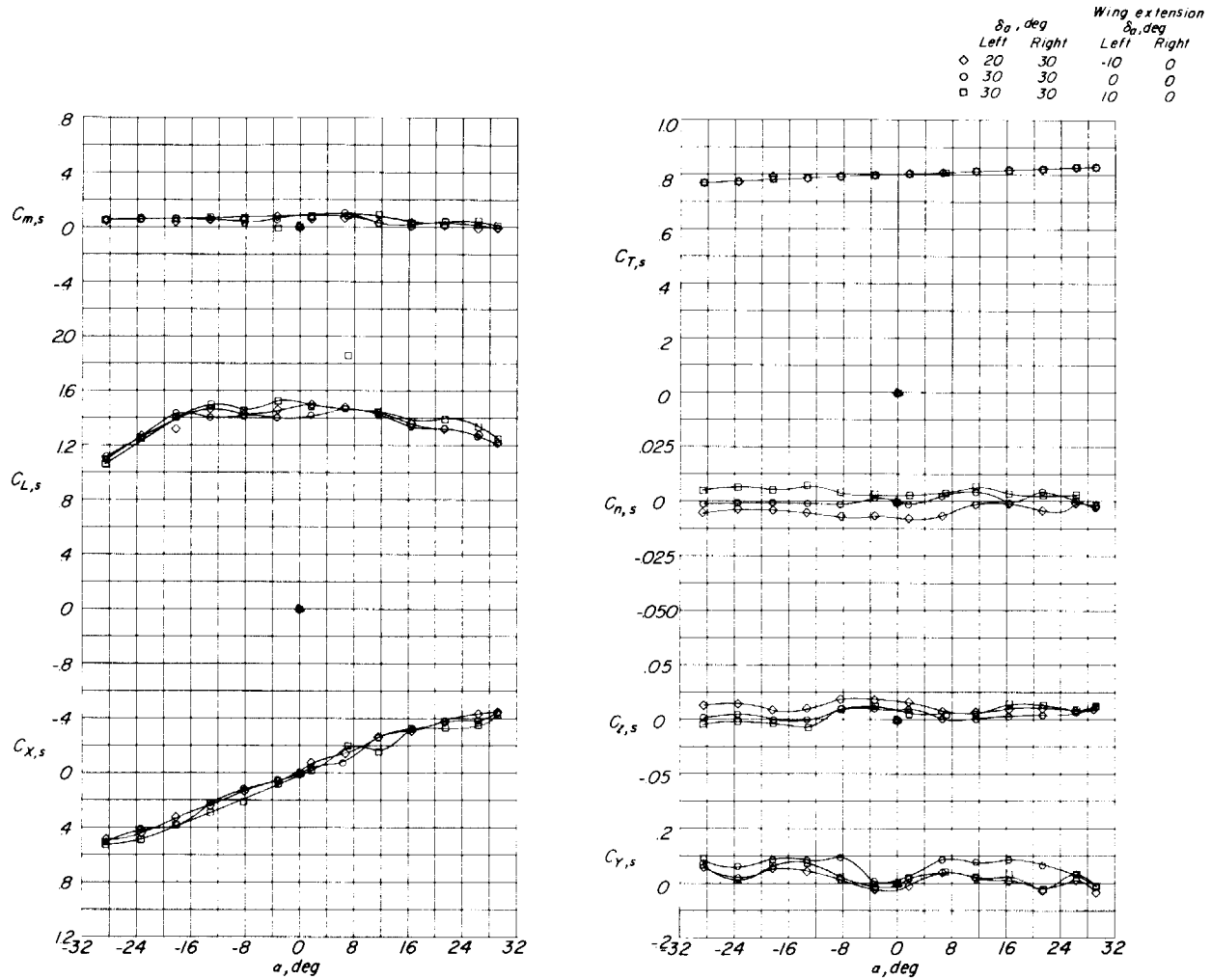

(b) Flapped configuration; $i_w = 45^\circ$; $i_t = 30^\circ$.

Figure 38.- Concluded.

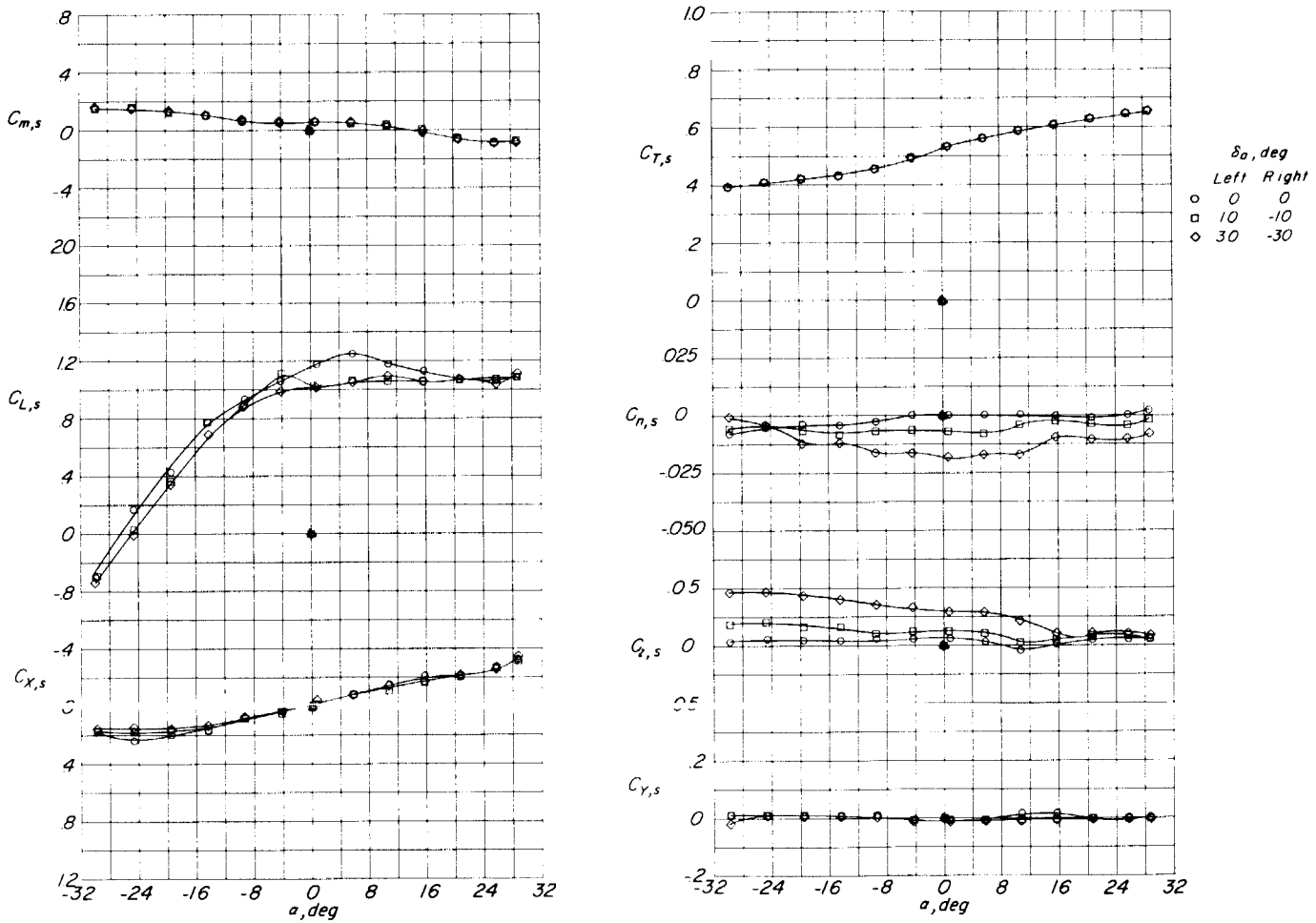

(a) Speed-brake configuration; $i_w = 30^\circ$; $i_t = 20^\circ$.

Figure 39.- Aileron effectiveness for speed-brake configuration for several thrust coefficients and wing tilt angles.

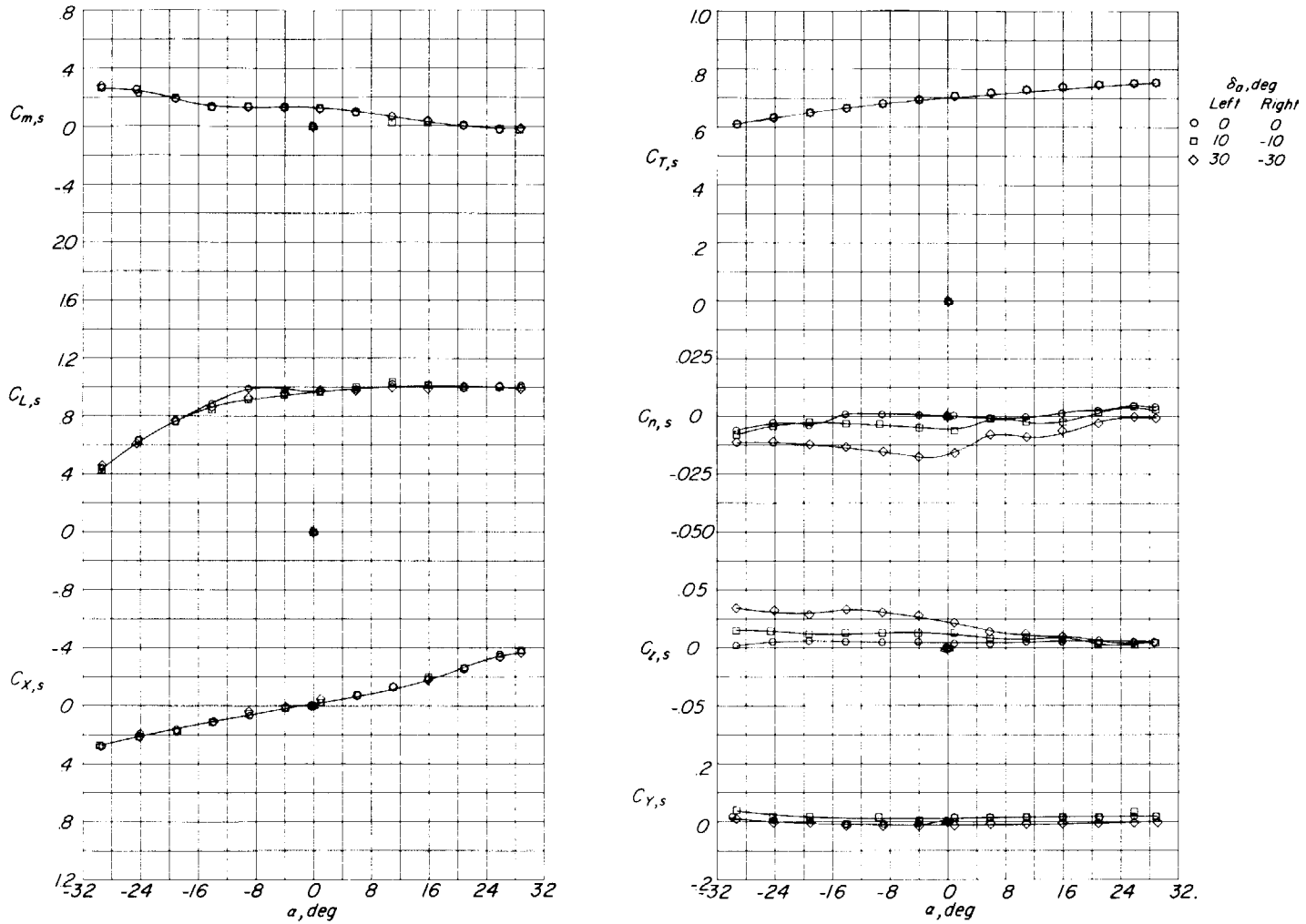

(b) Speed-brake configuration; $i_w = 45^\circ$; $i_t = 19.2^\circ$.

Figure 39.- Concluded.

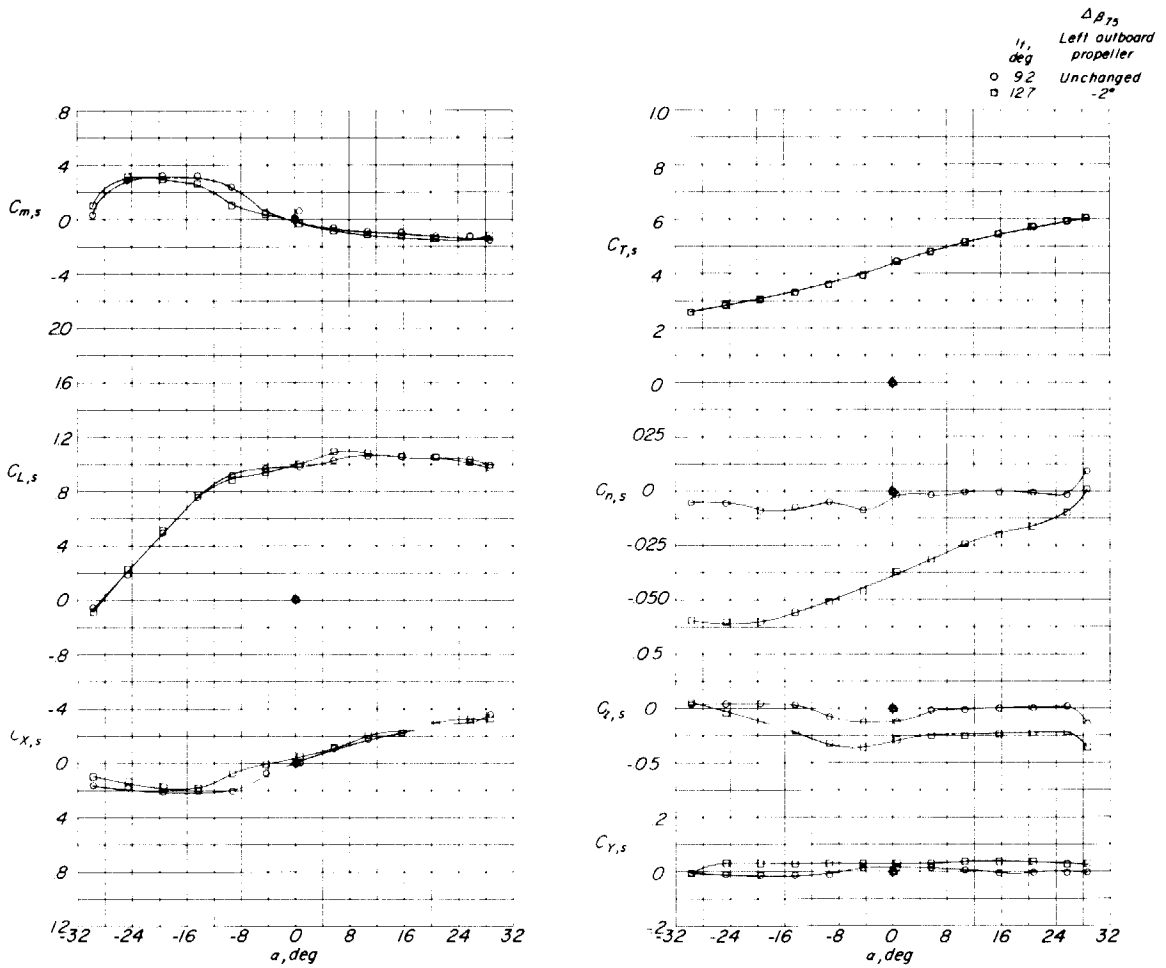

(a) Basic configuration; $i_w = 30^\circ$.

Figure 40.- Effect of reduction of blade angle of left outboard propeller for basic configuration for several thrust coefficients and wing tilt angles.

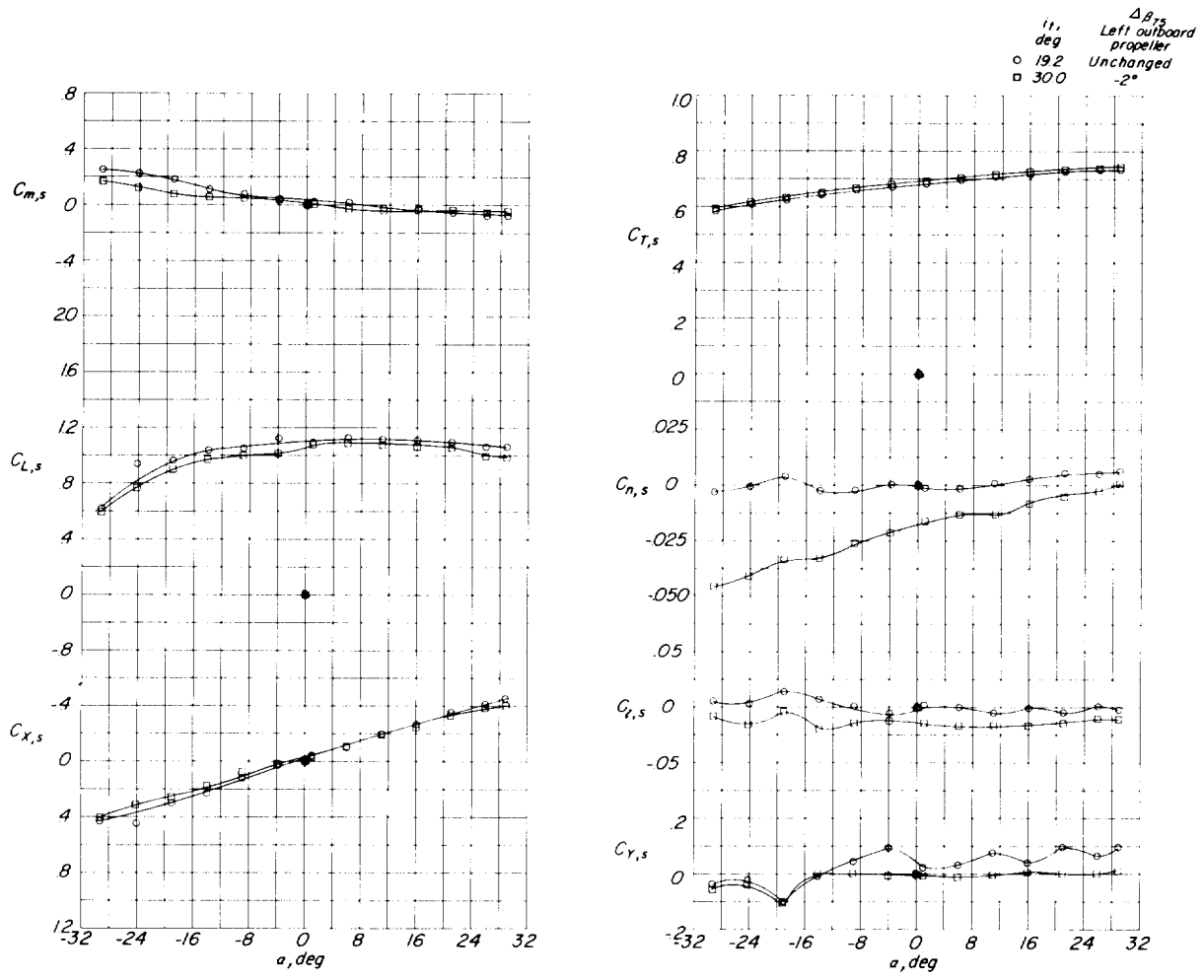

(b) Basic configuration; $i_w = 45^\circ$.

Figure 40.- Continued.

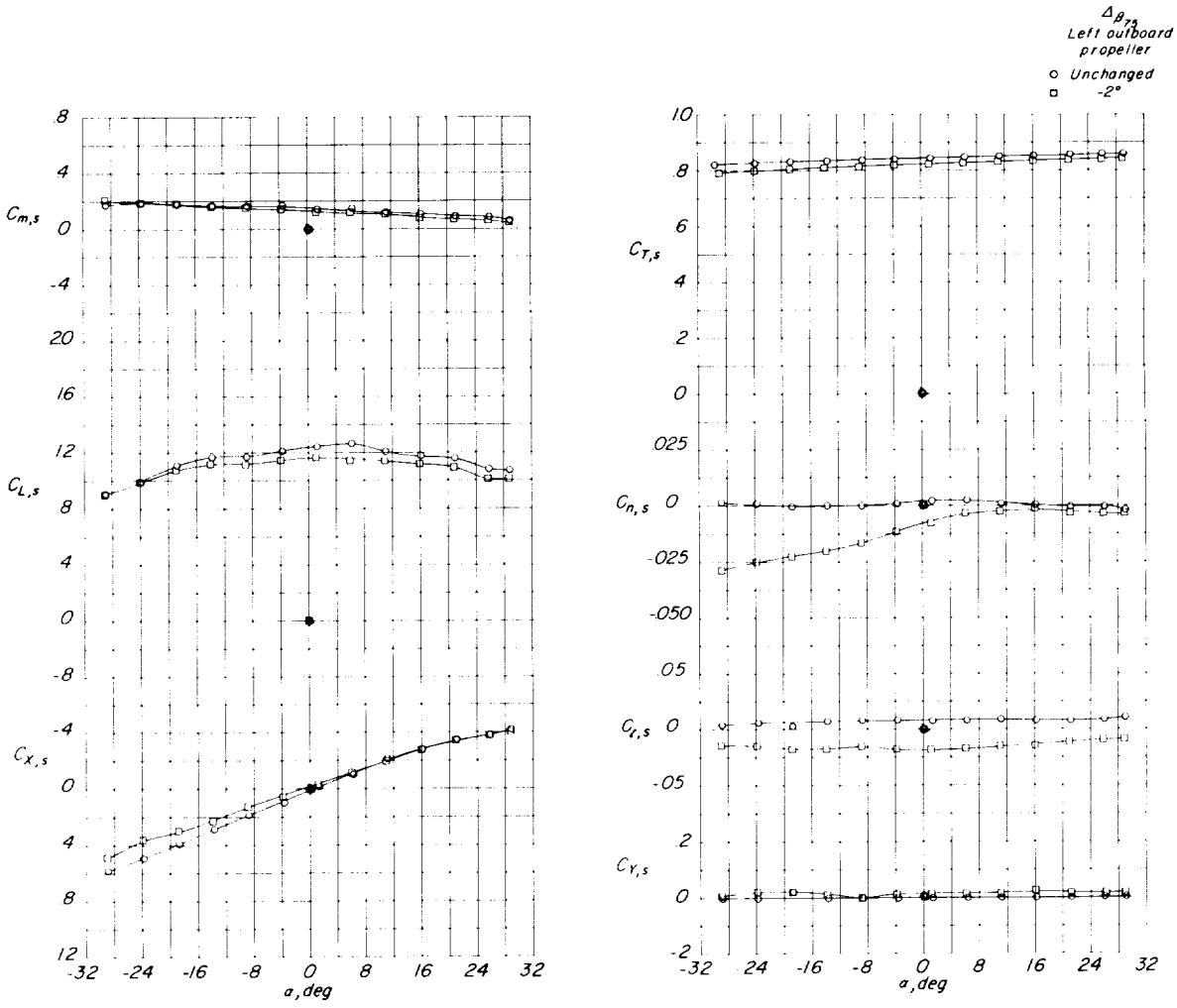

(c) Basic configuration; $i_w = 50°$; $i_t = 30°$.

Figure 40.- Continued.

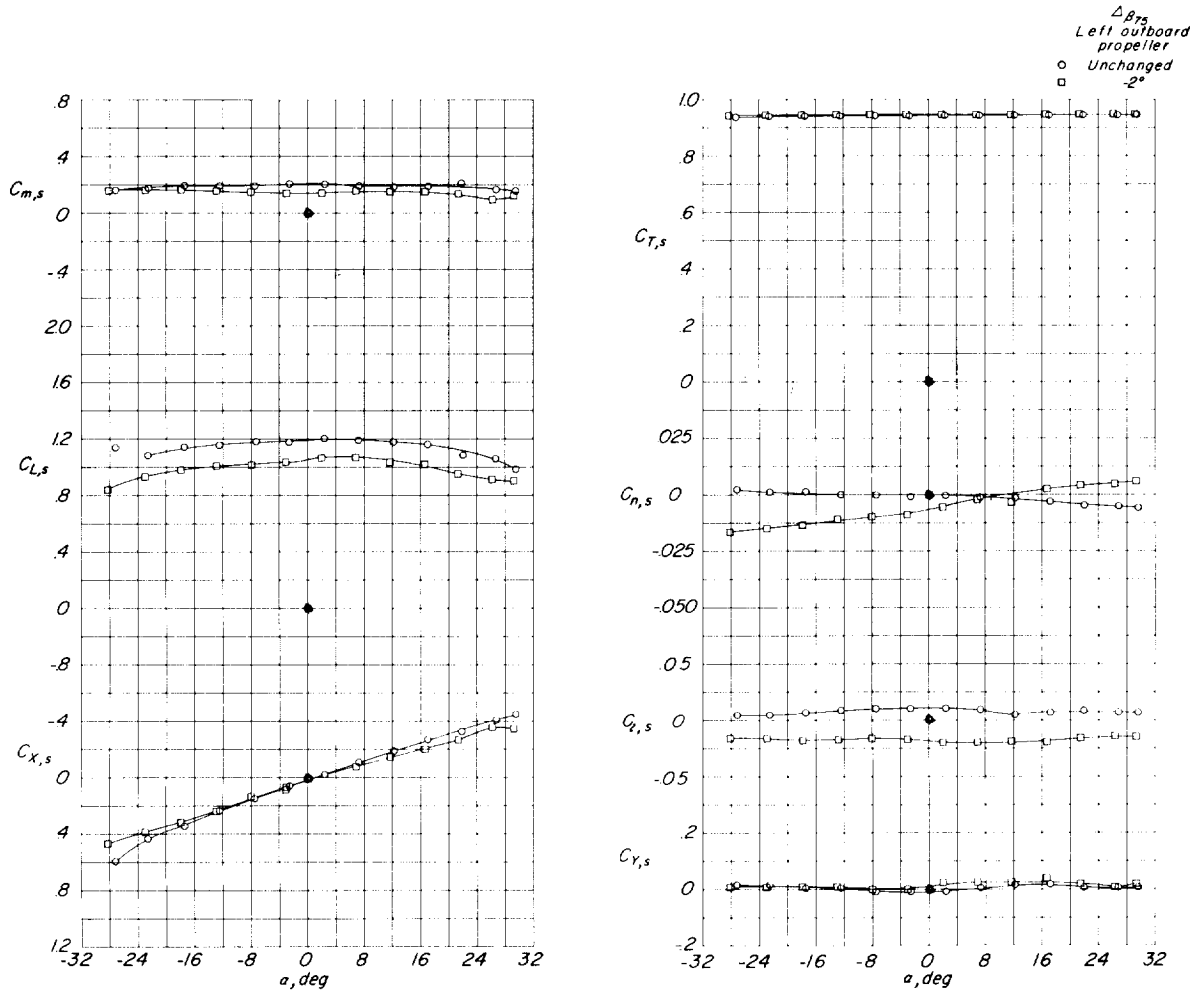

(d) Basic configuration; $i_w = 75°$; $i_t = 30°$.

Figure 40.- Concluded.

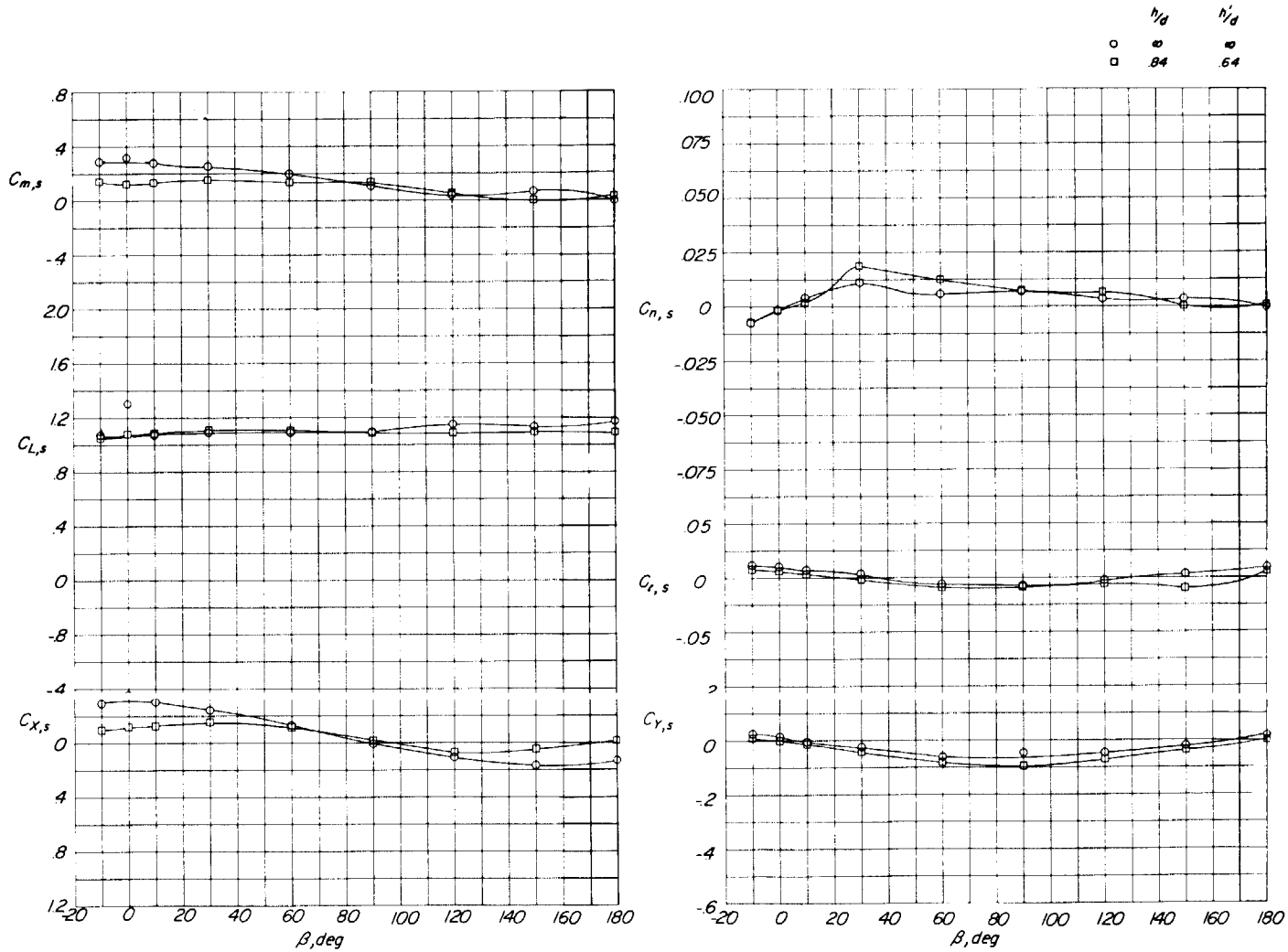

Figure 41.- Aerodynamic characteristics through 180° sideslip-angle range for basic configuration both in and out of ground effect. $\alpha = 0°$; $i_w = 90°$; $i_t = 30°$; $C_{T,s} = 0.965$.

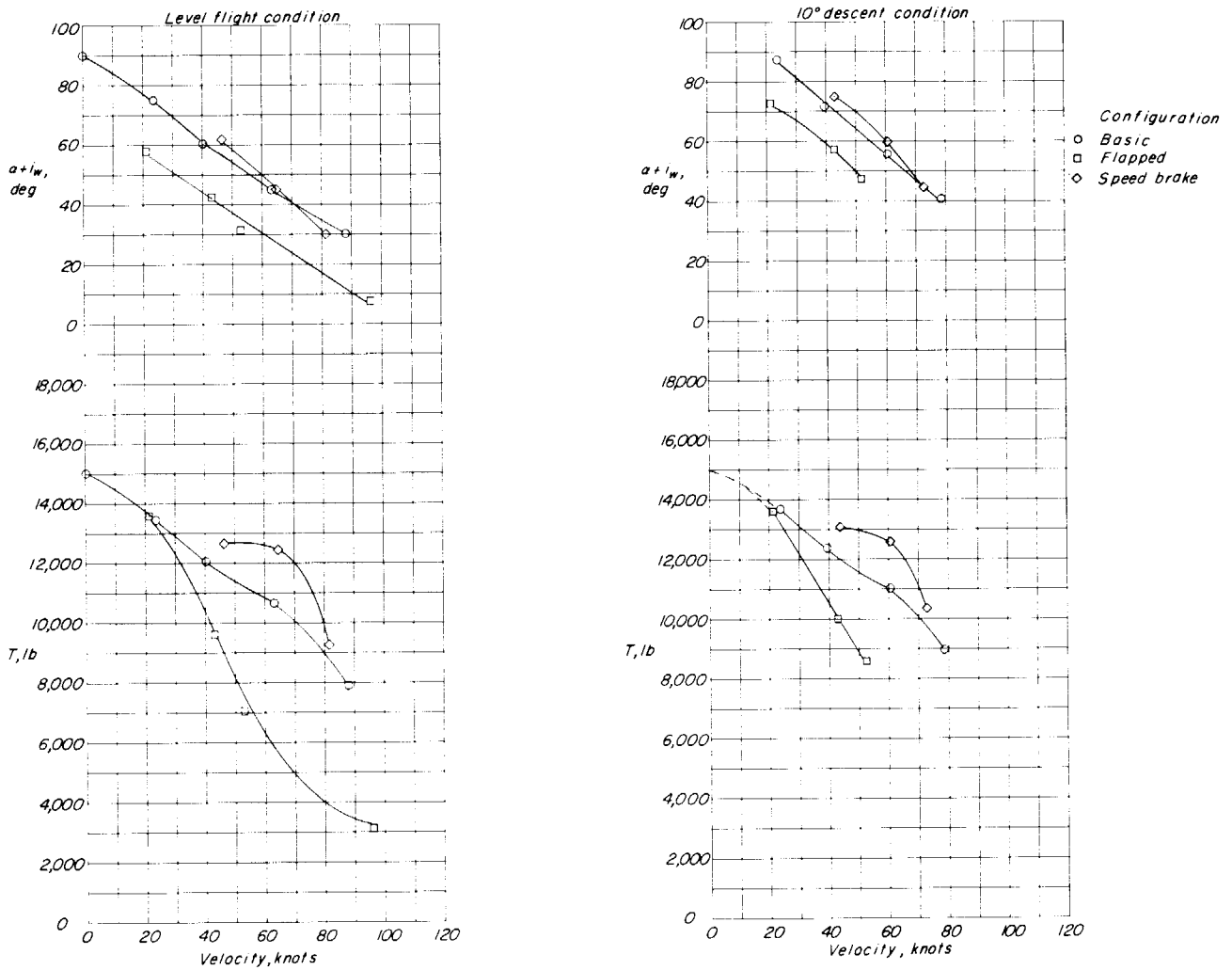

Figure 42.- Thrust and thrust-line incidence required in transition for an assumed 15,000-pound airplane.

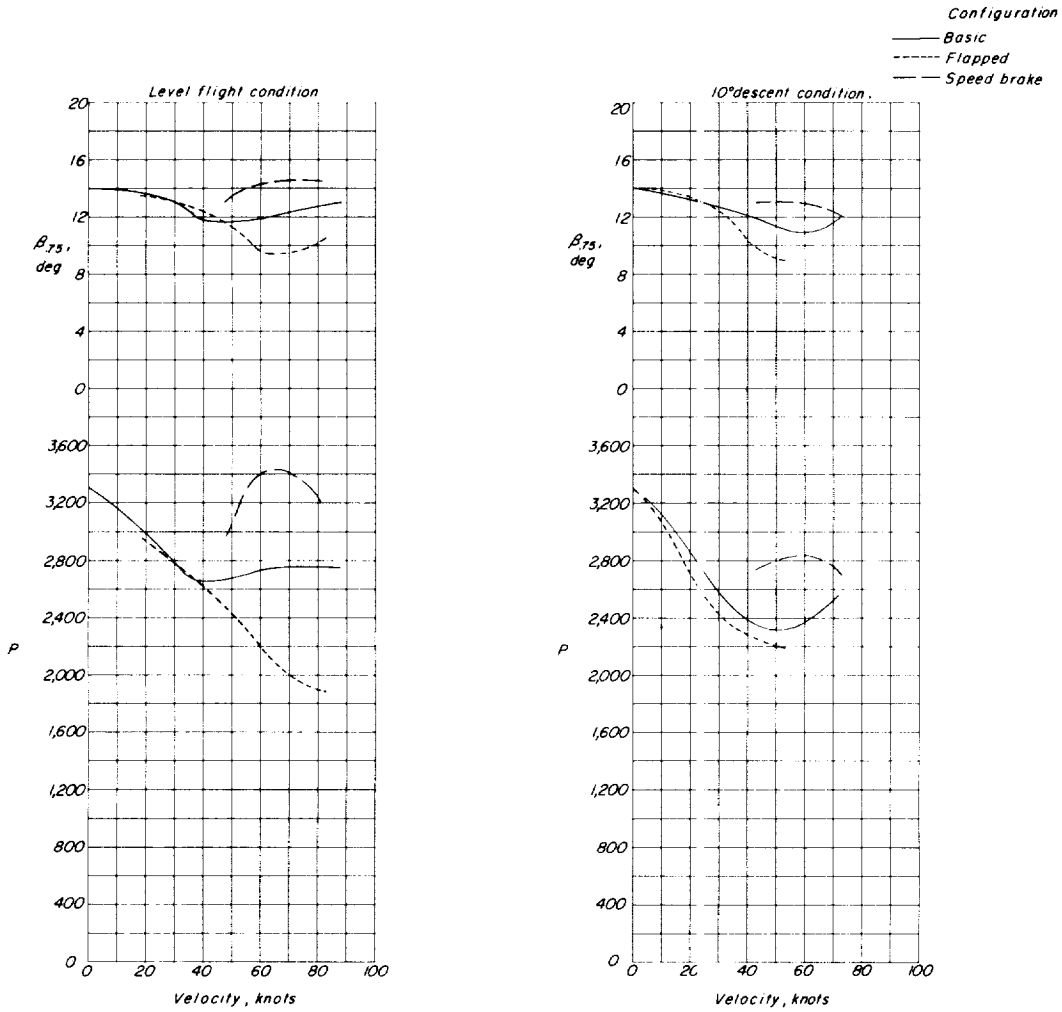

Figure 43.- Power and propeller-blade angle setting required in transition for an assumed 15,000-pound airplane.

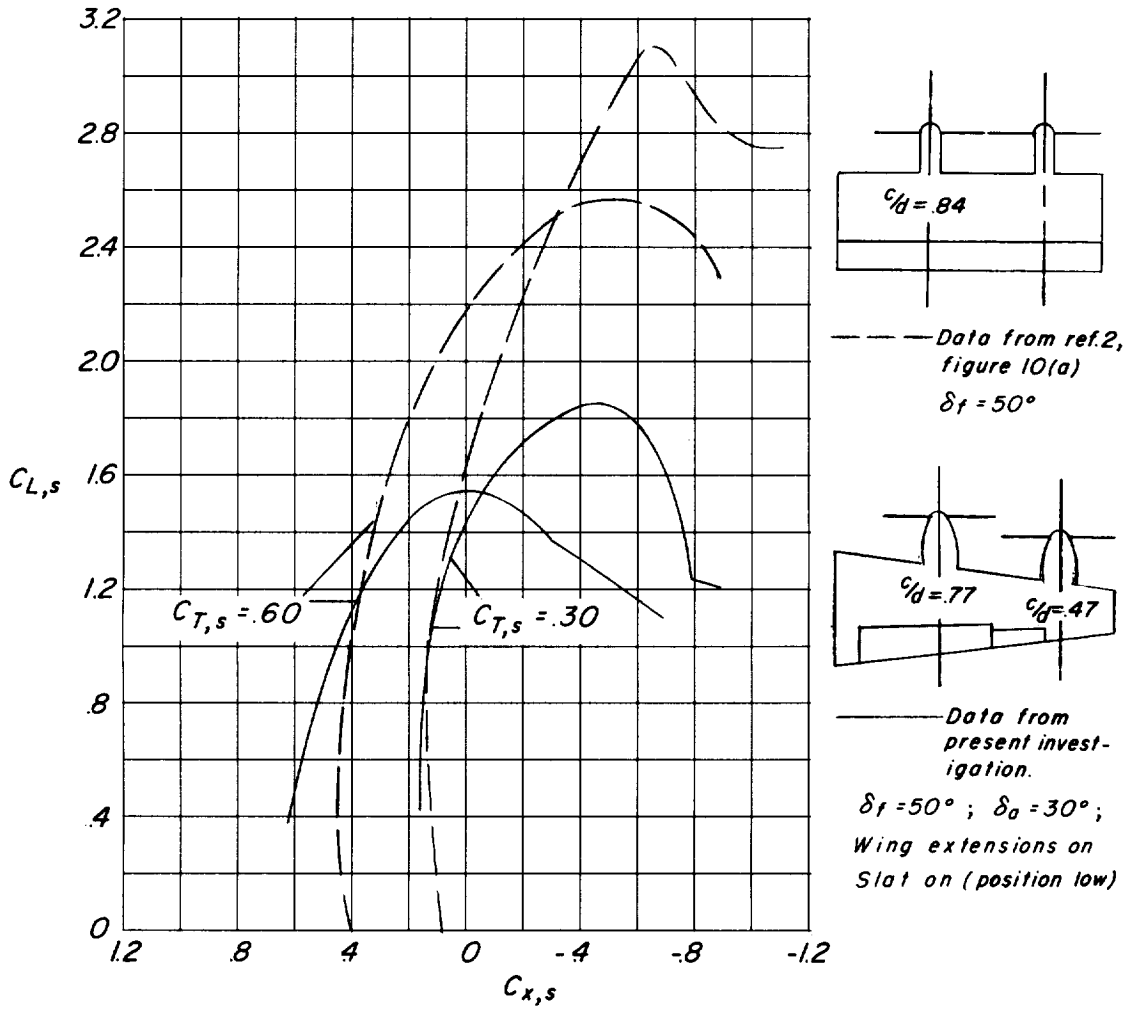

Figure 44.- Comparison of lift—longitudinal-force polars for the flapped configuration of reference 2 (fig. 10(a)) and flapped configuration of present investigation.

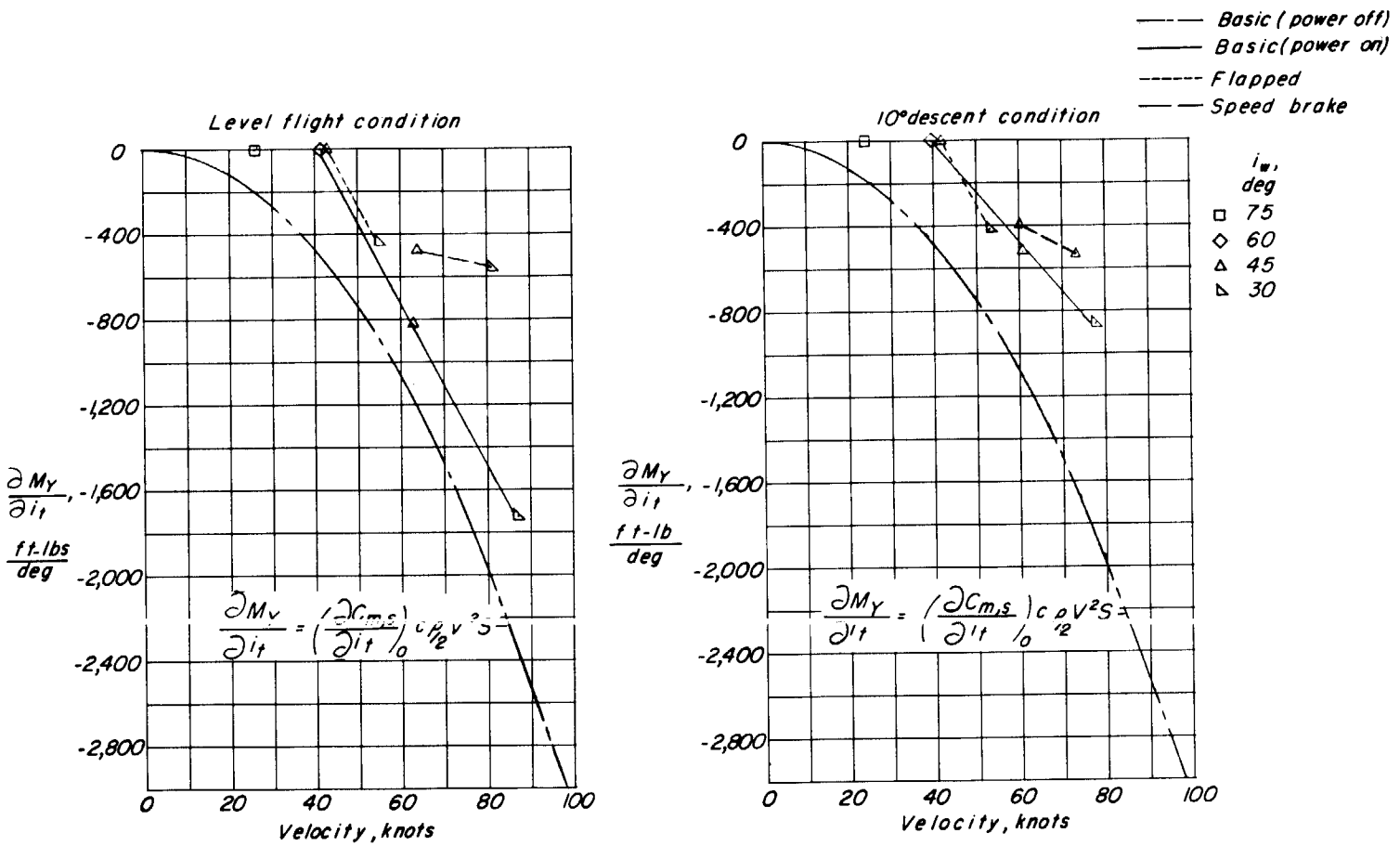

Figure 45.- Horizontal-tail effectiveness of assumed airplane in transition speed range out of ground effect.

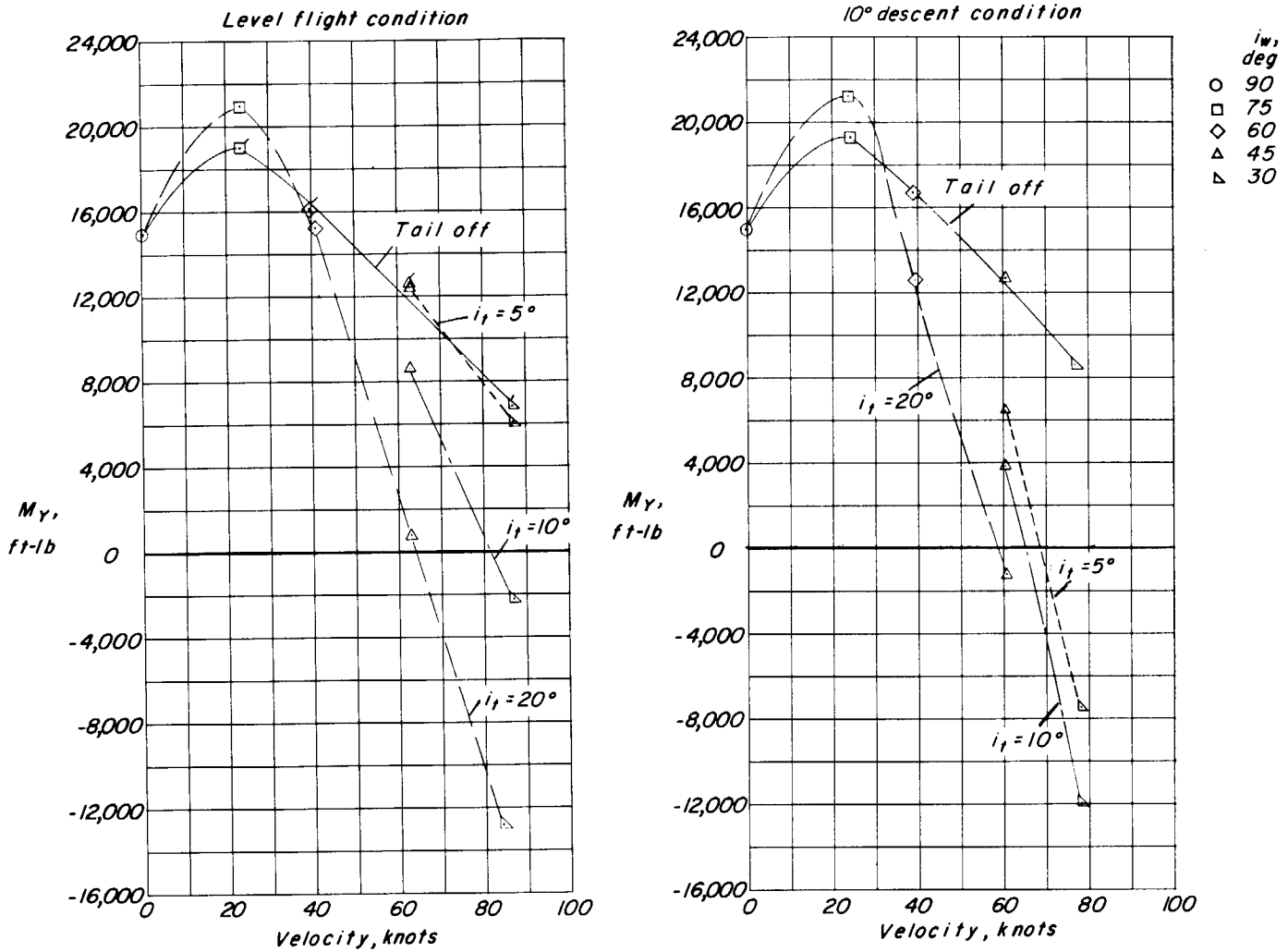

Figure 46.- Variation of pitching moment with speed in transition for several tail deflections of the assumed airplane (basic configuration).

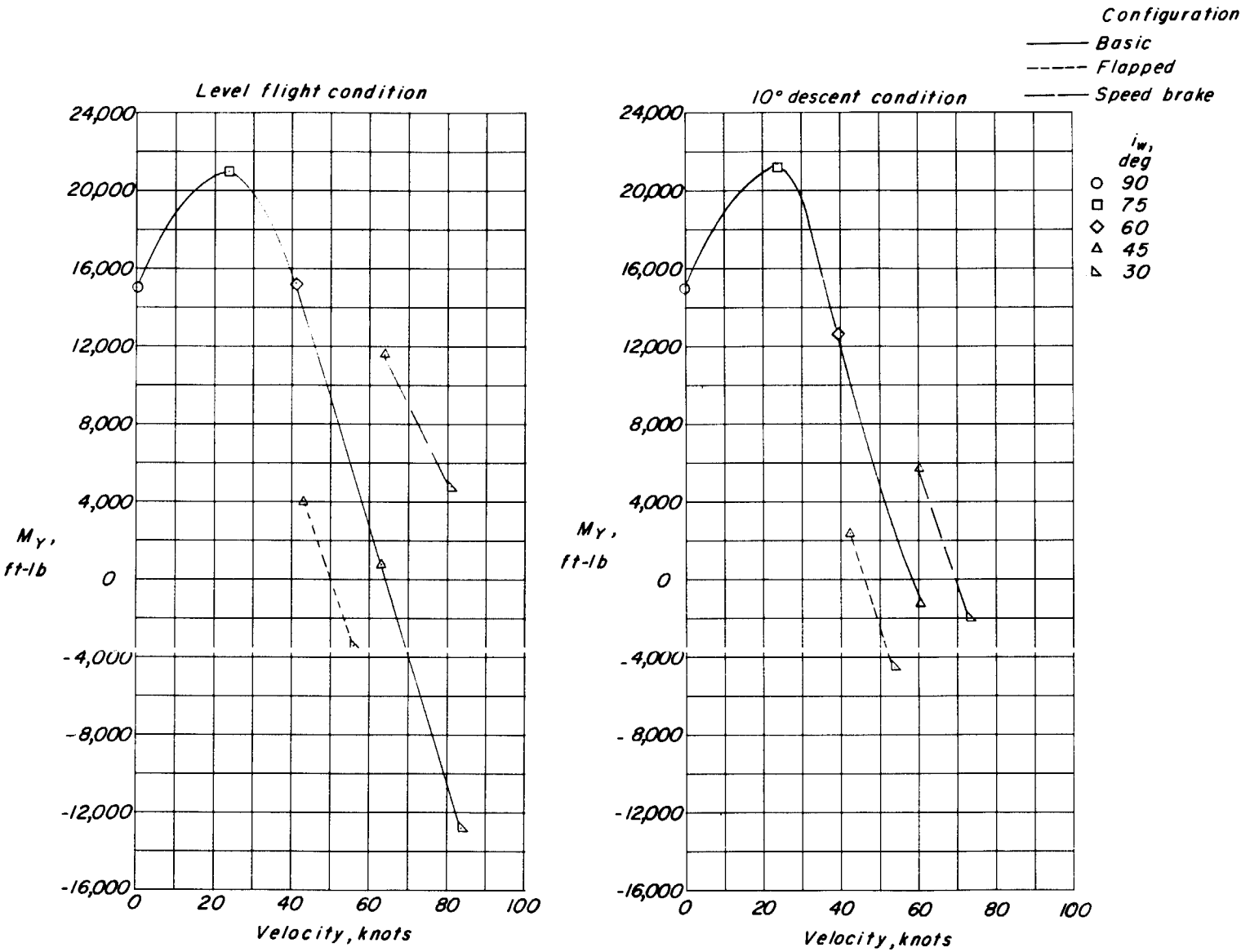

Figure 47.- Effect of configuration on pitching moments of the assumed airplane in transition. $i_t = 20^\circ$.

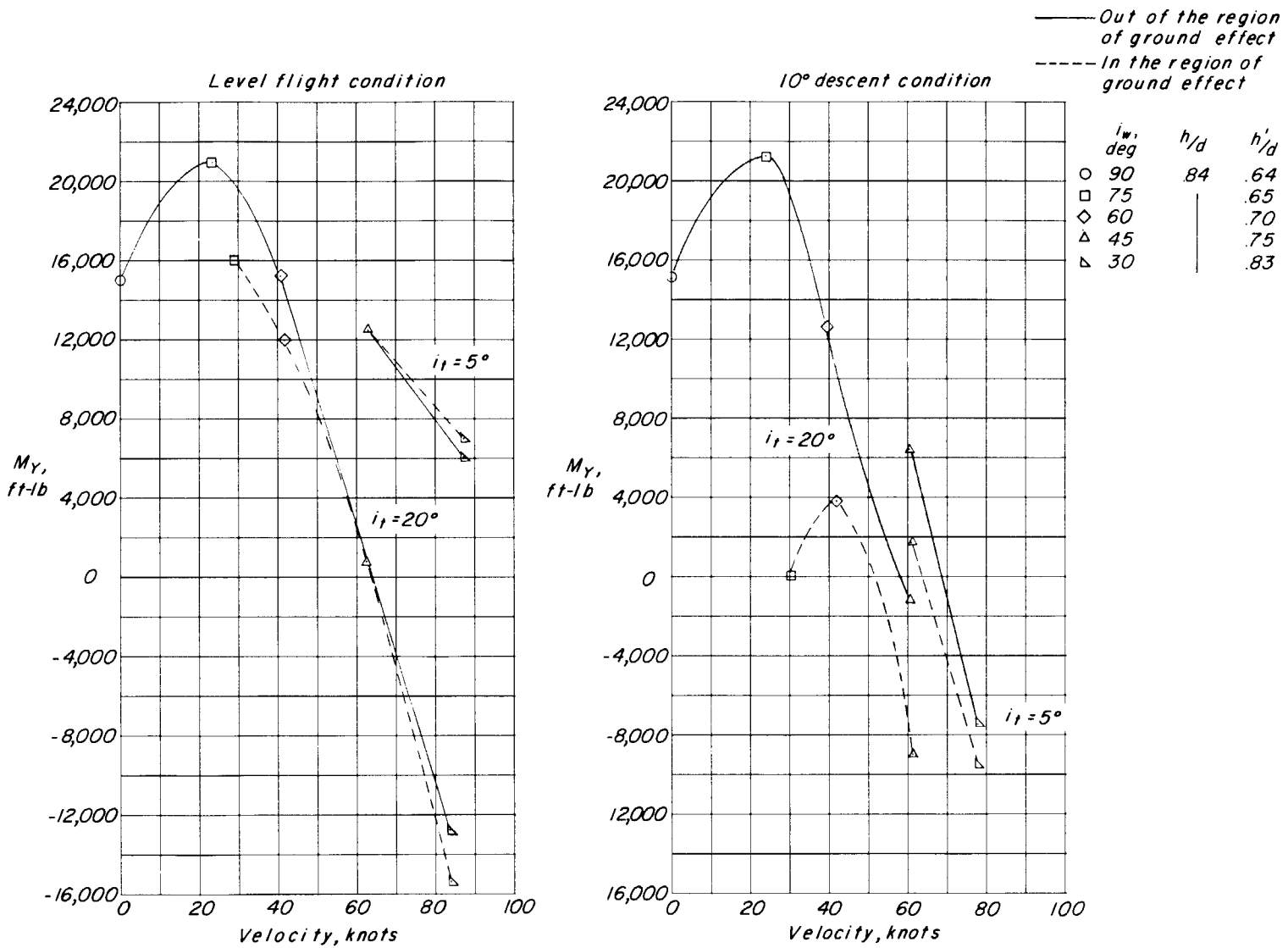

Figure 48.- Effect of ground on pitching moments of the assumed airplane in transition (basic configuration).

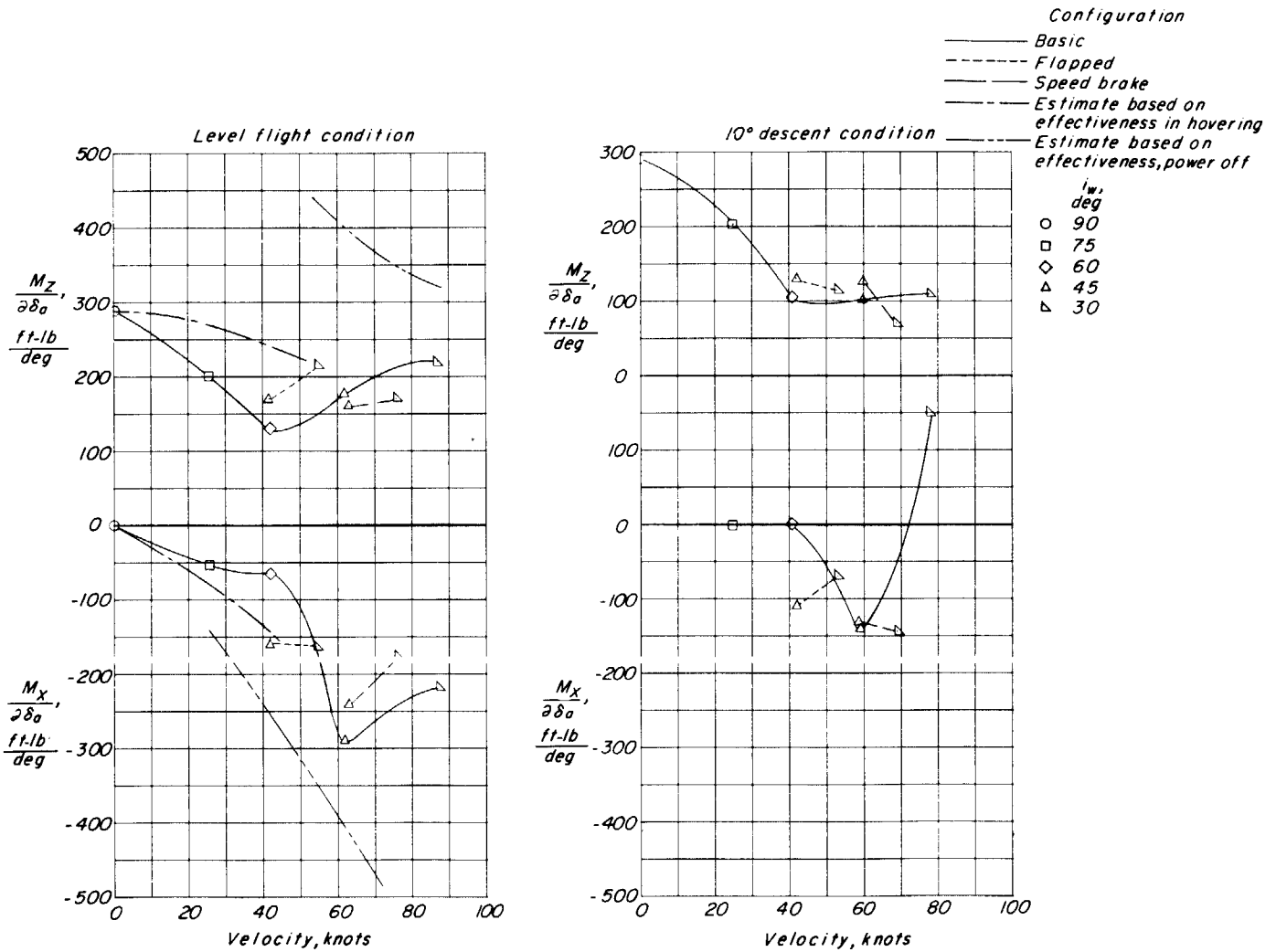

Figure 49.- Effect of configuration on aileron effectiveness for the assumed airplane in transition.

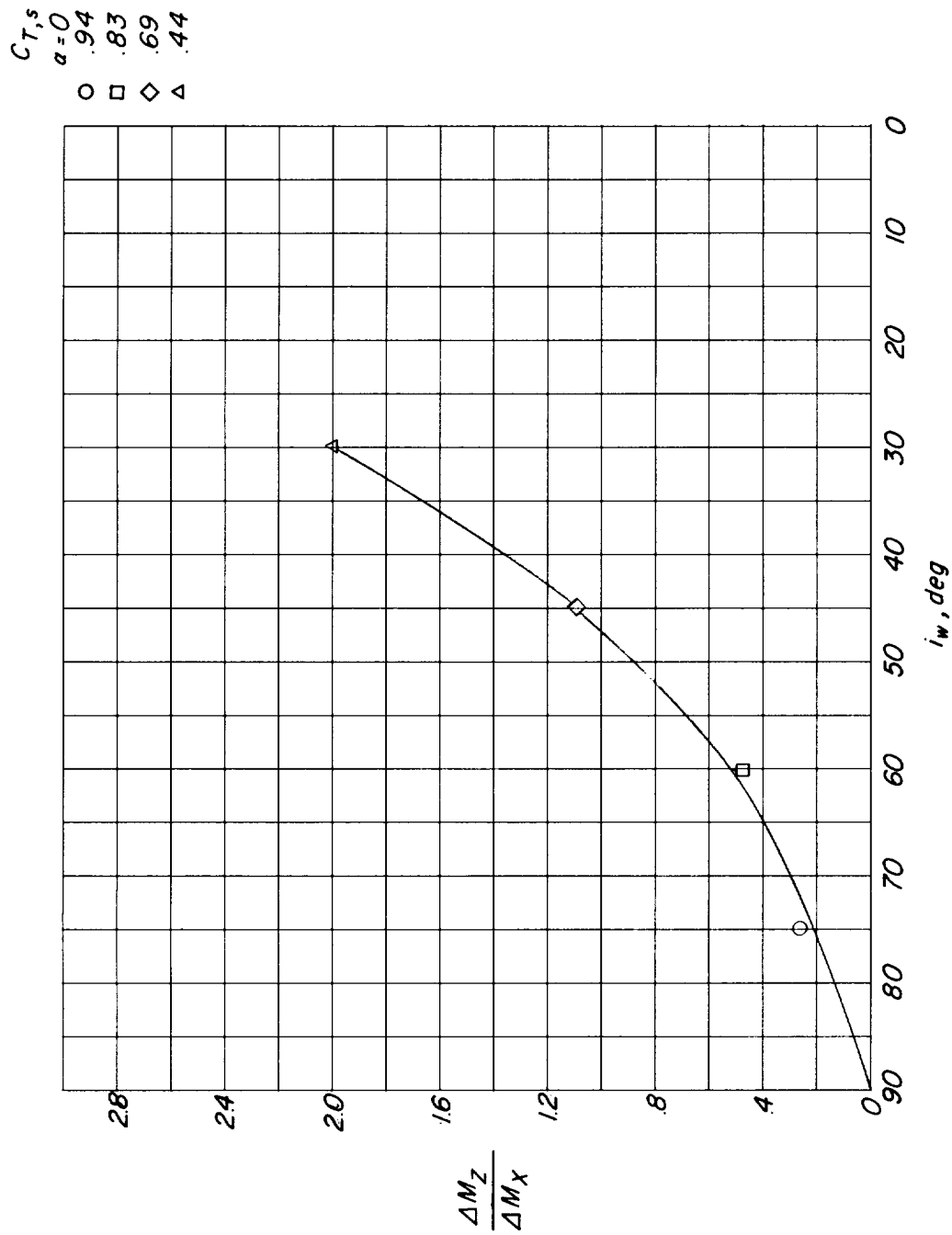

Figure 50.- Ratios of yawing moment to rolling moment obtained by changing the blade angle of the outboard propeller.

NASA - Langley Field, Va. L-1491